Design of Connections for Post Tensioned Rocking Timber Frames

Tom Armstrong

Supervisors

Prof. Andy Buchanan

Prof Stefano Pampanin

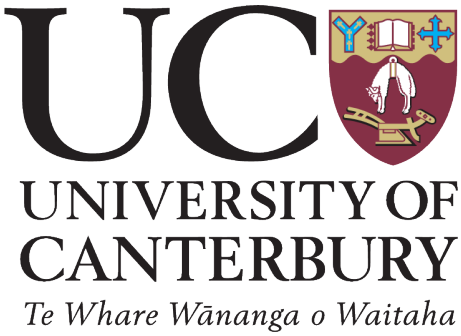

A Thesis In Partial Fulfilment of the Requirements for the Degree Master of Engineering

Contents

List of Figures

List of Tables

List of Acronyms

American Concrete Institute	ACI
Acceleration Displacement Response Spectra	ADRS
College of Creative Arts	CoCA
Displacement Based Design	DBD
Digital Read Out	DRO
European Technical Approval	ETA
Force Based Design	FBD
Laminated Veneer Lumber	LVL
Maximum Credible Event	MCE
Modified Monolithic Beam Analogy	MMBA
Non-linear Time History Analysis	NLTHA
Nelson Marlborough Institute of Technology	NMIT
Necked Plate Dissipater	NPD
Necked Rod Dissipater	NRD
PREcast Seismic Structural System	PRESSS
reinforced concrete	RC
Single Degree of Freedom	SDOF
Serviceability Limit State	SLS
Structural Timber Innovation Company	STIC
Timber Concrete Composite	TCC
Uniformly Distributed Load	UDL
U-shaped Flexural Plate	UFP
Ultimate Limit State	ULS

Chapter 1

Introduction

The introduction of Pres-Lam as a structural system aims to allow timber to stand alongside concrete and steel as a material of choice for multi-storey frame structures. It achieves this by combining Laminated Veneer Lumber (LVL) structural members with forces from post-tensioning to produce a strong, light-weight and resilient structural solution. The addition of external energy dissipation devices allows designers to concentrate inelastic behaviour into specified and appropriately detailed elements. This provides increases in hysteretic damping without sacrificing repairability

The development of Pres-Lam has followed from advances in pre-cast concrete (Priestley *et al.*, 1999). The PREcast Seismic Structural System (PRESSS) system combines controlled rocking at joints with re-centring from post-tensioned tendons to produce structures that; perform well during seismic events, have limited permanent displacement afterwards, and are fast and simple to construct. The use of timber in place of concrete for this application provides benefits including weight reductions, lowering seismic demands and allowing frames with long clear spans.

The 2011 earthquakes in Christchurch reinforced the importance of ensuring that structures not only protect life-safety during a seismic event, but also minimise damage and downtime afterwards (Canterbury Earthquakes Royal Commission, 2012). In many cases structures survived the ground motion but were left with more damage than was economical to repair. The self-centring behaviour of Pres-Lam frames can be used to minimise residual drifts, while energy dissipating 'fuses' limit damage to the structure.

1.1 Motivation for the research

Pres-Lam structural systems are transitioning from the laboratory to the construction site. At the time of writing, several Pres-Lam buildings have been built, with more planned and under construction. Each of these structures has, however required significant input from academia during design. This research aims to raise confidence in Pres-Lam frame systems among designers. It is hoped that this will facilitate more widespread adoption of the technology for new construction.

Like all timber, LVL is an anisotropic material, its strength and stiffness is greatly diminished perpendicular to the direction of the grain. Columns in moment frames are highly stressed in this direction in the beam column joint zone. This necessitates inclusion of reinforcement in the

joint zone. Designs for reinforcement require careful consideration to ensure their effectiveness. This research aims to provide designers with tested details for use in future construction.

The design of dissipative elements must also be undertaken with particular attention to detail to ensure effectiveness. Challenges which may be encountered include; restraining buckling under compressive loads, connection to timber elements and replacement after a seismic event. The experimental testing undertaken has enabled clarification of these challenges, and development of solutions.

1.2 Scope and Objectives

This thesis investigates beam column joints for post-tensioned timber frame buildings. The objective of this research is to provide design and detailing guidance to building designers. This will be achieved by meeting the following objectives.

- Design, construct and assemble a selection of joint details, to gain insights about their constructibility, complexity and repairability.
- Undertake an experimental testing campaign to assess each joint's seismic performance.
- Compare the observed behaviour with predictive models of joint response.
- Provide design and detailing recommendations for beam column joints.
- Show how these joints can fit into structural systems by designing and assessing case study structures.

1.3 Organisation

Chapter 2 describes the body of research supporting this thesis. Previous experimental testing efforts are presented and key findings are summarised. Past and current construction projects using Pres-Lam are detailed. Components necessary to successful joints including dissipation devices and connection systems are outlined.

Chapter 3 describes the full scale experimental testing of beam column joints undertaken as part of this research. The tested options for column reinforcement and dissipation devices are explained and details of the construction and fabrication procedures are given.

Chapter 4 presents the results of the testing campaign. The observed behaviour of each joint detail tested is described. Key details of each joint's performance are determined. These are used to compare the effectiveness of joint reinforcement, energy dissipation and overall behaviour.

Chapter 5 describes numerical and analytical modelling of joint behaviour. Analytical models are used to examine localised effects including connection stiffness and armouring effectiveness. Numerical models have been produced using design guidance available at the time of writing. These are compared to the observations of joint response seen in Chapter 4. This data is used to assess the accuracy of current design procedures.

Chapter 6 presents recommendations for the design and detailing of beam column joints. These incorporate observations from experimental testing and modelling. Construction considerations for joint details are highlighted.

Chapter 7 demonstrates how the joints considered may fit into a larger structural system. Three case study buildings are presented. Beam column connections have been designed and detailed for these structures. The seismic performance of these structures has been assessed using numerical modelling.

Chapter 8 concludes the thesis and summarises recommendations for designers.

Chapter 2

Research Background

This chapter describes the body of research supporting this thesis. It describes modern seismic design philosophy, including the use of controlled rocking to limit seismic demands on structures. The development of Pres-Lam as a technology is documented, with descriptions of past and current structures using this system given. Additionally, novel connection types are introduced; these are used to produce beam column joints tested in this research.

2.1 Performance Based Seismic Design

Most traditional building codes prescribe minimum standards for performance during earthquakes. They typically focus on the safety of occupants and do not explicitly consider damage sustained by the structure or reoccupation following an earthquake (FEMA, 2006). During the 2011 Canterbury earthquakes this approach resulted in buildings where collapse was prevented, although severe damage occurred. In many cases the structures were damaged beyond economic repair and were demolished (Canterbury Earthquakes Royal Commission, 2012).

Performance based seismic design explicitly evaluates the expected behaviour of the structure at each of several performance levels. Desired performance targets can be specified and the structure's design tailored to achieve these (FEMA, 2006). This ability to define and meet specific criteria enables designers, owners, regulators, and other affected parties to consult on the trade-off between cost and expected performance. Beyond this trade-off, new design approaches are appearing where performance targets are met without significantly increasing cost (Pampanin *et al.*, 2010, STIC, 2013, Gledhill *et al.*, 2008).

2.2 Rocking Structures

Damage observations following the 1963 Chilean earthquake identified that structures exhibiting rocking sustained less damage than expected (Housner, 1963). Controlled rocking has been used by designers to reduce damage from seismic events since the 1980s when a railway viaduct incorporated rocking piers with additional energy dissipation devices (McManus, 1980).

Rocking behaviour is caused by a geometric non-linearity. At the onset of rocking the system's stiffness is greatly reduced, resulting in a lengthening of its fundamental period and reduction in seismic demand.

Rocking can be incorporated into structures either at the foundations or at the joints between structural components. These options are compared below.

Footing rocking occurs when foundations are allowed uplift from the underlying ground. Foundation rocking of a frame and the equivalent Single Degree of Freedom (SDOF) model are shown in Figure 2.1. There is extensive supporting literature (Kelly, 2011) as well as codification and design notes (Kelly, 2011, Standards New Zealand, 2004, Stewart *et al.*, 1994) for this form of rocking. A major disadvantage of foundation based rocking is the reliance on soil properties for satisfactory behaviour. If soft soils are encountered, yielding of the underlying material may occur, causing permanent settlement to develop (Mergos & Kawashima, 2005).

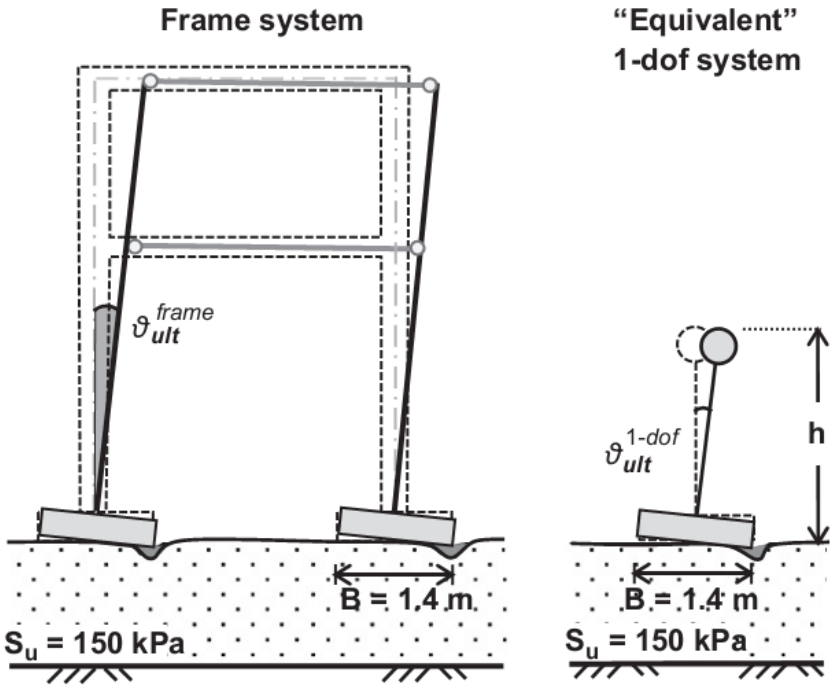

Figure 2.1: Footing rocking of frame and equivalent SDOF system (Gelagoti *et al.*, 2012)

Controlled rocking involves allowing gaps to open between various structural elements. This opening is forced to occur at locations targeted by the designer. Because of this, detailing can be produced to mitigate damage to the structure. If adequate re-centring capacity is available in the structure, residual displacements can be minimised. Re-centring may take the form of gravity loads or additional forces such as from post-tensioning tendons. This form of rocking and its effect on system stiffness is illustrated in Figure 2.2.

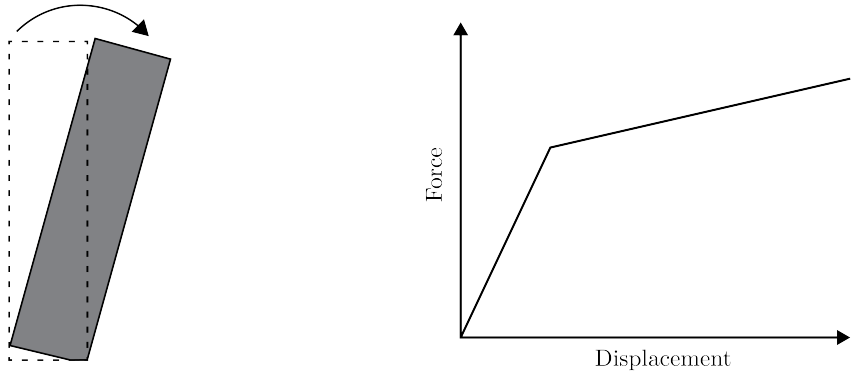

Figure 2.2: Rocking at structural interfaces, diagram (a) and stiffness response (b)

2.3 PRESSS

The PREcast Seismic Structural System research programme was undertaken by researchers in the US and Japan in the the 1990s. It aimed to develop precast concrete structural systems suitable for use in seismic regions (Priestley *et al.*, 1999).

The *"Hybrid"* system produced as part of this programme used pre-cast components connected using un-bonded post-tensioning tendons. When subjected to seismic loading, gaps at the connection interfaces produce localised rocking effects. Inelastic deformation was concentrated in mild-steel energy dissipation devices meaning that structural damage is avoided. The elongation of post-tensioning provided the system with re-centring. A schematic view of a PRESSS beam column connection together with a behavioural idealisation of each of the components of the system is given in Figure 2.3.

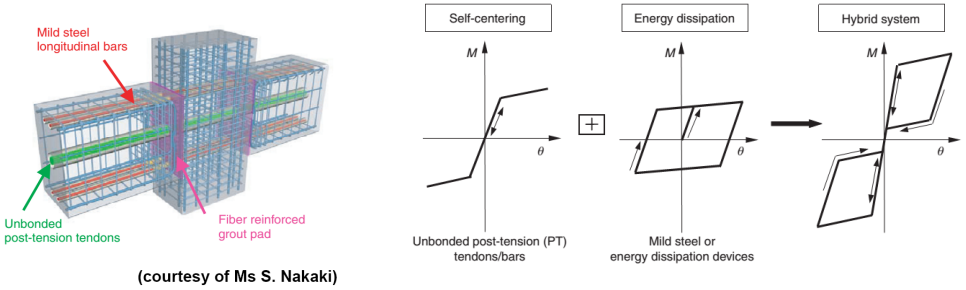

Figure 2.3: Hybrid PRESSS joint and behavioural idealisation (fib, 2003)

The total hysteresis profile shown in Figure 2.3 has a characteristic *"flag"* shape. This features energy dissipation, represented by the area enclosed in the loop. Additionally, the response returns through the origin, meaning that zero residual displacement is expected for this system.

The individual behaviour of the post-tensioning and mild steel components are shown individually

as well as the combined response. The contributions of each of these can be tuned by the designer to create a system with the desired characteristics.

The PRESSS programme included experimental verification of both sub-assemblies and structural systems (Priestley *et al.*, 1999). Figure 2.4 shows the experimental set-up for 60% scale tests of a structure using both frame and wall systems subjected to pseudo-dynamic loading. This test subjected the building to extreme lateral loadings, well in excess of code requirements, with only minor damage observed.

(a) PRESSS frame system (b) PRESSS wall system

Figure 2.4: PRESSS structural systems (Nakaki *et al.*, 1999)

Comprehensive design guidelines (Pampanin *et al.*, 2010) have been produced to support the design of PRESSS structures. The documents contain the theoretical and research background, design methodologies and examples as well as design charts enabling quick preliminary designs for components of PRESSS systems.

The success of the PRESSS research programme has seen a number of PRESSS buildings constructed in New Zealand. These include a hospital in Christchurch (Pampanin *et al.*, 2011), a university building in Wellington (Cattanach & Pampanin, 2008). These structures have been subjected to earthquakes and good seismic performance has been observed. Images of these structures are shown in Figure 2.5.

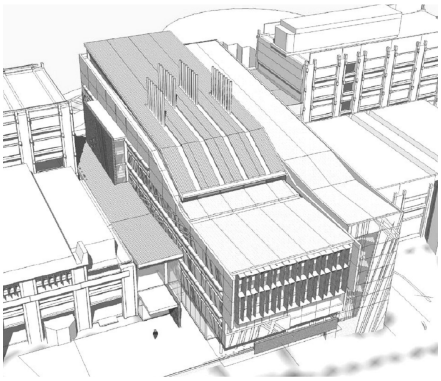

(a) Victoria University, Wellington
(Cattanach & Pampanin, 2008)

(b) Christchurch Hospital
(Pampanin *et al.*, 2011)

Figure 2.5: PRESSS buildings in New Zealand

2.4 Pres-Lam

The extension of jointed ductile technology to engineered timber was proposed in 2004 at the University of Canterbury (Palermo *et al.*, 2005). Preliminary tests of small-scale LVL specimens validated the performance of these systems. The potential to create a strong, resilient, light-weight structural system with benefits over both traditional construction techniques as well as PRESSS concrete systems was shown.

2.5 Beam Column Joint Testing

Previous experiential investigations into Pres-Lam beam column joints have been undertaken at the University of Canterbury. These are summarised in Table 2.1 and are described in more detail below.

Table 2.1: Summary of Pres-Lam beam column joint testing

Tests	Scale	Reinforcement	Dissipation	Notes
Newcombe	2/3	Steel Plate	Post-Tensioning only Internal Mild Steel	
Iqbal	full	Steel Plate Screws	Post-Tensioning only External Necked Rod	
Smith	2/3		External Mild Steel	
van Beerschoten	full	Screws Crossbanded LVL Rotated veneers	-	Gravity loading

2.5.1 Newcombe

Newcombe undertook 2/3 scale tests of beam, column and wall sub-assemblies (Newcombe, 2007). Seven tests were undertaken of the beam column sub-assembly. The test set-up used is shown in Figure 2.6. The quasi-static tests used an American Concrete Institute (ACI) loading protocol (ACI, 2001). Testing considered an external beam column joint specimen with:

- Post-tensioning only
- Fused internal mild steel dissipaters
- Fully bonded internal dissipaters
- Fused external dissipaters

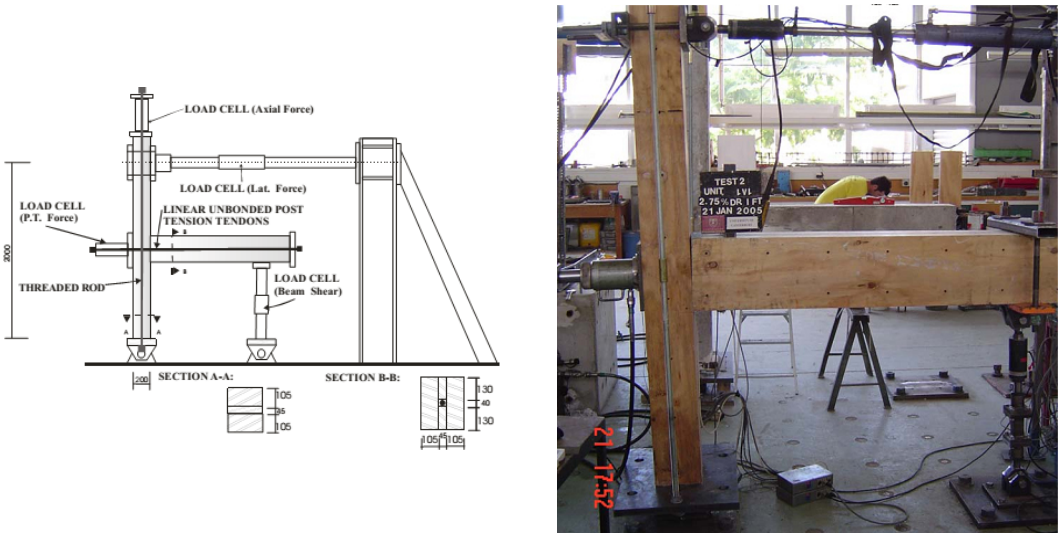

Figure 2.6: Diagram and photograph of 2/3 scale beam column test (Newcombe, 2007)

Representative moment-rotation results for these tests are shown in Figure 2.8 These show the response of the specimen with and without mild steel dissipaters. Two options for dissipaters are shown in figure 2.7, one connected to the outside face of the column and one epoxied inside the LVL. As expected, the response is approximately bilinear for the post-tensioning only case and exhibits a flag shaped hysteresis in the hybrid specimen.

(a) Internal dissipaters (b) External dissipaters

Figure 2.7: Dissipation devices (Newcombe, 2007)

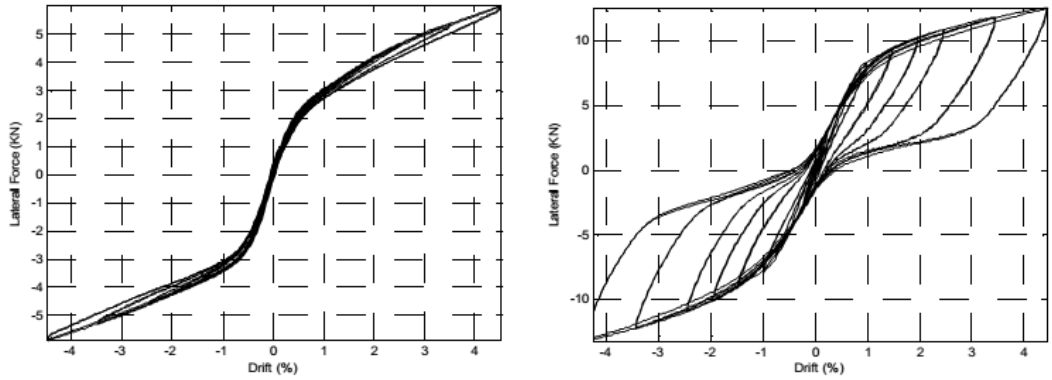

(a) Post-tensioning only (b) Mild steel dissipation

Figure 2.8: Representative results from 2/3 scale beam column joint testing (Newcombe, 2007)

These tests used a steel angle to armour the corners of the beam agains LVL splitting. This arrangement is shown in Figure 2.9. The angles concentrated stresses and so exacerbated the problem of low LVL strength and stiffness perpendicular to the grain in the column. This was detrimental to the performance of these systems.

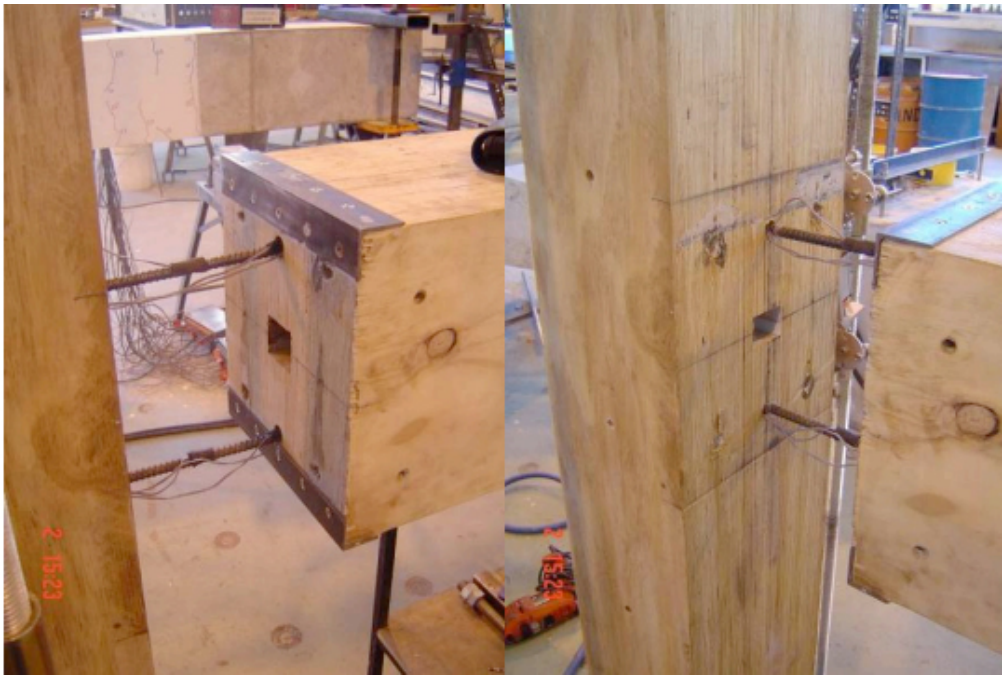

Figure 2.9: Beam edge reinforcement with steel angles (Newcombe, 2005)

Newcombe's results indicated that uncertainty in the response of hybrid beam column joints arises mainly due to dissipative elements. The connection of these dissipaters to the beam and column was highlighted as being critical to performance (Newcombe, 2005).

A two storey 2/3 scale test building was constructed by Newcombe (Newcombe *et al.*, 2010a). This is shown in Figure 2.10. The structure for this test was prefabricated and assembled by professional contractors. This allowed a more realistic assessment of advantages in terms of speed of construction to be quantified. The structural system took 15 hours to assemble "*on site*".

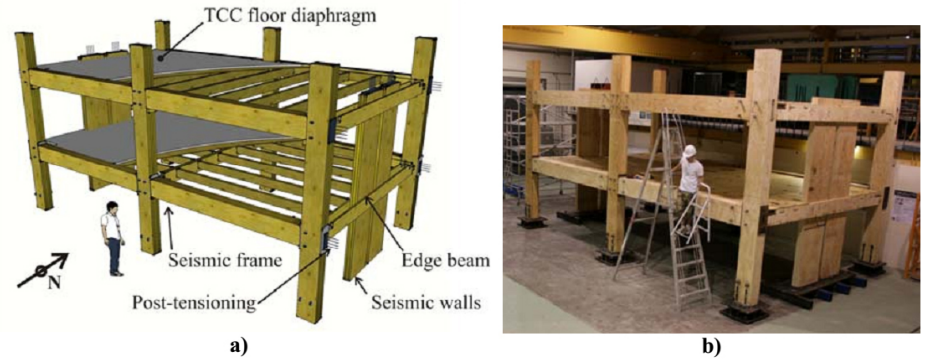

Figure 2.10: 2/3 scale test structure (Newcombe, 2011)

.

Ten tests were carried out on the structure, with six of these being loaded in either the frame direction or bi-directionally. Testing considered both hybrid and post-tensioned only joints. The effectiveness of the dissipative reinforcement at the beam column interface was severely reduced by elastic deformations in the frame and connection slip, both of which lowered the displacement imposed on the dissipater. The research indicates the need for further research into connection detailing for beam column joints, particularly the connection of dissipative elements to timber.

Beam to column joint interfaces were reinforced in one of two ways. Lower level joints were reinforced with internal steel plates while the upper joints used fully threaded screws. A comparison of these details is given pictorially in Figure 2.11 and diagrammatically in Figure 2.12. The level of joint reinforcement used, particularly in the screw reinforced, case is quite low, potentially explaining some of the limited performance observed in these joints.

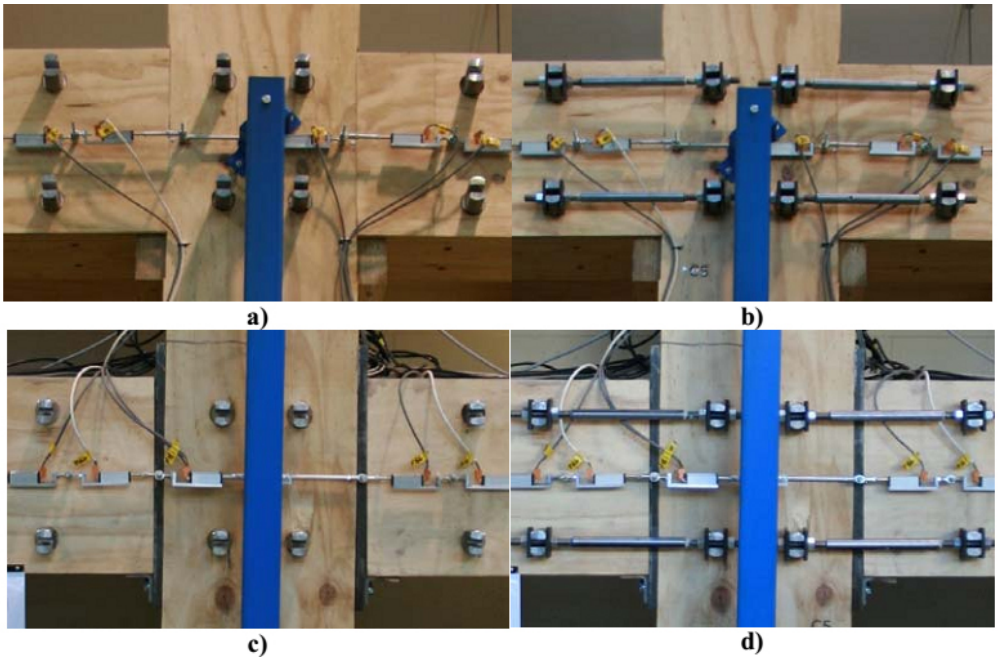

Figure 2.11: Beam column connection for test structure a) level 3 PT only, b) level 3 Hybrid, c) level 2 PT only, d) level 2 hybrid (Newcombe, 2011)

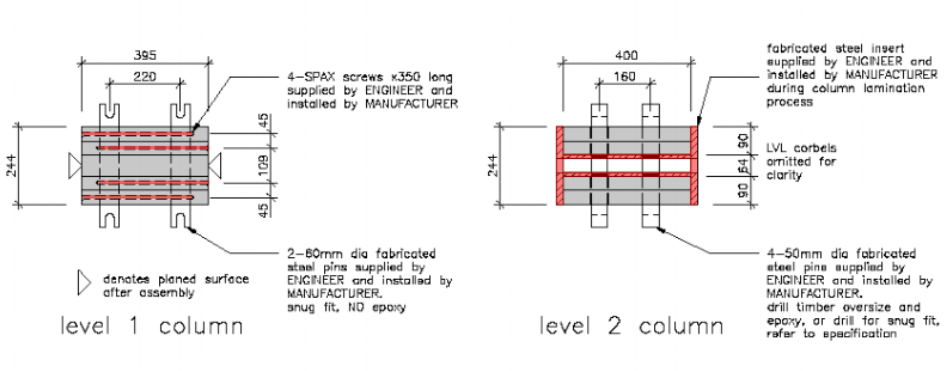

Figure 2.12: Joint details of test structure showing screw reinforced upper joint and steel reinforced lower joint (Newcombe, 2011)

Structural damage was minimal up to the design drift levels. For larger drift levels, up to 3%, there was some crushing of the column observed. This occurred around dissipation anchorage pins where LVL crushed perpendicular to grain. This increased the slop in the connection to the dissipative elements.

2.5.2 Iqbal

Testing of a full-scale a beam column specimen was undertaken at the University of Canterbury in 2010 (Iqbal, 2011). This was designed for the seismic frame of a six storey building in a high seismic zone. The frame used 9 m beam spans and a beam spacing of 6 m. The inter storey height was 3.6 m. This represented a realistic structural layout, albeit, one optimised for a timber framed system. Interior and exterior joint specimens were tested. These set-ups are shown in Figures 2.13 and 2.14, respectively.

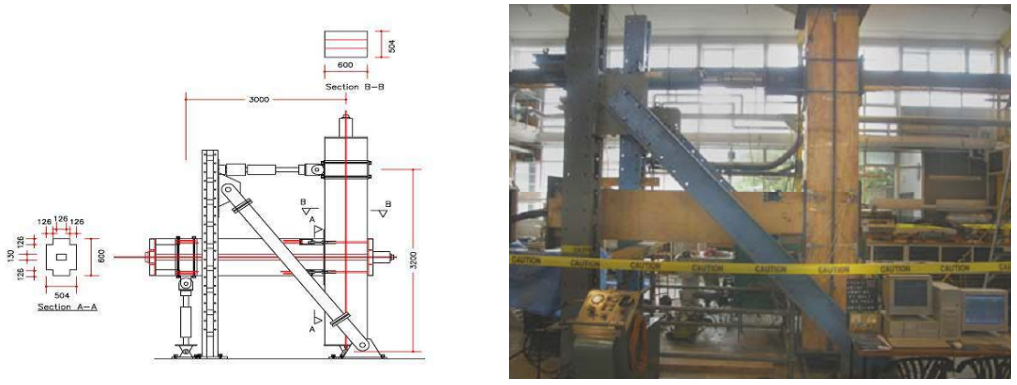

(a) Diagram (b) Photo of test set-up

Figure 2.13: Exterior beam column joint specimen (Iqbal *et al.*, 2010)

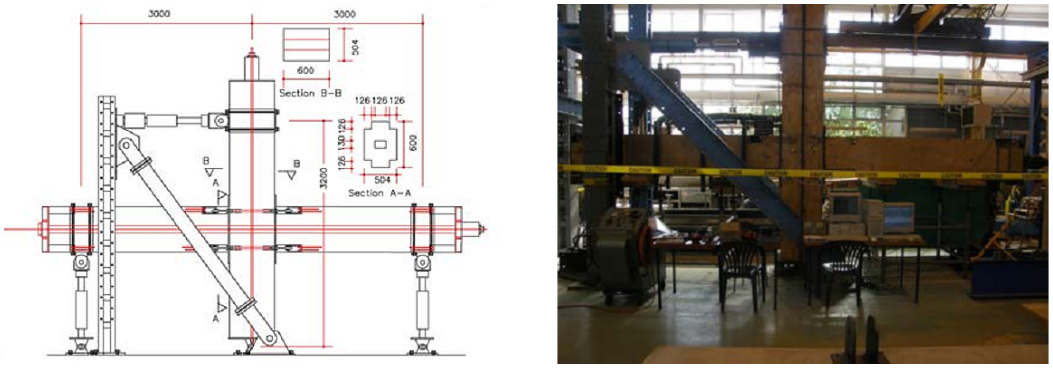

(a) Diagram (b) Photo of test set-up

Figure 2.14: Interior beam column joint specimen (Iqbal *et al.*, 2010)

A total of ten tests were carried out on the beam column specimen. These included four for the external arrangement and six for the internal joint. Post-tensioned only and hybrid designs were assessed. The impact of joint zone armouring was also tested. Armouring options included steel plates and diagonal screws. The steel joint armouring and dissipation details are shown in Figure 2.15.

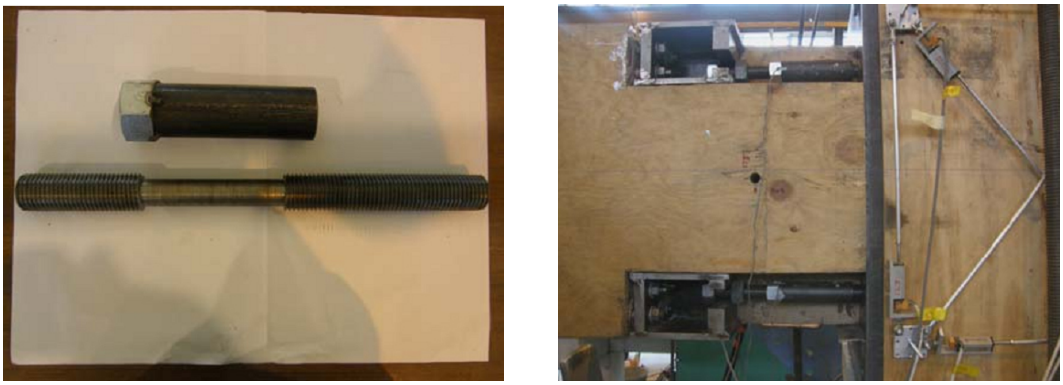

(a) Necked rod dissipater details (b) Close up of joint zone

Figure 2.15: Beam column joint details showing external dissipation devices (Iqbal *et al.*, 2010)

Typical results from a test are shown in Figure 2.16. This figure shows the cyclic performance of the system and illustrates the combination of energy dissipation and re-centring developed by the jointed ductile system.

Fully threaded screws were used to reinforce the joint zone for some of the test specimens. This involved 10mm diameter, 600mm long *SPAX* screws installed both horizontally and diagonally in the column. Figure 2.17 shows the installation of these screws. The force-displacement plot shown in Figure 2.17 shows that the screw reinforcement had little effect on the stiffness of the joint (Iqbal, 2011). There was however a noticeable decrease in post-tensioning losses during testing (Iqbal *et al.*, 2010). Increased joint stiffness would be expected given a reinforced joint zone. It

is possible that the number of screws used to reinforce the joint may have been insufficient to achieve this.

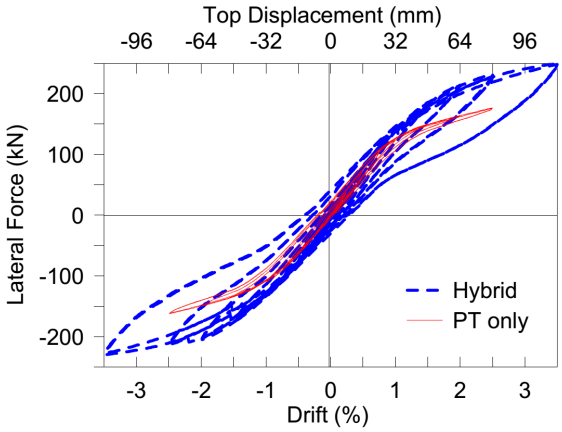

Figure 2.16: Moment rotation results from a typical test of a full scale beam column joint (Iqbal, 2011)

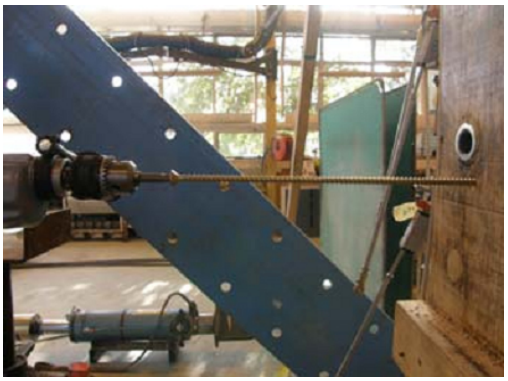

(a) 600 mm reinforcement screw installation

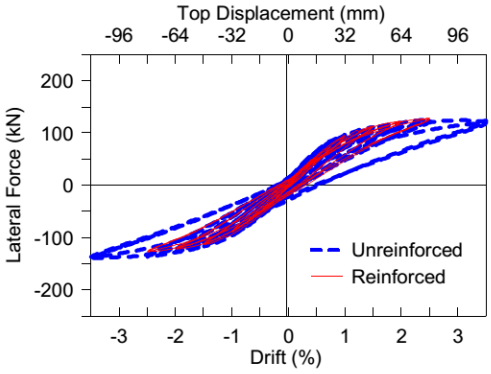

(b) Response comparison between screw reinforced joint and un-reinforced joint

Figure 2.17: Joint reinforcement using fully threaded screws (Iqbal *et al.*, 2010)

The testing performed as part of this campaign showed good results with almost complete re-centring observed in most specimens. Where residual displacements were observed, this was found to be largely due to sliding at the base connection. No structural damage was observed to the specimens. The research concluded that more testing of a greater variety of joint details should be undertaken to provide increased knowledge of sub-assembly behaviour (Iqbal, 2011). It additionally recognised the value of testing full-scale specimens in delivering accurate results.

2.5.3 van Beerschoten

Testing of beam to column connections by van Beerschoten focused largely on gravity loads. This involved the use of draped tendons to achieve longer spans while satisfying stiffness and deflection limits. The stiffness of the joint zone was again identified as a critical factor to the successful use of LVL in a frame based structural system (van Beerschoten, 2011).

This testing considered several reinforcing options for the joint zone including:

- Fully threaded screws and a steel bracket,
- Using cross-banded LVL, and
- Rotating the outer laminates of the LVL 90 degrees.

An overview of the testing is shown in Figure 2.18, details of the joint zone are shown in Figure 2.19.

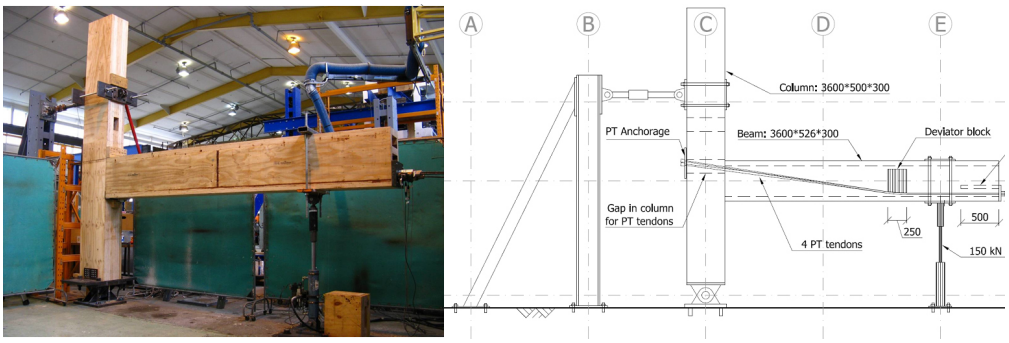

Figure 2.18: Test setup and diagram for draped tendon beam column test (van Beerschoten, 2013)

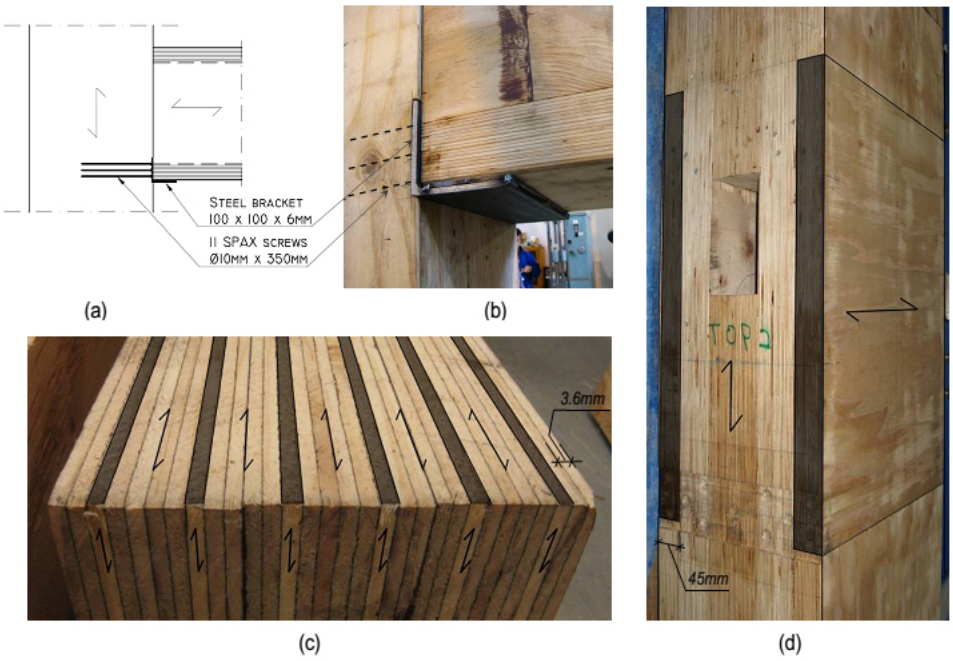

Figure 2.19: Joint reinforcement (van Beerschoten, 2011) including:
a,b) Corbel and screw reinforcement
c) Cross-banded LVL
d) Outer layers of joint zone rotated 90 degrees

For the specimens with regular LVL in the column zone, the inclusion of screw reinforcement was seen to increase the joint stiffness by 60%. The screws however showed no improvement when used with cross-banded LVL or where the LVL was rotated in the joint zone. Rotating the LVL in the joint zone also increased the joint stiffness by around 50% (van Beerschoten, 2011).

2.5.4 Smith

Smith undertook testing of a beam column specimen modified from Newcombe (Section 2.5.1). External dissipation was added to the 2/3 scale specimen to create a hybrid joint (Smith, 2006). The outline of the hybrid specimen and apparatus for the test is shown in Figure 2.20. Nine tests were undertaken These considered several external dissipation options and post-tensioning levels for each specimen. Photos of the specimen with post-tensioning only and the hybrid joint are shown in Figure 2.21.

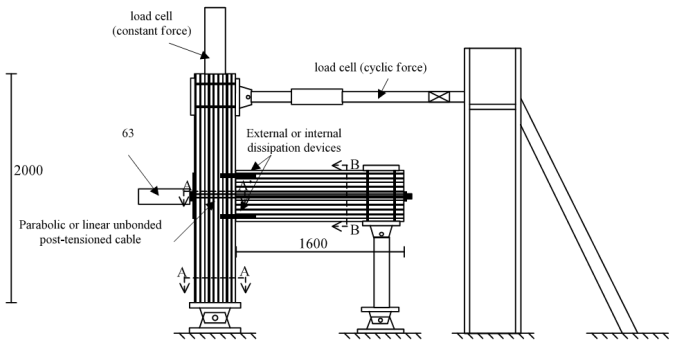

Figure 2.20: Experimental set-up for hybrid beam column joint testing (Smith, 2006)

(a) PT only joint (b) Hybrid joint

Figure 2.21: Beam column joint tests at 4.5% drift (Smith, 2006)

The response of a hybrid beam column joint test is shown in Figure 2.22. This shows the characteristic flag shaped hysteresis incorporating both re-centring and energy dissipation. The loops produced are stable with only slight degradation between cycles. Several other tests confirmed this behaviour. However in some cases, partial failure of the dissipater or its connection lead to poor response at extreme drift levels. This testing showed the critical importance of good detailing for external dissipation.

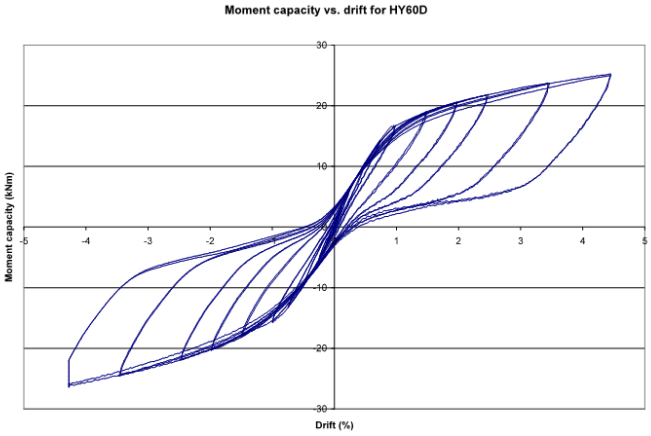

Figure 2.22: Response of hybrid beam column joint test (Smith, 2006)

A three storey 2/3 scale frame building was dynamically tested at the University of Basilicata (Smith *et al.*, 2014). This was a two way frame and was tested with and without dissipative joint reinforcement. The frame structure is shown in Figure 2.23. The frame was subjected to seven scaled earthquake records, applied uniaxially.

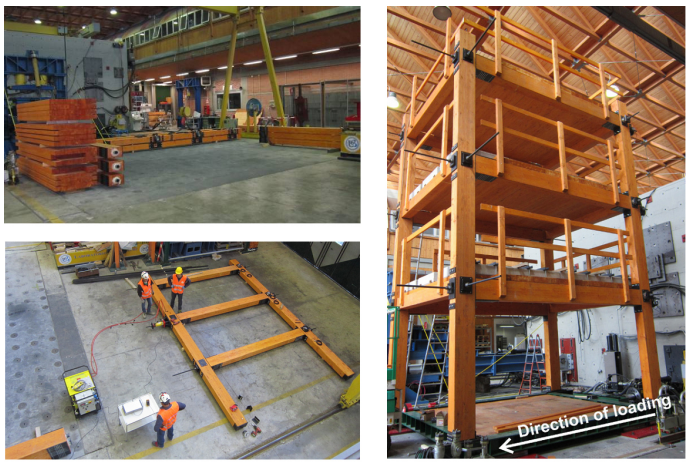

Figure 2.23: Shake table testing of frame at UNIBAS lab (Smith *et al.*, 2014)

Dissipation for this test took the form of yielding steel angles at the beam to column and column to foundation interfaces. These dissipaters used a steel angle where one leg was milled down to ensure yielding, they are shown in Figure 2.24. Slip in the connection between the steel dissipater and the timber beam was seen to reduce their performance in some tests. This again reinforces the need for adequate connection strength and stiffness to be provided to dissipative elements (Smith *et al.*, 2014). The inclusion of mild steel dissipative reinforcement was seen to reduce the peak drift of the structure by as much as 30% without a corresponding increase in floor acceleration.

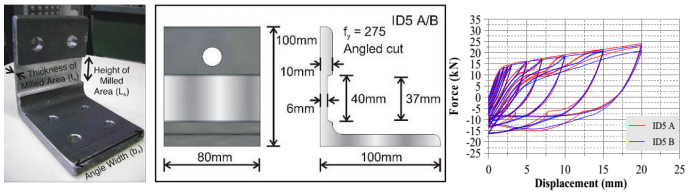

Figure 2.24: Angle dissipater used in frame test (Smith *et al.*, 2014)

2.6 Current Generation of Pres-Lam Buildings

Several structures utilising post-tensioned structural systems were either complete or under construction at the time of this research. These include buildings using both wall and frame systems. Examples of these buildings are discussed below. Additional details of these buildings and of buildings using wall based structural systems can be found in the Pres-Lam design guide (STIC, 2013).

2.6.1 Nelson Marlborough Institute of Technology (NMIT) Building

The NMIT building is a three storey educational building in Nelson (Devereux *et al.*, 2011). It was designed by ISJ Architects and Aurecon Engineers. The building uses rocking timber shear walls, post-tensioned using steel rods to realise a damage avoidance design philosophy. Completed in 2011, the building was the first in the world to be constructed using Pres-Lam technology.

Coupled rocking timber shear walls were used with high-strength steel bars to provide re-centring. Dissipation was provided using U-shaped Flexural Plates (UFPs) at the interface between the walls. The overall structure, including the walls, is shown in Figure 2.25.

Figure 2.25: The NMIT building under construction

2.6.2 College of Creative Arts (CoCA) Building

The Massey University College of Creative Arts (CoCA) building uses two storey post-tensioned timber frames on top of a concrete podium. The building was designed by Dunning Thornton consultants and construction was completed in 2012 (Dominion Post, 7 Feb 2012). The building is used to contain 3,600m^2 of teaching and exhibition spaces for Massey's College of Creative Arts as a link to other parts of the campus.

The beam column joints were reinforced using rotated blocks of LVL meaning that compression was carried parallel to the grain. Dissipation devices were located between a reinforced concrete wall and the first floor beams rather than at the beam column joint.

Exposed post-tensioning was used for this structure. Redundant load paths have been provided in case the post-tensioning is damaged in a fire.

(a) Exterior

(b) Post-tensioning at beam column joint

(c) Exposed post-tensioning at beam

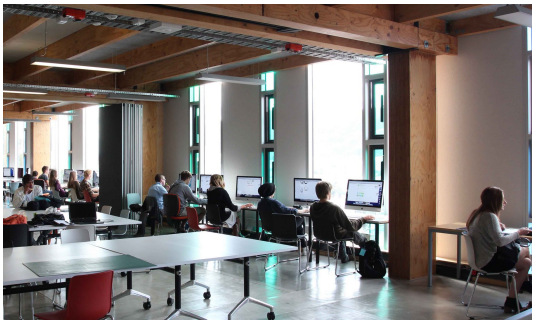

(d) Interior spaces showing exposed timber structure

Figure 2.26: CoCA building (Massey University, 2012)

2.6.3 EXPAN Building

The offices for EXPAN and the Structural Timber Innovation Company were located on the campus of the University of Canterbury. This structure began life as an experimental test specimen and was thoroughly tested in the laboratory (Newcombe *et al.*, 2010b). It was later demounted and reconstructed as offices. The test specimen was constructed at $^2/_3$ scale and so

extensions were added to bring it to full height. Post-tensioned frames were used in the long direction while rocking, post-tensioned walls were used in the other. The frames used both armoured and un-armoured beam column joints. The specimen in the lab is shown in Figure 2.27a

Due to the light-weight material and pre-fabrication techniques used, the erection of this building took only nine working days, two of which were for the erection of scaffolding (Smith *et al.*, 2011). Additionally, the construction required only eight workers on site. Images taken during the building's construction are shown in Figures 2.27b and 2.27c

The building was again sold and, at the time of writing, is expected to be demounted and relocated onto a site in Christchurch, for use as a commercial office.

(a) Test specimen
(Newcombe *et al.*, 2010c)

(b) Frame erection

(c) Erected structure

(d) Clad building

Figure 2.27: EXPAN Building

2.6.4 St Elmo's Courts

St Elmo's Courts was a brick apartment building severely damaged during the Christchurch earthquakes. The building was replaced with a hybrid timber-concrete post-tensioned structure, designed by Rick Proko Architects and Ruamoko Engineers.

The two-way frames used meant that LVL in the joint zone could not be reinforced economically. Because of this, pre-cast concrete columns were used with timber beams.

The building is on base isolators meaning that the upper structure is expected to remain essentially elastic. Due to this, additional dissipation devices were not included.

(a) Demolition of original building

(b) Architectural rendering

(c) New building under construction

Figure 2.28: St Elmo's Courts

2.6.5 Merritt Building

The Merritt building is a three storey office building constructed as part of the rebuild after the earthquakes in Christchurch. It was designed by Sheppard and Rout Architects and Kirk Roberts Engineers. It uses a steel based joint reinforcement system and replaceable necked rod dissipaters. Post-tensioning runs through voids in the beams and is anchored to the outside of the columns. Provisions for re-stressing have been included in the design.

This research was conducted during the construction of the Merritt building. The joint detail from this building was used as the basis of a specimen for the experimental campaign described in Chapter 3.

(a) Finished

(b) Under construction

Figure 2.29: Merritt Building

2.6.6 Trimble Building

Trimble's Christchurch office building was destroyed by a fire. A replacement building was constructed using Pres-Lam frames and walls. Engineering and architectural design was by Opus. This is a large 2 storey, open plan office building with $6000m^2$ of floor space. The structural systems uses both timber frames and walls. External Necked Rod dissipaters are connected to the beams and columns using timber rivets. Post-tensioning runs through the beams and columns on the lower level. Figure 2.30 shows the frame and the beam column joint detail.

(a) Two storey frame

(b) Beam column joint

Figure 2.30: Trimble Building

2.6.7 Review of Current Buildings

This review of some current Pres-Lam buildings found that significant design input from academia was required. This was largely due to each project featuring significantly differing design detailing. While this is feasible for small numbers of structures, the uptake of post-tensioned timber structures is likely to be improved with the availability of a greater number of more standardised design options

2.7 Energy Dissipation Devices

Discreet energy dissipation devices mean that designers are able to concentrate inelastic deformations in specified elements. If done correctly, this can mean that damage from a seismic event is limited to easily replaceable components with the remainder of the structure largely unaffected.

Research into energy dissipation devices has largely concentrated on devices using hysteretic or viscous damping. The behaviour of viscous damping based devices is dependant on velocity whereas hysteretic dissipaters are displacement governed.

Hysteretic damping arises due to the area contained within the force-displacement history of the device. Mild steel has well defined mechanical properties exhibiting both a long post yield region and low variability. This makes it ideally suited for use as a hysteretic damping devices.

Hysteretic damping devices using mild steel are simple to design and fabricate and are less costly than viscous damping solutions. For these reasons, this research focuses on mild steel hysteretic dissipaters.

Hysteretic mild steel damping has been used in many structures exposed to seismic risk. The first of these was a railway viaduct in the central North Island of New Zealand (Beck & Skinner, 1973), the bridge piers and dissipation details are shown in Figure 2.31.

(a) Base of piers (Ma & Khan, 2008)

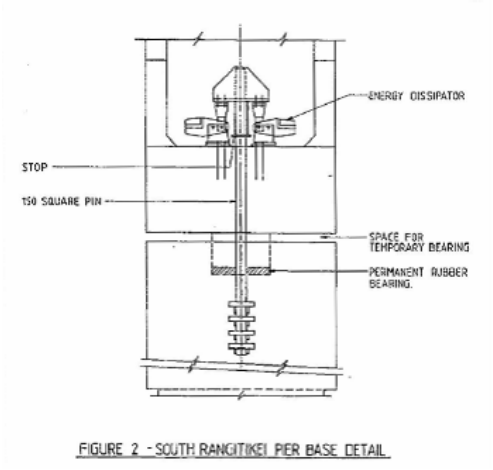

(b) Mild-steel dissipater in pier base (Cormack, 1988)

Figure 2.31: Stepping rail bridge with mild-steel dissipation

This review looks at several types of mild steel dissipaters including:

- Necked Rod / Plug and Play Dissipaters
- Milled Angle Dissipaters
- acplUFP Dissipaters

These all function similarly, with controlled yielding of mild steel dissipating energy. Yielding is most often controlled by reducing sectional area over a region of relative displacement during seismic movements.

2.7.1 Necked Rod / Plug and Play Dissipaters

Circular steel sections with a reduced cross section over a yielding zone have a long history of use in earthquake resisting structures (Tyler, 1978). These have well defined behaviour and are simple to design and fabricate. Variants of this type of dissipater has been the primary choice for both PRESSS and Pres-Lam frame systems. A schematic view of this dissipater type is shown in Figure 2.32.

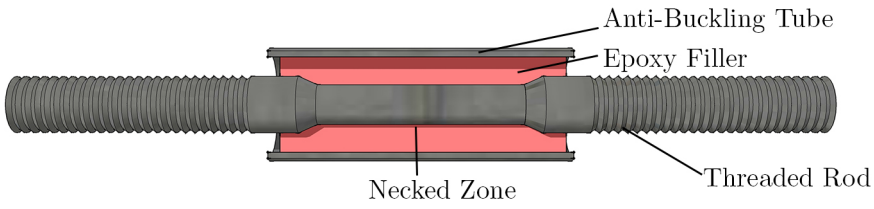

Figure 2.32: Necked rod dissipater

2.7.2 Milled Angle Dissipaters

Mild steel angles have been used to create energy dissipation devices. One face of the angle is connected to the beam and the other to the column. When the angle is subjected to differential displacements, a milled down area in the angle yields, dissipating energy. These dissipaters have been tested with good results (Smith *et al.*, 2014). This dissipater and its response are shown in Figure 2.33. Connection to the LVL using screws may be simplified with the use of these dissipation devices.

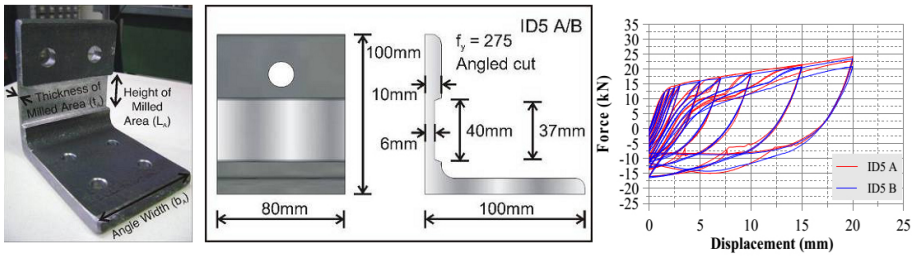

Figure 2.33: Milled angle dissipater (Smith *et al.*, 2014)

2.7.3 U-shaped Flexural Plates (UFPs)

UFP dissipation devices were introduced in 1972 as a method of dissipating the kinetic energy of an earthquake (Kelly *et al.*, 1972). These use a flat steel plate rolled into a U shape. A relative displacement between structural components during earthquake attack is used to yield the plate, dissipating energy. As the plate rolls, the yielding zone moves on the plate. This avoids concentrating inelastic demand in a single location, and reduces the susceptibility of UFPs to low-cycle fatigue.

These devices utilise large relative displacements to generate dissipation, they are therefore well suited to PRESSS and Pres-Lam applications. Examples of their use in these structures and a general diagram of the device are shown in Figure 2.34.

(a) (Pampanin *et al.*, 2011)

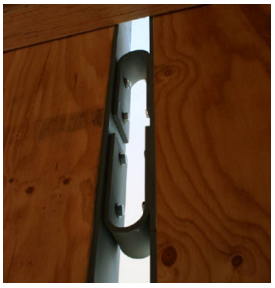

(b) (Iqbal *et al.*, 2007)

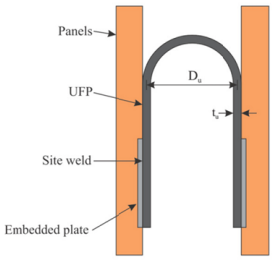

(c) (Baird *et al.*, 2014)

Figure 2.34: Details of UFP dissipaters

UFP based dissipation is more suited to wall based structural systems (Baird *et al.*, 2014) compared with frames. Because of this, these dissipation devices were not be tested as part of this research.

2.7.4 Additional Dissipation Types

Modifications to the dissipation systems described above were in development at the time of this research. One such system which showed promise was a modified Necked Rod Dissipater (NRD). This comprised a rod with slots milled into the side to create a trefoil profile. This system does not require grout or epoxy filling to provide buckling resistance (White, 2014). These were being developed by another project and testing results were not available at the time of testing for this research.

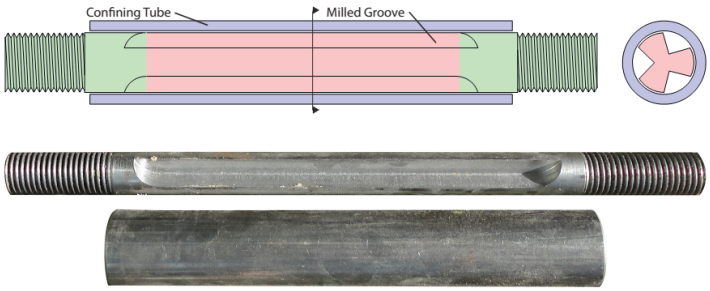

Figure 2.35: Clover leaf dissipater (White, 2014)

Additional, more complex dissipation systems including ring-springs, viscous dampers and shape-memory alloys were discussed for use in this project (Ringfeder, 2010, Kam *et al.*, 2008, Zhu & Zhang, 2007). These appeared to be able to meet the performance requirements of Pres-Lam frames. However cost and other factors meant that they weren't considered further in this research.

2.8 Dissipater Connection Methods

The connection of energy dissipation devices to timber in hybrid beam column joints has been identified as critical to achieving good performance (Newcombe, 2005). Several options for connecting to timber have been identified as being of use in this experimental campaign and are described below.

2.8.1 Timber Rivets

Timber rivets allow a strong, stiff connection to be made between a steel plate and timber. They are similar to nails. However, when driven through narrow holes in the steel plate they expand and produce a connection with minimal slip.

A comprehensive experimental and analytical campaign has been undertaken to investigate the performance of these devices in New Zealand LVL. This has resulted in a published design guide (Quenneville & Zarnani, 2013) and design software which enables rapid evaluation of riveted connections.

Figure 2.36: Timber Rivets (Quenneville & Zarnani, 2013)

2.8.2 Fully Threaded Screws

Long, fully threaded screws are available from a number of manufacturers (Würth GmbH & Co, 2011, SPAX Construction, 2012, Rotho Blaas s.r.l, 2012), with manufacturer produced design guides based on the Eurocode. The formulations in these guides contain modification factors based on timber density which enables their use with New Zealand produced LVL.

Where possible, these screws are used at an angle to the timber. Inclined screws have been shown to increase connection strength and stiffness. This is due to the screw being loaded in withdrawal rather than shear and the "rope effect" being engaged. Eurocode formulations explicitly consider this effect as opposed to the simpler formulae in New Zealand standards (Standards New Zealand, 1993, European Committee for Standardization, 2004).

Fully threaded screws have also been shown to be effective in reinforcing timber, particularly where it is loaded in tension or compression perpendicular to the grain. Guidance for the design of screws used in this configuration is given by some manufactures in their technical literature (Rotho Blaas s.r.l, 2012).

2.8.3 ZD Plates

ZD plates are a novel connection type allowing fully threaded screws to be loaded in tension and compression, increasing the capacity of a screw group. These consist of a pair of machined steel brackets which fit snugly together. Screws fit into sockets within the lower plate and the upper bracket locks these in place. This arrangement loads the screws in withdrawal and in compression. A diagram of these connections is shown in Figure 2.37.

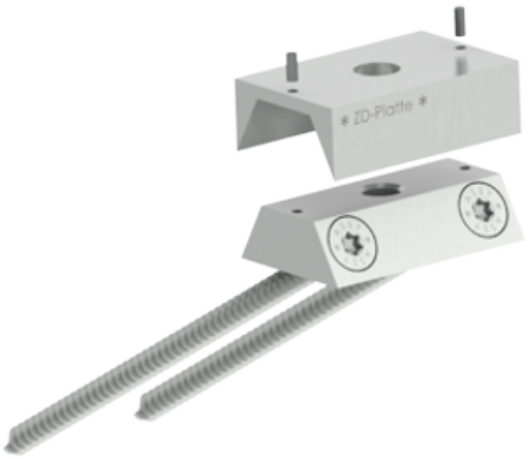

Figure 2.37: ZD Plate (http://www.swg-produktion.de/)

2.9 Summary

This literature review has outlined previous testing of Pres-Lam beam column joints as well as provided examples of the use of Pres-Lam in buildings. The need for greater investigation into the detailing of beam column joints has been noted, particularly around dissipation devices and armouring the joint zone. Options for dissipation devices and connection systems have been summarised.

Chapter 3

Experimental Testing

This research aims to provide design and detailing guidance for additional beam column joint options. This chapter describes the experimental campaign employed to test beam column joint details. It gives details of the specimens including design and fabrication, loading and reaction apparatus, and test protocol. Fabrication, assembly and testing was undertaken in the Structures Laboratory at the University of Canterbury.

3.1 Objectives

The primary objective of this series of tests is to gather data to assess the viability of several different reinforcement and energy dissipation options for the beam column connections. Joints were assessed on:

- Moment rotation response,
- Cyclic stability,
- Energy dissipation,
- Residual displacement,
- Constructability, and
- The ability current models to predict their behaviour.

3.2 Specimen Details

A single specimen which consisted of a full scale beam and column as described below was reused for each test. The first joint detail tested was reinforced using steel sections and used Necked Rod Dissipaters. The components for this were fabricated under commercial conditions by an external company. This was done to ensure that the specimen was as similar as possible to what will be used in structures. In subsequent tests, the specimen was modified in place to create each set-up. While the conditions were not entirely those of a commercial job, it was possible to assess construction issues found in each design.

Both the beam and column consisted of 800 mm $\times$ 315 mm rectangular LVL sections. The column was a solid section while the beam had a 100 mm $\times$ 100 mm duct in the centre for

post-tensioning strands. The beam length was 5,000 mm and the column length was 4,760 mm. Details of each of these sections are given in Figure 3.1

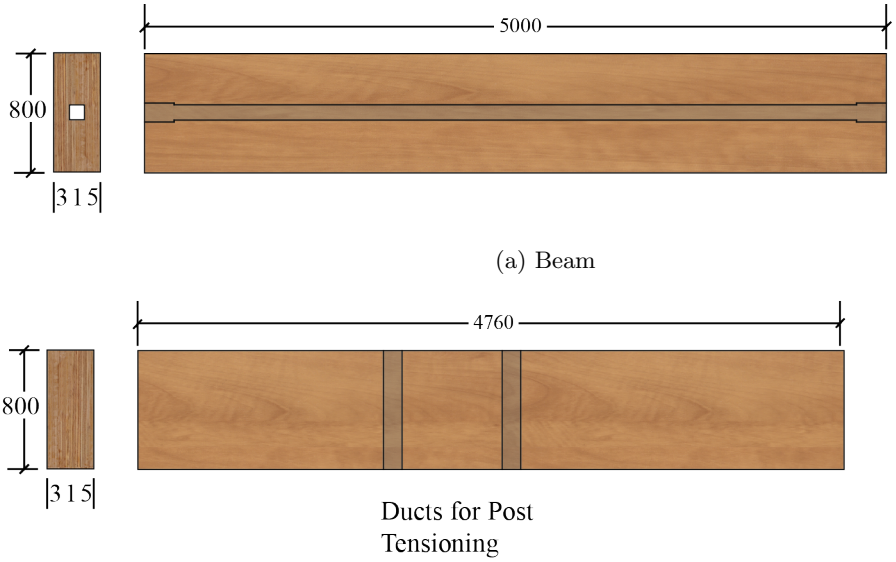

(a) Beam

(b) Column

Figure 3.1: Specimen sections used in test

Testing investigated both joint reinforcement and energy dissipation options. Steel and screw based reinforcement schemes were considered. Options for energy dissipation devices consisted of:

- Plug and Play dissipaters
- Necked Plate Dissipaters (NPDs) (similar to flattened Plug and Play dissipaters)
- A new dissipater design using LVL blocks and steel rods, these were named Timber Plus dissipaters

Each of these options is described more fully later in this chapter. Reinforcement and dissipation options were combined to form testable beam column joints. Plug and Play dissipaters were tested on the steel reinforced joint, the Timber Plus dissipater was tested on the screw reinforced joint, while Necked Plate Dissipaters were tested on both. The joints used in each test are summarised in Table 3.1. Details of each joint are shown in Figure 3.2.

Table 3.1: Testing schedule

Specimen Code	Joint Reinforcement	Dissipation	Dissipater Connection
A-B1	Steel	None	
A-B2	Steel	None	
A-P1	Steel	Plug and Play	Threaded Coupler
A-P2	Steel	Plug and Play	Threaded Coupler
A-D1	Steel	NPD[1]	Timber Rivets
A-D2	Steel	NPD	Timber Rivets
B-B1	Screws	None	
B-B2	Screws	None	
B-D1	Screws	NPD	ZD Plates
B-D2	Screws	NPD	ZD Plates
B-TP	Screws	Timber Plus	Diagonal Screws

[1] Necked Plate Dissipater

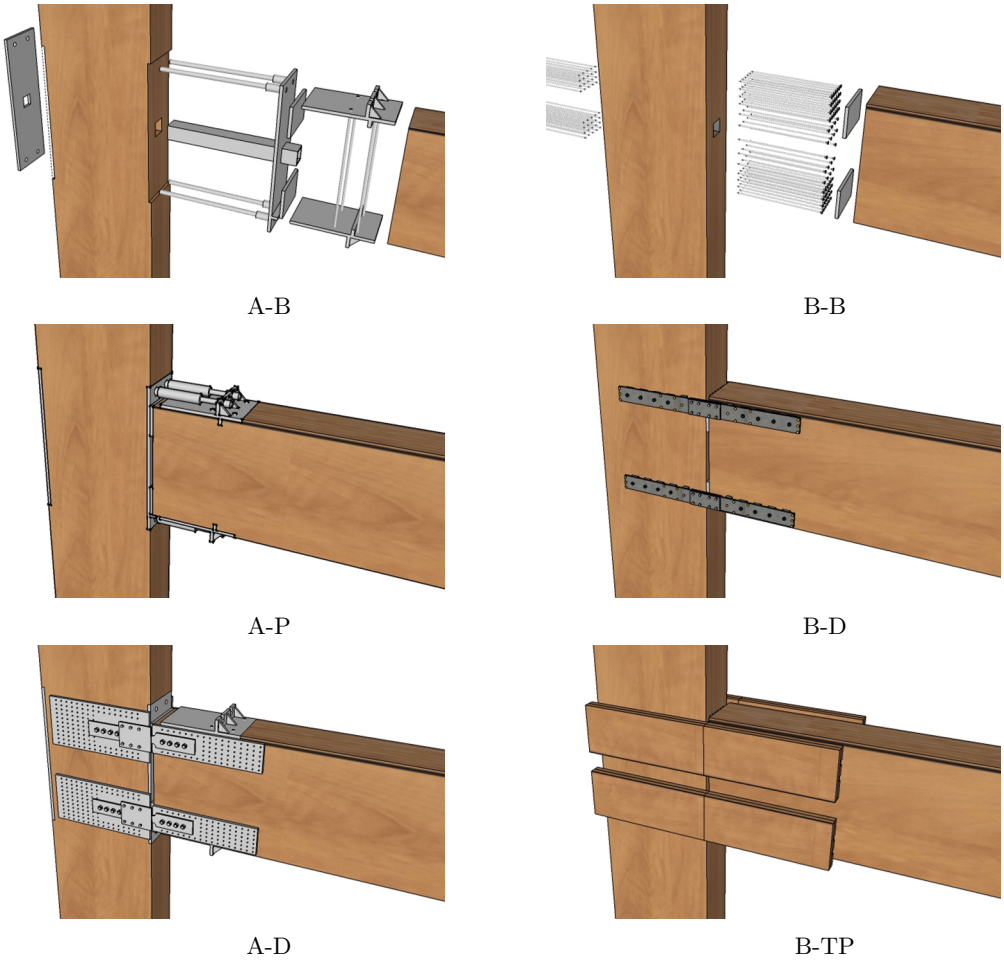

Figure 3.2: Details of joints tested

3.2.1 Assembly

Preparing the joints for testing required:

1. Placement of the beam and column
2. Post-tensioning the joint
3. Connecting dissipation devices

Propping was used to assemble the joints in the lab. In practice, full frames can be assembled flat on the ground before being lifted into place. A comparison of the two techniques is shown in Figure 3.3.

(a) Assembly of joint in lab (showing propping)

(b) Lifting frame into position (on construction site)

Figure 3.3: Frame connection and assembly methods for laboratory and construction site

Each joint was post-tensioned using a hydraulic jack. This elongated a single stand at a time. Two stages of stressing were used to balance the force in each of the five strands. Contractors have jacks sufficient to stress all strands simultaneously, which is preferable as it ensures similar forces in each strand. The jack, jacking frame, and load cell used in the laboratory are shown in Figure 3.4a. A close up of the strand anchorage block as used on site is shown in Figure 3.4b.

(a) Single strand jack used in lab

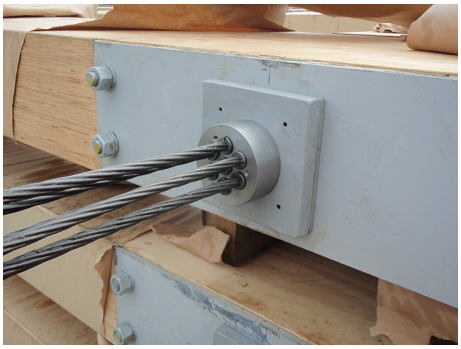

(b) On-site post-tensioning anchorage details

Figure 3.4: Post-tensioning details

The connection methodology for dissipation devices varied according to the type of device used. Details for each option are provided in Section 3.6.

3.3 Design Criteria

The first joint tested was designed for use in a building under construction at the time of this research (see Section 2.6.5). This building was a three storey office building with an average 3 6m interstorey height. The performance of this joint was assessed based on numerical models and tested to ensure the validity of the model. Subsequent joints were designed to match the

performance of this benchmark. Using joints designed to achieve the same response enabled a comparison of the effectiveness of each detail. Testing of these joints identified behaviour and aspects not considered in the structure's design.

3.4 Apparatus and Test Set-up

3.4.1 Reaction Frame and Loading Apparatus

The specimen was loaded at the mid storey height through a hydraulic ram and loading beam. Pin connections were used to ensure no extra moment was induced. The column was restrained at the base using a rocking foundation plate. The beam was supported at the free end with a dual pinned mechanism, allowing horizontal translation and rotation but effectively restricting vertical displacement. A schematic view of the test set-up is shown in Figure 3.5. The long loading beam extension was necessary due to space restrictions on the laboratory's strong floor.

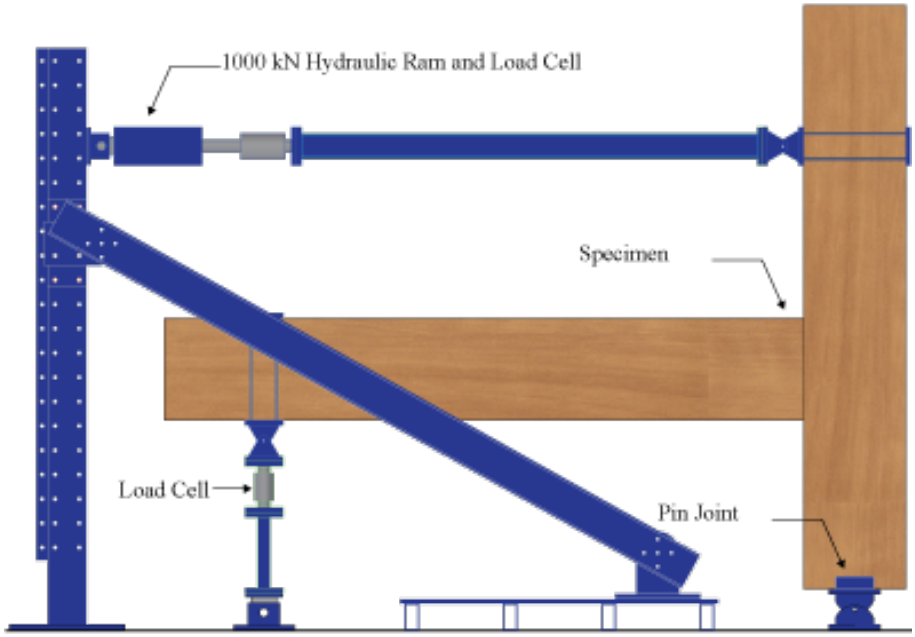

Figure 3.5: Laboratory setup

3.4.2 Loading Protocol

A quasi-static loading protocol was used for these tests. The loading protocol followed that of a modified American Concrete Institute (ACI) frame acceptance criteria. This was been adopted for Pres-Lam frames as in much of the literature consulted (Newcombe *et al.*, 2010d, Iqbal *et al.*, 2008, Iqbal *et al.*, 2010, Palermo *et al.*, 2005). The scope of this methodology is limited to reinforced concrete moment frames. However it was deemed applicable for use with Pres-Lam systems owing to the similarity of behaviour between concrete PRESSS systems and timber Pres-Lam. The

loading history applied to the column is shown in Figure 3.6. The protocol calls for three fully reversing cycles to each drift level with limits on the minimum and maximum increases between cycles.

Digital cameras were used to capture images of these tests. The displacement was held for around two seconds to allow the cameras to take and save photographs of the joint and overall specimen at each step of the loading history. This meant that a complete displacement history took around four hours to run.

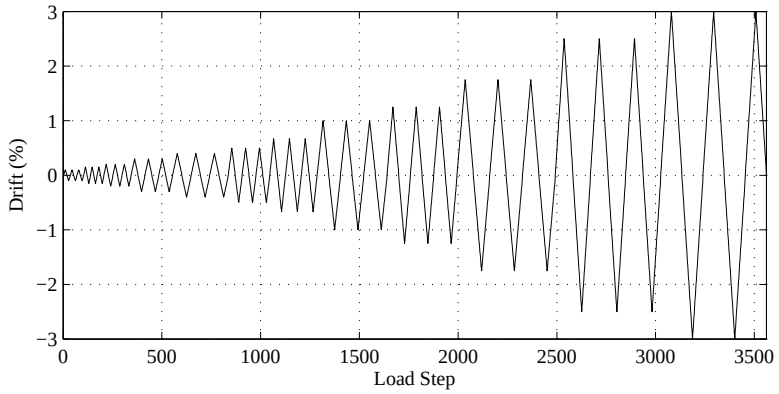

Figure 3.6: Modified ACI loading protocol used as input to hydraulic ram

3.4.3 Instrumentation

Each joint detail was instrumented with linear and rotary potentiometers to measure displacements and load cells to measure forces. Local deformations within the joint area were measured with a grid of linear potentiometers. These were also connected over the gap to measure opening. Using overlaid instruments it was possible to reduce the effect of timber deformation and obtain more reliable gap opening measurements. Diagonal pairs of potentiometers were employed to record shear deformations in the specimen. For each dissipation option tested, potentiometers were used to measure the extension of the dissipater devices as well as the connection stiffness. The layout of instrumentation over the joint zone is shown in Figure 3.7. A complete description of the instrumentation is given in Appendix A.

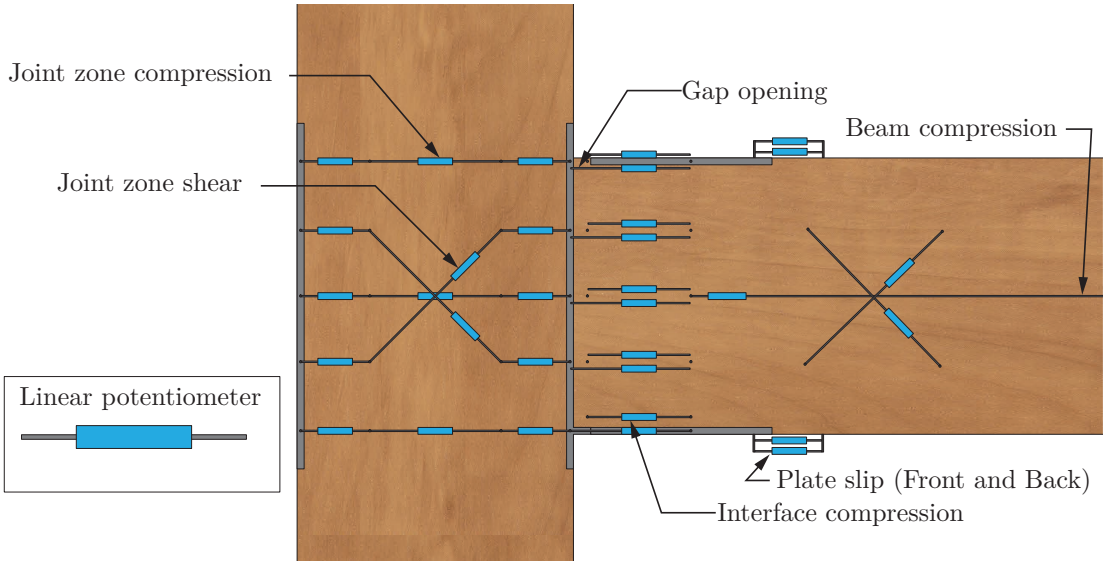

Figure 3.7: Joint zone instrumentation layout

3.5 Joint Reinforcement Options

The low perpendicular to grain strength of the LVL column required that reinforcement be provided to resist the high compressive stresses in the joint zone. Two reinforcement options were tested:

- Steel reinforcement using rods, plates and a square hollow section
- Screw reinforcement using long fully threaded screws acting similarly to piles, diffusing load and increasing stiffness.

3.5.1 Steel Based Joint Reinforcement

The first joint tested was reinforced using steel plates, rods and an SHS. This detail is shown in Figure 3.8. This specimen arrived fully fabricated with only connection of the beam to column and installation of instrumentation required prior to testing.

After preliminary testing, steel shims were added to force heel and toe rocking to occur, increasing the effectiveness of the post-tensioning.

This joint detail was taken from the design of a building under construction in Christchurch as part of the rebuild effort after the February 2011 earthquake. Interestingly, the design of these beam column joints had a Re-centring Ratio (λ) of less than 1.0 meaning that some residual displacement was expected. Instead, while local re-centring was not targeted, when combined with gravity loads and column to foundation connections, re-centring of the entire structure was specified. This building is described in Section 2.6.5.

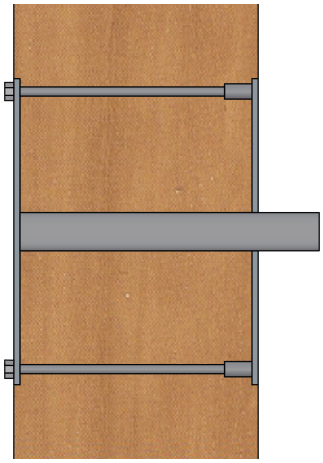

(a) Section showing steelwork

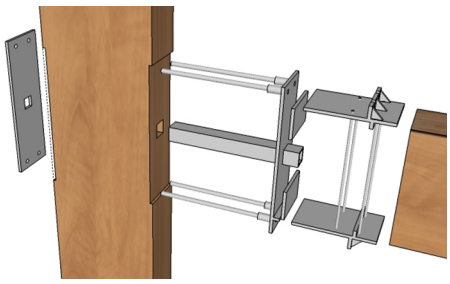

(b) Overview

Figure 3.8: Schematic of steel joint reinforcement

3.5.2 Screw Based Joint Reinforcement

An alternate joint detail was devised to use less steelwork to reinforce the LVL against perpendicular to grain compression at the interface. This used high strength fully threaded screws as reinforcement which act similarly to piled foundations to spread the load over a larger area. A steel plate was used to distribute compression over the screw group. Additional screws were provided to counteract medium and long term creep in the the joint zone, especially around the post-tensioning anchorage.

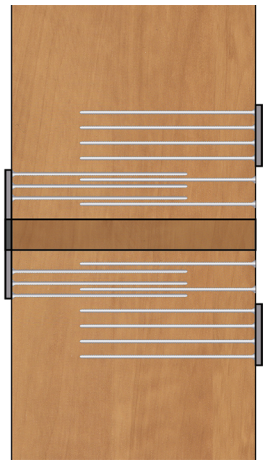

(a) Section showing screws

(b) Overview

Figure 3.9: Schematic of screw based joint reinforcement

Design

For the screw reinforced joint, the design parameters were changed slightly from the steel solution. Fully re-centring behaviour was targeted for the arrangements using this joint. This was achieved by increasing the post-tensioning proportion of the moment capacity at design level drifts.

Compressive load demand was evaluated using a Modified Monolithic Beam Analogy (MMBA) procedure (Palermo *et al.*, 2004). This gave both the maximum load and the neutral axis depth, allowing the design stress level to be determined. The design of screw reinforcement for compressive stresses imposed on the joint zone is covered in Chapter 6.

The screw groups were designed according to the procedure in the Würth design guide (Würth GmbH & Co, 2011). This dictated the number of screws, spacing requirements as well as minimum required lengths. The guide was written for Kerto[1] which has a density of 480 kg/m^3 (Metsä Wood, 2012) as opposed to the 570 kg/m^3 density typical of New Zealand LVL (Nelson Pine Industries Limited, 2012). The difference in density means that the values given for screw buckling resistance are likely to be conservative. It was decided to use screws longer than half the column depth and overlap them somewhat to provide a more direct load path for the compressive stresses imposed by the post-tensioning. This is also expected to reduce long term creep in the joint region, although this has not been experimentally verified.

The design solution chosen is shown in Figure 3.9. It is comprised of 580 mm long, 10 mm diameter Würth brand screws arranged into groups to resist bearing stresses from rocking and post-tensioning.

Fabrication

Screws were installed into pre drilled holes to allow for more accurate placement and to lower spacing limitations. A magnetic base drill and steel plate were used to ensure that these holes were made as square as possible. Several methods for inserting the screws were tried. These included; an electric hand drill with a high torque gear box, an air powered driver and an air powered impact wrench. The impact wrench was found to be the most effective, with good installation speed and reduced screw damage and operator fatigue. Even using these techniques, there were still some instances where screws from opposite sides of the joint clashed. Where this was the case, they were driven in as far as possible and ground flush. A layer of epoxy was spread over the screw heads to ensure a flush bearing surface on the screws even where heads had snapped off. Bearing plates to induce heel and toe rocking were screwed onto the column face.

[1] European trade name for LVL

(a) Screws awaiting installation

(b) Installing Screws with impact wrench

Figure 3.10: Assembly of screw reinforced joint

3.6 Dissipation Options

By including discrete energy dissipation elements in the joint, a fuse was provided to protect the structure from seismic damage. Several dissipation options were investigated. These were:

- Plug and Play Dissipaters
- Necked Plate Dissipaters
- Timber Plus Dissipaters

These devices are described in more detail in the following sections. A common feature of each of these dissipation options is that mild steel is forced to yield over a well controlled, specified length and sectional area. These two properties are chosen by the designer and allow force-displacement behaviour to be well defined at the design stage. The low variability of the mechanical properties of mild steel make it well suited for use in this application where the dissipater strength must be controlled within precise limits.

The reduced area in the critical region means that compressive loadings are likely to induce buckling. Because of this, each of the dissipation options designed features anti-buckling measures. The efficacy of these restraints was tested.

Post earthquake remediation options were considered for these dissipation options in order to significantly reduce repair cost and complexity. To assess this, each test was run twice, replacing the dissipative elements between each loading.

3.6.1 Plug and Play Dissipation

Plug and Play dissipaters consist of threaded rods with a necked down region in the centre. These are surrounded by a steel sleeve which is filled with grout or epoxy to restrain buckling.

Some of the dissipaters were provided as complete units, others were assembled in the laboratory. Dissipaters were fabricated using both cementitious grout and epoxy as buckling restraining elements. No difference in the performance of the dissipaters was observed between these materials.

These dissipaters were connected to the joint using threaded couplers. Couplers were connected to epoxied rods that ran fully through the joint and were anchored on the outside faces. The rod and coupler arrangement is shown in Figure 3.8.

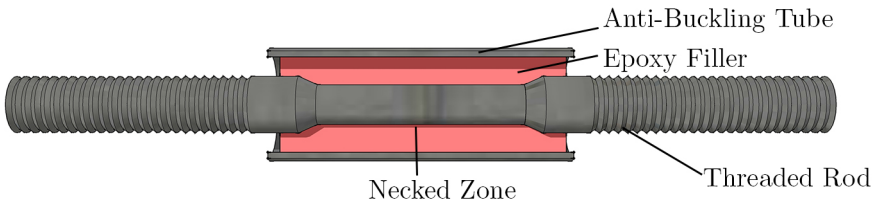

Figure 3.11: Plug and Play dissipater details

Fabrication

Several Plug and Play dissipaters were assembled in the laboratory. Necked threaded bars were provided by an external contractor. These were inserted into steel 60.3 × 4.5 CHS[2] tubes and fixed in place with timber end plugs. Sika grout or Ramset epoxy was injected into the tube and wedges held the bar in place while it cured. Figure 3.12 shows images of the assembly of these dissipaters.

(a) Dissipative element

(b) Epoxy Curing in anti-buckling tubes

Figure 3.12: Fabrcation of Plug and Play dissipaters using epoxy

3.6.2 Necked Plate Dissipaters (NPDs)

Necked Plate Dissipaters are flat steel bars which have been milled to provide a central yielding zone. A sample is shown in Figure 3.13. NPDs were connected to the joint using both a timber riveted plate as well as proprietary tension, compression screw anchors. The Necked Plate Dissipaters were designed using an iterative method which selected the length and sectional area of the necked region. A spreadsheet tool was used to rapidly evaluate the dissipater and joint

[2]Circular Hollow Section with diameter of 60.3 mm and wall thickness 4.5 mm

design parameters to achieve required moment and rotation goals. Previous research into mild steel dissipaters (Smith *et al.*, 2013) has shown that sharp transitions down to the necked area reduce cyclic performance. As a result, a smooth radius was used for these dissipaters.

Figure 3.13: Necked Plate Dissipater details without cover plates

The thin plates in these dissipaters experience considerable compression loadings. Buckling is a therefore a significant issue which must be addressed by the designer. The NPDs tested used additional cover plates to restrain against buckling. For the rivet plate connection, cover plates were bolted into threaded holes in the rivet plate. The screw anchor design used several configurations of plates which clamped over the necked region. These are summarised in Table 3.2.

Table 3.2: Buckling restraint options used for NPDs

Option	Test(s)	Image
Bolted to Rivet Plate	A-D1 A-D2	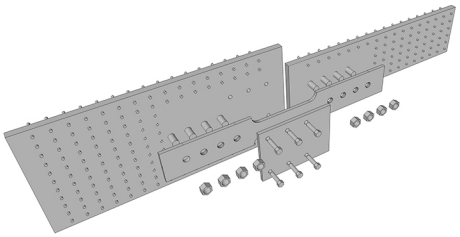
Short Screw	B-D1	
Long Screw	B-D2	
Slotted Stiffened Plate	B-D2	

Fabrication

Necked Plate Dissipaters were fabricated from flat sections of mild steel. These were cut to length and necked to the required dimensions using a milling machine. As the dimensional accuracy of the bolt holes was of critical importance, these were also drilled while on the mill. A Digital Read Out was used to aid fabrication of the test samples. In full scale production, efficiencies would be gained by using automated CNC machines.

These dissipaters were connected using groups of bolts on both the beam and column. The level

of energy dissipated is based on the extension of the dissipater. Because of this, any movement in the connection would have limited the dissipater's effectiveness. To prevent this, bolt holes were the exact diameter of the bolts rather than oversized, as is common practice in the construction industry. These tight tolerances imposed challenges on the design and fabrication of connections between the dissipaters and the timber.

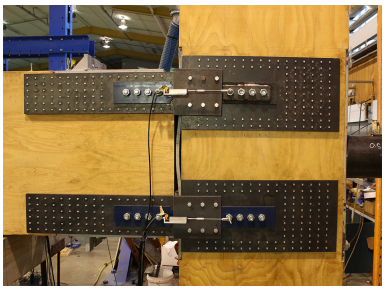

(a) Timber Rivets

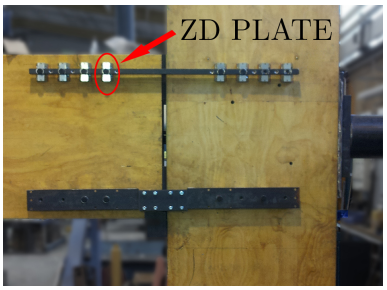

(b) ZD Plates
Top: Without Dissipater
Bottom: Dissipater Installed

Figure 3.14: Connection options for NPDs

The timber rivet plates used to attach the NPDs to the beam and column were straight forward to connect to the timber. Rivet plates were designed in accordance with the guide produced as a result of research at the University of Auckland as part of the Structural Timber Innovation Company (STIC) programme (Quenneville & Zarnani, 2013). While there were a large number of rivets to put in, for a building scale operation, tools similar to nail guns are available commercially. Plates for both the beam and column were attached at the same time. The dissipater was in place during this process to ensure that the plates were placed the correct distance apart.

Proprietary SWG ZD Connectors (SWG Schraubenwekr Gaisbach GmbH, 2011) were used for the screw anchored NPDs. These allowed the inclined screws to be loaded in both tension and compression, reducing the total number of screws required compared to simpler designs where only tension could be relied on. The European Technical Approval (ETA) (SWG Schraubenwekr Gaisbach GmbH, 2011) for the ZD connectors contained the equations used for the design of these connections.

The screw reinforced joint detail using NPDs was the most challenging to fabricate due to the large number of screws and their varying angles of installation. The complexity of this joint is shown in Figure 3.15. Installation would have been significantly easier if ZD Plates had been used with a less congested joint reinforcement system

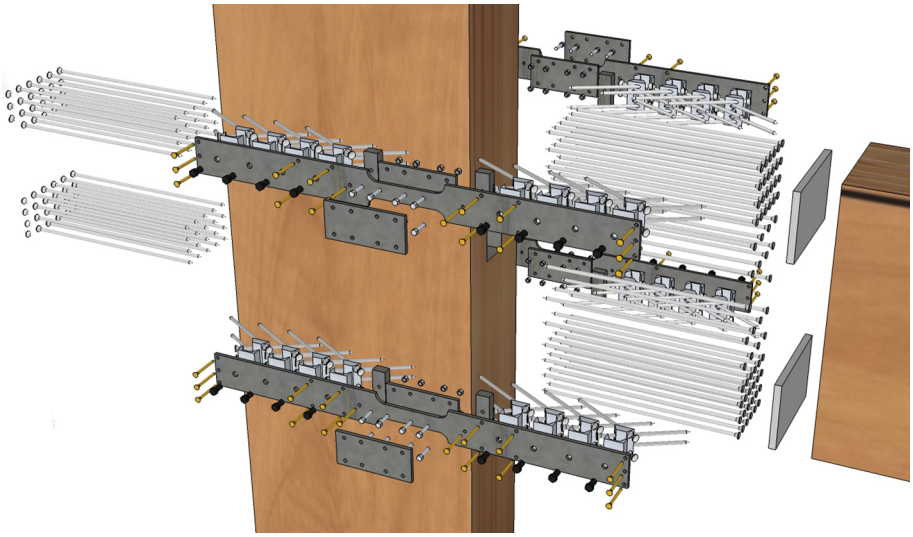

Figure 3.15: Exploded view of Necked Plate Dissipaters installed using inclined screws

Residual stresses in the NPDs after testing due to plastic elongation complicated replacement of the dissipaters. For the test with NPDs on the riveted plate it was necessary to cut the dissipaters in half and remove each section individually as shown in Figure 3.16a. In other cases, the dissipaters were able to be removed by hand, using a pry bar.

The NPDs bolted to the rivet plate required that the bolt groups on the beam and column be aligned exactly. As this was not the case after testing, enlarged holes on the dissipater were used with a snug fit washer welded to the NPD. This arrangement is shown in Figure 3.16b. The heat from welding caused the plate to bend, requiring them to be flattened prior to installation. This made replacement NPDs significanly more time and labour intensive than for screw in dissipaters.

(a) Removing NPD from joint with grinder after testing

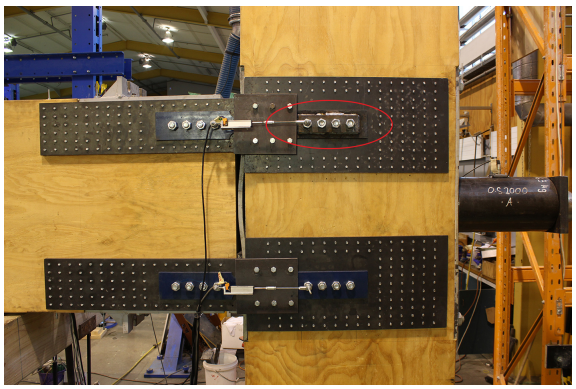

(b) Washer plate welded to replacement NPD on riveted plate

Figure 3.16: Replacement of NPDs

3.6.3 Timber Plus Dissipaters

Timber Plus dissipaters comprise threaded rods with a necked region epoxied into an LVL block. The LVL provides buckling resistance to the bar when it is loaded in compression. These blocks are fixed to the outside of the joint using inclined fully threaded screws. A pre-cut gap is positioned over the rocking interface between the beam and column to allow gap opening. A mild steel plain round bar was threaded rather than using standard threaded rod. The steel grade used was chosen to produced the ductile behaviour required of the dissipater. The steel rod in the necked down region spanning this gap is smooth and wrapped in tape to de-bond it from the epoxy. A schematic view of this dissipation option is shown in Figure 3.17.

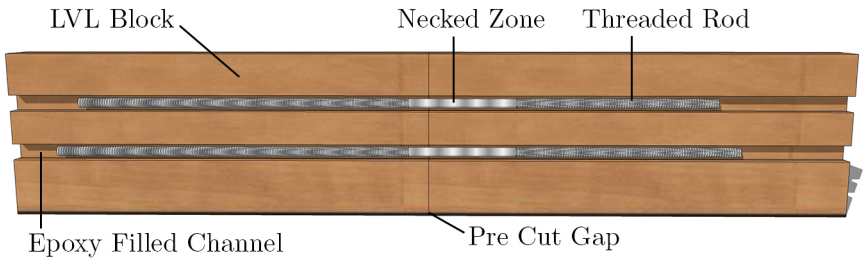

Figure 3.17: Timber Plus Dissipater details

Fabrication

The Timber Plus dissipaters were fabricated in the structures lab. Cross laminated LVL blocks were first screw glued into blocks 72 mm thick. The procedure from the Screw-Lamination design guide (EXPAN, 2012) was used for this. A router was used to create slots for the steel rods. After this, the two faces of the dissipater blocks were screw glued together. Once set, the rods were inserted and epoxied into place. Photographs taken during the fabrication of these dissipaters are shown in Figure 3.19.

The assembled dissipater blocks were attached to the joint using inclined SPAX screws. This connection detail was combined with screw reinforcing for the LVL in the column. Because of this, the joint was very congested, with screws installed in six directions. Figure 3.18 shows an exploded view of the joint. Construction required accurate placement of all screws to minimise clashes. Several such clashes were experienced during installation. However this was resolved by reinstalling the screws at a slight offset.

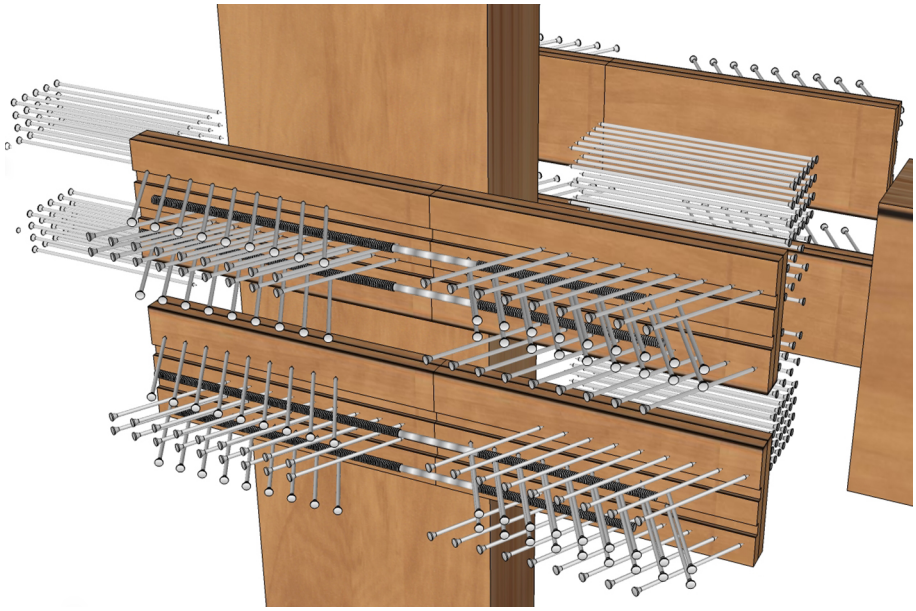

Figure 3.18: Exploded view of Timber Plus Dissipater installed using inclined screws

(a) Spreading adhesive

(b) Laying up boards

(c) Installing clamping screws

(d) Routed slots being glued

(e) Clamping applied to finished block

(f) Filling slots with epoxy

Figure 3.19: Fabrication of Timber Plus dissipaters

3.7 Test Summary

Reinforcement and dissipation options were combined to form testable beam column joints. The joints used in each test are summarised in Table 3.1. Plug and Play dissipaters were tested on the steel reinforced joint, the Timber Plus dissipater was tested on the screw reinforced joint while Necked Plate Dissipaters were tested on both. Geometric details of the dissipative steel in each test is given in Table 3.3.

The moment rotation behaviour of each joint is developed from dissipative steelwork and re-centring post-tensioning. The performance of dissipation devices is determined by both its area and distance from the neutral axis. These geometric details of the dissipative steel in each test are given in Table 3.3. The results of each of the tests are described in the next chapter.

Table 3.3: Specimen details

Specimen	Necked Area[a]	Dissipative Element Depth(s) [b]
A-B1	-	-
A-B2	-	-
A-P1	$241\,mm^2$	$-46\,mm$
A-P2 [c]	$314\,mm^2$ / $241\,mm^2$	$-46\,mm$
A-D1	$500\,mm^2$	$95\,mm$
A-D2	$500\,mm^2$	$95\,mm$
B-B1	-	-
B-B2	-	-
B-D1	$450\,mm^2$	$100\,mm$
B-D2	$450\,mm^2$	$100\,mm$
B-TP[d]	$2 \times 299\,mm^2$	$100\,mm$
		$200\,mm$

[a] Area for a single dissipater, Twice this value at both top and bottom.
[b] Depths are taken from top/bottom of the beam. Positive values are inside beam depth, negative values outside beam depth.
[c] Specimen used differing dissipaters on top and bottom of joint.
[d] Timber Plus dissipater has two layers of mild steel, see Figure 3.17.

3.8 Conclusions

A single beam column joint specimen was reused to test the effect of joint reinforcement and energy dissipation options. All options were designed to match the moment capacity of the initial reference joint. The target re-centring ratio varied between joints which meant differing contributions from post-tensioning and dissipation.

Steel and screw based joint reinforcement options were considered. The steel option was fabricated by an external contractor while the screw option was constructed on-site. The steel option appeared to be more straightforward to construct due to containing fewer components. The screws used to reinforce the joint zone required careful placement and installation to ensure they did not snap or interfere with one another.

The replaceability of each dissipation option was assessed. The Necked Rod Dissipaters were the simplest to replace. These were connected using a threaded coupler on one end and a slotted hole on the other. Because of this, there were minimal issues with tolerances when fitting replacement dissipaters.

The screw-in devices used to attach NPDs to the timber featured pins designed to lock upper and lower plates together. These were not installed for testing. This allowed a degree of adjustment when fitting replacement dissipaters by tightening screws on either side to move the attachment block. It was a time consuming process, requiring multiple passes to ensure a good fit. The adjustments required were still quicker than the welded plate option used for the rivet pates.

A large number of screws, inclined in both directions, were used in the Timber Encased Dissipaters. The high likelihood of these having bent during testing increased the risk of screws snapping during removal. This would have made installation of a replacement dissipater problematic. Because of this, these dissipaters were not considered to be replaceable. Supplementary dissipaters could be installed around these, if required, after an earthquake.

After testing, buckling and plastic elongations of the dissipaters meant in many cases that it was easiest to cut them with an angle grinder before removal. This process required care as the residual stresses in the dissipater could cause it to grip the cutter.

The results of this testing are analysed in the following chapters to assess joints based on moment-rotation response, energy dissipation, and residual displacement in accordance with the testing objectives set out at the beginning of this chapter.

Chapter 4

Results of Experimental Testing

This chapter describes the results of each experiment performed as part of this research programme. Key behaviour for each joint including moment rotation, post-tensioning and neutral axis depth is shown in the plots presented below. Observations of damage sustained in each test are also described. In addition, comparisons between tests for a range of key results are given. Aspects of data processing techniques used are also commented on.

4.1 Observations and Results

The following sections detail each test conducted as part of this campaign. Moment-rotation, post-tensioning activation and neutral axis depth plots are shown. In addition, tables of data including, stiffness, damping and residual displacement are provided. Any damage to the specimen which was observed during testing is also described below.

4.1.1 Tests A-B: Steel Reinforced Joint, No Additional Dissipation

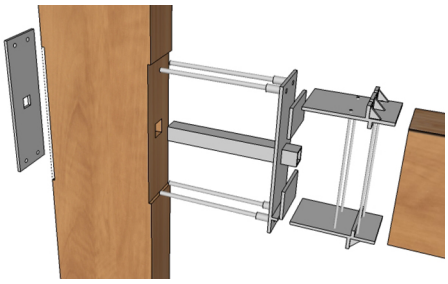

Figure 4.1: Steel reinforced joint with no dissipation

This specimen was the first tested. Several small tests were undertaken prior to subjecting the specimen to the full displacement history to ensure correct function of the test apparatus. On the first test cycle to 10 mm ($\approx 0.3\%$ drift), the epoxy behind the bearing plate on the column

face cracked. This crack extended from the bottom of the joint zone, upwards approximately 300 mm and was 0.35 mm wide at the base. The epoxy was present to aid constructibility and its cracking was not thought to materially affect the joint's response. Bolts were installed in the dissipater couplers in subsequent tests to hold the steel plate firmly against the joint, similar to if dissipaters were present. A photo of this arrangement is provided in Figure 4.2.

In initial testing to low drifts, gap opening was not observed. At the time this was thought to be due to interface stiffness being insufficient to generate observable rocking behaviour. Shims were introduced into the joint to increase stiffness and force a heel and toe rocking mode. This was accomplished by positioning steel plates (200 mm tall, 20 mm thick) between the armoured column face and the beam. When stressing this joint, the armouring plate bent away from the column face. This was due to the post-tensioning force's application directly to the Square Hollow Section (SHS) and the elimination of the restraint provided by the beam at the centre of the joint face. This is shown in Figure 4.3 and Figure 4.4. It was thought that this was a primarily aesthetic defect and would not significantly affect the response of the joint so testing was continued.

Figure 4.2: Bolt restraints for steel reinforced tests without dissipation

Figure 4.3: Bent armouring plate, after stressing, shims installed

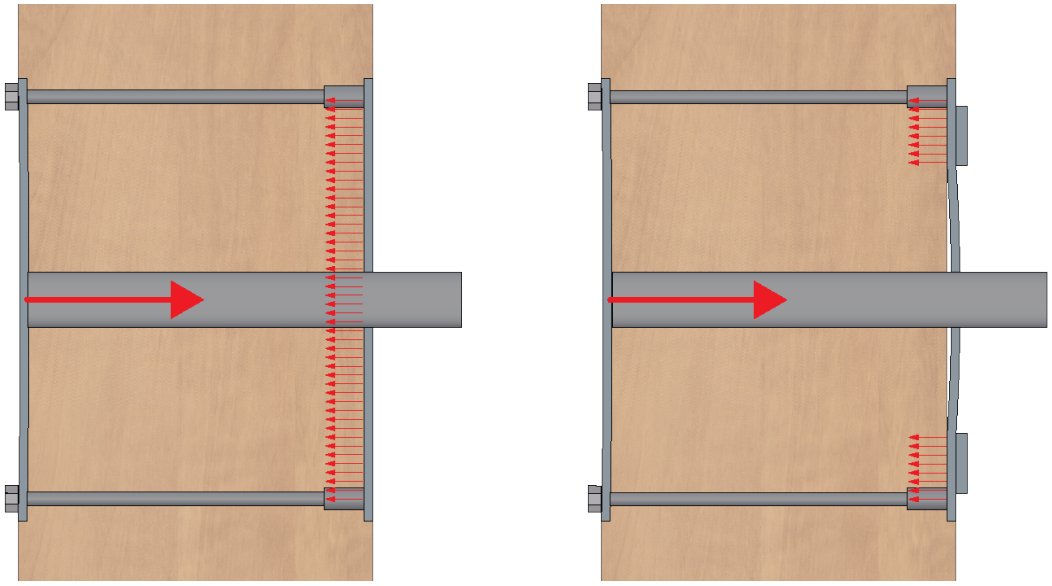

(a) Plate without shims
(forces transfer over whole plate)

(b) Plate with shims
(forces only transfer over edges)

Figure 4.4: Force diagram for bent plates

The moment rotation response of the steel reinforced joint without dissipation is shown in Figure 4.5. Energy dissipation was minimal, this joint produced narrow loops with little area contained. The stiffness discontinuity at gap opening is clearly evident in the moment - rotation plot shown. The response is stable from cycle to cycle, matching the backbone curve well. The moment capacity of the joint is symmetrical, without obvious discrepancies in stiffness when comparing extension and retraction of the ram. This test was run to a larger drift level than for the other specimens. It was pushed to 3.5%, compared with 3.0% for the other tests.

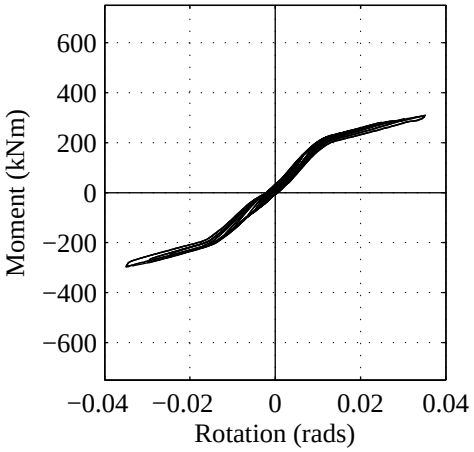

Figure 4.5: Moment rotation response for steel reinforced joint with no dissipation (A-B)

A plot of post-tensioning force against drift is shown in Figure 4.6. The behaviour is very well defined with a well defined, cyclically stable curve produced. There is a slight asymmetry in the post-tensioning force developed. At maximum drift the retraction of the ram produced 15% larger forces as compared to ram extension.

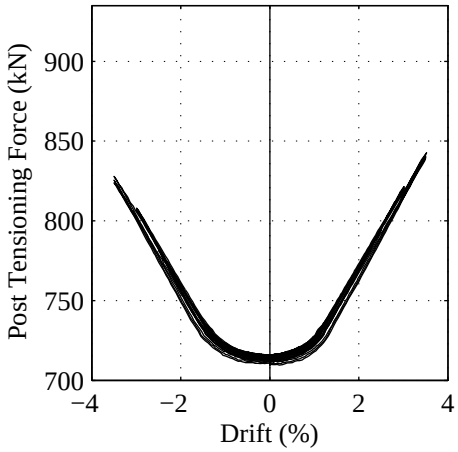

Figure 4.6: Post-tensioning force vs drift for steel reinforced joint with no dissipation (A-B)

The calculated neutral axis depth in the end of the beam is shown in Figure 4.7. There is large amount of scatter in the data but a general trend is evident. The influence of the steel shim plates can be seen at large drifts where the neutral axis depth is concentrated at around 200 mm from the centre of the joint. The neutral axis depth was calculated according to Section 4.3.4.

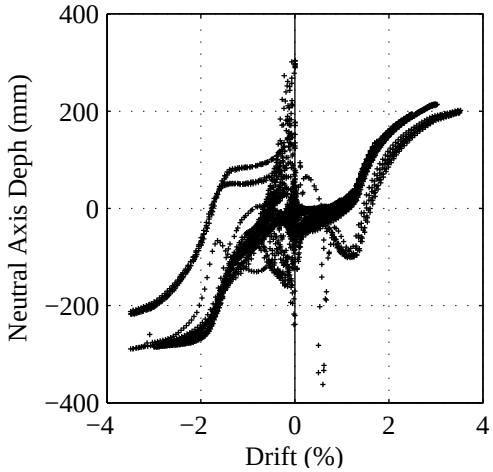

Figure 4.7: Neutral axis depth for steel reinforced joint with no dissipation (A-B)

Data from the test is summarised in Table 4.1. This table shows average moment at 1.25%, 2.5%

and 3.0% drift levels, stiffnesses as well as other quantities. These values are used to compare the results from each test later in this chapter.

Table 4.1: Data from A-B series tests

	A-B
1.25% Moment (kNm)	201
2.5% Moment (kNm)	267
3.0% Moment (kNm)	286
Yield Stiffness (MNm/rad)	21.5
Residual Displacement (mm)	-2.1
Yield Drift	1.03%
Joint Shear Stiffness[1](MPa)	651
3% Hysteretic Damping[2]	2.6%

[1] See Section 4.3.3.
[2] See Section 4.2.6.

4.1.2 Tests A-P: Steel Reinforced Joint with Plug and Play Dissipation

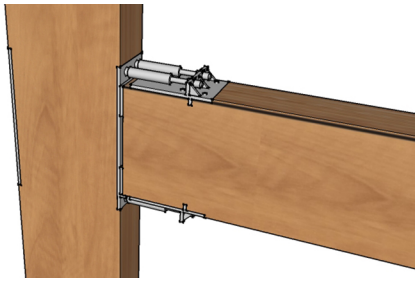

Figure 4.8: Steel reinforced joint with Plug and Play dissipation

Testing for this option was conducted on the steel joint modified to include the steel plates, forcing heel and toe rocking. During the first test, at a drift of 0.5%, cracks were noticed at the end of the steel plate on the beam. Testing continued to a drift of 2.7% where a sudden separation of the epoxy under the plate was observed. As this was early in the testing programme, it was decided to discontinue testing at this time. This was done to prevent further damage to the specimen which may have caused difficulties in further testing. After a visual inspection following the test, it was decided that this damage was likely to be primarily aesthetic and did not affect the load path of the dissipaters. The second test using this joint configuration was run as specified.

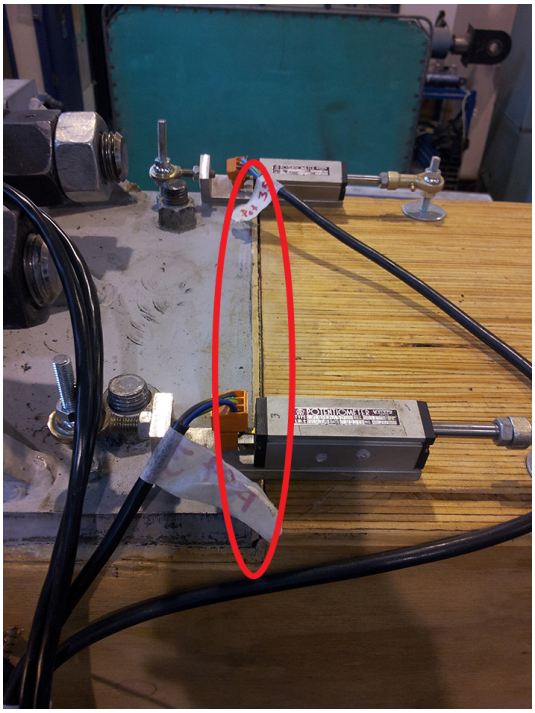

(a) Crack in back end of beam plate

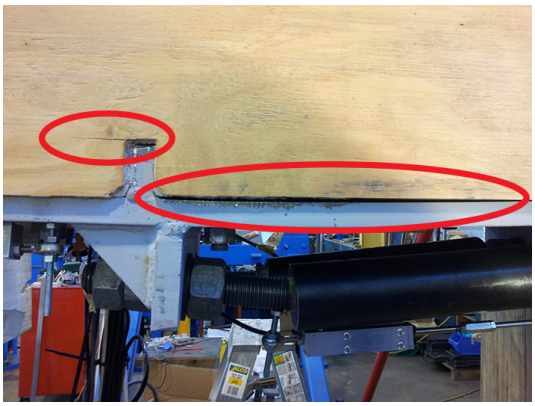

(b) Split in LVL at tip of shear key and approximately 200 mm long separation of epoxy under beam plate

Figure 4.9: Damage observed in steel reinforced joint with no additional dissipation.

The moment-rotation response of the steel reinforced joint with Plug and Play dissipaters is shown in Figure 4.10. The loops produced by this joint are far fatter than for the joint with no dissipation devices. The area contained within the loops is representative of the energy dissipated by the system. A more gradual change in stiffness is observed instead of the abrupt discontinuity seen in Figure 4.5. This is particularly evident in the second and subsequent cycles to each drift level. Connection softening is thought to be responsible for this.

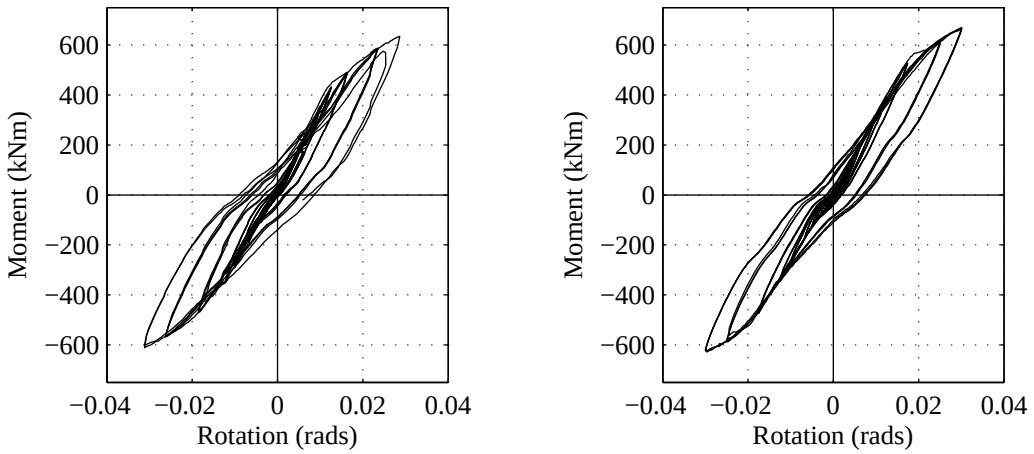

(a) A-P1

(b) A-P2

Figure 4.10: Moment rotation response for steel reinforced joint with Plug and Play dissipation

The post-tensioning activation plot in Figure 4.11 shows the relationship between post-tensioning force and applied displacement. There are larger losses in post-tensioning forces in this test as opposed to the same joint without dissipative elements. This is seen by the decrease in force at 0% drift after cycles to large displacements. The reduction is due to relaxation of the tendons following permanent deformations of the LVL. A permanent compression across the centre of the joint zone in the column of 3.6 mm was recorded by potentiometers placed across this region. This represents a drop in length of 0.45%. This is similar to the reduction in post-tensioning force from around 720 kN to 715 kN seen in the tests. Bearing from the post-tensioning anchorage plate and shim plates at the beam column interface mean that stresses and deformations should be concentrated near the anchorage location. The data confirms this with deformation concentrated near the post-tensioning anchorage.

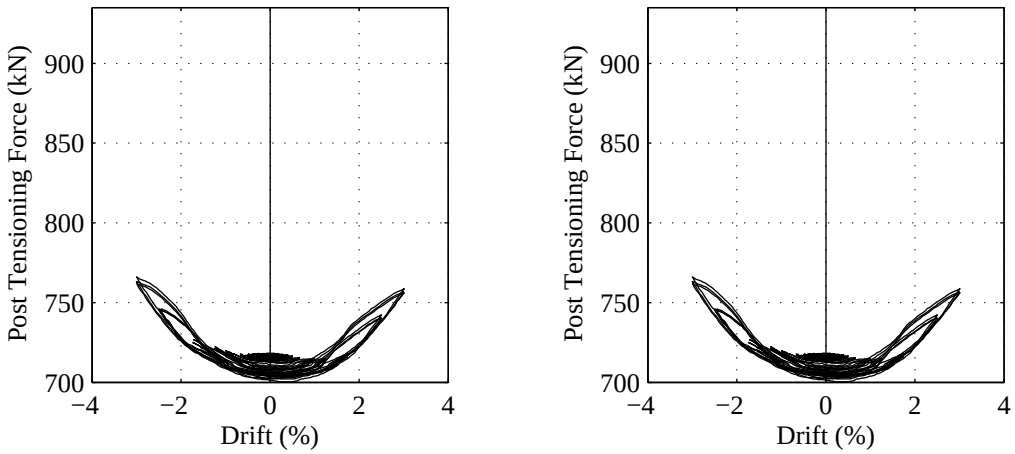

(a) A-P1 (b) A-P2

Figure 4.11: Post-tensioning force vs drift for steel reinforced joint with Plug and Play dissipation

Figure 4.12 shows the variation in the neutral-axis depth at the end of the beam for a range of column top displacements. The effect of the shims is apparent in these plots as, at large drifts, the neutral-axis depth is concentrated in the location of the shims at 200 mm from the centre of the joint. The relationship is slightly more clearly defined than for the joint without additional dissipation.

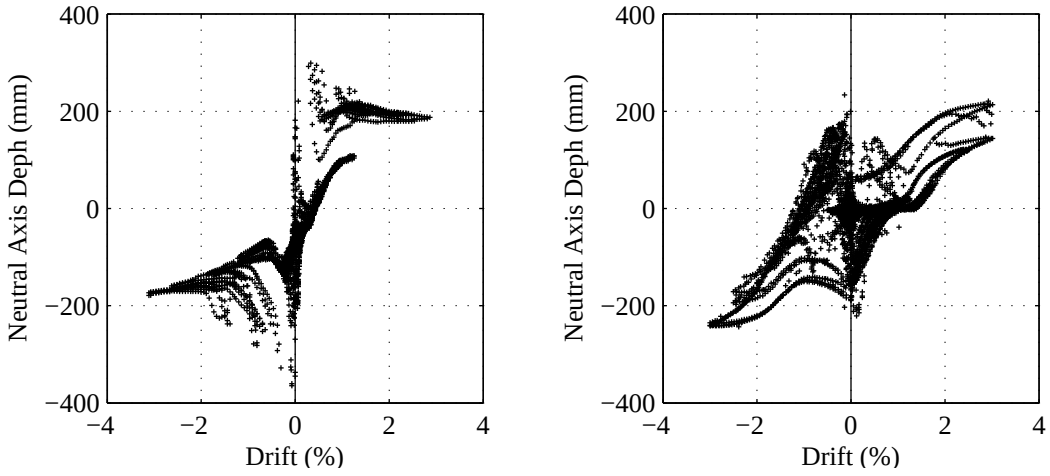

(a) A-P1 (b) A-P2

Figure 4.12: Neutral axis depth for steel reinforced joint with Plug and Play dissipation

Table 4.2: Data from A-P series tests

	A-P1	A-P2	Average
1.25% Moment (kNm)	357	385	371
2.5% Moment (kNm)	571	593	582
3.0% Moment (kNm)	616	645	631
Yield Stiffness (MNm/rad)	37	32	34
Residual Displacement (mm)	-26	-24	-25
Yield Drift	1.17%	1.84%	1.51%
Joint Shear Stiffness (MPa)	738	660	699
3% Hysteretic Damping[1]	11.5%	10.2%	10.8%

[1] See Section 4.2.6 for the details

4.1.3 Tests A-D :Steel Reinforced Joint with Necked Plate Dissipaters on Riveted Plates

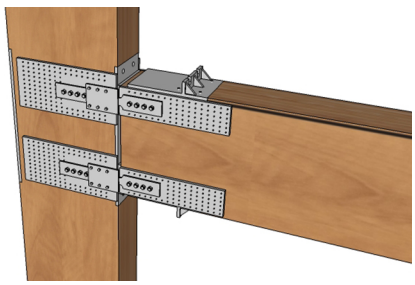

Figure 4.13: Steel reinforced joint with Necked Plate Dissipaters

Two tests of the steel reinforced joint with NPDs were completed with no visible damage to either the dissipaters, connections or timber observed. The anti buckling arrangement consisted of a steel plate covering the necked down area of the dissipater and bolted back into the rivet plate on the column. This appeared to work extremely successfully. No buckling was directly observed, nor was the effect detected in the recorded data. Once these plates were removed however, it was apparent that significant buckling forces were restrained as the compressed NPD then buckled.

The moment rotation behaviour of these tests is shown in Figure 4.14. These specimens were designed for a lower moment at ultimate drift than the joint with Plug and Play dissipaters. A result of this is the increased re-centring behaviour shown in the moment-rotation response.

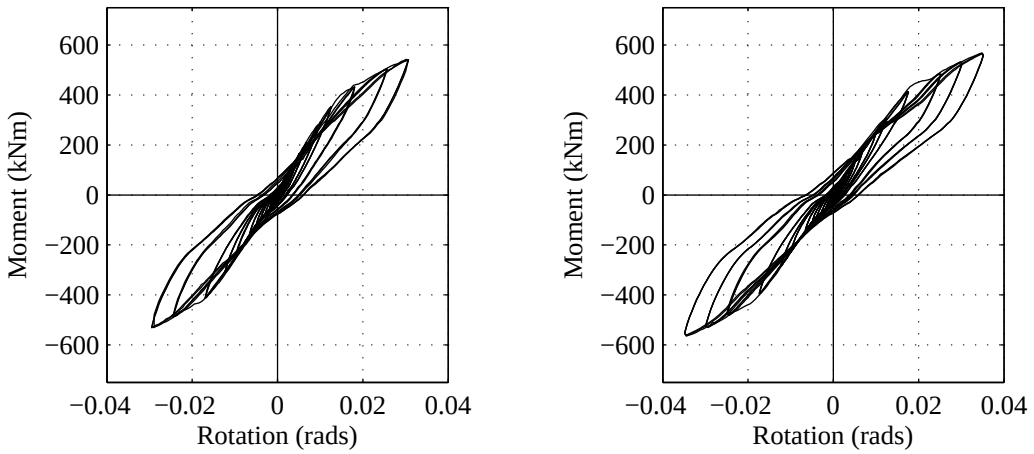

(a) A-D1 (b) A-D2

Figure 4.14: Moment rotation response for Necked Plate Dissipaters on steel reinforced joint

The post-tensioning activation relationship shown in Figure 4.15 is better defined than for the Plug and Play dissipation. Post-tensioning force losses in both of these tests were minimal. The residual centreline compressive deformation at the end of these tests was on average 0.7 mm. This is considerably less than the 3.6 mm recorded in the previous test.

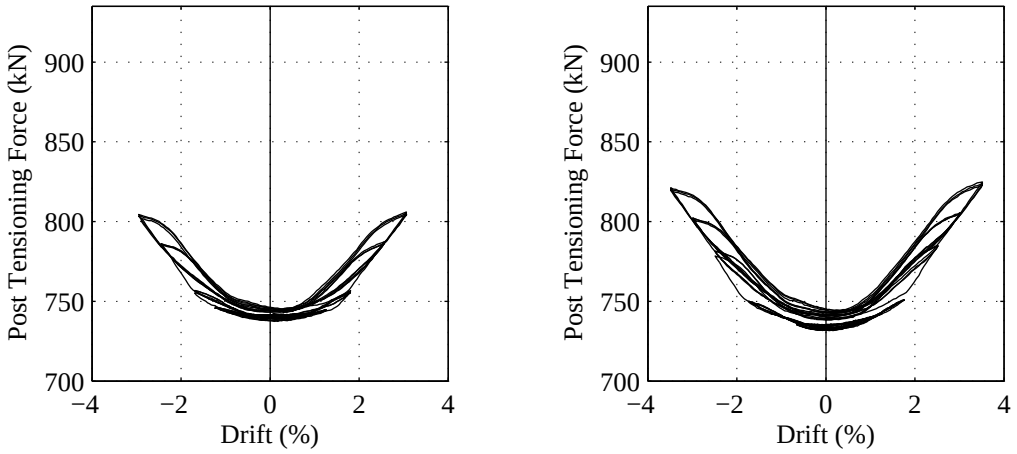

(a) A-D1 (b) A-D2

Figure 4.15: Post-tensioning force vs drift for Necked Plate Dissipaters on steel reinforced joint

The neutral-axis depths in the end of the beam in these tests is given in Figure 4.16. The data obtained for these is quite poor and does not appear to follow that of other tests. A slight trend toward the location of the shim plates is evident at large drift levels in both tests. The plots suggest that the neutral axis depths are located in the centre of the joint at low drifts. The shim

Table 4.3: Data from A-D series tests

	A-D1	A-D2	Average
1.25% Moment (kNm)	325	293	309
2.5% Moment (kNm)	491	482	487
3.0% Moment (kNm)	532	531	532
Yield Stiffness (MNm/rad)	30	25	28
Residual Displacement (mm)	-21	-21	-21
Yield Drift	1.84%	1.80%	1.82%
Joint Shear Stiffness (MPa)	94	92	93
3% Hysteretic Damping[1]	9.4%	8.5%	9.0%

[1] See Section 4.2.6 for the details

plates mean there is no contact between the beam and column at this location. Because of this, it is unlikely that this neutral-axis location is correct. It is possible that data was incorrectly obtained for this test, leading to these incorrect results.

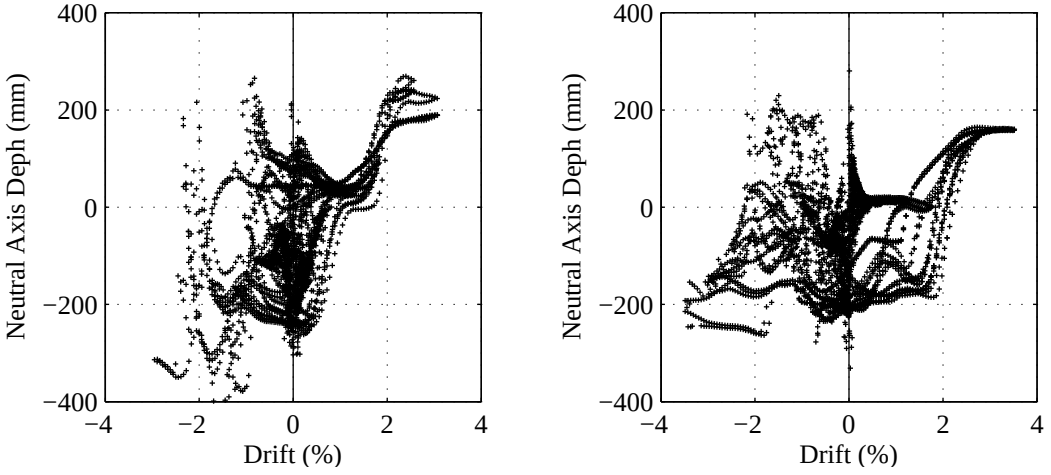

(a) A-D1 (b) A-D2

Figure 4.16: Neutral axis depth for Necked Plate Dissipaters on steel reinforced joint

4.1.4 Tests B-B: Screw Reinforced Joint, No Additional Dissipation

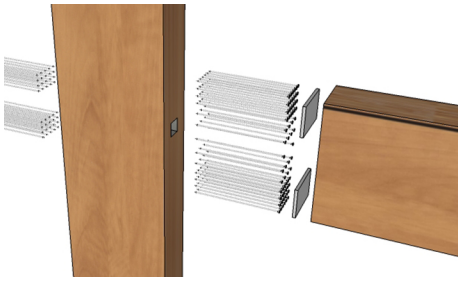

Figure 4.17: Screw reinforced joint with no dissipation

The moment-rotation response of the screw reinforced joint without additional dissipation is shown in Figure 4.18. This data shows similar narrow loops and well defined stiffness discontinuity as the steel reinforced joint without dissipation (Figure 4.5). Again, the response is symmetrical, showing no difference between moment or stiffness for either loading direction.

Results from the second test of this joint are shown in Figure 4.18b. The response from the first test are overlaid on this plot. They show that the second test had a greater cyclic stability. This may be due to any slack between the timber and screw reinforcing being removed in the first test.

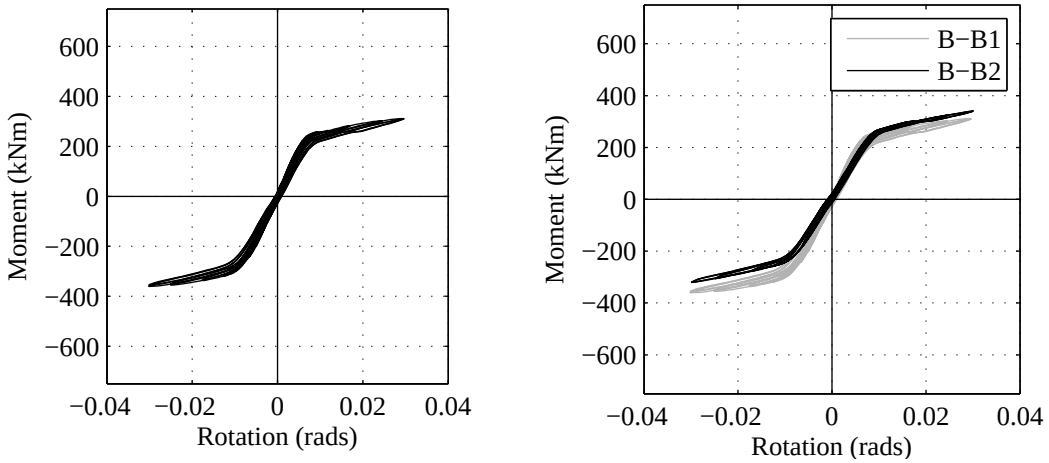

(a) B-B1

(b) B-B2

Figure 4.18: Moment rotation response for screw reinforced joint with no dissipation

Figure 4.19 shows the post-tensioning activation for the screw reinforced joint. Similarly to Figure 4.6, the response for this test is very well defined, with loops containing minimal area.

A drop in post-tensioning force of 2.5% is seen in Figure 4.19a. The effect of this change in post-tensioning force can be seen in Figure 4.18a where there is a slightly larger area contained within the loops as compared to Figure 4.18b. The residual compression in the column after this

test was approximately 0.1 mm. This corresponds to a reduction in post-tensioning force close to the 2.5% recorded. It it therefore likely that this accounts for the majority of the losses observed.

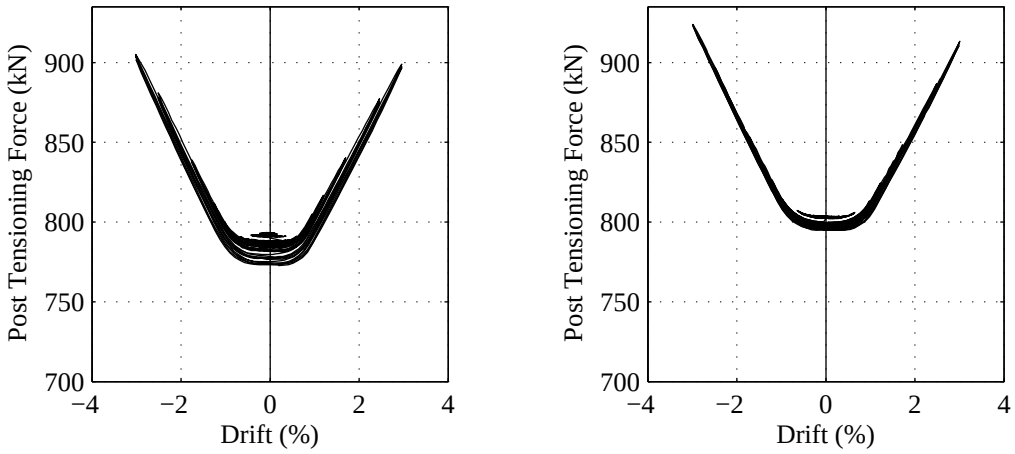

(a) B-B1 (b) B-B2

Figure 4.19: Post-tensioning force vs drift for screw reinforced joint with no dissipation

Neutral-axis depths for the screw reinforced joint without additional dissipation are given in Figure 4.20. The relationship is very clear in Figure 4.20a while it is less pronounced in Figure 4.20b, particularly for low drifts. This may be due to errors in measurement. In Figure 4.20a it is evident that the neutral-axis resides in the shim plates for large drift levels.

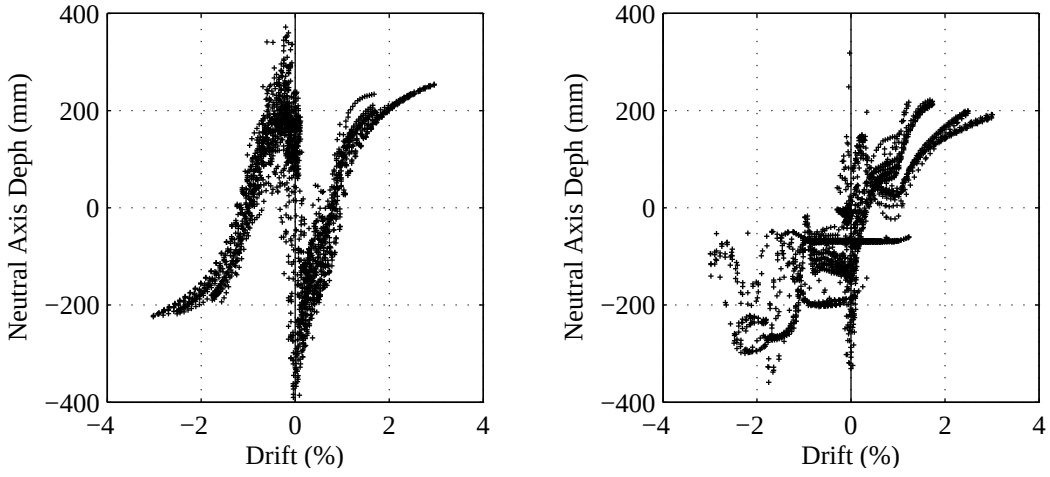

(a) B-B1 (b) B-B2

Figure 4.20: Neutral axis depth for screw reinforced joint with no dissipation

Table 4.4: Data from B-B series tests

	B-B1	B-B2	Average
1.25% Moment (kNm)	290	268	279
2.5% Moment (kNm)	327	314	321
3.0% Moment (kNm)	333	328	331
Yield Stiffness (MNm/rad)	34	30	32
Residual Displacement (mm)	-4	-2	-3
Yield Drift	0.68%	0.85%	0.77%
Joint Shear Stiffness (MPa)	587	926	757
3% Hysteretic Damping[1]	2.0%	1.7%	1.9%

[1] See Section 4.2.6 for the details

4.1.5 Tests B-D : Screw Reinforced Joint with Necked Plate Dissipaters on Screw in Devices

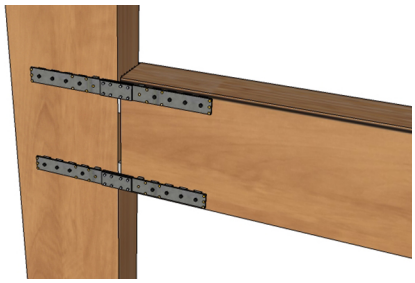

Figure 4.21: Screw reinforced joint with Necked Plate Dissipaters

Anti-Buckling Devices

During the first test run, at drifts of 3%, the NPDs buckled on one side of the joint. The buckled shape of the dissipaters is shown in Figure 4.22. As seen in Figure 4.22a the anti buckling block placed under the NPD was not connected sufficiently well to the timber. The screws used to connect this plate to the timber were 80 mm long, meaning that the thread embedding length into the timber was only approximately 30 mm. To remedy this, in the second test, two options were developed; using longer screws to have greater threaded length embedded in the timber, and increasing the size and stiffness of the anti buckling plate as well as using longer screws. During this test, both options successfully restrained buckling. Each option was placed on either the top or bottom of the joint to allow the impact of each to be separated. Even with this buckling, the ultimate response of the joint was not significantly affected. As shown in Figure 4.23, buckling only occurred on the final cycle to 3.0 % drift. Even with this buckling, the reduction in moment capacity was less than 5%.

(a) Buckled dissipater on joint

(b) Dissipaters after removal

Figure 4.22: Buckled Necked Plate Dissipaters after testing

The moment rotation behaviour of these tests show a marked difference when compared to tests on the joint using steel reinforcement. This is due to the increased re-centring ratio (λ) which means that the response passes close to the origin on the unloading branch. Reduced residual displacement was achieved while maintaining a similar moment capacity by increasing the proportion of the moment taken by post-tensioning.

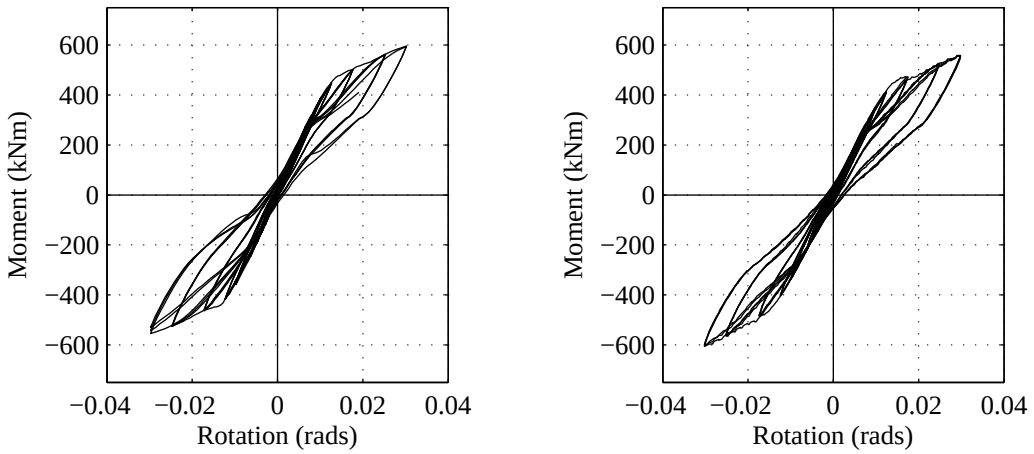

(a) B-D1 (b) B-D2

Figure 4.23: Moment rotation response for screw reinforced joint with Necked Plate Dissipaters

The post-tensioning force to drift relationship for the screw reinforced joint with NPDs is shown in Figure 4.24. These exhibit well defined behaviour with good cyclic stability. There is negligible post-tensioning force loss after the test in either of the specimens. A slight asymmetry is observed for the test shown in Figure 4.24a. In this test, post-tensioning force is larger when the ram is extended. The effect is small, resulting in an increase of overall post-tensioning force of only 0.6%.

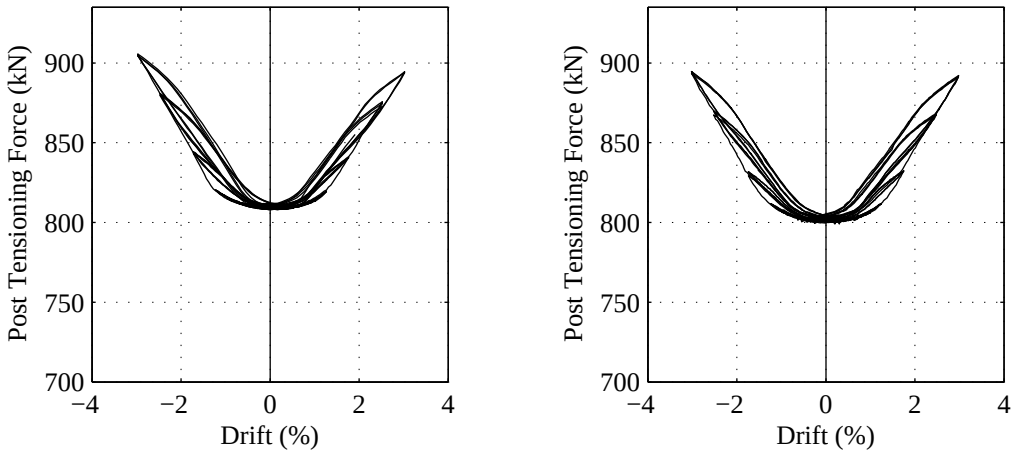

(a) B-D1 (b) B-D2

Figure 4.24: Post-tensioning force vs drift for screw reinforced joint with Necked Plate Dissipaters

The calculated neutral-axis depth for the screw reinforced joint with NPDs is shown in Figure 4.25. The effect of shim plates can be seen for some of the data in Figure 4.25a where the neutral axis depth trends toward $\pm$ 200 mm. Figure 4.25b shows the neutral-axis located at the centre of the

Table 4.5: Data from B-D series tests

	B-D1	B-D2	Average
1.25% Moment (kNm)	420	401	411
2.5% Moment (kNm)	536	538	537
3.0% Moment (kNm)	558	576	567
Yield Stiffness (MNm/rad)	40	36	38
Residual Displacement (mm)	7	-9	-1
Yield Drift	1.22%	1.27%	1.25%
Joint Shear Stiffness (MPa)	862	839	851
3% Hysteretic Damping[1]	6.8%	6.9%	6.9%

[1] See Section 4.2.6 for the details

joint for large negative drifts. This is thought to be erroneous, possibly due to the high sensitivity of the method used to calculate the neutral axis depth and errors in measurement.

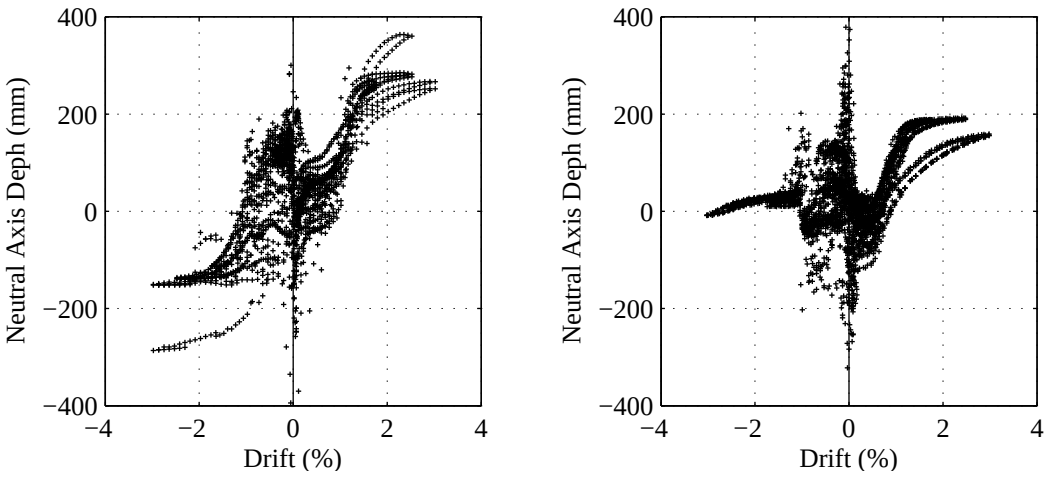

(a) B-D1 (b) B-D2

Figure 4.25: Neutral axis depth for screw reinforced joint with Necked Plate Dissipaters

4.1.6 Tests B-TP: Screw Reinforced Joint with Timber Encased Threaded Rod Dissipation

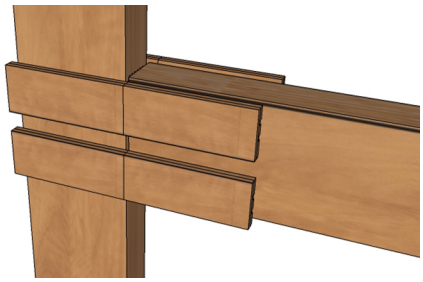

Figure 4.26: Screw reinforced joint with Timber Plus dissipaters

The moment-rotation response of the screw reinforced joint with Timber Plus dissipaters is presented in Figure 4.27. A clear backbone curve can be seen in the data. This displays a gradual loss of stiffness as gap opening and steel yielding occurs as opposed to the sharp transition of the joints without dissipation. This is believed to be due to crushing of the timber at the gap interface and slip of the connecting screws. The joint behaviour is symmetrical with similar moments and stiffnesses in each direction.

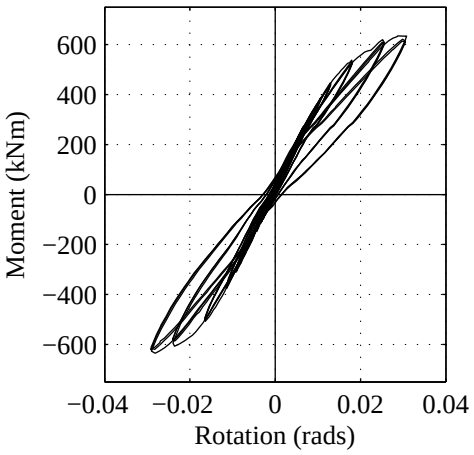

Figure 4.27: Moment rotation response for Timber Plus dissipater on screw reinforced joint

Post-tensioning activation is shown in Figure 4.28. No significant losses in post-tensioning are observable in the data. The response is asymmetric. A difference of 2% of the total post-tensioning force between each direction is observed at maximum drift levels. This difference, while pronounced in Figure 4.28 is not particularly apparent in the moment-rotation response shown in Figure 4.27.

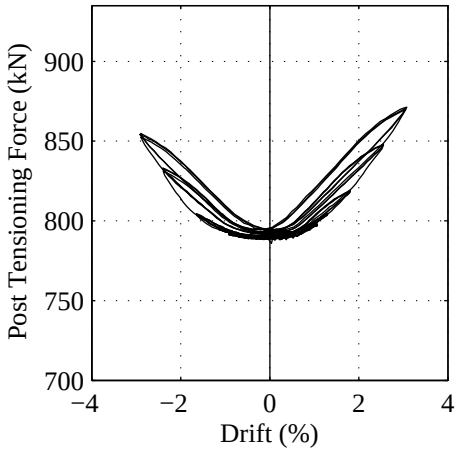

Figure 4.28: Post-tensioning force vs drift for Timber Plus dissipater on screw reinforced joint

The neutral-axis depth in the beam for the screw reinforced joint with Timber Plus dissipation devices is given in Figure 4.29. The data is quite scattered and the relationship is not as apparent as for other specimens. During testing it was noted that the dissipation devices exhibited localised gap opening, with a secondary neutral-axis present inside the timber blocks. This behaviour is likely to have interfered with the determination of the neutral axis depth in the beam section. From the figures it appears that the neutral axis is located further from the centre of the joint than in other tests. This is consistent with the increased compression area due to the dissipater transferring compressive stresses across the joint. The increased stiffness of the dissipater block when compared to the column due to grain orientation is also likely to contribute to this phenomenon.

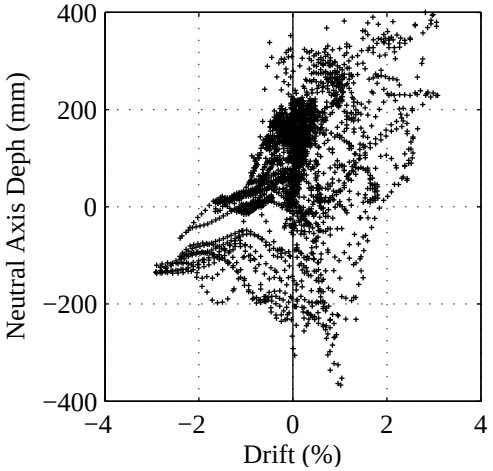

Figure 4.29: Neutral axis depth for Timber Plus dissipater on screw reinforced joint

Table 4.6: Data from B-TP series tests

	B-TP
1.25% Moment (kNm)	418
2.5% Moment (kNm)	601
3.0% Moment (kNm)	630
Yield Stiffness (MNm/rad)	38
Residual Displacement (mm)	-5.5
Yield Drift	1.79%
Joint Shear Stiffness (MPa)	310
3% Hysteretic Damping[1]	6.2%

[1] See Section 4.2.6 for the details

4.2 Summary of Results

A summary of the results of all of the tests conducted in this program is given below. These sections detail differences in:

- Moment-Rotation
- Post-Tensioning Forces
- Neutral Axis Depth
- Stiffness
- Hysteretic Damping
- Residual Displacement
- Cyclic Stability

Comparisons between each joint for the factors considered enables the effectiveness of each design to be evaluated.

4.2.1 Moment Rotation

Moment-rotation response is the primary measure of a joint's performance. Key elements of this behaviour include; moment capacity at target drift levels, yield stiffness, and ultimate stiffness, as illustrated in Figure 4.30.

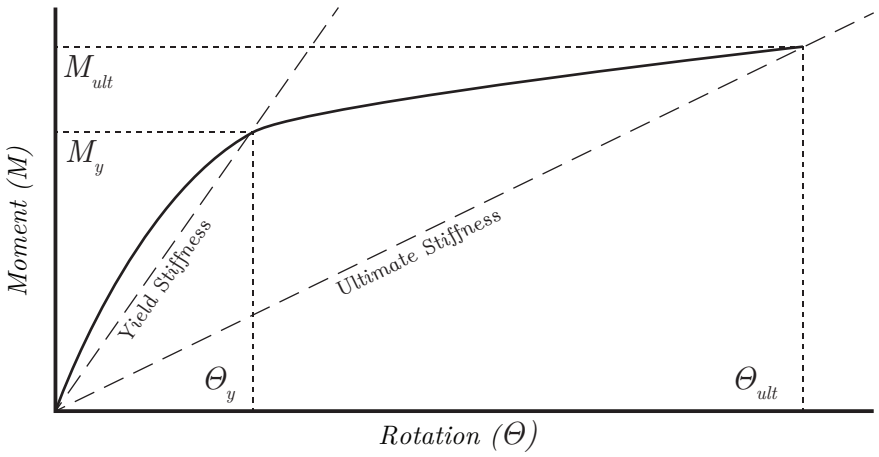

Figure 4.30: Terminology used in moment rotation discussion

The moment capacity of each joint at a drift level of 3.0% is shown in Table 4.7. This information can be used to evaluate each joint against its design parameters.

The joints using additional dissipation devices were designed to achieve a moment of 585 kNm at a connection rotation of 3%. The rotation experienced by the connections at a 3% drift level are less than 3% due to deformation of the beam, column and joint zone (Newcombe, 2007).

For design, the frame contribution was assumed as 0.4% based on frame geometry. This was based on analyses of the three storey prototype structure described in Section 2.6.5.

Table 4.8 provides a comparison between the ultimate design moment and that achieved for each specimen. Slight reductions in moment capacities were predicted due to post-tensioning losses. Most connections however performed in line with expectation. However the joint with Timber Plus dissipaters achieved approximately 15% greater moment than designed.

Table 4.7: Connection moment at 3.0% Drift

Joint Reinforcement	Dissipation	Test	Test Value (kNm)	Average (kNm)	Increase (%)[a]
Steel	None	A-B2	286	286	
	Plug and Play	A-P1	616		
		A-P2	645	631	120%
	NPDs	A-D1	532		
		A-D2	531	532	86%
Screw	None	B-B1	333		
		B-B2	328	331	
	NPDs	B-D1	558		
		B-D2	576	567	72%
	Timber Plus	B-TP	630	630	91%

[a] Increase over same joint without additional dissipation

Table 4.8: Connection ultimate design moments

Joint Reinforcement	Dissipation	Test	Design (kNm)	Observed[a] (kNm)	Difference
Steel	Plug and Play	A-P	623	631	1%
	NPDs	A-D	578	532	-8%
Screw	NPDs	B-D	567	567	0%
	Timber Plus	B-TP	553	630	14%

[a] Average observed value for each test series.

The drift at which the joint's stiffness changes abruptly is a combination of the gap opening and subsequent increase in post-tensioning force, as well as yielding of the mild steel dissipative elements. The yield drift reported in Table 4.9 represents the drift maximising the change in slope of the moment-rotation response. A stiff frame with a low yield drift will have larger ductility than a structure with a lower yield drift.

Table 4.9: Yield drift

Joint Reinforcement	Dissipation	Test	Test Value (%)	Average (%)	Increase (%)[a]
Steel	None	A-B2	1.0%	1.0%	
	Plug and Play	A-P1	1.2%		
		A-P2	1.8%	1.5%	50%
	NPDs	A-D1	1.8%		
		A-D2	1.8%	1.8%	80%
Screw	None	B-B1	0.7%		
		B-B2	0.9%	0.8%	
	NPDs	B-D1	1.2%		
		B-D2	1.3%	1.2%	50%
	Timber Plus	B-TP	1.8%	1.8%	125%

[a] Increase over same joint without additional dissipation

4.2.2 Stiffness

The secant stiffness to yield of each test is compared in Table 4.10. This initial stiffness is very important to the overall response of the structure containing these joints, as it will determine the performance of the building in low to moderate seismic events. Reductions in stiffness increase a building's period. This lowers seismic moment and shear demands but increases displacement, possibly causing non structural damage to the building and its contents.

Compared to the steel reinforced joint, the screw reinforced joint had a pre-yield stiffness around 50% greater. Post-tensioning doesn't increase stiffness before gap opening. The screw based joint reinforcement is therefore likely to account for the majority of the increase in stiffness.

In the cases tested, the stiffness in both the positive and negative directions have been similar. There is a slight difference in the low drift stiffness between the tests without dissipation for Joint A and Joint B (Figure 4.5 and Figure 4.18). This difference is likely to be due to the steel channel interfering with the slot in the beam, restraining joint rotation. While this difference may be significant in joint level testing, frame behaviour can be expected to be approximately the average of the two directions.

Table 4.10: Yield stiffness

Joint Reinforcement	Dissipation	Test	Test Value (MNm/rad)	Average (MNm/rad)	Increase (%)[a]
Steel	None	A-B2	21.5	21.5	
	Plug and Play	A-P1	36.7		
		A-P2	31.6	34.2	47%
	NPDs	A-D1	29.8		
		A-D2	25.2	27.5	17%
Screw	None	B-B1	34.1		
		B-B2	30.2	32.1	
	NPDs	B-D1	40.4		
		B-D2	36.4	38.4	21%
	Timber Plus	B-TP	38	38	26%

[a] Increase over same joint without additional dissipation

4.2.3 Post-Tensioning Activation

The initial post-tensioning force applied to each specimen is given in Table 4.11. In all cases, this force was below the level targeted by the design. This was due to tendon relaxation and other short-term losses. The moment capacity of the joints will be reduced because of this. As real structures are unlikely to experience an earthquake immediately after construction, they too will to have lower post-tensioning forces. Because of this, the slight losses in post-tensioning forces seen here are worthy of note, not concern.

Table 4.11: Initial post-tensioning

Joint Reinforcement	Dissipation	Test	Target (kN)	Test (kN)	Average (kN)
Steel	None	A-B2	750	716	716
	Plug and Play	A-P1	750	721	
		A-P2	750	718	720
	NPDs	A-D1	750	741	
		A-D2	750	732	737
Screw	None	B-B1	810	793	
		B-B2	810	804	799
	NPDs	B-D1	810	812	
		B-D2	810	803	808
	Timber Plus	B-TP	810	795	795

Long term testing

The specimen was assembled and stressed prior to conducting seismic tests of the joint. The joint was configured with steel reinforcing and no dissipation devices (A-B). It was left for a period of 28 days and post-tensioning force was monitored. During this time, the tendon force was seen to vary by around 4%. The data from this test is compared with environmental data (NIWA, 2007) in Figures 4.31 and 4.32. Variations in post-tensioning force can be seen to be highly correlated to both temperature and humidity. There is also a clear reduction in forces over time. This variation in post-tensioning force may be responsible for some of the differences in moment capacity observed between tests of the same joint.

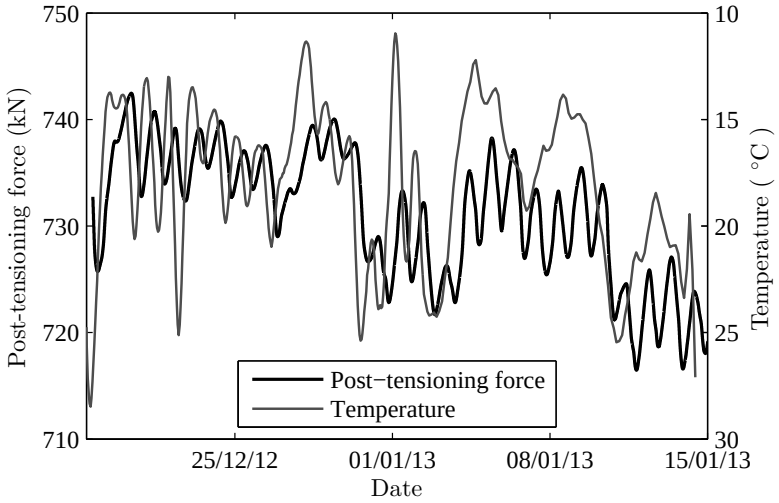

Figure 4.31: Comparison of post-tensioning force and temperature

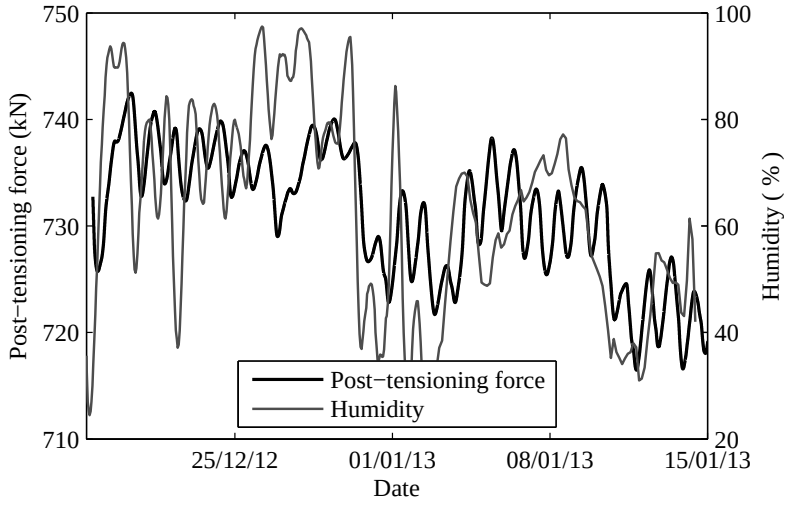

Figure 4.32: Comparison of post-tensioning force and humidity

4.2.4 Neutral Axis Depth

The data for the depth of the neutral axis in the joint was quite scattered, and as such, the differences between all joints were not apparent. This data would likely have been

improved by increasing the number of potentiometers across the joint zone to better capture compression deformations near the rocking interface. Chapter 5 shows the goodness of fit between computational models for joint behaviour and the data obtained.

4.2.5 Re-centring Ratio

The re-centring ratio (λ) is the ratio between moment components acting to centre the joint and moment components dissipating energy. It is defined as:

$$\lambda = \frac{M_{Re-centring}}{M_{Dissipating}} \tag{4.1}$$

This quantity was determined from the results of each test by comparing the total moment rotation response to that of the post-tensioned only response. While this is not exactly correct, as there is some small dissipative component of the post-tensioned joint, it is deemed adequate for this comparison. The results of this procedure are averaged for the cycles to 3% drift and are shown in Table 4.12. The joint without additional dissipation will have larger rotations for a given seismic demand than the hybrid joint. Because of the relatively constant re-centring ratios at large drifts as shown in Figure 4.33 this simplification was deemed to be acceptable.

The relationships between re-centring ratio and drift for each test are shown in Figure 4.33. These show the difference between steady state re-centring ratio at large drifts and the rapidly changing ratios near zero displacement. The results presented in the table are values for λ at large drifts so are not fully indicative of actual re-centring performance. The figures shown present a more complete view of re-centring behaviour. A unity ratio threshold has been marked on the plots. Where the observed re-centring ratio is above this line, full re-centring performance is expected. All specimens have a large 're-centring' ratio at large drifts. The re-centring ratio must be larger than 1.0 at low drift levels to achieve full re-centring. The first specimen tested, with steel reinforcing and Plug and Play dissipation, was designed for the Merritt building and did not target full re-centring. Figure 4.33a and Figure 4.33b show the re-centring ratio reducing at low absolute drifts. Connections on the screw reinforced joint connections were designed to achieve full re-centring. This can be seen in the upward trend at low displacements of Figure 4.33e and Figure 4.33f.

Table 4.12: Re-centring ratio for cycle to 3% drift

Joint Reinforcement	Dissipation	Test	Test Value	Average
Steel	None	A-B2	-	
	Plug and Play	A-P1	1.79	
		A-P2	1.79	1.79
	NPDs	A-D1	2.20	
		A-D2	2.23	2.23
Screw	None	B-B1	-	
		B-B2	-	
	NPDs	B-D1	2.10	
		B-D2	2.20	2.20
	Timber Plus	B-TP	1.94	1.94

[a] Increase over same joint without additional dissipation

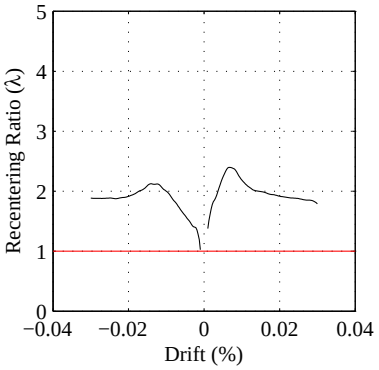

(a) A-P1

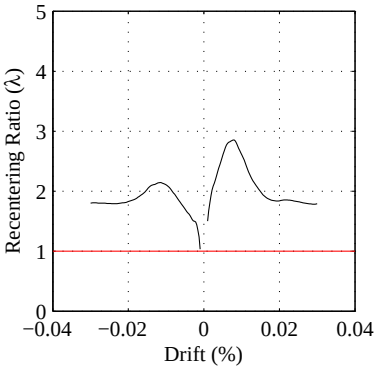

(b) A-P2

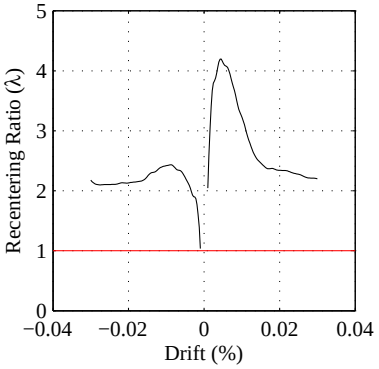

(c) A-D1

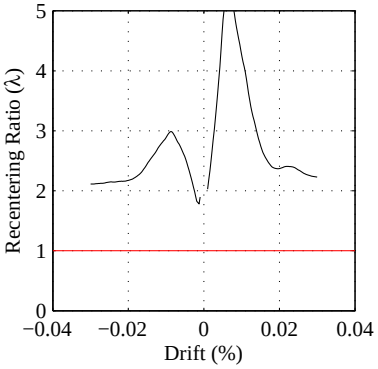

(d) A-D2

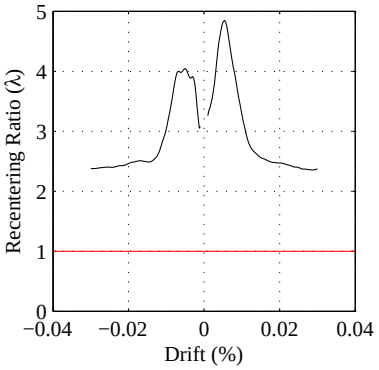

(e) B-D1

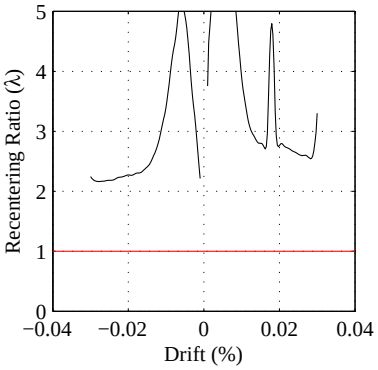

(f) B-D2

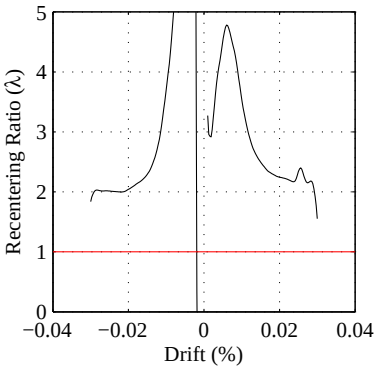

(g) B-TP

Figure 4.33: Re-centring ratio (λ) vs drift for each test

4.2.6 Hysteretic Damping

The hysteretic damping for each specimen tested is outlined in Table 4.13 The values shown are for the displacement cycle to 3%. Displacement cycles from the origin to a single peak and returning to the origin were used instead of full positive/negative cycles. An average of each of the cycles to 3% is presented. As this was the design level drift, it was considered to be representative of the energy dissipation of the system.

Hysteretic damping was calculated according to the procedure outlined in Section 4.3.5. An example of this process is given below for the second test using Necked Plate Dissipaters on a steel reinforced joint (Test A-D2). The area contained in the cycle under consideration as well as that of an elastic viscous damper are shown in Figure 4.34.

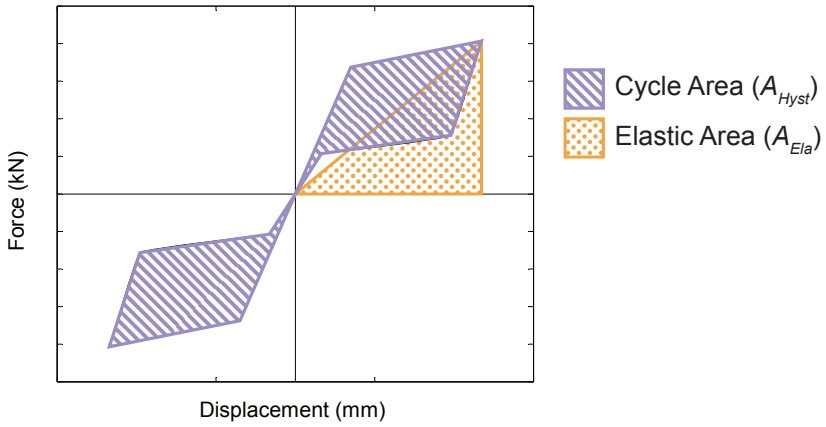

Figure 4.34: Illustration of the procedure for obtaining hysteretic damping for 3% loop of steel reinforced joint using Necked Plate Dissipaters.

The areas derived from this process were:

$$A_{Hyst} = \int_{cycle} \mathrm{F}(\Delta)\mathrm{d}\Delta \tag{4.2}$$

$$= 9770\mathrm{kNmm} \tag{4.3}$$

$$A_{Ela} = \frac{1}{2}\Delta_{peak}F_{peak} \tag{4.4}$$

$$= \frac{1}{2} \times 110\mathrm{mm} \times 150\mathrm{kN} \tag{4.5}$$

$$= 8275\mathrm{kNmm} \tag{4.6}$$

The hysteretic damping was then calculated according to:

$$\xi_{Hyst} = \frac{1}{4\pi}\frac{A_{Hyst}}{A_{Ela}} \tag{4.7}$$

$$= \frac{1}{4\pi}\frac{9770}{8275} \tag{4.8}$$

$$= 9.4\% \tag{4.9}$$

This process was repeated for each of the cycles to a drift level of 3.0%, an average was produced for the specimen. This average is the value reported in Table 4.13.

Both of the solutions without dissipative elements are seen to have very little hysteretic damping. This is to be expected, and in design the damping contribution of post-tension only solutions are generally neglected (Pampanin *et al.*, 2010).

The effect of targeting a higher re-centring ratio for the tests using Joint B are apparent in the reduction hysteretic damping when comparing the B-D series to that of A-P or A-D. Because of the lower mild steel contribution to the moment response, the loops produced are thinner, dissipating less energy.

Table 4.13: Hysteretic damping at 3% drift

Joint Reinforcement	Dissipation	Test	Test Value (%)	Average (%)	Increase (%)[a]
Steel	None	A-B2	2.6%	2.6%	
	Plug and Play	A-P1	11.5%		
		A-P2	10.2%	10.8%	415%
	NPDs	A-D1	9.4%		
		A-D2	8.5%	9.0%	346%
Screw	None	B-B1	2.0%		
		B-B2	1.7%	1.9%	
	NPDs	B-D1	6.8%		
		B-D2	6.9%	6.9%	363%
	Timber Plus	B-TP	6.2%	6.2%	326%

[a] Increase over same joint without additional dissipation

The Displacement Based Design (DBD) (Priestley *et al.*, 2007) guide gives the following formulation for hysteretic damping in systems with flag shaped dissipation.

$$\xi_{Hyst} = \left(\frac{2}{1+\lambda}\right)\left(\frac{\mu-1}{\pi\mu}\right) \tag{4.10}$$

Table 4.14 compares the values obtained from testing with this approach.

Damping of around 2% was observed for the specimens without external dissipation where none was predicted. This damping is relatively minor and should continue to be neglected in design.

Error in damping predictions for systems with additional dissipation was up to 45%. Predictions were more accurate for the steel reinforced joint than in the screw reinforced joint.

The screw reinforced joint had a more pronounced yield point. This meant that ductilities were more clearly defined. As a result earlier yielding was identified and larger ductilities reported. These large apparent ductilities lead to an overestimate of hysteretic damping.

Table 4.14: Comparison of observed and theoretical damping (ξ_{hyst})

Test	Ductility (μ)	Re-centring Ratio (λ)	Hysteretic Damping		Error	
			Predicted	Actual	Test	Average
A-B2	3.0	-	-	2.6%	-	
A-P1	2.5	1.8	13.6%	11.5%	-15.7%	
A-P2	1.7	1.8	9.4%	10.2%	9.0%	-3.4%
A-D1	1.7	2.2	8.2%	9.4%	14.7%	
A-D2	1.7	2.2	8.2%	8.5%	3.8%	9.3%
B-B1	4.3	-	-	2.0%	-	
B-B2	3.3	-	-	1.7%	-	
B-D1	2.5	2.1	12.3%	6.8%	-44.8%	
B-D2	2.3	2.2	11.2%	6.9%	-38.6%	-41.7%
B-TP	1.7	1.9	9.0%	6.2%	-31.4%	-31.4%

4.2.7 Effective Joint Panel Shear Modulus

The nominal shear modulus of plain LVL is 550 MPa. The shear deformations across undisturbed sections of the column were used to assess the shear modulus of the LVL in the specimen. The average modulus calculated was 873 MPa, 60% higher than the nominal value provided. Although prior testing may have impacted the shear stiffness of LVL outside the joint zone, this effect is unlikely to be large and no significant pattern was seen in the data. As all the material used came from the same manufacturer, this single average value was used to compare the joint reinforcement schemes.

The effective shear modulus across the joint zone was found for each specimen. These values are shown in Table 4.15. A comparison is provided between the recorded value and that for a plain LVL section.

Table 4.15: Effective shear modulus for the joint zone

Joint Reinforcement	Dissipation	Test	Test Value (MPa)	Average (MPa)	Increase (%)[a]
Steel	None	A-B2	868	868	-
	Plug and Play	A-P1	983		
		A-P2	880	932	7%
	NPDs	A-D1	126		
		A-D2	123	125[b]	-86%
Screw	None	B-B1	783		
		B-B2	1235	1009	16%
	NPDs	B-D1	1150		
		B-D2	1119	1135	30%
	Timber Plus	B-TP	413	413	-53%

[a] Increase above average shear modulus measured outside joint region
[b] Value thought to be erroneous

The values obtained suggest that the steel reinforcing scheme showed little improvement over a plain LVL section while the screw reinforcing improved stiffness by around 30%. This is due to the steel plates being only on the surface of the timber rather than embedded in the column. It is therefore not surprising that the steel reinforcing did not improve shear panel stiffness.

The effect may also be influenced by the higher post-tensioning loads used with the specimens including the screw reinforced joint. This may have caused a greater proportion of the shear force to act with a reduced lever arm, causing a reduction in the shear deformation over the total joint zone. This would present an apparent increase in shear stiffness.

4.2.8 Residual Displacement

The residual displacement of each test is directly related to the re-centring ratio of the joint. A direct comparison of the residual displacement from each test is not an appropriate description of the performance of the joint due to different design parameters between Joint A and B. Because of this, meaningful comparisons can only be made for tests from the same joint.

It can be seen from the results in Table 4.16 that there is a higher degree of variability in the residual displacements from the screw reinforced joint. The residual displacements vary between tests by as much as 28% in the case of the NPD tests. In absolute terms however, the total residual displacement is far lower than for the steel reinforced joint. In the case of the NPD tests, the residual displacement of the screw reinforced joint is only 38% of that of the steel reinforced joint. This is to be expected as the joints were designed with different target re-centring ratios.

The residual displacement of the joints without external energy dissipation devices was very low, averaging less than 3 mm. The difference in average residual displacement between the steel and screw reinforced joints without additional dissipation is minimal.

Table 4.16: Residual displacement

Joint Reinforcement	Dissipation	Test	Test Value (mm)	Average (mm)	Increase (%)[a]
Steel	None	A-B2	2	2	
	Plug and Play	A-P1	26		
		A-P2	24	25	1150%
	NPDs	A-D1	22		
		A-D2	21	22	1000%
Screw	None	B-B1	4		
		B-B2	2	3	
	NPDs	B-D1	7		
		B-D2	9	8	167%
	Timber Plus	B-TP	6	6	100%

[a] Increase over same joint without additional dissipation

4.2.9 Cyclic Stability

The moment rotation response of the first cycle to each drift level was compared to that of subsequent cycles. Ideally there would not be any significant degradation with each cycle, as this may indicate unacceptable damage to components of the system. However, all tests using mild steel dissipative elements exhibited marked reductions in stiffness on the second and later cycles to each drift level. This is particularly apparent in Figure 4.14 and Figure 4.23. In each case, cycles were affected only after the dissipaters have yielded. When subjected to inelastic cyclic loading, the response asymptotically approaches previous peaks, following a lower stiffness branch than the elastic portion of the backbone curve. Several explanations for this behaviour have been proposed, they include:

- The hysteretic properties of steel.
- Dissipater connection slip.
- Crushing of timber.
- Dissipater buckling.

Similar behaviour has been noted in previous testing (Iqbal, 2011). This behaviour was attributed to yielding and bending of the dissipaters.

The observed behaviour appears very similar to examples of this phenomenon found in literature (Lowes, 1999, Chapter 3). This means that the behaviour is likely to be at least partially governed by the hysteretic properties of mild steel.

In each case, the third loading cycle follows the response of the second, without further significant degradation. This indicates that the damage is only done when displacement exceeds previous maxima. Because of this, it is proposed that at least some of the reduction in moment response is due to slip in the connection from the dissipater to the beam and column. This was directly observed in tests A-P1 and A-P2 where the cracking of timber and splitting of epoxy around the plate connecting the dissipaters to the beam was noted. This phenomonon and its effect are shown diagramatically in Figure 4.35.

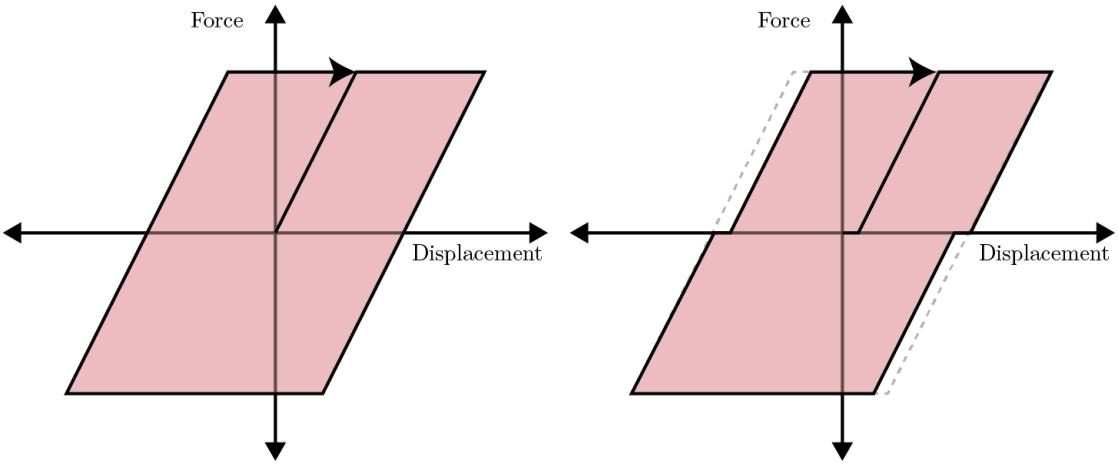

(a) No Dissipater Slip (b) Dissipater Slip

Figure 4.35: Reduction in stiffness of moment rotation response for second and subsequent cycles

This softening resulted in a reduction of the area contained in the loops of later cycles. This could mean that the displacement response of structures is larger for ground motions with several large pulses than may otherwise be expected. Because of the uncertainty in the source of this behaviour, a numerical model was not able to capture this behaviour.

Only very minor crushing of the timber was observed visually. Potentiometers placed across the joint zone also measured the permanent deformation of the timber after the completion of each test. The values recorded were small and are unlikely to account for the reduction in stiffness seen.

4.2.10 Energy Dissipation Per Cycle

The development of energy dissipation for each of the tests has been assessed for each cycle. The area of each loop in force-displacement space was calculated. The figures below show both the energy dissipated per cycle and the cumulative energy dissipation for each drift level.

For tests without external dissipation devices, cumulative dissipated energy appears approximately linear. Where dissipation is added, the slope of the cumulative energy dissipation curve is discontinuous. Dissipaters activate for drifts larger than the yield point and considerably greater

energy dissipation is achieved. The second, steeper slope is also roughly linear. This is shown most clearly in Figure 4.38b where a drift of 3.5% was attained. As the yield point did not occur exactly at a change in drift level, the intermediary drift level exhibits a combination of the pre and post yield stiffnesses. This gives rise to the appearance of an exponential relationship for bi-linear behaviour.

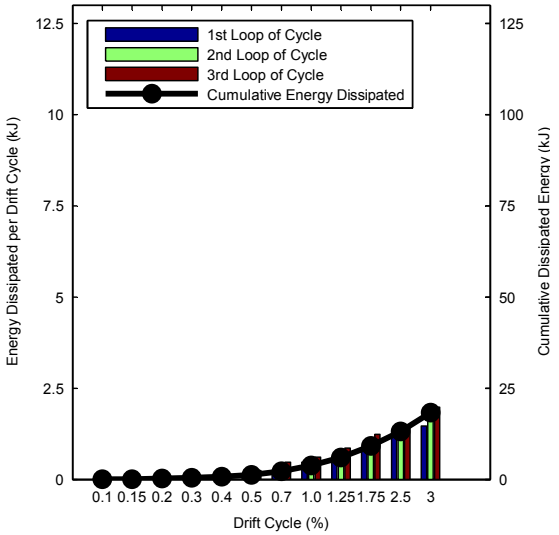

Figure 4.36: Energy per cycle for steel reinforced joint with no dissipation

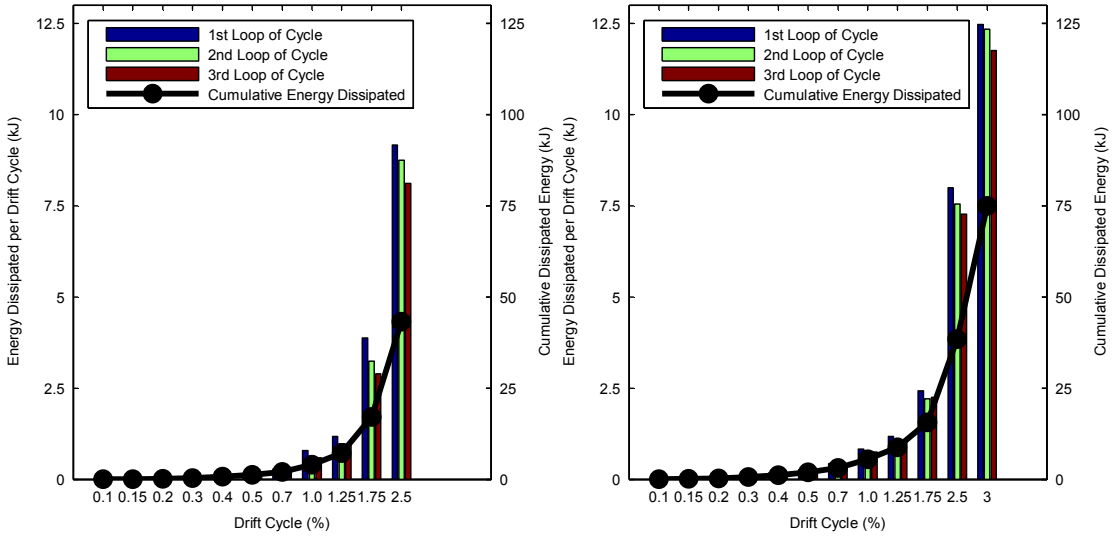

(a) First test (b) Second test

Figure 4.37: Energy per cycle for steel reinforced joint with Plug and Play dissipation

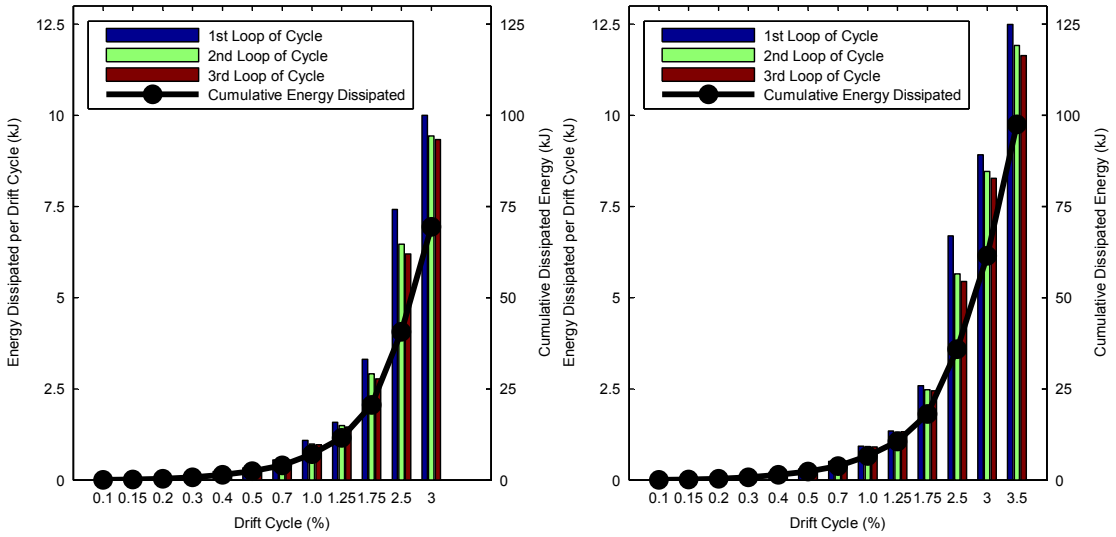

(a) First test (b) Second test

Figure 4.38: Energy per cycle for steel reinforced joint with Necked Plate Dissipaters

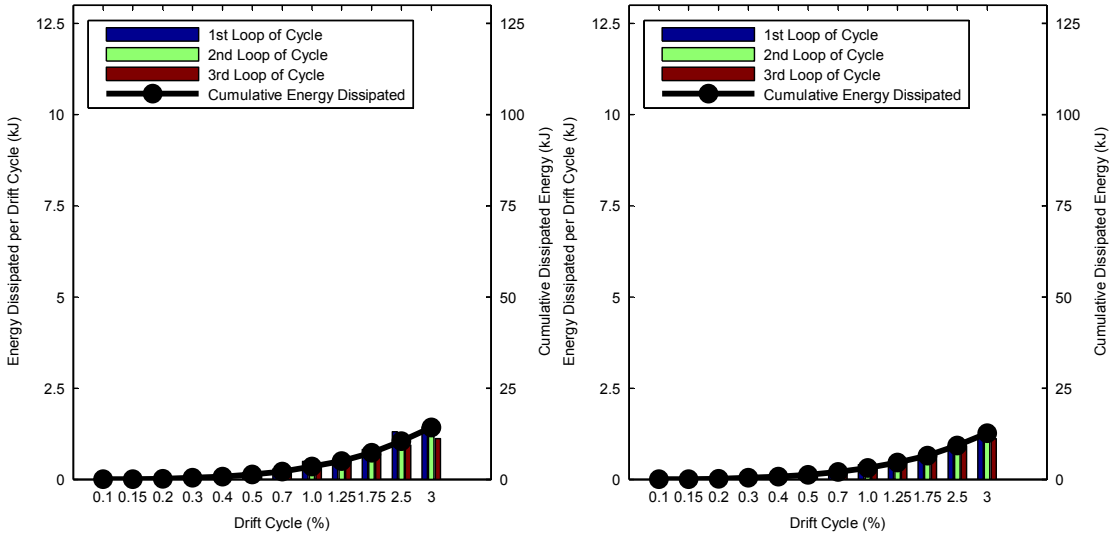

(a) First test

(b) Second test

Figure 4.39: Energy per cycle for screw reinforced joint with no dissipation

The reduction in moment capacity due to dissipater buckling seen in Figure 4.23 is also apparent in the energy dissipated for each cycle. Figure 4.40a shows a large drop in the cyclic energy for second and subsequent cycles at each drift level. The increased performance of the additional anti buckling measures used in the second test is apparent in Figure 4.40b where energy actually increase for the second cycle.

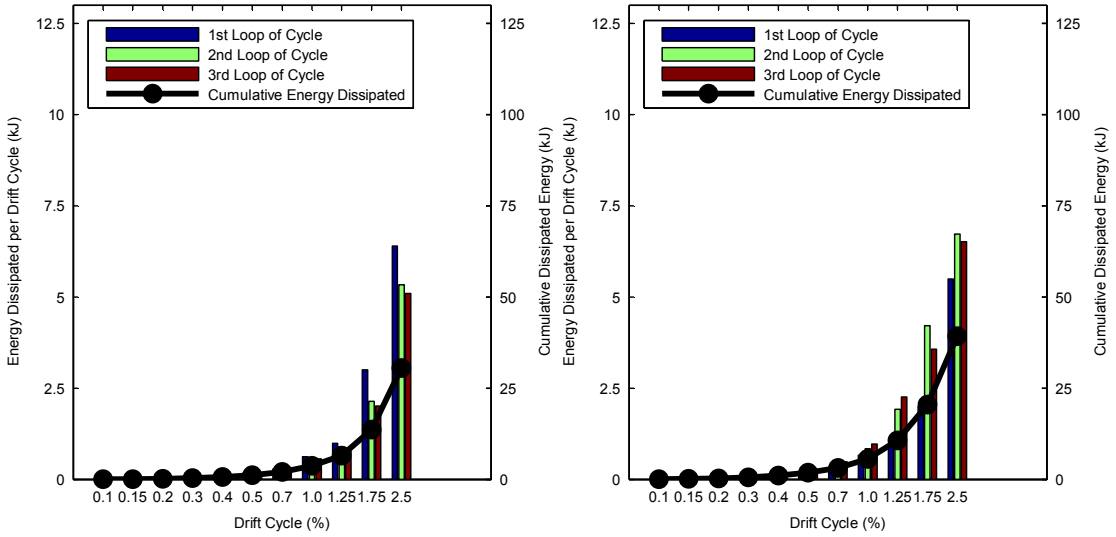

(a) First test (b) Second test

Figure 4.40: Energy per cycle for screw reinforced joint with Necked Plate Dissipaters

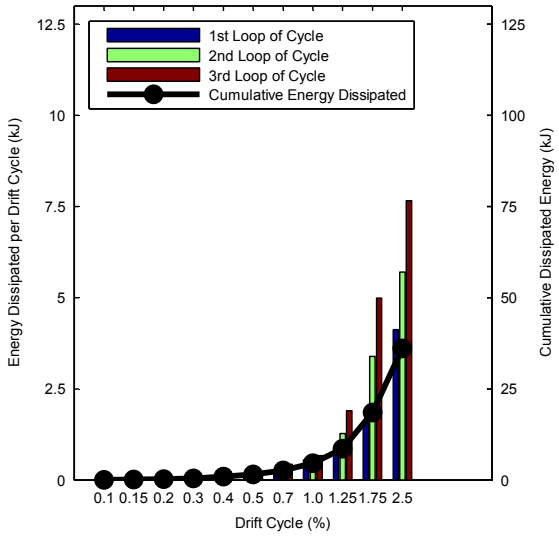

Figure 4.41: Energy per cycle for screw reinforced joint with Timber Plus dissipation

4.3 Derivation of Results

MATLAB scripts and functions were created to manipulate and process the raw data contained in the files from each experiment. Some processing was applied to the records before analysis in order to correct for erroneous data points. The key results considered from each test were:

- Moment Rotation
- Post-Tensioning Activation
- Neutral Axis Depth

Several other secondary items were also evaluated including hysteretic damping, cyclic stability and residual displacement.

4.3.1 Pre Processing and Filtering of Results

The data from every channel except for post-tensioning force was zeroed before being used to derive output. Several data points with zero displacement were saved at the beginning of the record. The data was zeroed by subtracting these points from the rest of the data.

One rotary potentiometer from A-P1 was found to give faulty data. The displacement recorded on the logger stepped suddenly even though the controller recorded no such displacement. To counteract this, the jump was removed from data points.

4.3.2 Moment Rotation

Because of the pinned base connection, the moment at the joint centre line was calculated simply based on the ram height and applied force. The rotation of the joint was measured in two distinct ways; directly using a rotation transducer, and indirectly using applied displacement.

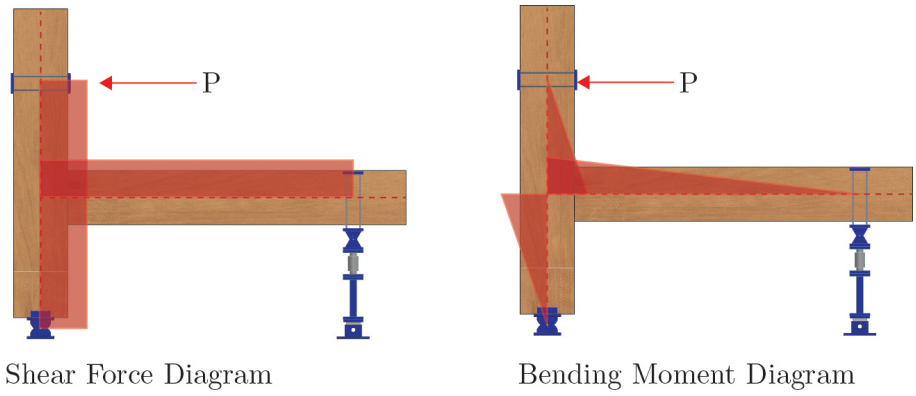

Figure 4.42: Bending moment and shear force diagrams

4.3.3 Shear Deformation

The shear modulus of plain LVL is 550 MPa. The efficacy of joint reinforcement methods was assessed by comparing the effective shear modulus (G_{eff}) across the joint zone to that for plain LVL. The effective shear modulus was determined using:

$$G_{\text{eff}} = \frac{\tau}{\gamma} \tag{4.11}$$

The shear deformation (γ) was measured using pairs of diagonal potentiometers across the zones of interest. As the measured zone was subjected to shear stresses (τ), the potentiometers underwent deformations shown in Figure 4.43. Using Equation (4.12), the shear deformation was determined.

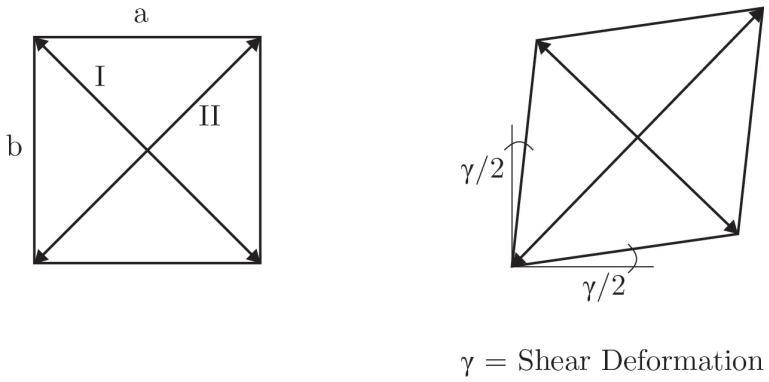

Figure 4.43: Deformations of potentiometers subjected to shear after Ma (Ma, 2010)

$$\gamma = (\Delta_a + \Delta_b)\frac{\sqrt{a^2 + a^2}}{2ab} \tag{4.12}$$

where

γ = shear deformation
a, b = side lengths
Δ_a, Δ_b = change in side lengths

The average shear stress was determined by dividing the shear force by the member's plan area. The bending moment diagram in Figure 4.42 indicates an instantaneous change in shear force at the joint zone. In reality this change in moment is caused by localised shear forces across the joint. The shear force in this zone was taken as the joint moment divided by the 75% of depth of the beam. This factor was chosen due to joint geometry which suggested the lever arm between compression forces and the tension from the dissipater would be around 600 mm.

In several instances, anomalous values for stiffness were obtained from the data. This is thought to be either the potentiometers exceeding their range or being incorrectly installed. The affected data was discarded for subsequent analyses.

4.3.4 Neutral Axis Depth

The neutral axis depth at the end of the beam for each specimen was determined by considering the opening over the gap at the beam column interface. Linear interpolation between the gap opening and the height was used to determine the height of zero stress. At some of the data points, especially where stresses were low, this process returned no clear neutral axis. For the purpose of this analysis, these points were discarded. The result of this analysis was a scatter plot showing discrete neutral axis depths for many points in the loading protocol. Trend lines have been fitted to the data by eye. These give a general idea of the neutral axis depth, even where it is not clearly distinguished.

4.3.5 Hysteretic Damping

The hysteretic damping (ξ_{visc}) for each joint was obtained according to the procedure outlined below (Jacobsen, 1960). A derivation of this process can be found in more specialised literature on this subject (Blandon, 2004). This process consisted of comparing the area of the hysteretic response to that of a purely elastic viscous damper as shown in Figure 4.44. It is important to recognise that the damping calculated below is limited to the sub-assemblies tested. Additional deformations from the structure will reduce effective damping where these are incorporated into larger systems (Priestley *et al.*, 2007).

The dissipated energy was equated to the area beneath the force-displacement curve for a given loop.

$$E_{Diss} = A_{Hyst} \tag{4.13}$$

The equivalent damping was calculated by assuming that the sub-assembley was a SDOF system excited at it's natural frequency. This assumption holds for systems with low hysteretic energy absorption (Priestley *et al.*, 2007), including Pres-Lam frames.

$$\xi_{visc} = \frac{1}{4\pi}\frac{E_{Diss}}{E_{sto}} = \frac{1}{2\pi}\frac{A_{Hyst}}{F_0 u_0} \tag{4.14}$$

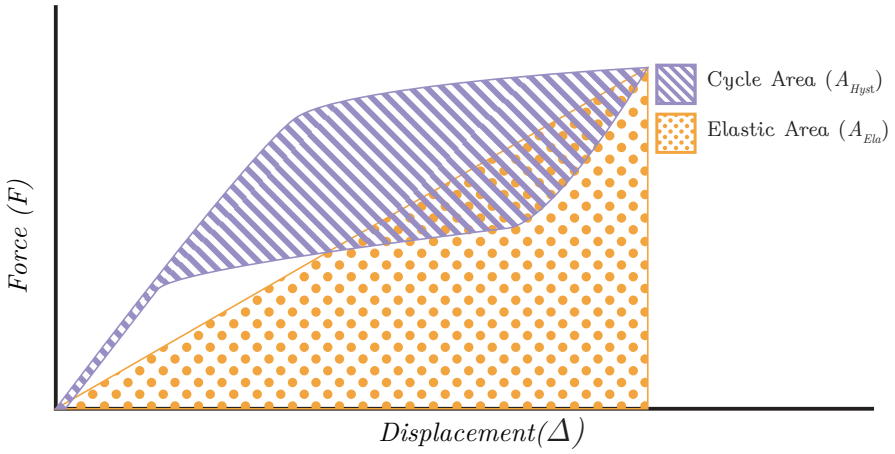

Figure 4.44: Comparison of hysteretic area to get hysteretic damping

Hysteretic damping for the joint is used as an input to the displacement based design procedure and is therefore of critical importance to designers of these structures. When comparing the effectiveness of the dissipation in each of these joints, this parameter was used. The development of damping at different drift levels was calculated and is presented for each of the joints discussed. A comparison of hysteretic damping between each test allows the designer to compare the energy dissipated by each joint detail. This is primarily a function of the performance of yielding dissipative elements in the joint.

4.4 Conclusions

The behaviour of each joint has been shown in Section 4.1. In addition, key parameters have been compared in Section 4.2.

The moment capacity of all joints matched the design values well at design level drifts. Where differences were observed, they were within $\pm 15\%$. Some reduction in moment capacity was expected due to post-tensioning losses prior to testing. This reduction was minor however, the worst case was seen in the test with NPDs and a steel reinforced joint where a reduction of 8% was measured.

Some slight damage to the timber was seen in the tests using a steel reinforced joint. This damage was minor and did not affect the performance of the joint. No significant damage was observed for the tests using screw reinforcing.

The effect of joint reinforcement on the effective shear stiffness of the joint zone was assessed using diagonal potentiometers. A comparison between the stiffness within and outside of the joint zone was made to assess the increase in stiffness obtained from the reinforcement. The data obtained was faulty for some tests. Representative values can still be obtained from the remaining data. The steel reinforcement option produced only minimal stiffness changes while the screw reinforcement increased stiffness by $20 - 30\%$.

The tests using the steel joint reinforcing were not designed to be fully re-centring while those using the screw reinforcing were not. This can be seen in the shape of the loops produced on the moment-rotation plots as well as in the residual displacements for each test. Additionally, due to the larger post-tensioning component of the moment, screw reinforced joints exhibited lower energy dissipation. This can be seen in the plots of energy dissipation per cycle and the hysteretic damping values for these tests.

The yield stiffness of the screw reinforced joints was approximately 50% larger than for the steel reinforced joint. This was due to the fact that the screws extended into the timber whereas steel reinforcing was only located at the surface. This increased stiffness will mean lower drifts in structures subjected to minor seismic events and could result in reduced damage to non-structural elements.

Chapter 5

Analytical and Numerical Modelling of Joints

This chapter outlines the modelling used to predict and assess the performance of beam column joint sub-assemblies. The observed behaviour of each joint tested is compared to the response of a non-linear computational model. The effect of dissipater connection slip was assessed using spring based analytical models.

5.1 Analytical Models of Localised Behaviour

5.1.1 Steel Reinforcement Plate Bending

Bending of the steel armouring plate was observed during testing. Bending was first seen to occur with the application of the post-tensioning load, prior to testing. This bending is shown in Figure 5.1. During testing, this caused the beam to rock about its centre rather than outer edges. Because of this, post-tensioning activation was delayed, limiting the performance of the joint detail. To ensure that the joint behaves effectively, it is necessary to consider the differential displacement of the plate when subjected to post-tensioning loading.

An analytical model has been created to investigate the effects of geometry and plate properties. The plate has been approximated as a symmetrical, two span, spring supported beam subjected to a Uniformly Distributed Load (UDL) over its entire length. While this is not strictly representative of the actual geometry, it gives an adequate approximation of behaviour for this comparison. The model derived the deformed shape of the plate from first principles. This derivation is shown in Appendix B. A schematic view of this model is shown in Figure 5.1. The plate will act against the column face, acting perpendicularly to the grain of the LVL. Because of the lower stiffness in this direction, the model neglected the contribution of the timber to assess the worst case scenario for differential displacement.

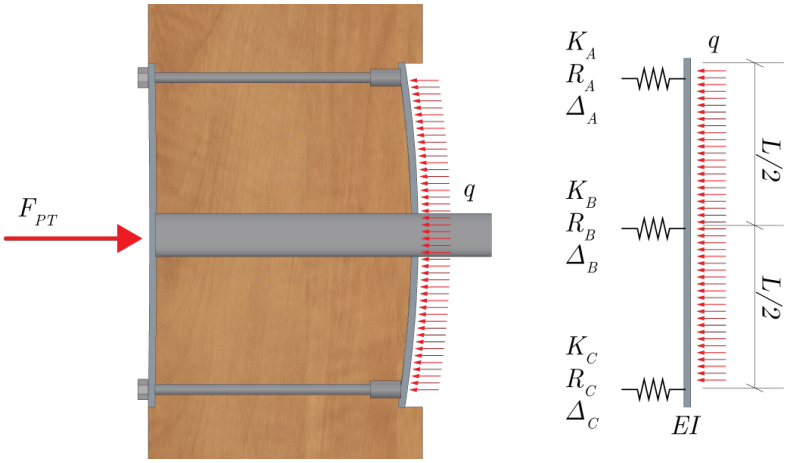

Figure 5.1: Bent plate resulting from post-tensioning forces

This model is used to provide recommendations to designers, assisting them to detail the bearing plate for a steel reinforced joint. The equations derived show that the differential displacement tends to zero when the stiffness of the central support is $3\frac{1}{3}$ times that of the outer supports. Relative displacements for a given plate thickness increase when stiffnesses vary from this value. This may cause the plate to bow when subjected to stresses induced by the post-tensioning forces.

5.1.2 Dissipation Device Performance

Spring based models of dissipaters were used to investigate dissipater performance. The model used springs in series to represent the displacement components of the dissipater. Bi-linear properties were assigned to the springs to capture yielding. Figure 5.2 shows a schematic view of the model used. The key parameters of the model are shown in Table 5.1. Elongation in each region of the dissipater was represented by a discrete spring. Spring constants were determined according to elastic theory, shown below

$$k_i = \frac{A_i E_i}{L_i}$$

The design of dissipation devices neglected elongation outside the necked region. The effect of including this additional deformation was investigated using the model.

Dissipater elongation in the transition zone was initially considered and found to be on the order of 0.1 - 0.2% of total displacement. Due to its small contribution to dissipater behaviour, this source of elongation has been neglected in the analysis.

The efficiency of each dissipater was determined by comparing the proportion of displacement from the yielding zone. As total displacement is governed by gap opening, this value represents the effectiveness of the dissipation unit in transforming a limited displacement to energy dissipation. Under this system, dissipation efficiency is largely governed by the distance from the necked zone to the supports (e.g bolts or threaded couplers).

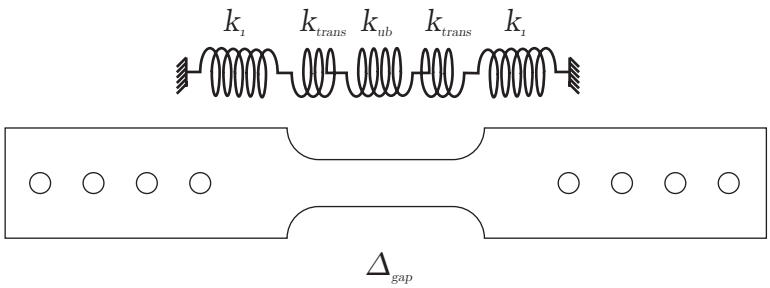

Figure 5.2: Details of spring model for dissipater displacement components

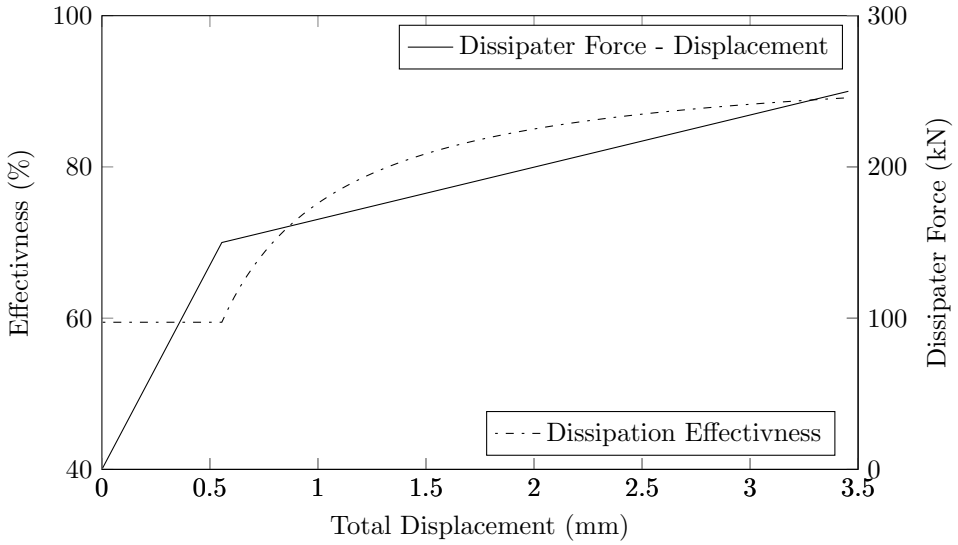

Figure 5.3: One result from the dissipater model

Table 5.1: Dissipater spring model parameters

Parameter	Description
A_1	Area of non-yielding region
A_{ub}	Area of unbonded region
L_1	Length of one non-yielding region
L_{ub}	Length of unbonded region
f_y	Yield Stress of dissipater

Each of the dissipater designs investigated in this programme was used as input to the model. This was used to assess the efficiency of each design over a range of dissipater displacements. The results of this are shown in Figure 5.4. The displacement corresponding to a 3.0% rotation in the

joint is marked in the plot by a cross[1].

The yield point of each dissipater is shown in Figure 5.4. Efficiencies remain constant up to the yield point; deformation is entirely elastic and is shared amongst each spring according to stiffness. In reality, all deformation below this displacement is elastic so no energy is dissipated. The dissipaters can be seen to yield at low displacements compared to their design levels. This is beneficial as it means that dissipation is maximised. Efficiency increases very sharply after yielding, asymptotically approaching 100%.

The second Plug and Play dissipater has far lower efficiency than the first tested, particularly at low displacements. This is due to the larger necked area resulting in later onset of yielding, and increased stiffness leading to lower elongation in the necked zone. Although still lower, this dissipater reached within 2% the efficiency and developed a higher force than that of Plug and Play 1.

In order to facilitate connection to the beam and column, the second NPD had a far greater length between the necked zone and fixity (L_1). This resulted in increased elastic deformations which delayed the onset of yielding and reduced ultimate efficiency. The decrease in efficiency of the Plug and Play dissipaters is minimal when displacements reach ultimate levels.

[1]The displacement for the Plug and Play dissipater with a 20 mm necked diameter was taken at a rotation of 2.1% as this corresponded to the ultimate strain capacity of the dissipater in the necked region.

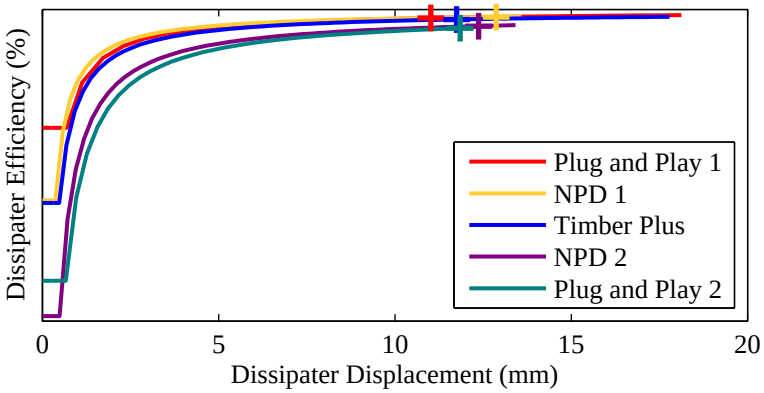

(a) Normal scale

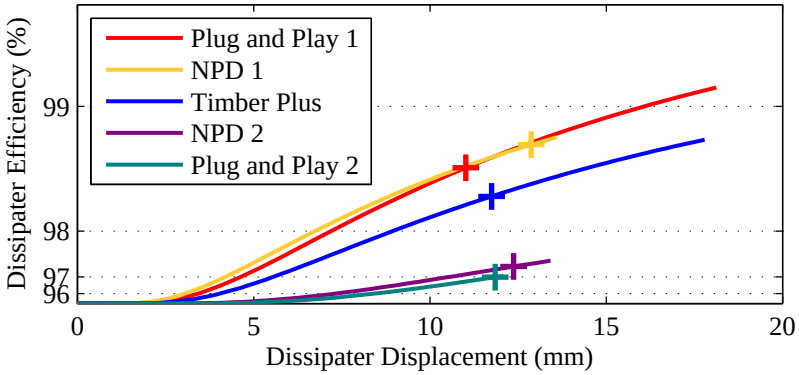

(b) Exponential scale

Figure 5.4: Comparison of dissipater efficiencies from analytical model (Cross represents dissipater displacement at 3.0% drift)

Table 5.2: Comparison of dissipater model results and parameters

Device	Specifications		Efficiency[a]
Plug and Play 1	$A_1 = 707\,\text{mm}^2$, $A_{ub} = 241\,\text{mm}^2$, $f_y = 500\,\text{MPa}$	$L_1 = 155\,\text{mm}$, $L_{ub} = 225\,\text{mm}$	98.6%
Plug and Play 2	$A_1 = 707\,\text{mm}^2$, $A_{ub} = 314\,\text{mm}^2$, $f_y = 500\,\text{MPa}$	$L_1 = 260\,\text{mm}$, $L_{ub} = 150\,\text{mm}$	96.9%
NPD 1	$A_1 = 1000\,\text{mm}^2$, $A_{ub} = 500\,\text{mm}^2$, $f_y = 300\,\text{MPa}$	$L_1 = 150\,\text{mm}$, $L_{ub} = 170\,\text{mm}$	98.7%
NPD 2	$A_1 = 1000\,\text{mm}^2$, $A_{ub} = 450\,\text{mm}^2$, $f_y = 300\,\text{MPa}$	$L_1 = 355\,\text{mm}$, $L_{ub} = 165\,\text{mm}$	97.2%
Timber Plus	$A_1 = 904\,\text{mm}^2$, $A_{ub} = 597\,\text{mm}^2$, $f_y = 300\,\text{MPa}$	$L_1 = 150\,\text{mm}$, $L_{ub} = 220\,\text{mm}$	98.5%

[a] Dissipater efficiency at 3% joint rotation

5.1.3 Performance Implications of Dissipater Connection Stiffness

The analytical model for dissipater performance described in Section 5.1.2 was extended to account for displacements due to connection slip and elongation. This was achieved by adding additional springs to account for these effects. The updated model is shown in Figure 5.5.

Some difficulty was found in estimating the stiffness of the connections designed for this programme. While design literature comprehensively covers the strengths of connection devices, stiffness properties are often given less attention. Where stiffness values were provided, these tended to be simple formulations providing rough estimates or in conflict with other results. Stiffness for each connection type are summarised in Table 5.3.

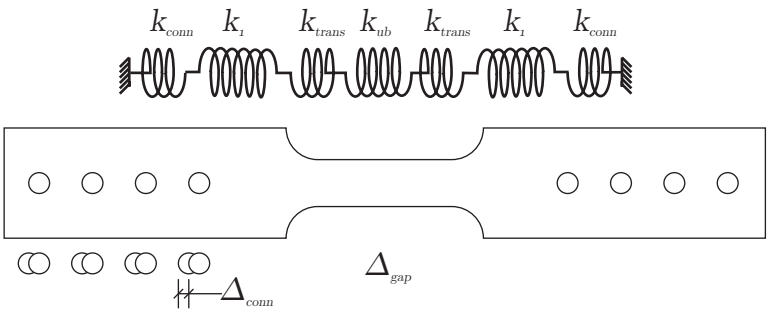

Figure 5.5: Details of spring model for dissipater displacement components, extended to account for connection displacements

Table 5.3: Connection stiffness formulations

Connection Type	Stiffness	Typical Stiffness (K_{conn})[a]
Threaded Couplers	None Given Assumed to be perfectly fixed.	∞[b]
Timber Rivets	1 kN/mm Per Rivet[c]	50.4 kN/mm
Inclined Screws	$K_{\text{ser}} = 780 d^{0.2} l_{\text{eff}}^{0.4}$ N/mm for Würth Screws (Würth GmbH & Co, 2011)	32.0 kN/mm for ZD Plates
ZD Connectors	$K_{\text{ser}} = 100$ kN/mm [d]	200 kN/mm

[a] Stiffness calculated inclusive of both beam and column connection for test specimen.
[b] Couplers assumed to be connected to rigid steel section passing through joint.
[c] The timber rivet design guide provides formulations for serviceability level displacements. However these are load dependent so do not give a unique stiffness value (Quenneville & Zarnani, 2013).
[d] For connections with additional screws perpendicular to the shear plane.

Connection stiffness' impact on the effectiveness of the dissipater designs used in this testing programme was assessed. Each connection stiffness was estimated using the formulations in Table 5.3. The proportion of total elongation from the necked region was assessed for a range of imposed displacements.

The results of this modelling show that the effectiveness of dissipation devices are heavily impacted by the rigidity of the connection systems used.

The change in efficiencies for each model is shown in Table 5.4. The Plug and Play connections were not impacted by this model as the threaded couplers used were assumed to be infinitely

rigid. Typical connection stiffness resulted in a drop in efficiency by 20-45%. This is obviously of great importance to designers and should be taken into consideration when specifying connection systems. The stiffnesses for screwed connections assumed that all load was carried in tension and neglected compression screws. The model ignores any slip in the connections, assuming all deformations are elastic. Any slip in the connections would further reduce the effectiveness of the dissipation devices attached.

Table 5.4: Result of connection stiffness model

Model	$E_{\text{ff,initial}}$	$E_{\text{ff,conn}}$	Change
Plug and Play 1	99 %	99 %	0 %
Plug and Play 1	97 %	97 %	0 %
NPD 1	99 %	66 %	−33 %
NPD 2	97 %	75 %	−22 %
Timber Plus	99 %	73 %	−26 %

Construction and fabrication tolerance issues may cause the dissipaters to slip before elongating. For designs where this was an issue, this slip was expected to be around 1 to 2 mm. The connection with the ZD plates was most at risk of slippage while no slip was expected for threaded couplers or rivets. The effect of this slip on the ZD plates is shown in Figure 5.6. This shows that even a modest slip of 2 mm can reduce the efficiency of the dissipater by around 10%, highlighting the importance of understanding and controlling construction tolerances.

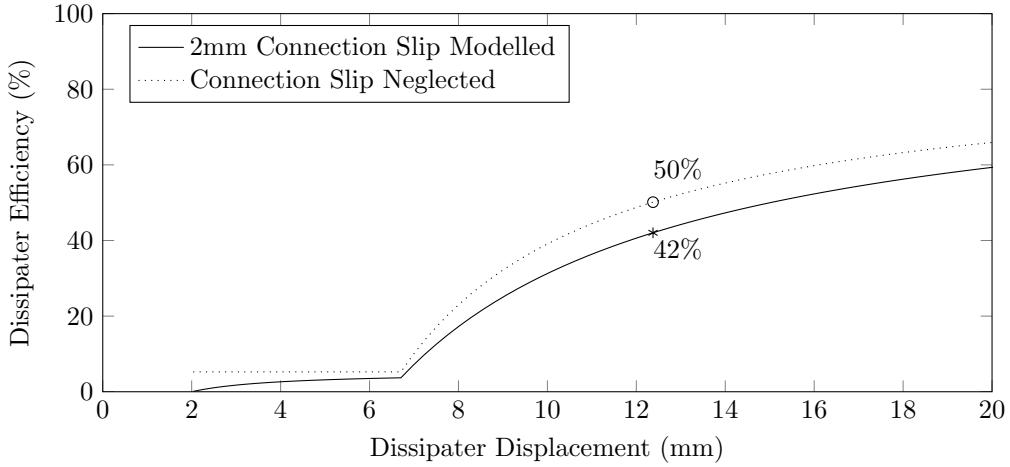

Figure 5.6: Effect of joint slip on ZD connector

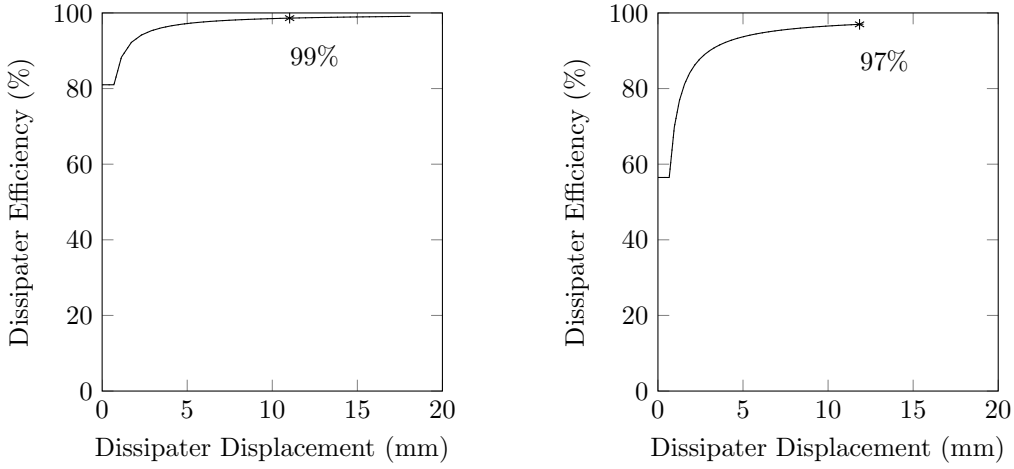

(a) Plug and Play 1

(b) Plug and Play 2

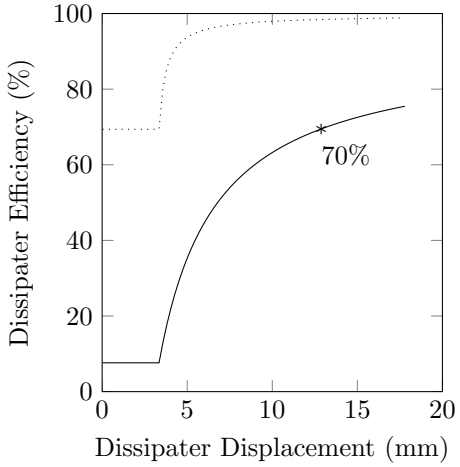

(c) NPD 1

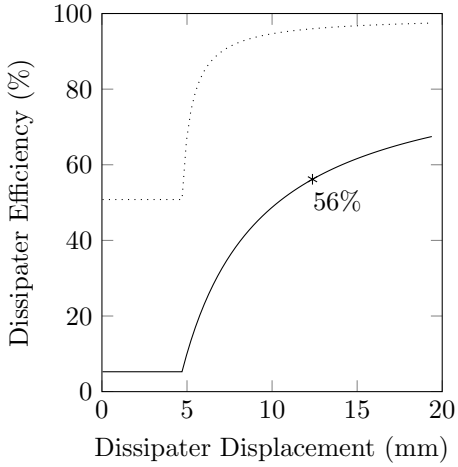

(d) NPD 2

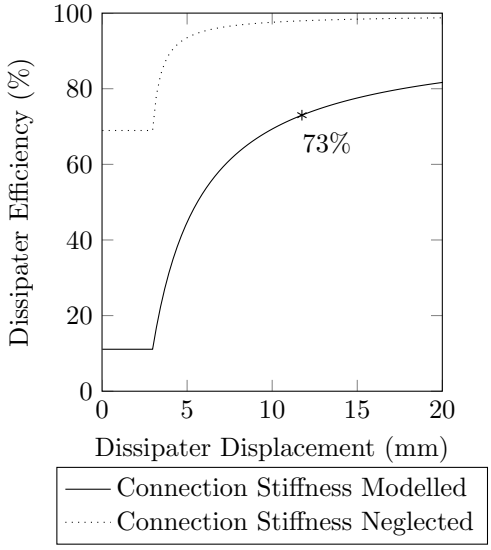

(e) Timber Plus

Figure 5.7: Reduction in dissipater efficiencies from connection flexibility

5.1.4 Neutral Axis Depths

The neutral axis depth determined from the MMBA design procedure was compared to that identified in the tests. The analytical solution is overlaid on the plots in Figures 5.8 to 5.13.

The analytical procedure for the steel reinforced joint without dissipation, shown in Figure 5.8, shows a general agreement with the envelope of recorded data. This matches reasonably well for large displacements, when the variance in the data decreases.

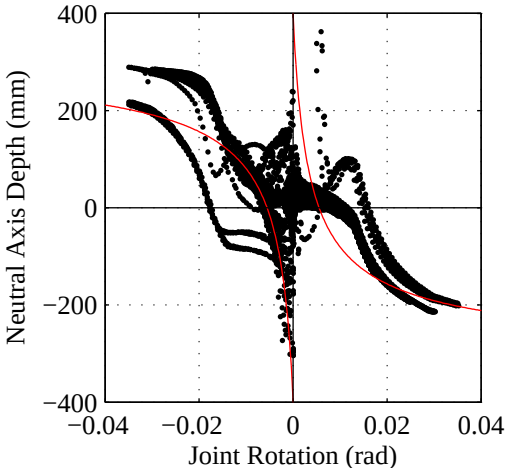

Figure 5.8: Observed neutral axis depth vs MMBA procedure for steel reinforced joint with no additional dissipation (A-B)

The neutral axis depth from tests with steel joint armoring and Plug and Play dissipation is shown in Figure 5.9. This data shows generally good agreement at large drift levels. At low drifts the data obtained is more scattered and the correlation with predictions from the MMBA procedure is worse. This is thought to be due to the limitations of instrumentation used to derive the neural axis depth in the beam during testing.

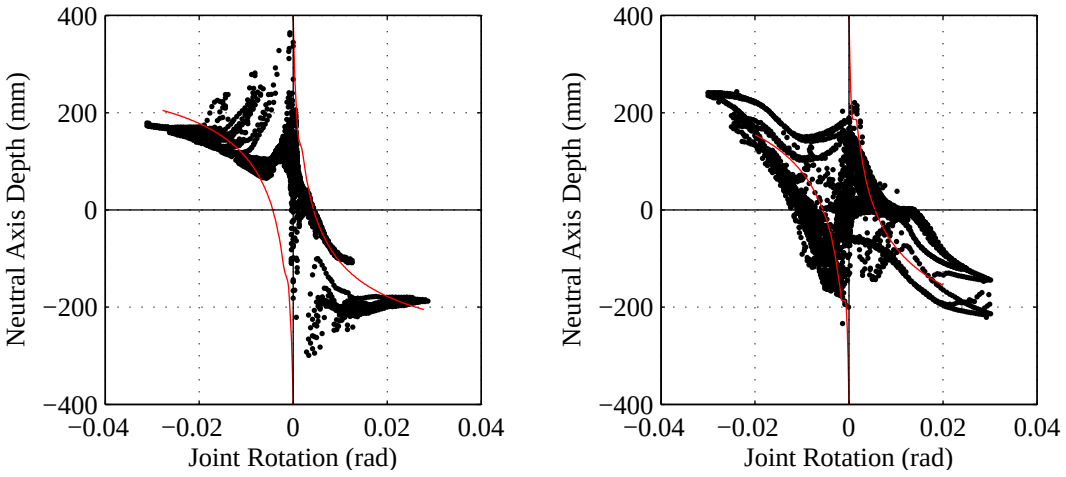

(a) A-P1 (b) A-P2

Figure 5.9: Observed neutral axis depth vs MMBA procedure for steel reinforced joint with Plug and Play dissipation

The neutral axis depth observed in the test using a steel reinforced joint with NPDs shows very poor correlation to the MMBA procedure. This is seen in Figure 5.10. The high degree of scatter in the first test makes determining a trend impossible. At large displacements there is a slight trend toward the locations of the shim plates at $\pm$ 200 mm.

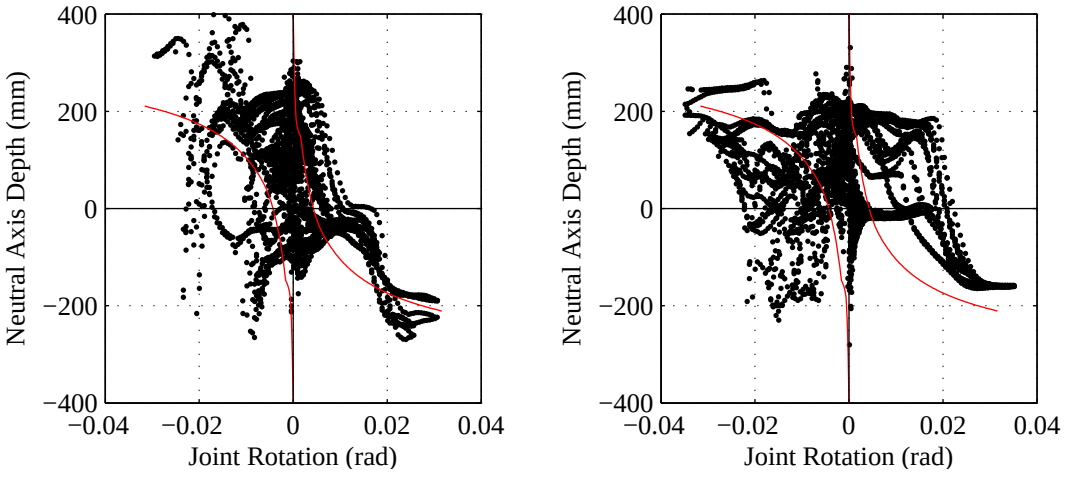

(a) A-D1 (b) A-D2

Figure 5.10: Observed neutral axis depth vs MMBA procedure for steel reinforced joint with NPDs

The tests from the screw reinforced joint without dissipation, shown in Figure 5.11, display tendencies towards the MMBA procedure's predictions. This is particularly true of the first test

where a definite trend is evident. In the second test this trend is less evident. However, some similarity between the predictions and observations remains. A trend toward the locations of shim plates is also evident in the data.

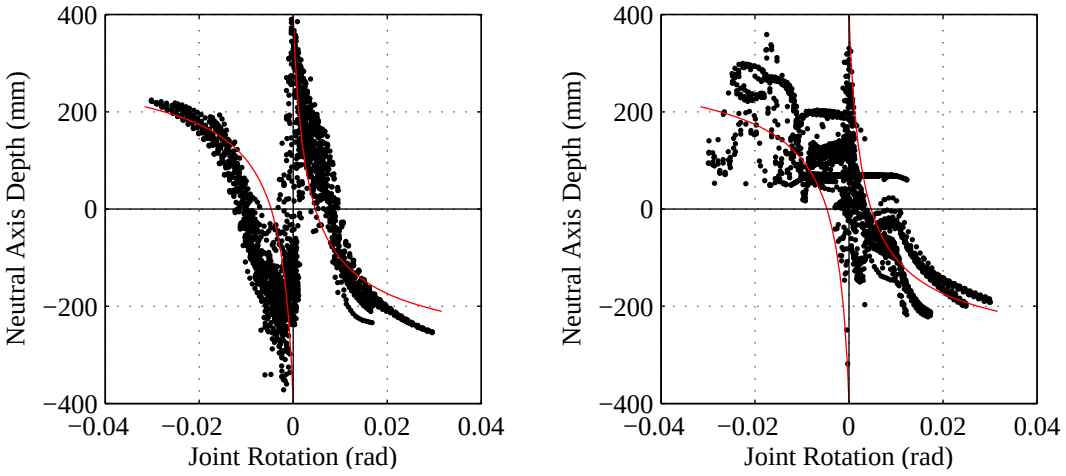

(a) B-B1 (b) B-B2

Figure 5.11: Observed neutral axis depth vs MMBA procedure for screw reinforced joint with no additional dissipation

The first of the tests of the Screw reinforced joint with NPDs shown in Figure 5.12 shows a slight match to predictions. Observed points are clustered around the MMBA procedure results large displacements Significant errors introduced from the measurement apparatus are evident however.

The second of the tests shows no clear match to the data. For large negative displacements in this test, the neutral axis depth is seen to tend to the mid point of the section. This is thought to be erroneous, particularly as, due to the heel-and-toe rocking plates, there is no contact between the beam and column at this location.

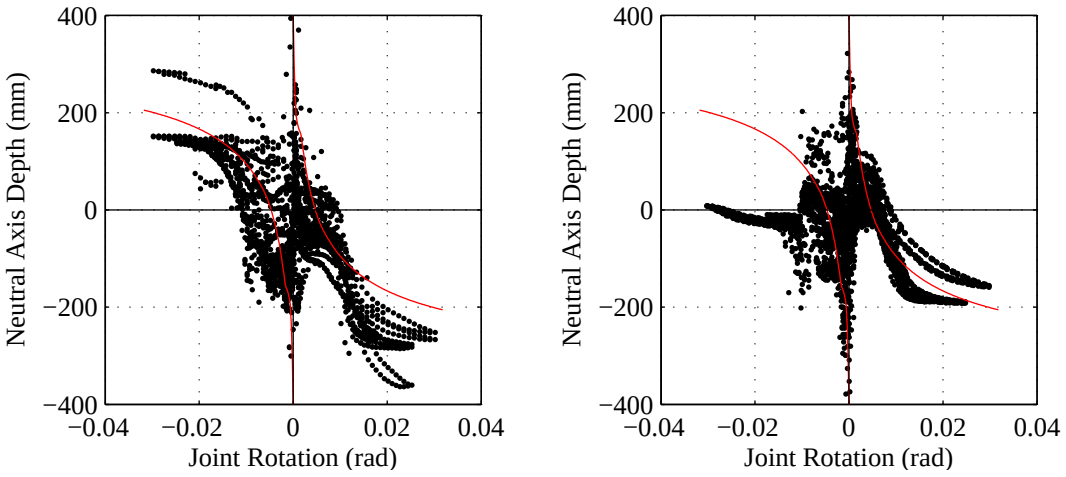

(a) B-D1 (b) B-D2

Figure 5.12: Observed neutral axis depth vs MMBA procedure for screw reinforced joint with NPDs

The data for the Screw reinforced joint with Timber Plus dissipation shown in Figure 5.13 is highly scattered. No clear trend toward the anticipated results can be seen in the data. The increased scatter in the data for this test is thought to be due to the fact that potentiometers were mounted to the timber blocks of the dissipaters rather than directly to the column.

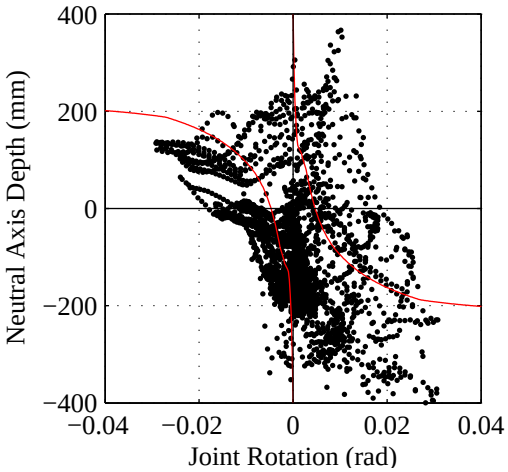

Figure 5.13: Observed neutral axis depth vs MMBA procedure for screw reinforced joint with Timber Plus dissipation

Data obtained for the neutral axis depth in the beam was highly variable. Accordingly, only qualitative matches to MMBA predictions were made. In many cases, the data could be seen to trend towards predictions, particularly at large rotations. The impact of the shim plates

can be seen in the data from many of the specimens, with clear trends to ±200 mm at large displacements. For other cases, no match could be observed. These discrepancies are largely due to inadequacies in the measurement techniques for determining the neutral axis depth and are not thought to reflect behaviour in the specimen.

5.2 Numerical Modelling of Joints

Numerical models of the beam column sub-assembly were created. The computer program Ruaumoko (Carr, 2008) was used to solve these models. The beam and column were modelled using elastic beam elements, and required only section and material properties. Modelling of the joint behaviour was achieved using non-linear rotational springs in parallel to simulate the contributions of the post-tensioning and mild steel components. Post-tensioning was modelled using bi-linear elastic springs while yielding steel was modelled with bi-linear plastic springs. The shear rotation inside the joint panel zone was represented using a rotational spring and rigid elements. A schematic overview of the model used is shown in Figure 5.14.

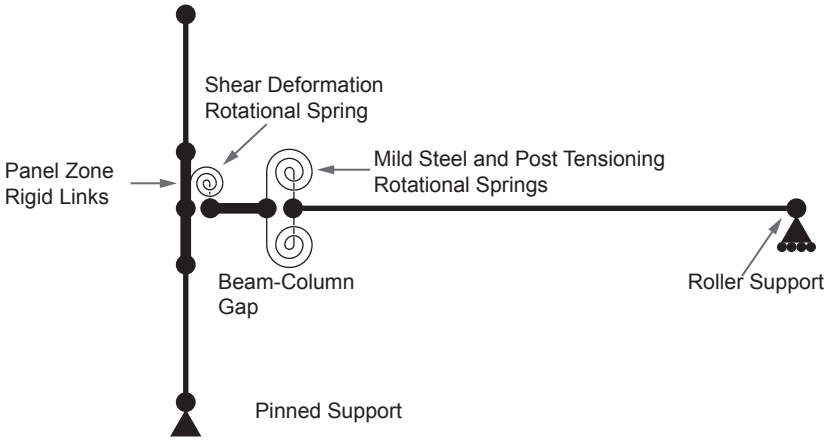

Figure 5.14: Schematic view of numerical joint sub assembly model

Conclusions from literature (Newcombe *et al.*, 2010d, Cusiel *et al.*, 2010) have shown that lumped plasticity models using rotational springs at joints achieve satisfactory levels of accuracy to model global frame behaviour. These models are comprised of two infinitesimally small rotational springs at each gap interface, modelling either the post-tensioning or mild steel dissipation. The properties of these springs are calibrated based on the backbone hysteresis curves of each component as calculated using the analytical methods described above. An alternative to rotational springs are models which use multi-spring elements. These are more difficult and time consuming to implement and calibrate and do not achieve significant gains in accuracy for frame behaviour (Newcombe *et al.*, 2010d). Due to these factors, predictive models for experimental testing use the rotational spring method.

Predictive models were created before each experimental test. These were based on the results of an MMBA procedure. This produced moment rotation behaviour for the mild steel and post-tensioning components of the joint. A bi-linear function was fitted to each constituent. This

procedure gave the yield moment (M_y), initial stiffness (k_0), and post yield stiffness reduction factor (r) for each of the non linear springs in the model. A summary of the parameters used is given in Table 5.5.

Table 5.5: Predictive numerical model spring parameters

Model	Post-Tensioning			Mild Steel		
	M_y (kNm)	k_0 (MNm/rad)	r	M_y (Nm)	k_0 (MNm/rad)	r
A-B	162	347	0.016	1	0	0.018
A-D	189	413	0.009	214	137	0.024
A-P1[a]	186	387	0.017	240	130	0.017
A-P2	170	617	0.019	314	219	0.019
B-B	201	383	0.011	1	0	0.018
B-D	202	436	0.009	193	116	0.025
B-TP	213	449	0.007	179	72	0.042

[a] A-P1 and A-P2 used different dissipater diameters (17.5 mm vs 20 mm) so separate models were created

Some discrepancy between the predictive models and observed data is due to variances in post-tensioning force. Post-tensioning force was measured during the stressing operation. This force is applied to the column through steel wedges which fit into anchor blocks. These wedges were hit back into the anchor block before the force was released from the jack. The force applied after releasing was heavily dependant on these wedges, sometimes dropping by as much as 25 kN. Post-tensioning force was also seen to vary daily by as much as 15 kN. As discussed in Chapter 4, this was apparently heavily dependant on temperature and humidity.

Updated models were created following each test. These used recorded post-tensioning forces at the start of testing to generate the parameters used in the models. This was done to compare the difference between the predictive models, useful in design and models of actual conditions.

5.3 Comparison of Tests to Model Results

The figures below show a comparison between experimental observations and output from the model. Two models are shown for each specimen; the predictive model made prior to testing, and, an updated model using accurate post-tensioning values.

5.3.1 Tests A-B: Steel Reinforced Joint with no Additional Dissipation

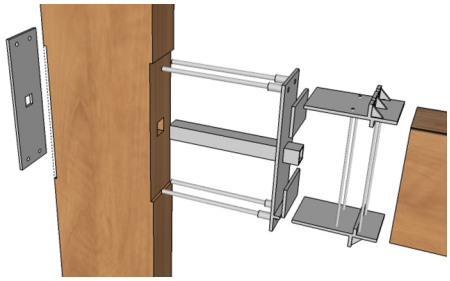

Steel reinforced joint with no dissipation

The moment-rotation response of the steel reinforced joint without additional dissipation devices is shown in Figure 5.15. The ultimate moment capacities of the model and observed data agree quite well, although the model tends to over-estimate slightly. The observed stiffness to yield for this joint is much less than the model. The increased displacement is likely to be due to the shear stiffness of the joint being lower than expected. This results in a later onset of yielding. In a structure, this is likely to result in larger drifts for Serviceability Limit State (SLS) events.

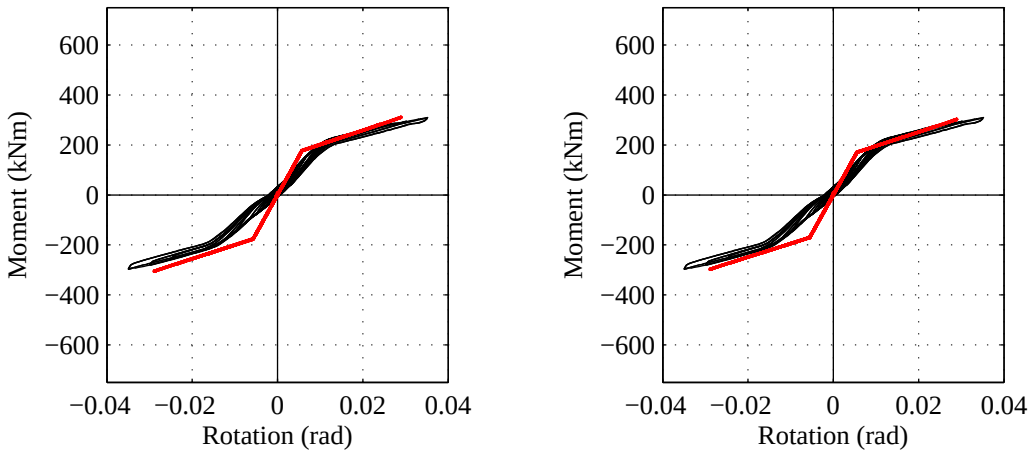

(a) pre experiment

(b) Post experiment

Figure 5.15: Model vs experimental results for steel reinforced joint with no dissipation.

5.3.2 Tests A-P: Steel Reinforced Joint with Plug and Play Dissipation

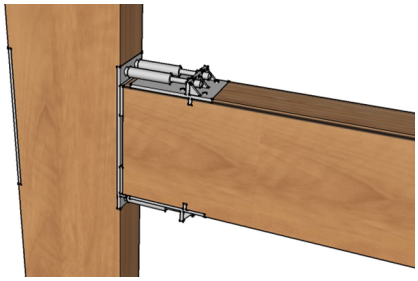

Steel reinforced joint with Plug and Play dissipation

The moment-rotation behaviour of the joint with the Plug and Play dissipation is shown in Figure 5.16. There is good agreement between experimental and model moment capacity. The pre-yield stiffness of is modelled quite accurately for this joint detail. The secant stiffness to yield point is in good agreement when visually comparing the predictions to the data.

Initial stiffness match well for low drift cycles. After excursions to large drifts, stiffness does not match as well because the system is not fully re-centring.

The initial unloading behaviour seen in the experiments is reflected in the models. Observed initial unloading stiffness match the model well. Later in the unloading cycle, the models are less accurate. This results in an under prediction of the energy dissipated by the system as well as the residual displacements. This is due to the bi-linear approximations used in the model failing to capture the full curve. Straight line approximations are seen instead. These errors are particularly apparent after large displacement cycles. Bauschinger effects need to be modelled by the spring model for dissipaters to capture this cyclic softening behaviour. The added complexity of such a model was not deemed to be justified for a small increase in accuracy on unloading cycles.

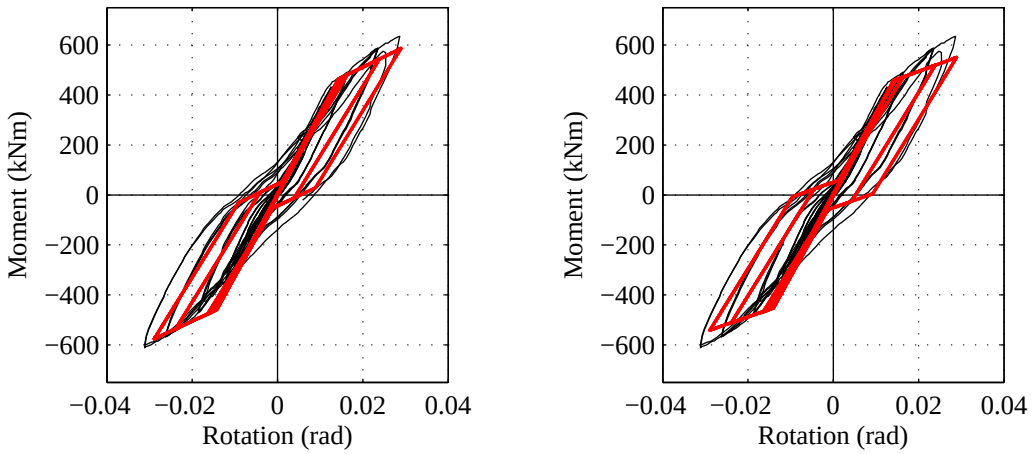

(a) A-P1 - pre experiment

(b) A-P1 - updated

Figure 5.16: Model vs experimental results for steel reinforced joint with Plug and Play dissipation.

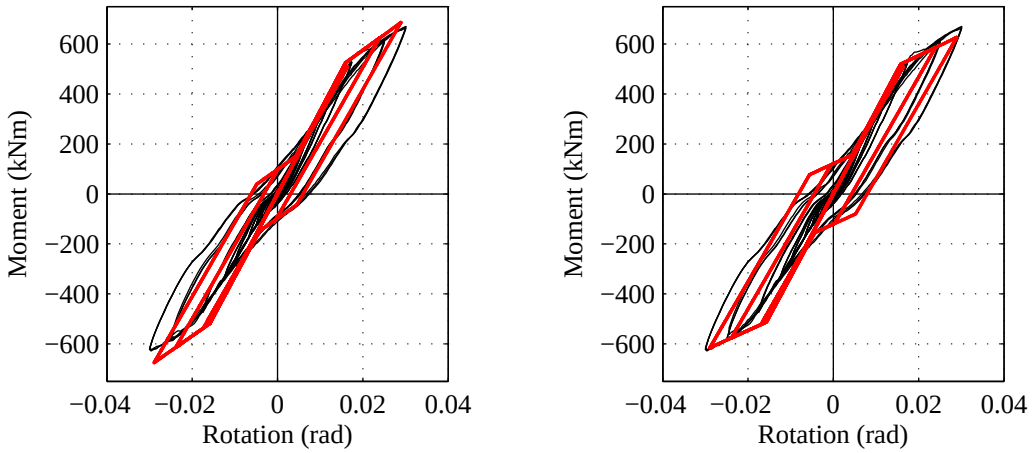

(a) A-P2 - pre experiment

(b) A-P2 - updated

Figure 5.17: Model vs experimental results for steel reinforced joint with Plug and Play dissipation.

5.3.3 Tests A-D : Steel Reinforced Joint with Necked Plate Dissipaters on Riveted Plates

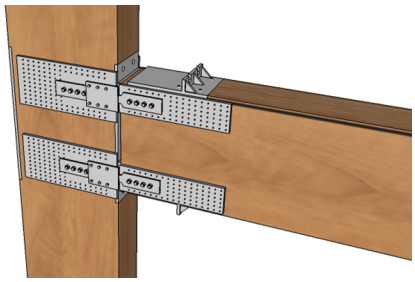

Steel reinforced joint with Necked Plate Dissipaters

The ultimate moment capacity is well predicted by both models. The initial model predicted an ultimate moment of 534 kNm, compared to an observed moment capacity of 532 kNm, a difference of 0.4%. Interestingly, the initial predictive model matched the ultimate moment better than the updated model. This suggests that material properties were conservative in the model's inputs. This produced a discrepancy between the model and observation of 4%. This is a small difference and is likely due to stochastic differences in material properties.

The reduction in stiffness observed during yielding of this specimen was more gradual than predicted by the model. This leads to an overestimation of the area contained within each cycle.

Residual displacements were larger than predicted. After large displacement cycles, residual displacements in the order of 22 mm were present. This was double that predicted by the model.

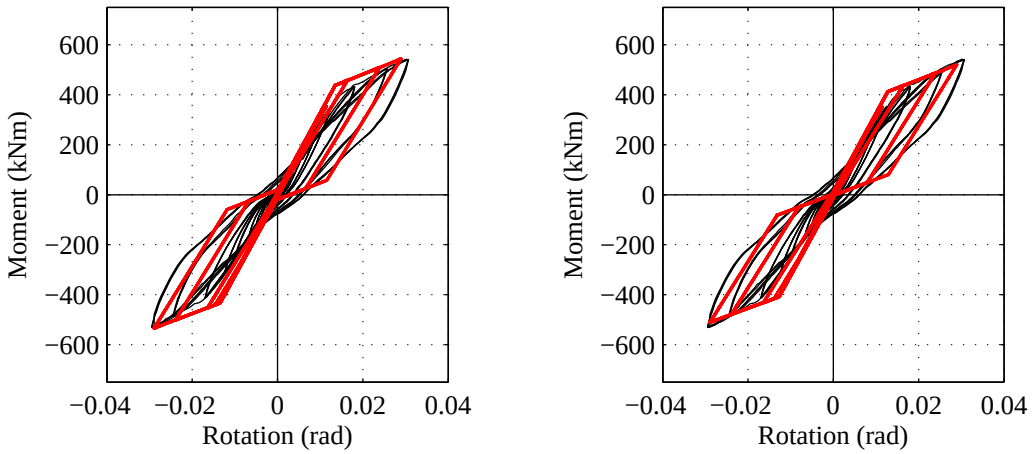

(a) A-D1 - pre experiment

(b) A-D1 - updated

Figure 5.18: Model vs experimental results for steel reinforced joint with NPDs.

The second test, shown in Figure 5.19, was run to 3.5% drift. The model is in good agreement with the 3.0% moment although it tends to over predict stiffness.

The models predicted a sharp change in unloading stiffness at gap closing. In practice, the change was more gradual, leading to increased residual displacements. Neither model accurately predicted the residual displacements observed in these tests.

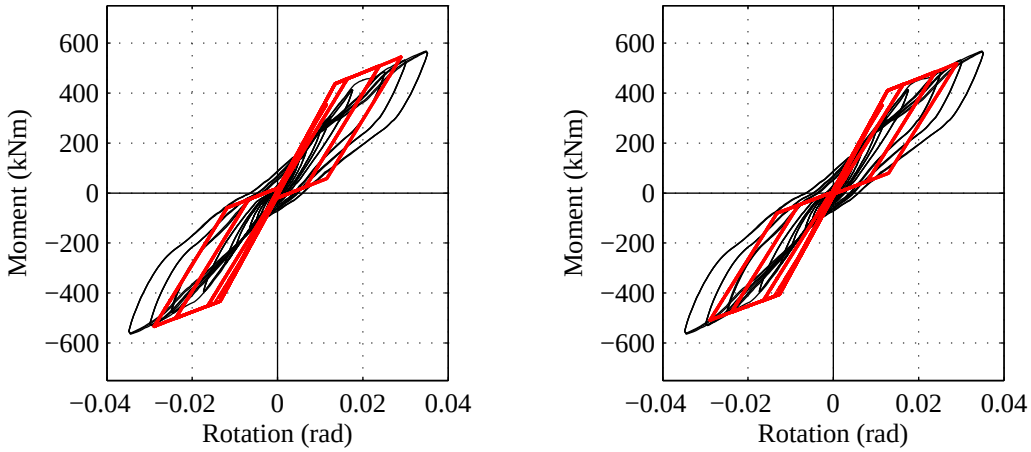

(a) A-D2 - pre experiment

(b) A-D2 - updated

Figure 5.19: Model vs experimental results for steel reinforced joint with NPDs.

5.3.4 Tests B-B: Screw Reinforced Joint with No Additional Dissipation

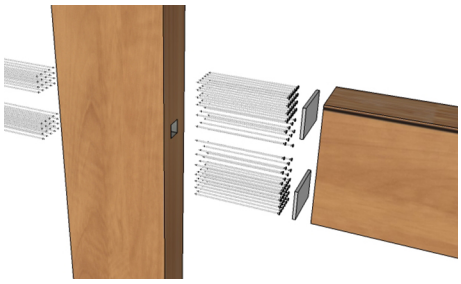

Screw reinforced joint with no dissipation

The models for screw reinforced joints with no additional dissipative elements shown in Figures 5.20 and 5.21 predict behaviour well. Both the pre-yield and post-yield stiffness are accurately captured. A slight asymmetry of response can be seen in Figure 5.20 where both models under predict the magnitude of the negative moment. In all cases, the ultimate moment is within 6% of that observed. The model predicts the yield point of this specimen's response accurately.

As there is no influence from dissipative elements in these specimens, behaviour is essentially governed by post-tensioning. The models updated to include more accurate post-tensioning values can be seen to more closely match the moment-rotation behaviour observed in the tests.

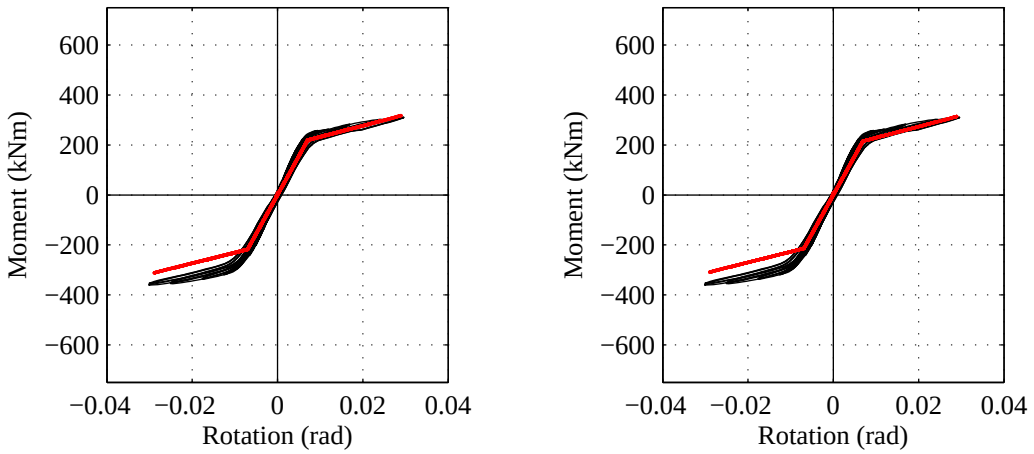

(a) B-B1 - pre experiment

(b) B-B1 - updated

Figure 5.20: Model vs experimental results for first test of screw reinforced joint with no dissipation.

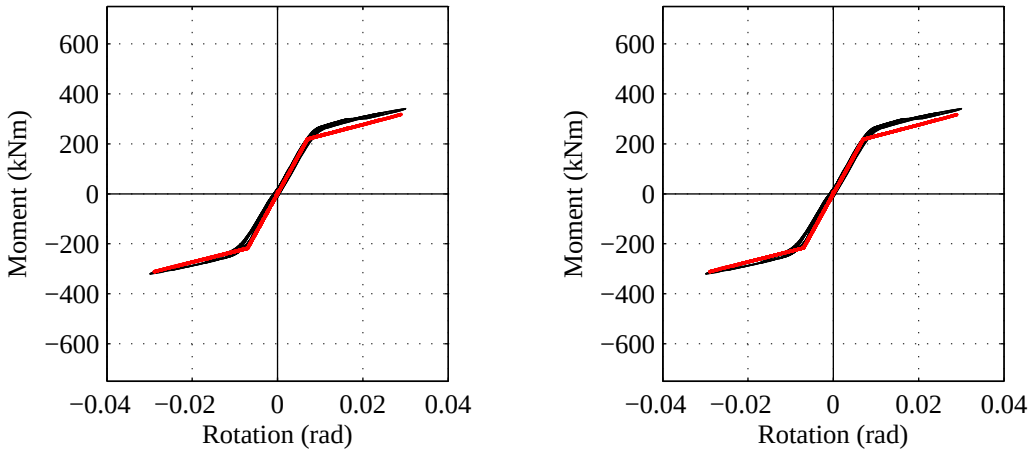

(a) B-B2 - pre experiment

(b) B-B2 - Updated

Figure 5.21: Model vs experimental results for second test of screw reinforced joint with no dissipation.

5.3.5 Tests B-D : Screw Reinforced Joint with Necked Plate Dissipaters on Screw in Devices

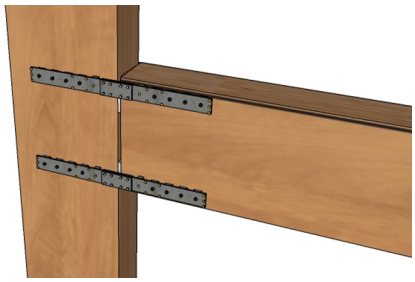

Screw reinforced joint with Necked Plate Dissipaters

The initial stiffness and yield points are captured well by the models.

The post yield stiffness and ultimate moments are generally captured well by the models. There is some asymmetry in the tests which was not described in the models. This has lead to an under prediction of the post-yield stiffness and moment capacity of the joints for one direction.

The initial unloading stiffness matches that predicted by the model well. Further along the unloading curve the accuracy of this match decreases as the observed unloading stiffness decreases. While buckling of the dissipaters was observed in the tests, if this did occur and was not seen, it may explain the softening behaviour.

The residual displacements recorded in the specimen after each cycle are captured well by the model. There are however some small residual displacements following large displacement cycles that were not predicted by the model.

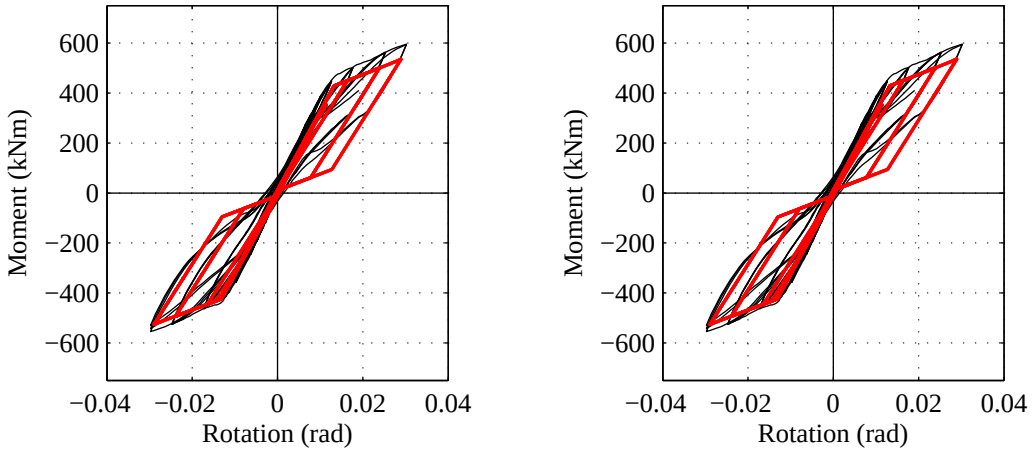

(a) B-D1 - pre experiment

(b) B-D1 - updated

Figure 5.22: Models vs experimental results for first test of screw reinforced joint with NPDs.

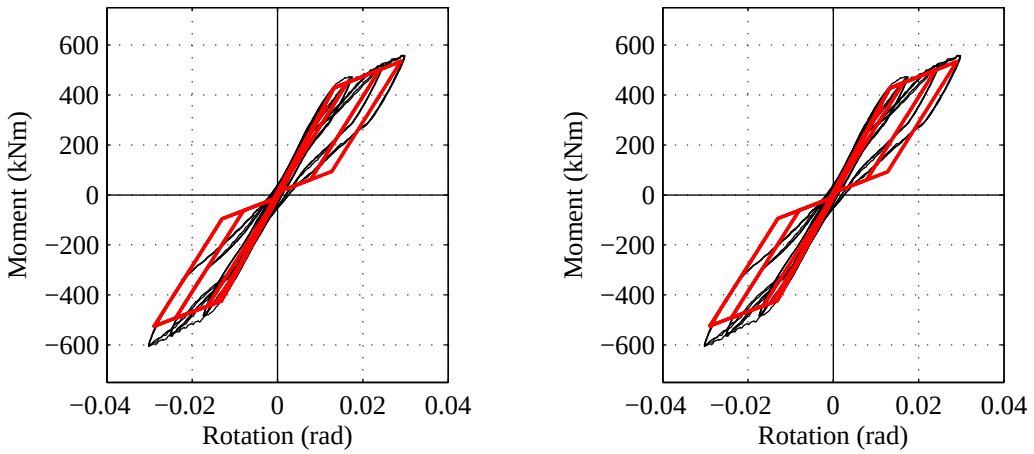

(a) B-D2 - pre experiment

(b) B-D2 - updated

Figure 5.23: Model vs experimental results for second test of screw reinforced joint with NPDs.

5.3.6 Tests B-TP : Screw Reinforced Joint with Timber Encased Threaded Rod Dissipation

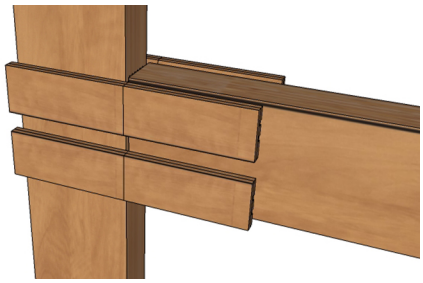

Screw Reinforced joint with Timber Plus dissipaters

The model for the screw reinforced joint with Timber Encased Threaded Rod Dissipation is shown in Figure 5.24. The initial stiffness observed in the test closely matches that predicted by the model. The post-yield stiffness is much larger than that predicted by the model. This is thought to be due to compression being carried by the dissipater blocks as well as the beam column interface.

The residual displacement is well predicted by the model for low cycles. There are however some minor residual displacements which are not captured by the model for cycles to larger drifts.

The unloading stiffness initially matches the model well. The observed stiffness decreases further along the unloading curve, reducing the accuracy of the model.

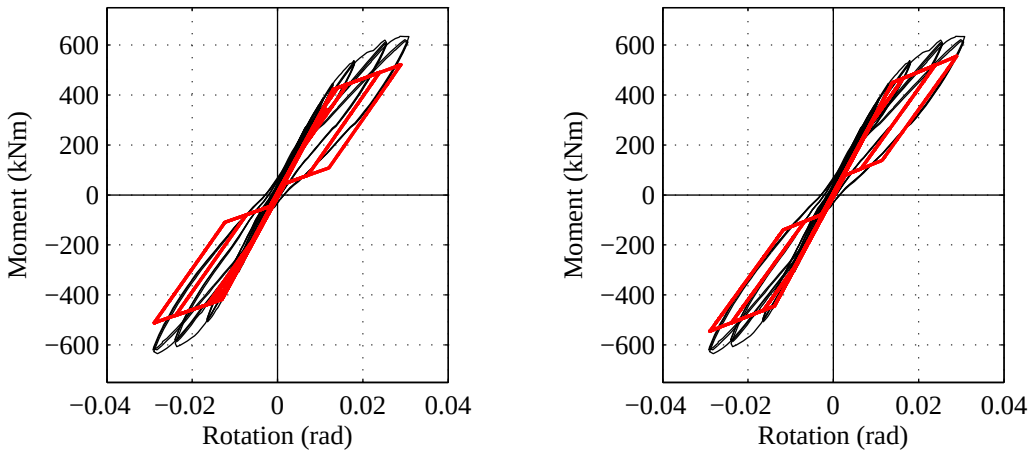

(a) B-TP - Pre experiment

(b) B-TP - updated

Figure 5.24: Model vs experimental results for screw reinforced joint with Timber Plus dissipation

5.3.7 Comparisons

Moment capacity

The models shown above have tendency to slightly underestimate the moment capacity of the joint at ultimate drift levels. As shown in Table 5.6, this was less than 10% for all tests except the joint with Timber Plus dissipaters. This should be conservative when used for the design of structures.

Table 5.6: Data vs. model comparison for moment at 3.0% drift (kNm)

Model	Predictive Model			Updated Model		
	Experiment	Model	Difference	Experiment	Model	Difference
A-B	286	306	7%	286	298	4%
A-P	631	675	7%	631	615	-4%
A-D	532	534	0%	532	509	-4%
B-B	331	312	-6%	331	309	-7%
B-D	567	525	-7%	567	526	-7%
B-TP	630	512	-9%	630	545	-13%

Yield drift

Yield drift was generally under-predicted by the model. This is shown in Table 5.7. This increase in yield above levels assumed by designers will reduce the effectiveness of dissipative elements. Slop in dissipater connections may have caused some of this increase. The numerical models used are unable to account for this phenomenon. Designers should therefore consider how sensitive their structures are to this parameter.

Table 5.7: Data vs. model comparison for yield drift (%)

Model	Predictive Model			Updated Model		
	Experiment	Model	Difference	Experiment	Model	Difference
A-B	1.00%	0.56%	-44%	1.00%	0.55%	45%
A-P	1.50%	1.59%	6%	1.50%	1.56%	4%
A-D	1.80%	1.34%	-26%	1.80%	1.27%	-29%
B-B	0.80%	0.71%	-11%	0.80%	0.73%	-9%
B-D	1.20%	1.33%	11%	1.20%	1.34%	12%
B-TP	1.80%	1.31%	-27%	1.80%	1.38%	-23%

Stiffness

The initial stiffness is generally well predicted by the models. In this range, the elastic properties of the LVL govern behaviour. For systems with yielding mild-steel dissipaters, the decrease in stiffness is often spread over a wider range of rotations meaning that the bi-linear stiffness of the model only captures this behaviour up to the point of first-yielding. A comparison between model and experimental stiffnesses is shown in Table 5.8. This table shows the models generally over-predicting yield stiffness. This is due to the secant stiffness being shown for the experimental values, which exhibit a gradual reduction in stiffness compared to the instantaneous reduction from the numerical models.

Table 5.8: Data vs. model comparison for yield stiffness (MNm/rad)

Model	Predictive Model			Updated Model		
	Experiment	Model	Difference	Experiment	Model	Difference
A-B	21.5	30.2	40%	21.5	30.2	40%
A-P	34.2	31.7	-7%	34.2	31.6	-8%
A-D	27.5	31.1	13%	27.5	31.1	13%
B-B	32.1	30.5	-5%	32.1	30.4	-5%
B-D	38.4	31.1	-19%	38.4	31.1	-19%
B-TP	38.0	31.1	-18%	38.0	31.2	-20%

Residual displacements

The models under-predict residual displacements of the specimens. A comparison between model and experimental values is shown in Table 5.9. Where designers are targeting full re-centring, this may lead to unconservative designs. To counteract this, a larger re-centring ratio could be targeted in design or a more accurate steel hysteresis model used.

Table 5.9: Data vs. model comparison for residual displacement (mm)

Model	Predictive Model			Updated Model		
	Experiment	Model	Difference	Experiment	Model	Difference
A-B	2	0		2	0	-
A-P	25	22	-12%	25	29	16%
A-D	22	11	-50%	22	3	-86%
B-B	3	0	-	3	0	-
B-D	8	2	-75%	8	2	-75%
B-TP	6	2	-67%	6	1	-83%

Damping

There were significant discrepancies between the hysteretic damping predicted by the model compared to that calculated from the experimental data. A comparison between the model and experimental values is given in Table 5.10. Error was generally reduced for the the updated models.

The models predicted very low damping for specimens without additional energy dissipation. Damping of around 2% was seen in the data. The numerical model used was not sufficiently complex to predict this phenomenon.

The error in the model ranged from 15-45% for tests with additional damping. Error was lower in the models for steel reinforced joints. This aligns with the comparison with damping relationships to ductility and re-centring ratio shown in Chapter 4.

Backbone force-displacement curves were captured with reasonable accuracy by the model for most specimens. The unloading behaviour of the models was not as representative of observed behaviour. This is likely to account for most of the error in hysteretic damping values produced from the model.

Table 5.10: Data vs. model comparison for hysteretic damping (%)

Model	Predictive Model			Updated Model		
	Experiment	Model	Difference	Experiment	Model	Difference
A-B	2.6%	0.1%	-98%	2.6%	0.0%	-99%
A-P	10.9%	8.6%	-21%	10.9%	10.9%	1%
A-D	9.0%	10.6%	17%	9.0%	10.5%	17%
B-B	1.9%	0.0%	-97%	1.9%	0.0%	-99%
B-D	6.9%	9.7%	42%	6.9%	9.7%	42%
B-TP	6.2%	8.8%	42%	6.2%	7.2%	16%

Post-Tensioning

The post-tensioning force varied from day to day and was never exactly what was specified by the design. The force was measured, enabling refined models to be created, compensating for these differences. Details of the differences are given in Table 5.11. As the maximum variation in

post-tensioning force was less than 5%, this is not expected to significantly alter the performance of the joint. In the interests of completeness however, modifications to the stiffness of the post-tensioning spring were made and the simulations were re-run.

Table 5.11: Initial post-tensioning force comparison

Test	Post-Tensioning (kN)			PT Spring Stiffness (MN/rad)		
	Model	Actual	Difference	Model	Revised	Difference
A-B2	750	739	−1 %	347	334	−4 %
A-P1	750	716	−5 %	387	375	−3 %
A-P2	750	721	−4 %	617	595	−3 %
A-D1	750	718	−4 %	413	405	−2 %
A-D2	750	741	−1 %	413	401	−3 %
B-B1	810	732	−10 %	383	376	−2 %
B-B2	810	793	−2 %	383	381	−1 %
B-D1	810	804	−1 %	436	437	0 %
B-D2	810	812	0 %	436	433	−1 %
B-TP	810	803	−1 %	449	523	16 %

5.4 Limitations of Models

As discussed in Chapter 4, after yielding, there were significant differences between the first excursion to a drift level and later cycles. The causes of this decrease are not well quantified but are likley due to a combination of inelastic timber compression and dissipater connection slip. The simple bi-linear models used in the predictive models described above fail to capture this behaviour. A more complex model could be developed, using non-linear multi-spring elements for local timber behaviour and non-linear springs modelling connection slip. This was not deemed necessary for the design engineers as the observed reductions in stiffness occurred for large displacement cycles and had little effect on the maximum moment achieved.

5.5 Additional Joint Configuration

The joint models developed above were used to predict the performance of an additional joint configuration. A screw reinforced joint with Plug and Play dissipation, attached by timber rivets was proposed. This combination of joint reinforcement and energy dissipation system was not experimentally tested but has the potential to perform well. As this joint used screw reinforcement, it was designed to the re-centring ratio requirements of the B series joint. This joint achieved better re-centring performance through an increase in initial post-tensioning force and a reduction in the effect of the dissipative steel elements. Because of this, the contribution of the dissipative elements will be reduced when compared to the other joint details. The joint was designed to achieve a similar moment capacity to the design requirements provided in Section 3.3.

Details of the joint are shown in Figure 5.25. Anchorages are comprised of a 200 PFC (Parallel Flange Channel) section riveted to the beam or column. The dissipaters are connected to these anchorages by a washer and lock nut system. This design allows for simplified assembly on site as tolerance issues are reduced.

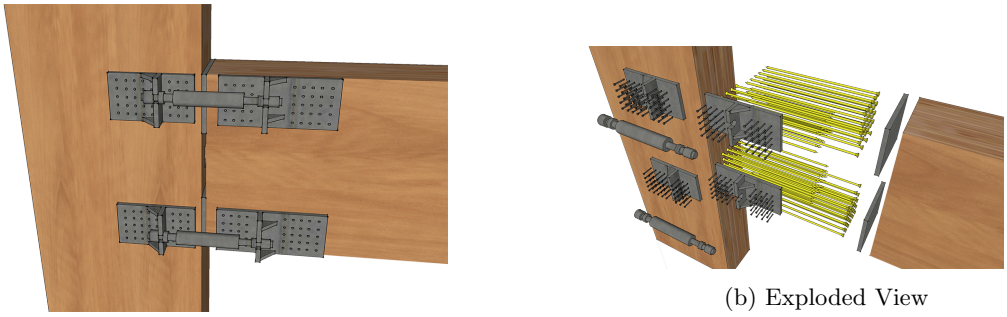

(a) Outline

(b) Exploded View

Figure 5.25: Details of screw reinforced joint with riveted Plug and Play dissipaters

The modelled performance of this joint configuration is shown in Figure 5.26. This shows the good re-centring performance expected of this design. Previous testing gives good confidence in the joint performing as predicted. However validation is required for this design.

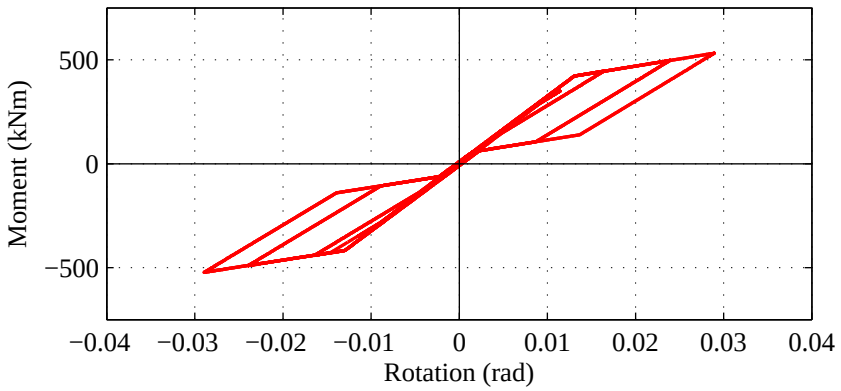

Figure 5.26: Predicted response of screw reinforced joint with Plug and Play dissipation

5.6 Conclusions

Numerical and analytical models have been created to investigate both joint and localised behaviour.

Predictions made on the basis of current design procedures were compared with experimental results. In general these models agreed well with the observed behaviour, capturing the initial stiffness and ultimate moment capacity well in most cases. The accuracy of the models was worse for predictions of residual displacement, yield rotation, and the area contained within loops for each cycle.

The models used did not capture the observed stiffness degradation observed for the second and subsequent cycles to maximum drift. More complex models have been proposed to capture this.

This added complexity was not deemed to be warranted for design by practising engineers.

The model was updated to use more accurate post-tensioning forces following testing. The model with updated parameters fits the observed data with greater accuracy. Results from the model using initial values fit the data with acceptable accuracy for most purposes.

An additional joint configuration has been proposed. This was not tested directly. However the individual components showed promise in other tests.

The length of dissipaters outside of the necked region decreases their initial efficiency. However, at large displacements, this effect diminishes. As these regions do not yield there is no effect on ductility.

Connection slip and connection stiffness can cause significant degradation in the performance of dissipation devices. Connections should be designed as stiffly as possible and sources of slip mitigated to prevent this.

Where steel armouring is used, the ratio of the stiffness between the central and outer support points should exceed 3.5 to prevent differential displacements. If this can not be achieved, the stiffness of the plate should be increased.

The data obtained for the neutral axis depth in the beam were highly scattered and, in some cases were thought to be erroneous due to imperfections in measurement techniques. Nevertheless, where good data were obtained, predictions derived from the MMBA were able to give reasonable estimates for the position of the neutral axis depth in the section. This was particularly true at large rotations.

Chapter 6

Recommendations for Design

This chapter summarises the findings of this research and provides suggestions to designers of Press-Lam beam column joints. The effect of uncertainties in design and construction on the joint's response are quantified. Joint reinforcement options are compared to ascertain the maximum moment capacity of several likely joint sizes. Connection options are assessed for a range of dissipater demands. Comparisons are made between designs for both joint reinforcement and dissipation connection.

6.1 Joint Design

6.1.1 Tolerances

It is important to consider the tolerances available for each variable when specifying design values. Discrepancies between the connection's design and as-built reality may be significant if the connection's moment capacity is required to fall within narrow limits. In this case, a sensitivity study should be performed, considering the likely variability sources of uncertainty. Tolerance issues are also an important consideration for the constructibility of the structure.

As LVL is an engineered wood product, produced in factory conditions, construction tolerances achievable using this are tight. Due to the LVL's low modulus of elasticity, consideration should be given to tolerances during assembly. This is particularly important where the timber is compressed after stressing. LVL, like all timber, is an orthotropic material and is affected by changes in humidity. Designers should consider possible shrinking and swelling when detailing components with very tight tolerances.

In laboratory testing, post-tensioning was applied to each of the five strands individually. This meant that the stress in each tendon changed as additional tendons were stressed. In order to offset this effect, the tendons were all stressed to an intermediate level before raising them to the final stress level. The potential for unequal forces in each tendon may be of concern if tendons approach yielding. Should a tendon (or tendons) yield and elongate, it will be less effective in subsequent cycles, raising stress in the remaining tendons and lowering stiffness. It is therefore recommended that a jack capable of stressing all tendons simultaneously be employed.

Long term application of post-tensioning forces to the LVL will cause creep in the timber and a relaxation in post-tensioning force will be observed. A seismic event is unlikely to occur immediately after stressing, thus allowance must be made for a reduction in post-tensioning force when the joint is activated in an earthquake. Reduced post-tensioning will affect the moment capacity of the joint as well as its re-centring properties. Regular scheduled checks should be made on the post-tensioning to ensure adequate performance for the lifetime of the building.

The yielding area and geometry of the dissipative element can be controlled precisely using milling equipment with high precision Digital Read Out. Attention must be paid to the grade of steel specified in the design. While time savings may be achieved by using Grade 4.6 threaded rod, the more consistent mechanical properties of Grade 300 mild steel make it more suited for use in dissipative elements. The increased ductility of lower grade steel means that it should be used where possible. Higher grade steel may be specified, but its ductility must be checked.

The assembly methodology of the joint must be considered when assessing tolerance issues. For factory assembled details, tight tolerances are achievable however, where components are assembled on site, constructibility considerations should be considered early in the design process. Checks of tolerances should be made prior to assembly on site. Components that do not meet tolerance specifications are likely to be forced into place on site, and as a consequence, may be damaged in the process.

A design example showing the potential variations in moment capacity of a joint is presented in Figure 6.1. The behaviour of this joint is taken from one of the joints tested as part of this experimental campaign. The specimen using screw reinforcement and NPDs[1] is assessed.

The ranges given to each parameter of the design are shown in Table 6.1 below. These values are indicative only. More accurate estimates should be obtained through consultation with relevant parties early in the design process. The following assumptions were made regarding the parameters used in this model:

- LVL sections were fabricated in a factory with 2 mm dimensional tolerances.
- Significant elapsed time since first stressing without adequate maintenance and re-stressing.
- Steel components were fabricated with a tolerance of 0.1 mm.
- Dissipaters were attached on site, leading to a tolerance of ± 10 mm in their positioning.

[1] Test Specimen B-D

Table 6.1: Variances in input parameters to joint performance model

Property	Specified	Variance	Parameters Affecting Moment	
			Upper Bound	Lower Bound
Section Depth (mm)	800	2	802	798
Section Width (mm)	315	2	317	313
Post-Tensioning Force (kN)	810	+5,-40[a]	815	770
Dissipater Area (mm^2)	450	5.5	456	445
Dissipater Yield (MPa)	300	15	315	285
Dissipater Overstrength	1.4	0.1	1.5	1.3
Dissipater Depth (mm)	50	10	40	60

[a] A significant decrease in post-tensioning force is more likely than an increase.

The monotonic moment rotation performance of the joint is given in Figure 6.1. The likely variation in moment capacity is shown over the entire rotation range of the connection. These parameters produce a 100 kN variance between highest and lowest case moment capacity. This represents 17% of the base connection's moment capacity and highlights the need for strict quality control and appropriate design choices.

There is a slight increase in the maximum rotation achieved in the lower bound case. This is due to reductions in steel strain given its lower distance from the neutral axis and longer unbonded length.

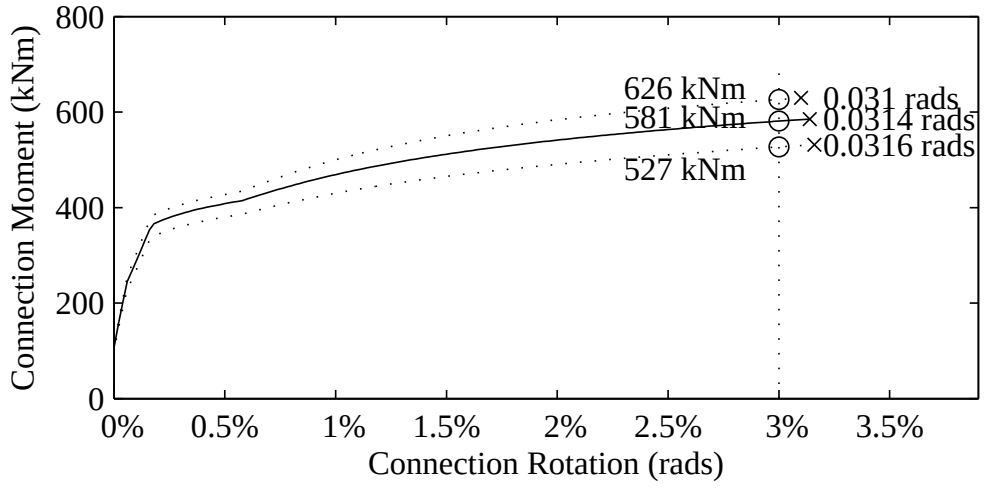

Figure 6.1: Moment - rotation sensitivity study results, showing upper and lower bound capacities (○) as well as expected ultimate rotations (×)

Changes to the joint's re-centring ratio are shown in Figure 6.2. The re-centring ratio decreases in the upper bound moment capacity case due to the larger mild steel dissipative component. In this case, the re-centring ratio is still greater than unity indicating that the joint should exhibit complete re-centring although, it is apparent that this may not always be the case. The designer must check for this possibility if re-centring is to be assures for the structure.

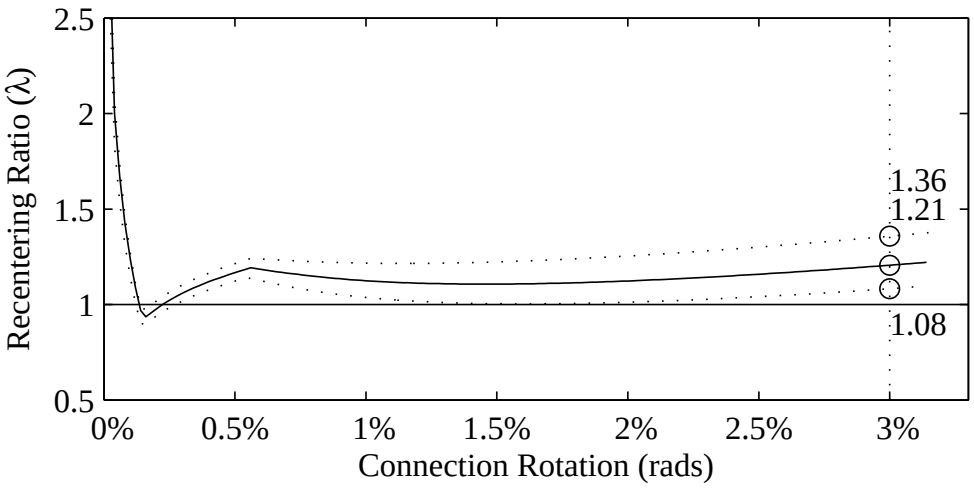

Figure 6.2: Re-centring ratio - rotation sensitivity study results

While this example presents an extreme case, it highlights the need to consider tolerances and material variability in design.

6.2 Joint Reinforcement

Reinforcement of the LVL in the joint zone against perpendicular to grain stresses has been identified as key to joint performance (Newcombe *et al.*, 2010a). Two reinforcement options have been considered in this research. Considerations for steel plate and screw based reinforcement systems are described below.

6.2.1 Steel Based Reinforcement

Issues arising from the stiffness of the armouring plate and relative stiffness of supports reduced rocking behaviour in one of the joint details tested. This was due to the plate bending and causing rotation about the centre of the joint rather than heel and toe rocking. The main cause of this was the differential displacement of the armouring plate between inside and outside supports. This is outlined in Figure 6.3.

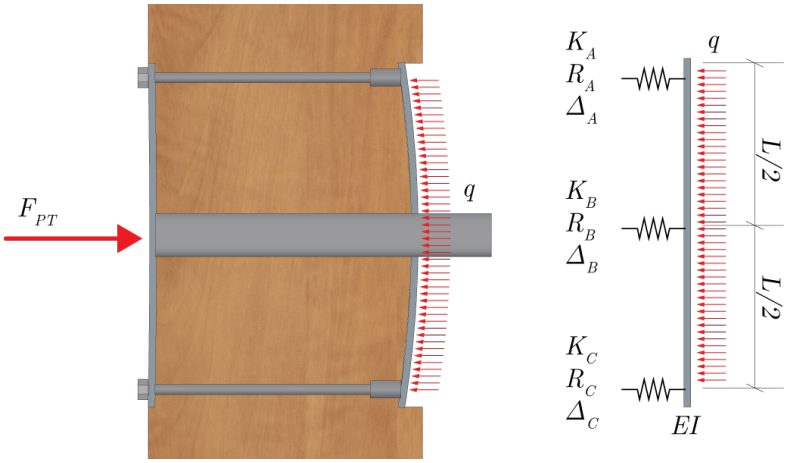

Figure 6.3: Differential displacement of armouring plate

An analytical model has been developed to predict differential displacement of the plate. The key variables considered in the mode are:

- Length between exterior supports.
- Loading applied to the plate.
- Plate stiffness.
- Stiffness of interior and exterior supports.

This model is described in Appendix B.

This model demonstrated that displacements are minimised when:

- The armouring plate's stiffness is increased.
- The interior support is as close as possible to 3 times as stiff as the exterior supports.

Although plate length and applied loading have an impact on the differential displacement, these are generally fixed before the design of the joint armouring. As a result, these factors were not considered as viable methods for reducing differential displacements.

As the exact stiffness of the plate's supports will be difficult to quantify, a combination of the approaches above is recommended.

Design charts

Steel based joint reinforcement details were investigated for a variety of likely member sizes. This was used to determine the maximum reinforced strength of a joint. From this, an estimate of the largest achievable moment capacity was produced.

The system and some of the key dimensions are outlined in Figure 6.4.

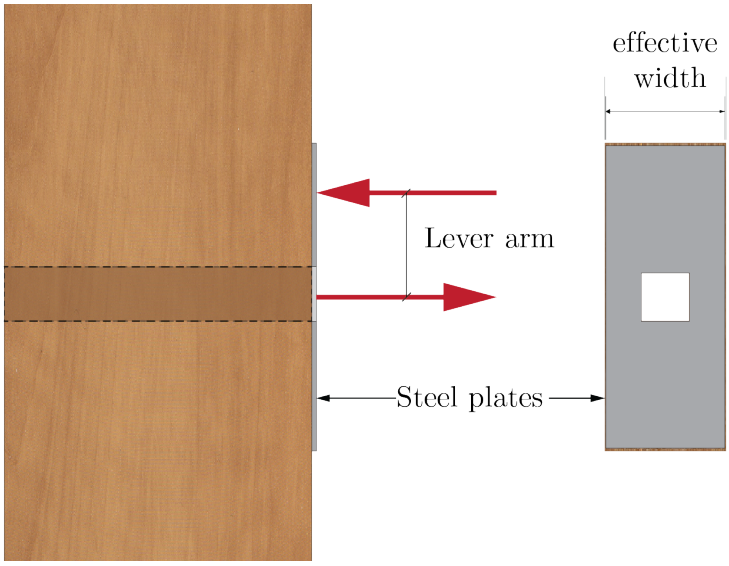

Figure 6.4: Steel joint reinforcement outline

The results of this investigation are summarised in Table C.1.

Table 6.2: Steel reinforcing maximum moment capacities ($\phi = 0.9$)

Depth \ Width	252 mm	315 mm	378 mm	441 mm	504 mm
600 mm	119 kNm	149 kNm	179 kNm	208 kNm	-
800 mm	167 kNm	208 kNm	250 kNm	292 kNm	333 kNm
1000 mm	-	269 kNm	321 kNm	375 kNm	429 kNm
1200 mm	-	327 kNm	393 kNm	458 kNm	524 kNm

6.2.2 Screw Based Reinforcement

Reinforcement of the LVL against perpendicular to grain crushing was with long, fully threaded screws.

These screws were designed following guidance set out in the manufacturer's design guides. (Würth GmbH & Co, 2011, SPAX Construction, 2012, Rotho Blaas s.r.l, 2012). These guides considered failure of the steel in the screws and failure of the timber, causing buckling of the screw. The total resistance of the connection accounted for both the timber and screw contributions.

A large number of screws were required in this reinforcement scheme. Reduction factors for screw groups were used in the design. A steel cover plate was used in the design to ensure that each screw in the group was loaded evenly.

The moment capacities using screw based reinforcement were significantly greater than those achieved for steel plate reinforcing. The design basis for the screw reinforcement considered the compression spreading at 45°, rather than at the surface as for the steel reinforcing. This may be at least partially attributable to the design basis assumed for each of these options. The screw based reinforcement was designed according to the more modern provisions of Eurocode 5 (European Committee for Standardization, 2004), while the steel based option was designed according to NZS3603 (Standards New Zealand, 1993). This may result in an overly conservative design for the steel reinforcement option.

Design Charts

Screw based joint reinforcement details were investigated for a variety of likely member sizes to determine the maximum reinforced strength of a joint. From this, an estimate of the largest achievable moment capacity was produced. An outline of this reinforcement as well as some of the key dimensions are shown in Figure 6.5.

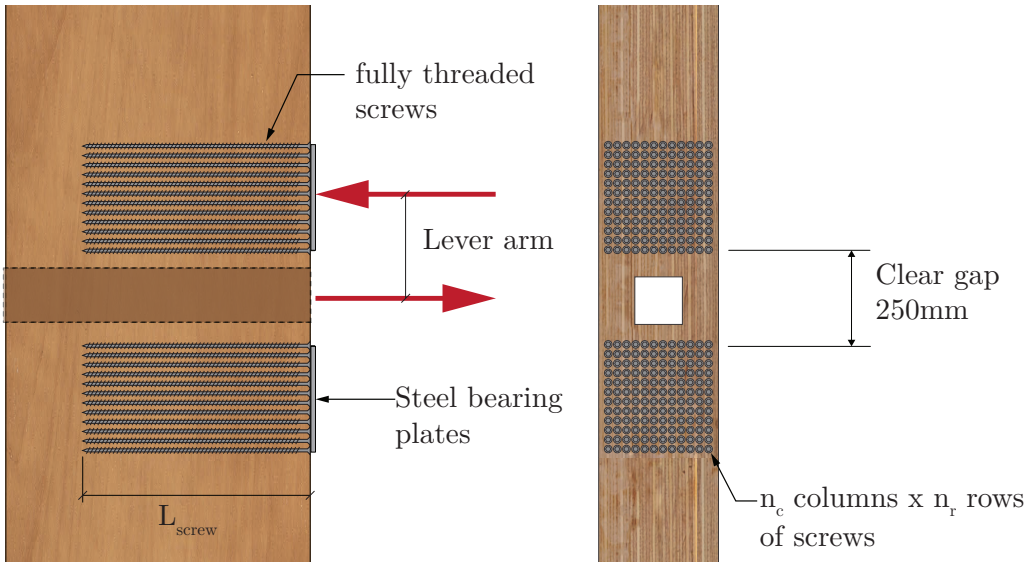

Figure 6.5: Screw joint reinforcement outline

The results of this investigation are summarised in Table 6.3. This table presents theoretical moment capacities for each joint size considering the highest screw density achievable. The largest moment capacity considering 6 mm, 8 mm and 10 mm screws is shown. These values are an upper bound on the moment capacity available in this system and should be used for initial sizing of joints prior to a more rigorous analysis.

Table 6.3: Screw reinforcing maximum moment capacities

Depth \ Width	252 mm	315 mm	378 mm	441 mm	504 mm
600 mm	428 kNm 380 ×8[a] 5 × 11[b]	523 kNm 380 ×8 5 × 14	633 kNm 380 ×8 5 × 17	743 kNm 380 ×8 5 × 20	-
800 mm	740 kNm 580 ×8 7 × 11	925 kNm 580 ×8 7 × 14	1110 kNm 580 ×8 7 × 17	1295 kNm 580 ×8 7 × 20	1480 kNm 580 ×8 7 × 23
1000 mm	-	1422 kNm 520 ×8 10 × 14	1706 kNm 520 ×8 10 × 17	1991 kNm 520 ×8 10 × 20	2275 kNm 520 ×8 10 × 23
1200 mm	-	2007 kNm 650 ×10 10 × 11	2408 kNm 650 ×10 10 × 13	2810 kNm 650 ×10 10 × 16	3221 kNm 650 ×10 10 × 18

[a] Screw length and diameter (mm)
[b] Screw layout ($n_{rows} \times n_{columns}$).

6.2.3 Reinforcement comparison

Screw reinforced joint achieve strengths of 3-5 times that of steel reinforced joints. This increase in strength comes with significantly increased costs and complexity, both in terms of material and labour. The joint designs shown in Table 6.3 use the maximum theoretical screw density in each joint size. Reductions in the number of screws will greatly reduce costs and simplify construction. An strength increase over the steel reinforcing option will likely be achieved even with a significant number of screws removed.

6.3 Energy Dissipation Device Connections

The design of energy dissipation devices is covered in more detail in the literature (STIC, 2013). These devices have been shown to function well if fabricated with the correct grade of steel and provided with adequate buckling restraint. The connection of dissipaters to the beam and column is a more challenging problem and has been investigated below.

The connection of dissipation systems to the LVL in the beam and column is critical to the performance of these beam column joints. Connections using threaded couplers, timber rivets and fully threaded screws have been investigated in this research. Threaded couplers are well understood (Standards New Zealand, 2006) by engineers and have been shown to perform well in this application. They have not been explored further in this section. The remaining connection options are explored in more detail in the following sections.

Design options have been investigated for a range of connection sizes using systems explored in this research. A summary of the standard connection capacities investigated is provided in Table 6.4.

Table 6.4: Standard connection sizes for dissipation devices

Connection force	Equivalent Area [1]	Equivalent Diameter [2]
80 kN	190 mm^2	16 mm
120 kN	280 mm^2	19 mm
160 kN	380 mm^2	22 mm
200 kN	475 mm^2	25 mm
240 kN	570 mm^2	27 mm

[1] Equivalent area and diameter of steel with 300 MPa yield stress and over-strength factor of 1.4
[2] Equivalent diameter for a circular dissipater

6.3.1 Riveted plates

Designs for riveted connections to satisfy the load limits in Table 6.4 were produced. Rivet design guidelines (Quenneville & Zarnani, 2013) for LVL were used to evaluate the capacity of each connection. These designs satisfied the minimum strength requirements for each connection type. The stiffness of each connection was also evaluated. Designers will likely wish to increase the number of rivets used to achieve stiffer connections.

The capacity of timber rivets is dependant on the loading direction. Designs for connections into the beam (acting parallel to grain) and column (perpendicular to grain) have been produced. These are shown in Tables 6.5 and 6.6.

The connections designed below were evaluated using the minimum timber sections from those evaluated in the reinforcement options above.

The stiffness of each of the connections presented was evaluated to determine a lower bound for this connection type. A stiffness of 1 kN/mm per rivet was adopted (Quenneville & Zarnani, 2013). The connections considered have stiffness of 25−50kN/mm.

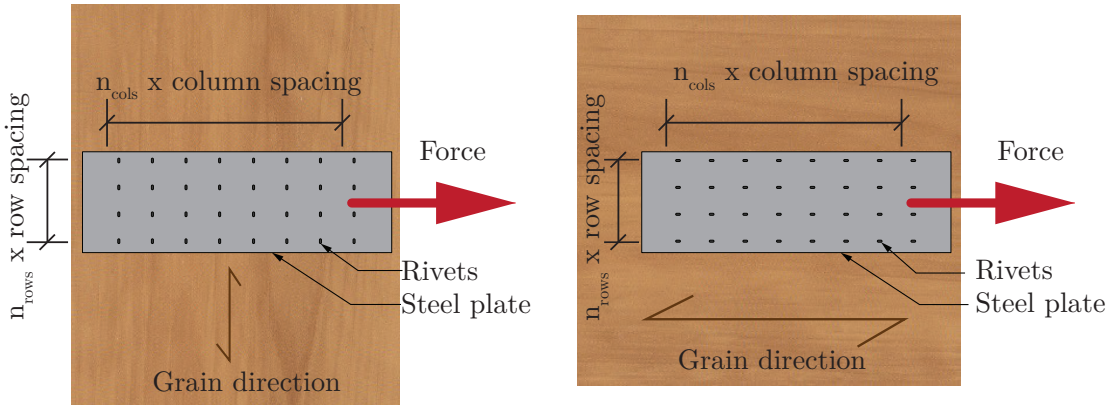

(a) Perpendicular to grain

(b) Parallel to grain

Figure 6.6: Schematic view of riveted connection

Table 6.5: Design data for riveted connections loaded parallel to grain (Beam)

Connection Class	Capacity	Rivets	Min Width
80 kN	88 kN	4×7	315 mm
120 kN	128 kN	4×8	315 mm
160 kN	163 kN	4×13	315 mm
200 kN	201 kN	4×16	315 mm
240 kN	241 kN	4×20	315 mm

Table 6.6: Design data for riveted connections loaded perpendicular to grain (Column)

Connection Class	Capacity	Rivets	Min Depth
80 kN	91 kN	4×8	$600mm$
120 kN	125 kN	4×10	$600mm$
160 kN	160 kN	6×9	$800mm$
200 kN	215 kN	6×12	$800mm$
240 kN	245 kN	6×14	$800mm$

6.3.2 Inclined screw connections

Connections were designed using inclined screws and proprietary anchorages. This connection type is shown in Figure 6.7. These connections were designed to satisfy the strength requirements of Table 6.4. The stiffness of these connection types was also evaluated.

A summary of the connections designed is shown in Table 6.7. Some of the connections in this chart are significantly above the required strengths. This is due to the minimum screw limits imposed in the ZD connector ETA (SWG Schraubenwekr Gaisbach GmbH, 2011). Minimum section sizes have been determined considering the extend of inclined screws in each option.

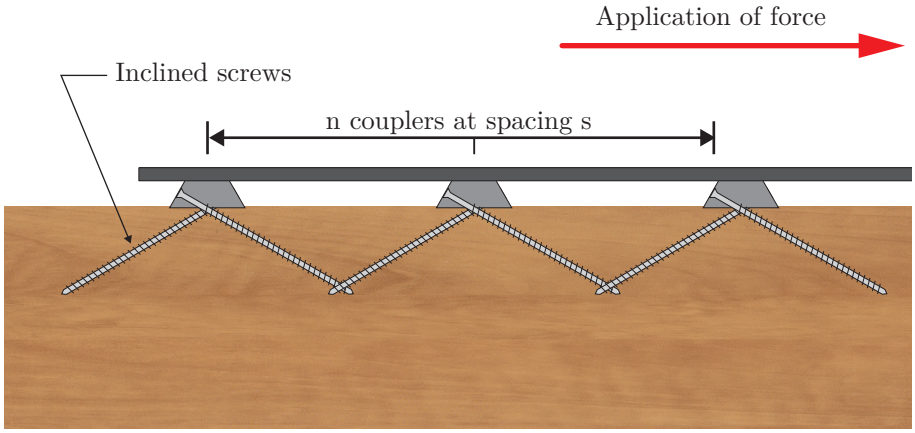

Figure 6.7: Schematic view of screwed connection

Table 6.7: Design data for screwed connections

Connection Class	Capacity	Screw Length	ZD Plates	Minimum Section Size
80 kN	86 kN	250 mm	1	600 mm × 315 mm
120 kN	143 kN	250 mm	2 @ 150 mm	800 mm × 315 mm
160 kN	171 kN	300 mm	2 @ 200 mm	800 mm × 315 mm
200 kN	215 kN	250 mm	3 @ 100 mm	800 mm × 315 mm
240 kN	257 kN	300 mm	3 @ 100 mm	800 mm × 315 mm

The ETA for the ZD connectors (SWG Schraubenwekr Gaisbach GmbH, 2011) used specifies a stiffness of 100 kN/mm per connector for arrangements with screws restraining movement perpendicular to the shear plane. This gives connection stiffnesses of 100-200 kN/mm for the connections described in Table 6.7.

6.3.3 Connection comparison

Both timber rivets and inclined screws were used to generate connection details. These satisfied load requirements and geometric limits for each connection in Table 6.4. Connection strength was better able to be tailored to requirements when using timber rivets. This is due to screw length limits imposed in the ETA for ZD connectors. This is unlikely to be an issue as connections are likely to be designed based on stiffness properties.

Minimum designs for strength were produced for each load case. This allows consideration of lower bound stiffnesses for each option. The screwed connections were 3-5 times stiffer than rivets. Rivets are cheap and simple to install therefore an increase in connection stiffness will be easily achievable.

Timber rivets produced a more compact connection detail. This was true both for plan area and connection depth. For this reason, timber rivets may be better suited to smaller timber members, for which depth may be governed by the screw embedment requirements.

6.4 Conclusions

The effect of uncertainties in material and geometric parameters as well as inaccuracies arising from construction tolerances has been assessed. An example has been used to illustrate the variability of joint performance expected considering maximum likely ranges for these values. The calculated moment-rotation behaviour had a range of up to 17% due to these variances. This illustrates the importance of both sensitivity studies and proper quality control.

Maximum moment capacities for a range of practical joint geometries were produced for both steel and screw reinforced joints. These can be used by designers as an initial sizing guide and to check the viability of proposed connection options.

Screw reinforced joints were seen to achieve strength of 3-5 times those of steel reinforced joints. This gain is due to the internal spreading of compression perpendicular to grain forces within the timber member. Steel bearing plates are key to obtaining good performance from these joints. The increase in strength from this reinforcing system is offset by increased cost and complexity in fabrication.

Timber rivets and fully threaded screws with a proprietary connection system were investigated as methods for attaching dissipation devices to the beam and column. Connection systems were designed for a range of dissipation forces corresponding to dissipaters with diameters of ranging from 16 mm to 27 mm. Both systems were able to achieve these strength requirements. The riveted connection was more compact and therefore able to be used in smaller members.

Chapter 7

Case Study Structures

7.1 Introduction

Three hypothetical frame structures have been designed using the connection details discussed in the experimental phase of this research. DBD methodologies have been used to arrive at initial designs for these structures. The performance of each initial design has been assessed against design criteria and comments about the suitability of design methods have been made. Modifications to the design have been made where required. The expected performance of these buildings under seismic excitations has been assessed using Non-Linear Time History Analyses (NLTHA) with a suite of ground motion records.

7.2 Design of Structures

Three structural configurations were investigated. These structures all used frames in one direction and walls in the other. Only seismic loading in the frame direction was considered in the analysis. Readers are referred to other literature for wall specific design guidance (STIC, 2013). The structures considered are shown in Figure 7.1.

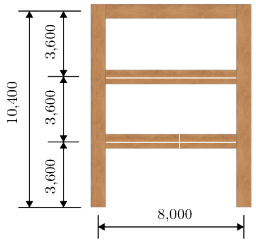

(a) Structure A: 3 storey 1 bay frame

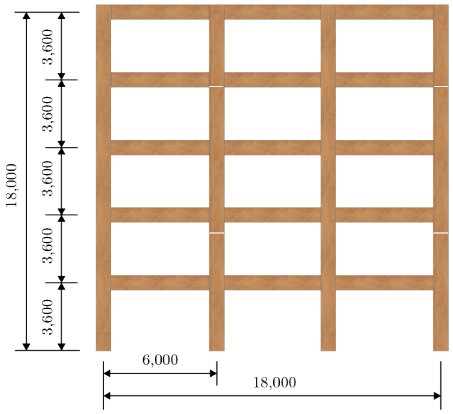

(b) Structure B: 5 storey 3 bay frame

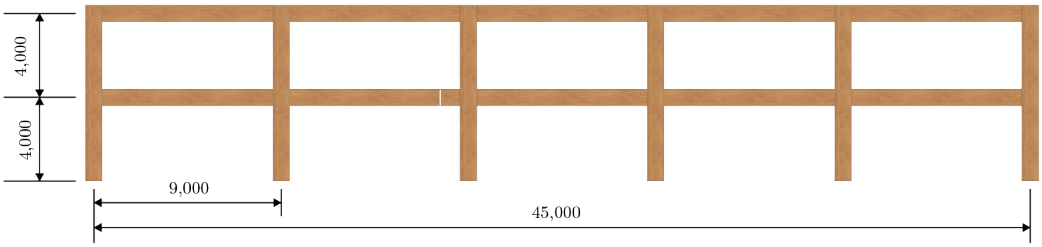

(c) Structure C: 2 storey 5 bay frame

Figure 7.1: Case study structures

The structures were designed according to NZS1170.5. They were:

- Office buildings (Q =3.0 kPa)
- Importance Level 2 as they have less than 10 000 m^2 of floor space and hold fewer than 5,000 people
- Designed assuming a life of 50 years, meaning a return period of 1/500 years was used
- Located in Wellington ($Z = 0.4$)
- On soil class C
- Designed for a 2.0% inter storey drift under Ultimate Limit State (ULS) conditions.

The following design criteria were used to assess the performance of the structures:

- SLS drift limit of 0.5%
- No gap opening at SLS
- ULS drift limit of 2.0%
- Maximum Credible Event (MCE) drift limit of 3.5%
- Joint rotations capacity to exceed MCE rotation demand

A DBD methodology was used to assess the lateral loads applied to each structure. Both DBD and Force Based Design (FBD) procedures can be used to satisfactorily evaluate demand on the structure (STIC, 2013), however, as the behaviour of the connections in the system is governed by rotation, a DBD approach is more direct. A comparison between DBD and FBD methodologies

for Pres-Lam structures is provided in literature (STIC, 2013).

It was assumed that gravity loads did not interact with seismic resisting systems for the purpose of these designs. This is the case where external dissipation devices are installed after the structure is carrying dead loads. If dissipaters were installed prior to erection the seismic performance of the frames would be somewhat compromised by frames carrying gravity loading. Dissipaters above the beams would be elongated under dead load and therefore have a reduced rotation capacity. Designers may need to account for these effects in structural systems.

7.3 Initial Designs

Initial designs for each of the structures were developed using simplified methods. These designs were later verified using numerical analyses.

Member sizes were selected with consideration of available material sizes. Element widths were selected as multiples of 63 mm while depths were chosen to minimise waste from 1200 mm billets. The sizes were chosen from those in Chapter 6.

A seismic load take-down was performed for each structure to determine the seismic mass at each floor. This was done according to NZS1170 using:

$$W_E = G + \psi_E Q \tag{7.1}$$

The structure's weight was made up from:

- Beams and columns
- Timber Concrete Composite (TCC) flooring
- Superimposed dead load
- Façade cladding
- Applied live load

DBD was used to determine the effective period, overturning moment and base shear according to the NZS1170.5 design spectra. The shear forces determined from this analysis were distributed through the frame using the Equilibrium Method (Priestley *et al.*, 2007, Pampanin *et al.*, 2010). This method allows the designer to set the moment capacity of the beam column joints in the structure. The design of the structures was rationalised using this method by selecting at most two different joint types per frame.

The DBD procedure was developed for reinforced concrete (RC) structural systems. Because of this, it does not consider frame flexibility when predicting yield rotations. This is an acceptable simplification for RC structures. However it is not appropriate for timber frames where stiffness is around $\frac{1}{3}$ that of concrete. Underestimating rotations at yield causes an over-prediction of ductility and hence damping. This results in an underestimation of base shears and therefore an under-designed structure. To remedy this, an alternate formulation for yield rotation was used (Newcombe, 2007).

The design moments chosen from the frame force distribution were used as targets when developing designs for the joints themselves. A MMBA based approach was taken for the designs. The target rotation was approximated by subtracting the yield drift from the structure's drift target.

Each of the joints specified by the design were detailed using:

- Screw reinforcement and NPDs.

- Steel plate reinforcement and Plug-and-Play dissipaters.

Moment capacity was distributed between mild steel and post tensioning by targeting a recentring ratio (λ) of 1.25. This was modified in some cases to ensure full recentring.

A summary of this process for each of the structures is given in the following sections.

7.3.1 Structure A

A summary of the initial design outputs for Structure A is shown in Table 7.1. This table shows the moment demands for the two joints to be detailed for this frame. One joint detail is proposed for the top floor and another for the lower two floors.

Table 7.1: Structure A: Design parameters

Analysis Step	Parameter	Value
Load Takedown	Seismic weight	1180 kN
DBD	Target displacement	216 mm
	Effective period	1.1 s
	Base shear	491 kN
	Overturning moment	4148 kNm
Beam Design Moments	Level 1,2	540 kNm
	Level 3	310 kNm

Joint Designs

Joint options considering both Plug and Play dissipaters and NPDs have been produced for lower and upper storeys. Due to the large moment demands, both joints use screw reinforcing.

Levels 1,2

The joint options considered for the lower storeys are shown in Figure 7.2. Post-tensioning in both joints consists of 7 13.5 mm diameter strands initially stressed to 1050 MPa (1050 kN total initial post-tensioning).

Plug and Play dissipaters are located 50 mm outside the beam depth and have a necked diameter of 23 mm. These are connected to the column using threaded couplers and to the top and bottom of the beam using riveted base plates.

NPDs have a necked down area of 15 mm $\times$ 35 mm. These are located 50 mm within the beam. Dissipaters are connected with three ZD connectors and inclined screws on each side.

Screw reinforcing is provided according to the maximum set out in the design chart in Chapter 6.

The joints have been detailed to produce similar moment-rotation responses and re-centring behaviour. A comparison of responses of the two joints is shown in Figure 7.3. Because of their similarity, only a single numerical model has been produced for this joint.

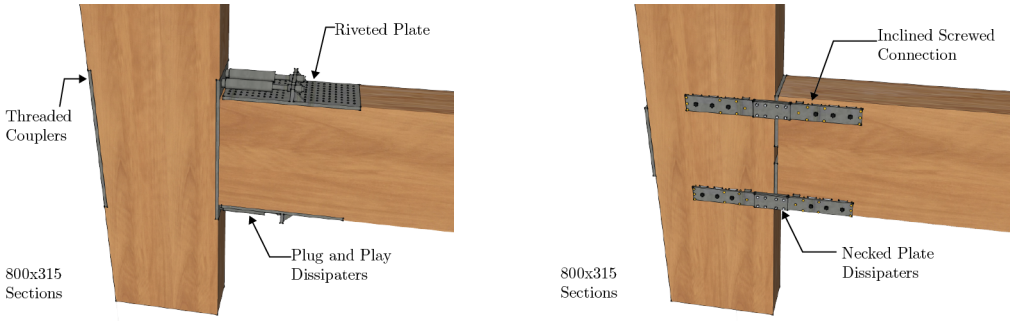

(a) Plug and Play dissipation (b) NPDs

Figure 7.2: Details for joints of levels 1,2 of Structure A

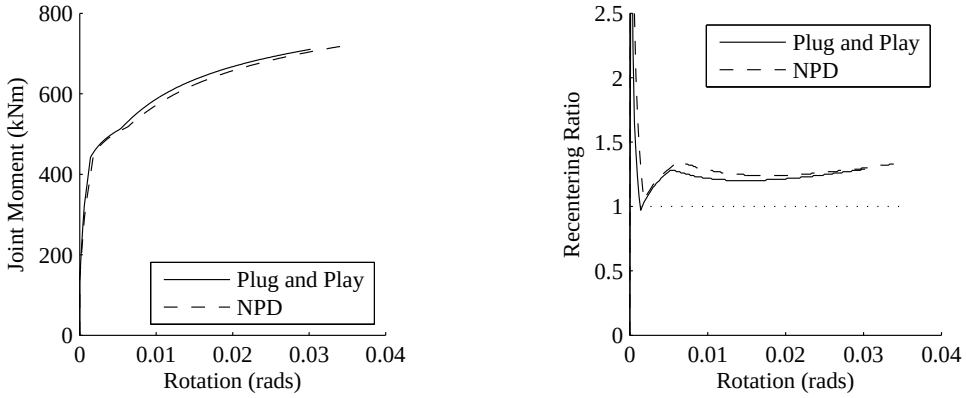

(a) Plug and Play dissipation (b) NPDs

Figure 7.3: Moment-rotation and re-centring ratio for for joints of levels 1,2 of Structure A

Level 3

Joint design options for the joints at level 3 are shown in Figure 7.4. The detailing adopted is similar to that used on the lower floors.

Due to lower moment demands, the post-tensioning has been reduced to 5 strands stressed to 900 MPa.

Plug and Play dissipation has a necked diameter of 18.75 mm. The unbonded length is unchanged at 250 mm. The riveted connection has been reduced from the lower joints. This is evident when comparing the size of attachment plates in Figure 7.2 and Figure 7.4.

NPDs with a necked down zone of 10 mm $\times$ 36 mm have been used. These are connected using two ZD connectors on each side of the dissipater.

Screw reinforcing has again been taken according to the maximum shown in the design charts in Chapter 6. Because of the lower demand, the number of screws could be reduced to produce a more economical joint detail.

Joint performance is compared in Figure 7.5. Because of the similarity of predicted response, only a single numerical has been used.

(a) Plug and Play dissipation (b) NPDs

Figure 7.4: Details for joints of level 3 of Structure A

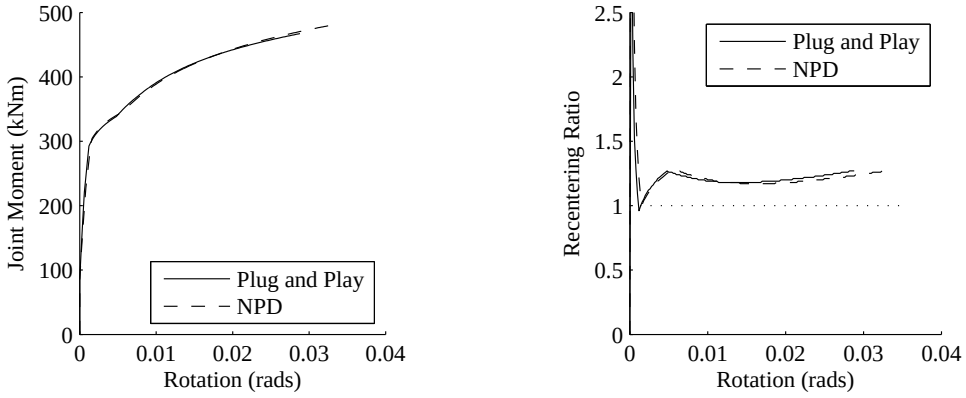

(a) Plug and Play dissipation (b) NPDs

Figure 7.5: Moment-rotation and re-centring ratio for for joints of level 3 of Structure A

7.3.2 Structure B

Structure B's initial design parameters are shown in Table 7.2. As shown in Section 7.5.1, the original design produced using this output did not yield satisfactory performance. Predicted drift at ULS was 15% larger than permitted. To remedy for this, the joint capacity was increased to reduce ULS displacements. Joint design moment was altered later in the design.

Two separate joint details are used in this structure. The lower three floors use a common detail while a separate one is used for levels 4 and 5.

Table 7.2: Structure B: Design parameters

Analysis Step	Parameter	Value
Load Takedown	Seismic weight	3483 kN
DBD	Target displacement	360 mm
	Effective period	1.7 s
	Base shear	872 kN
	Overturning moment	11,657 kNm
Frame Distribution	Beam Design moments	
	Level 1,2	346 kNm
	Level 3	187 kNm

Joint Designs

Two options have been detailed for each joint in the structure. Both use screw reinforcing. Plug and Play dissipation as well as NPDs is used.

As stated above, the the design was modified after deficiencies were noted in its performance. The joints described here are for the improved design.

Levels 1-3

The joint options for the lower three floors are shown in Figure 7.6. Both options use 5 13.5 mm diameter strands initially stressed to 850 MPa (610 kN initial post-tensioning).

Plug and Play dissipaters are located 50 mm above and below the beam. These have a necked down diameter of 18.5 mm and are attached using riveted plates and threaded couplers.

NPDs have a yielding section of 10 mm × 35 mm. These are attached using two ZD connectors on each end of the dissipater.

Screw reinforcing is provided according to the design chart in Chapter 6.

As shown in Figure 7.7, the response of these joints is nearly identical. Because of this, only a single numerical model was used.

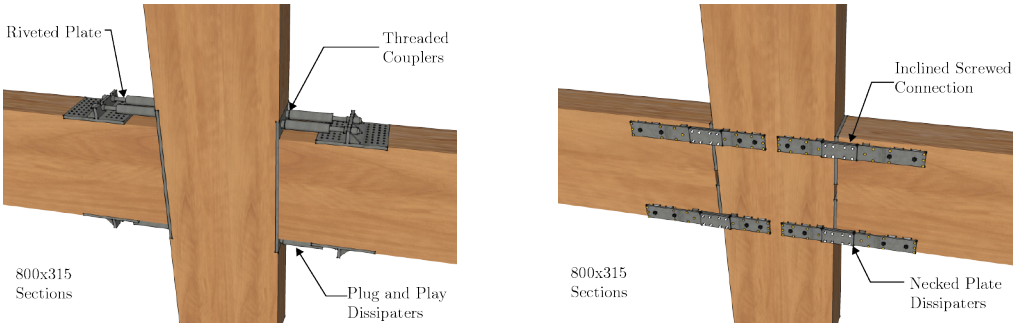

(a) Plug and Play dissipation (b) NPDs

Figure 7.6: Details for joints of levels 1-3 of Structure B

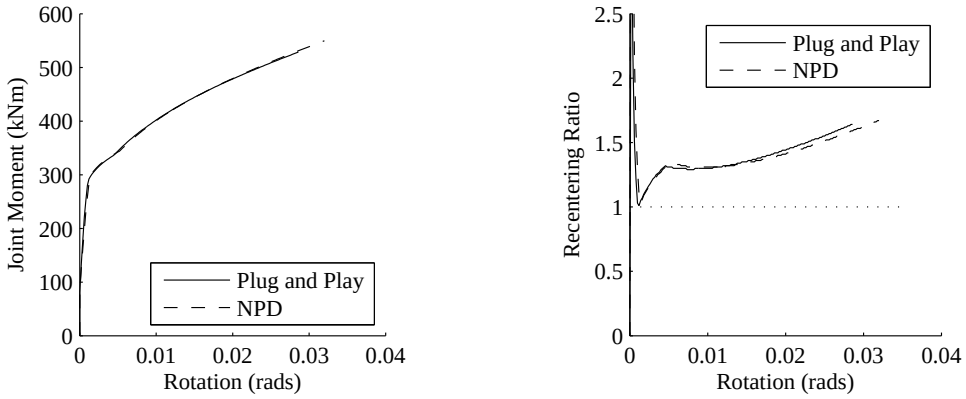

(a) Plug and Play dissipation (b) NPDs

Figure 7.7: Moment-rotation and re-centring ratio for for joints of levels 1-3 of Structure B

Levels 4,5

The joint options for levels 4 and 5 are shown in Figure 7.8. These joints both use 3 13.5 mm strands stressed to 700 MPa (300 kN initial post-tensioning).

Plug and Play dissipation is located 50 mm above and below the outer edge of the beam. The dissipaters have a necked diameter of 12.5 mm. These are connected using threaded couplers and riveted plates.

NPDs are located 75 mm within the beam depth. These have a necked section of 10 mm × 17 mm. Because of their low diameter, these dissipaters are connected using a single ZD connector on each side of the joint.

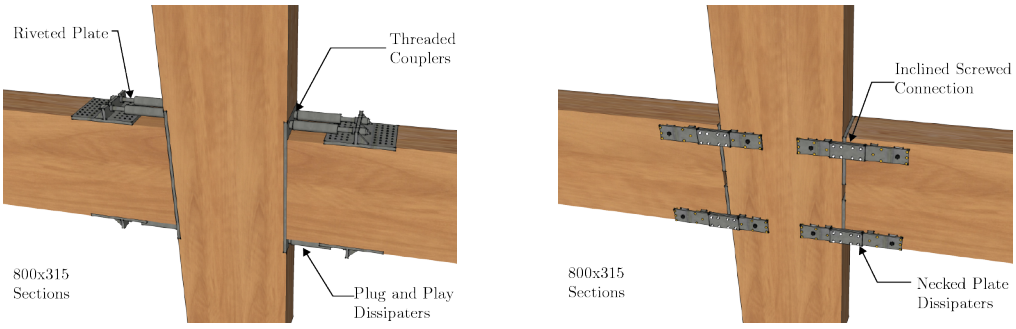

(a) Plug and Play dissipation (b) NPDs

Figure 7.8: Details for joints of levels 4-5 of Structure B

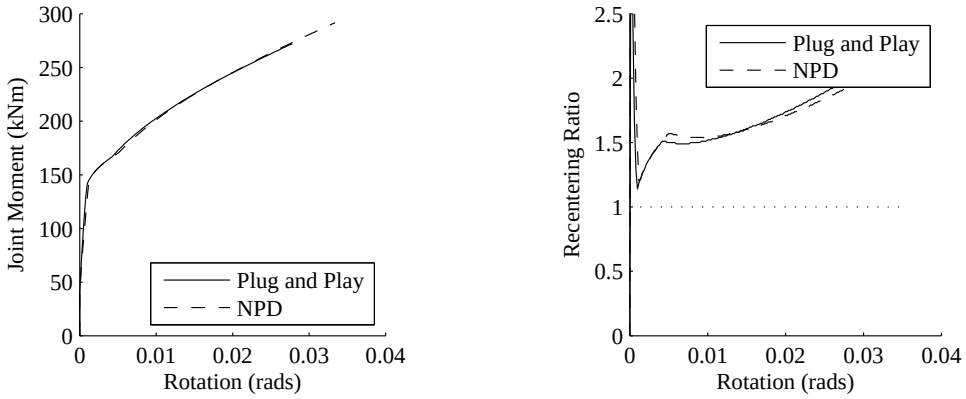

(a) Plug and Play dissipation (b) NPDs

Figure 7.9: Moment-rotation and re-centring ratio for for joints of levels 4-5 of Structure B

7.3.3 Structure C

Initially 600 mm beams and columns were chosen for this structure. Using this member size resulted in an initial predicted yield drift of 2.1%, larger than the ULS target drift. This rendered the dissipating joints ineffective. An increased member size of 800 mm was chosen to remedy this.

The design outputs from the DBD and frame load distribution procedures are shown in Table 7.3. Only a single joint design moment was chosen for this structure.

Table 7.3: Structure C: Design parameters

Analysis Step	Parameter	Value
Load Takedown	Seismic Weight	2982 kN
DBD	Target Drift	160 mm
	Effective Period	1.0 s
	Base Shear	1395 kN
	Overturning Moment	9,488 kNm
Frame Distribution	Beam Design Moments	
	All levels	280 kNm

Joint Designs

Two options were considered, using Plug and Play dissipaters or NPDs. Both joints used screw based reinforcement. Details of each joint are shown in Figure 7.10.

The joints used 5 13.5 mm diameter post-tensioning strands with an initial stress of 750 MPa (535 kN initial post-tensioning).

Plug and Play dissipaters were located 50 mm above and below the beam face. These had a necked diameter of 17 mm and an unbonded length of 250 mm. The dissipaters were connected using riveted plates and threaded couplers.

NPDs were located 75 mm within the beam section. These had a necked region of 30 mm × 10 mm. Connection to the beams and column were using 2 ZD connectors and inclined screws.

Screw reinforcing was according to that set out in the design charts in Chapter 6. The number of screws can be reduced as part of detailed design to arrive at a more efficient reinforcement scheme.

The joint's behaviour is shown in Figure 7.11. Because of the similarity between these joints, only a single numerical model was produced.

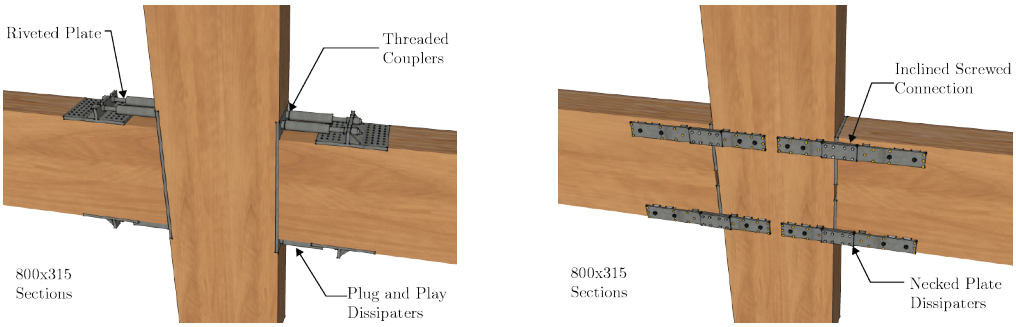

(a) Plug and Play dissipation (b) NPDs

Figure 7.10: Details for joints of levels 1,2 of Structure C

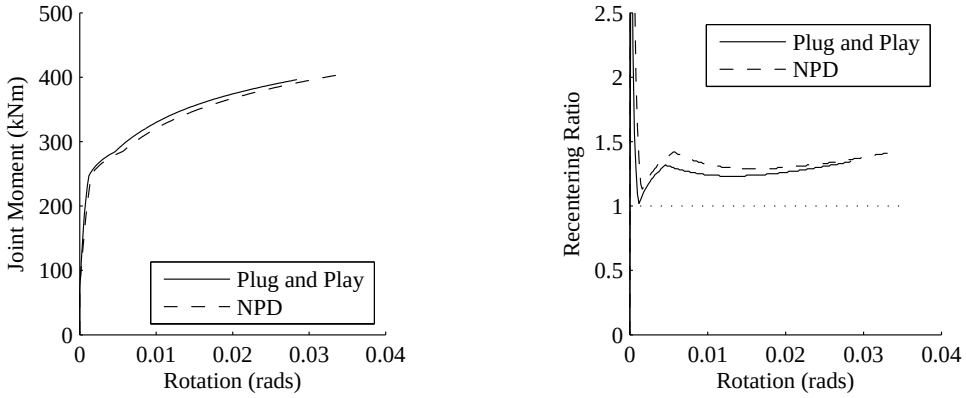

(a) Plug and Play dissipation (b) NPDs

Figure 7.11: Moment-rotation and re-centring ratio for for joints of levels 1,2 of Structure C

7.4 Description of models

OpenSEES (McKenna *et al.*, 2014) was used to generate computational models of each structure. These were lumped plasticity models using non-linear rotational springs to represent the moment-rotation properties of the joints.

The joints were modelled using three rotational springs, representing:

- Dissipative steel
- Re-centring from post-tensioning
- Joint panel rotation

Fictitious rigid members were used to ensure the model's geometry match that of the joint in reality. A detailed view the model and each joint is shown in Figure 7.12. Note that the figure shows Structure A, however other structures were modelled similarly.

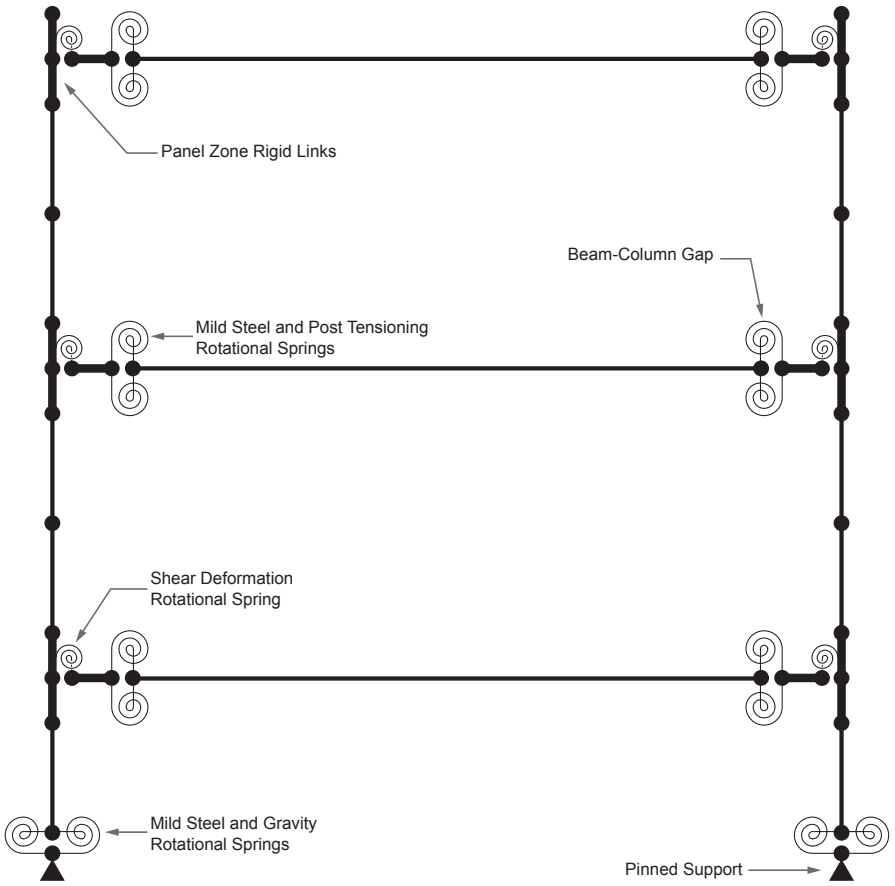

Figure 7.12: Arrangement of numerical model

7.4.1 Column base springs

These case study structures were analysed to assess the impact of beam column joint detailing. In order to achieve drift limits, particularly at SLS, column base connections were required to be detailed with mild steel dissipation. Re-centring arising from dead load in the columns was also modelled. Sizing of base dissipaters was undertaken but specific detailing was not undertaken as part of these case studies.

7.4.2 Beam column joint springs

Beam-column joints were modelled using zero-length rotational springs to represent:

- Post-tensioning, using a bi-linear elastic hysteresis
- Mild steel, using *STEEL01*, a bi-linear plastic hysteresis.

These springs were located at the interface between the beams and columns. The layout of these springs in the joint zones of the models is shown in Figure 7.12.

7.4.3 Column Shear Deformation Springs

Linear-elastic springs were used to model shear deformation in each joint zone. The arrangement of this spring is shown in Figure 7.12. The method used to derive these spring stiffness's was adopted from Newcombe (Newcombe, 2011) and is shown below.

$$K_r = GA_{sh}\left(\frac{h_b}{1-\frac{h_c}{L_b}-\frac{h_b}{H}}\right) \tag{7.2}$$

K_r = rotational stiffness
G = shear modulus of LVL
A_{sh} = horizontal shear area
h_b, L_b = depth and length of beam
H = inter-storey height

7.5 Analysis Methods

A series of non-linear analyses were performed for each model considered. These were:

- Displacement controlled pushovers
- Displacement controlled cyclic loadings
- Time history analyses.

7.5.1 Pushover analysis

Non-linear, displacement controlled pushover analyses were conducted on the structures. These were used to assess the preliminary designs of each of the structures.

Acceleration Displacement Response Spectra (ADRS)(Chopra & Goel, 1999) were used to compare the performance of the structure under likely seismic loadings. The pushover curves were plotted against displacement spectra from NZS1170.5. SLS, ULS and MCE seismic demand spectra are shown in Figures 7.13, 7.15, 7.16 and 7.18. This allows an evaluation of structural performance at each limit state. Demand spectra were scaled by the damping levels predicted in the DBD procedure.

Joint activation, the order in which yield occurred in each joints, was assessed for each case. This was used to ensure that joint activation was prevented under SLS loadings to prevent premature damage to non-structural elements. The plots shown for each structure display the total joint rotation for each level in the structure.

Structure A

The results of the pushover analysis for Structure A are shown in Figures 7.13 and 7.14. A comparison between the performance criteria and observed values is given in Table 7.4. With the exception of MCE joint rotation, all of the performance criteria were exceeded by the initial design.

As shown in Table 7.4, rotation demand exceeded capacity by 7% at MCE level drifts. Failure was located in the mild-steel dissipaters so residual moment capacity from the post-tensioning strand can be expected. This design was therefore deemed acceptable.

No modifications were made to the initial design as a result of the pushover analysis.

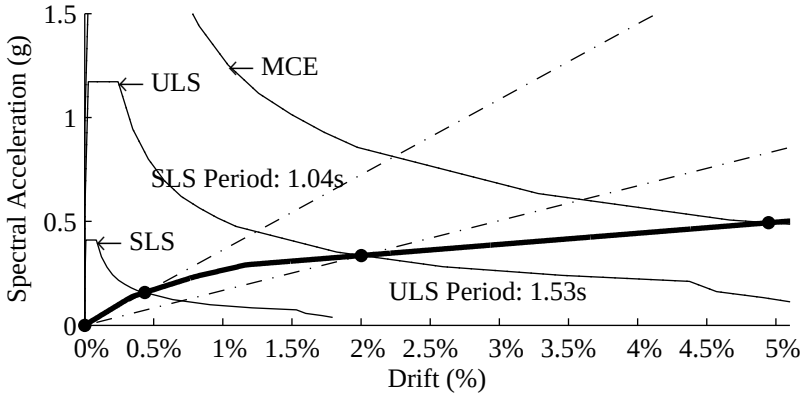

Figure 7.13: ADRS for Structure A

The plot in Figure 7.13 shows that a drift of 2.0% is expected for ULS seismic loadings. This is in line with the design assumptions from the DBD procedure used to design joints.

Table 7.4: Joint A Design criteria assessment

Performance Criteria	Design Value	Limiting Value	Acceptable
SLS Drift	0.43%	$\leq 0.5\%$	✓
SLS Joint Activation	1.04%	$\geq 0.5\%$	✓
ULS Drift	2.0%	$\leq 2.0\%$	✓
MCE Drift	4.9%	$\leq 5.0\%$	✓
MCE Joint Rotation Demand	0.032 rad	≤ 0.029 rad	✗

Figure 7.14 illustrates the expected behaviour of the joints at each level of the structure. This shows that the joint in the upper storey will yield first and sustain larger inelastic rotations than at lower levels. These plots can guide the assessment of the structure in rapid post earthquake assessments. If the upper joint has not yielded, it is unlikely that the remaining joins will be significantly damaged.

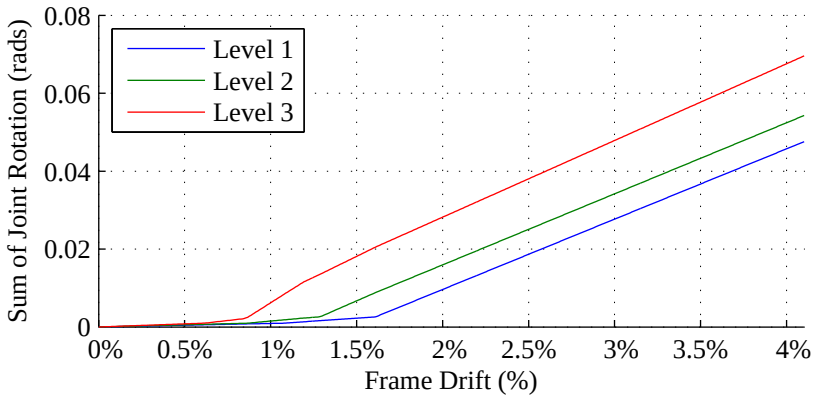

Figure 7.14: Joint activation sequence for Structure A

Structure B

The pushover curve original design for Structure B is shown in Figure 7.15. This frame was too flexible; the predicted 2.3% ULS drift exceeds the 2.0% design limit. The 15% increase in displacement is likely to represent inaccuracies in the DBD procedure's ability to capture the increased flexibility of timber. The discrepancy is small and doesn't reflect a fundamental unsuitability of the DBD method, rather, it reinforces the value of ADRS analyses for the design of structures.

The structure's design was revised to reduce ULS drift levels. The joint designs were revised to increase moment capacity at the target drift. An iterative process was used to achieve the design limits.

This increase in frame stiffness has meant that predicted deflections were lowered to:

- 2.0% for ULS
- 0.5% for SLS

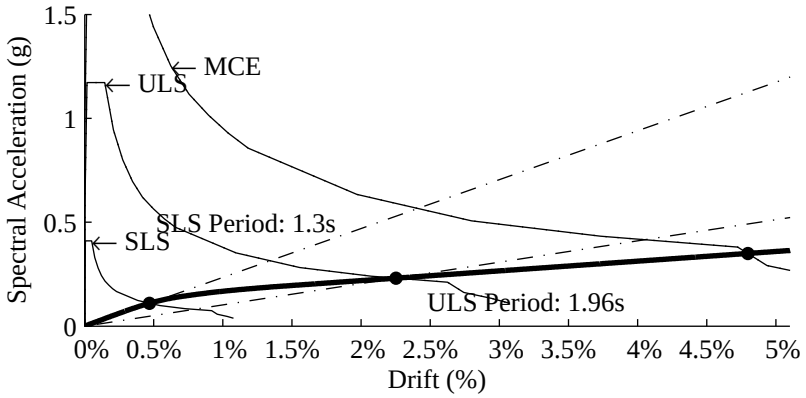

Figure 7.15: ADRS for Structure B

Table 7.5: Structure B Design criteria assessment

Performance Criteria	Design Value	Limiting Value	Acceptable
SLS Drift	0.47%	$\leq 0.5\%$	✓
SLS Joint Activation	0.68%	$\geq 0.5\%$	✓
ULS Drift	2.3%	$\leq 2.0\%$	✗
MCE Drift	4.8%	$\leq 5.0\%$	✓
MCE Joint Rotation Demand	0.023 rad	≤ 0.029 rad	✓

The ADRS for the revised design is shown in Figure 7.16. Compliance with design criteria is shown in Table 7.6. A comparison with Table 7.5 shows that the updated design fulfils design objectives.

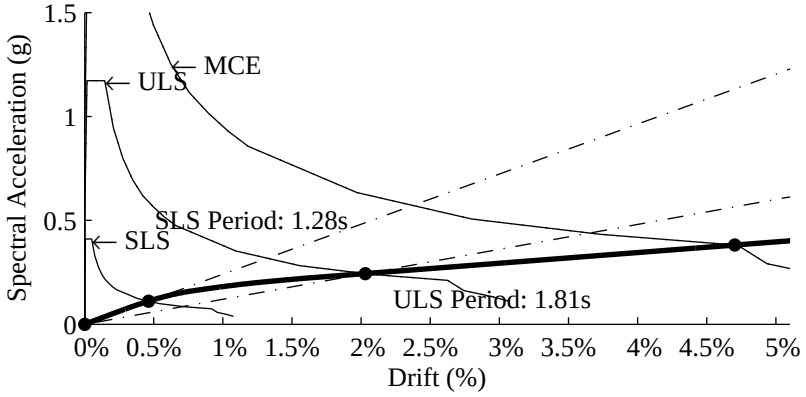

Figure 7.16: ADRS for revised Structure B

Table 7.6: Structure B revised design criteria assessment

Performance Criteria	Design Value	Limiting Value	Acceptable
SLS Drift	0.46%	$\leq 0.5\%$	✓
SLS Joint Activation	0.74%	$\geq 0.5\%$	✓
ULS Drift	2.0%	$\leq 2.0\%$	✓
MCE Drift	4.7%	$\leq 5.0\%$	✓
MCE Joint Rotation Demand	0.020 rad	≤ 0.29 rad	✓

The sequence of joint activation in the updated structure is shown in Figure 7.17. This plot shows that the upper level's joints are activated significantly before the others. This plot predicts that lower joints will not be activated until around ULS levels drifts.

Engineers may use the information contained in these plots when assessing structures following earthquakes. For example, if no damage is observed to the upper dissipaters, the structure is unlikely to have been subjected to drifts larger than 1.5%. Alternatively, if damage is seen to lower dissipaters, the structure is likely to have undergone severe displacement cycles.

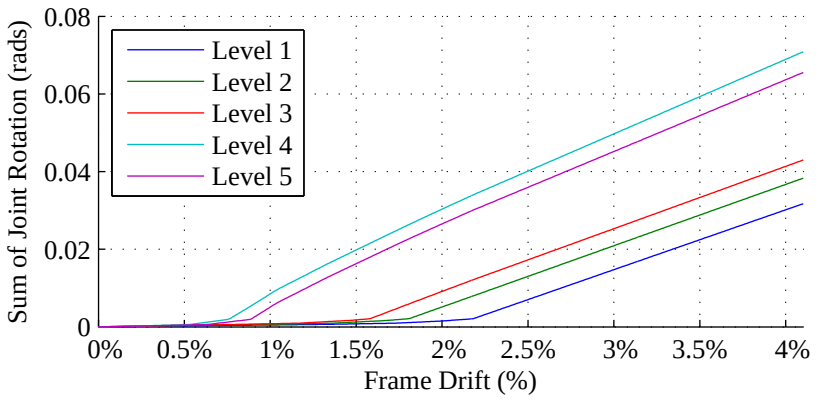

Figure 7.17: Joint activation sequence for Structure B

Structure C

The ADRS and compliance with design criteria of the design for structure C is shown in Figure 7.18 and Table 7.7. The initial design is shown to meet all of the specified criteria. Therefore no modifications were made.

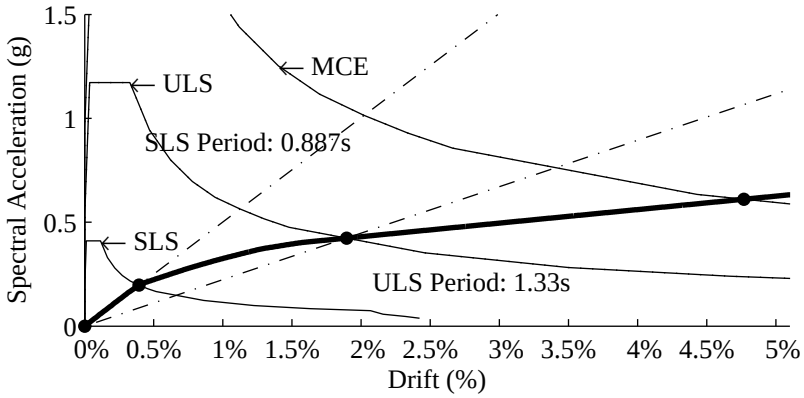

Figure 7.18: ADRS for structure C

Table 7.7: Structure C design criteria assessment

Performance Criteria	Design Value	Limiting Value	Acceptable
SLS Drift	0.39%	$\leq 0.5\%$	✓
SLS Joint Activation	1.17%	$\geq 0.5\%$	✓
ULS Drift	1.9%	$\leq 2.0\%$	✓
MCE Drift	4.8%	$\leq 5.0\%$	✓
MCE Joint Rotation Demand	0.030 rad	$\leq$0.029 rad	✓

Figure 7.19 shows the relationship between joint rotation and frame drift. This shows that the the joints are not expected to activate until just before ULS level drifts. A yield point is seen in the ADRS plot for the structure at around 0.3%. This is due to gap opening at the column base rather than at beam column joints.

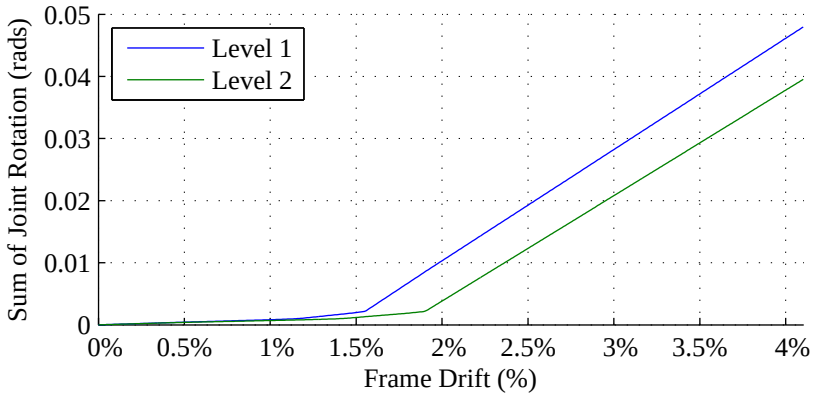

Figure 7.19: Joint activation sequence for Structure C

7.5.2 Cyclic displacement histories

The structures were subjected to cyclic displacement histories with cycles to expected SLS, ULS and MCE drifts. The hysteretic damping (ξ_{hyst}) at each level was directly determined from this analysis using the area contained within each cycle. Unlike the experimental tests, there were no post-tensioning only results to calculate the re-centring ratio (λ) with. A relationship between ductility (μ), damping and re-centring ratio was derived considering a perfectly elasto-plastic flag shaped hysteresis. The expression below was used to determine re-centring ratio for each structure:

$$\lambda = \frac{1 - \frac{1}{\mu}}{2\pi\xi_{hyst}} - 1 \tag{7.3}$$

This was considered to provide a sufficiently accurate re-centring ratio and was a further verification of the frame designs.

Structure A

The re-centring behaviour of the Structure A is shown in Figure 7.20. The structure can be expected to fully re-centre at all performance levels up to MCE.

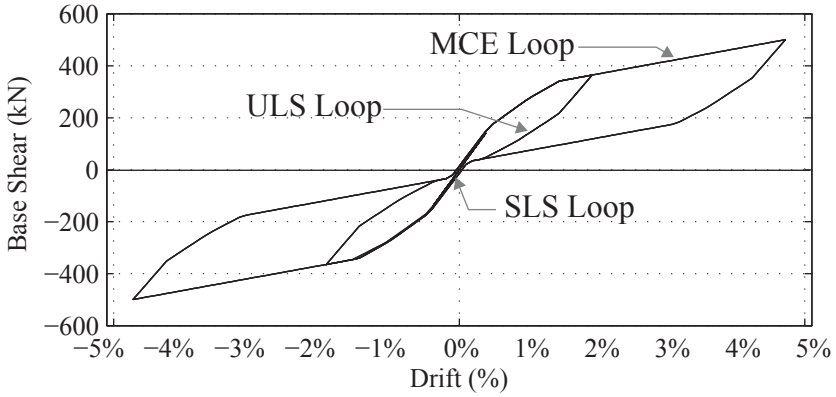

Figure 7.20: SLS, ULS and MCE cyclic displacement histories for Structure A

The energy dissipation developed for loops to each displacement level is shown in Table 7.8. This shows the expected re-centring ratio of the overall structure. The structure remains below yield at SLS drift levels so no additional hysteretic damping is achieved and an infinite re-centring ratio is obtained. For larger drift levels, the re-centring ratio is larger than predicted by the initial design. This is likely due to the column base connection's contribution to re-centring. Although re-centring is a positive quality of Pres-Lam structures, a trade-off is made between this and dissipated energy.

Table 7.8: Re-centring ratios for Structure A

Load Case	Ultimate Drift	Ductility (μ)	Hysteretic Damping (ξ_{visc})	Re-centring Ratio (λ)
SLS	0.4%	-	-	-
ULS	2.0%	4.2	4.3%	1.89
MCE	4.9%	10.2	5.7%	1.50

Structure B

Structure B's cyclic response is shown in Figure 7.21. This shows the behaviour of the frame when subjected to push-pull displacement histories to drifts predicted at each limit state. The plot shows that full re-centring is expected, even after MCE events.

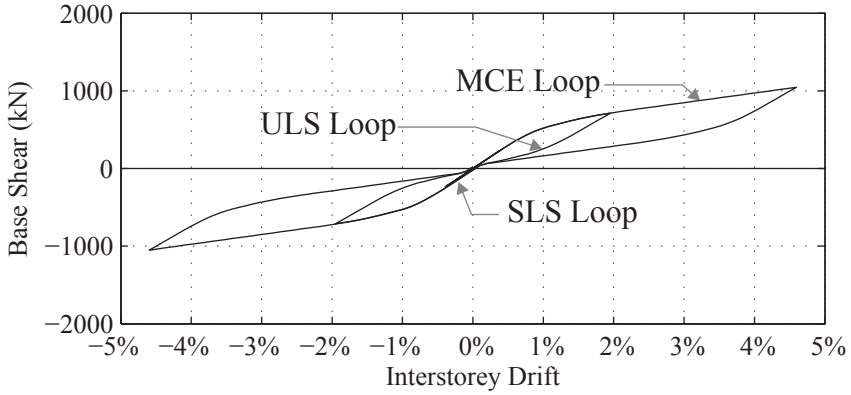

Figure 7.21: SLS, ULS and MCE cyclic displacement histories for Structure B

The energy dissipation developed on each of these cycles was determined from the moment-rotation response. This is used to compute the hysteretic damping and ductility. The re-centring ratio of the structure was back-calculated from these values.

The initial DBD procedure assumed damping of 3.7%. The observed damping was slightly larger than this for ULS. This means that the theoretical seismic demand will be slightly lower than predicted.

Table 7.9: Re-centring ratios for Structure B

Load Case	Ultimate Drift	Ductility (μ)	Hysteretic Damping (ξ_{visc})	Re-centring Ratio (λ)
SLS	0.46%	-	-	-
ULS	2.0%	2.64	4.0%	1.49
MCE	4.7%	6.21	5.0%	1.67

Structure C

The behaviour of this structure when subjected to reversing displacement histories is shown in Figure 7.22. Re-centring is expected even after MCE limit state.

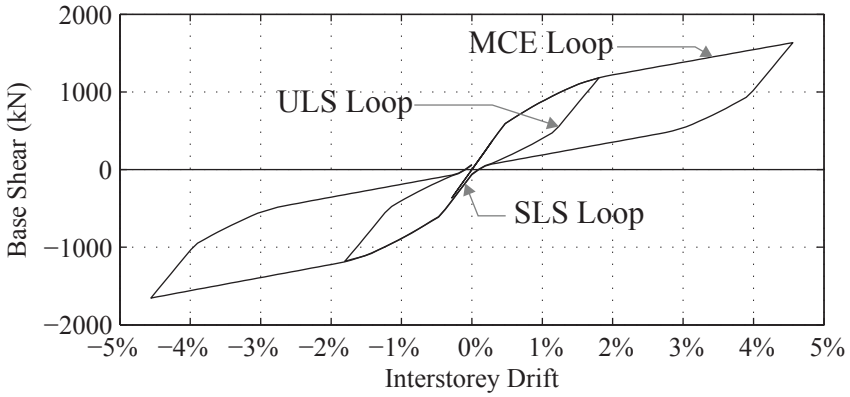

Figure 7.22: SLS, ULS and MCE cyclic displacement histories for Structure C

The ductility and damping observed from these simulations are shown for each limit state in Table 7.10. The structure is essentially elastic under SLS. Figure 7.22 shows that there is not a clearly defined yield point. Instead there is a gradual drop in stiffness as each joint yields. This means that the ductility figure reported contains some uncertainty. Because of this, actual structural ductility is larger than reported in the Table 7.10. This issue also exists for the other structures and is dependant on the activation drifts of each of the joints in the structure.

The simplistic formulations to calculate re-centring ratio from damping and ductility were not able to determine re-centring ratios for this structure. The formula was a based on a perfectly elasto-plastic model. Because of this, the post yield stiffness was not accounted for. The low ductilities and relatively large damping reported for this structure suggest that the structure does not re-centre. Figure 7.22 demonstrates clearly that this is not the case.

A more rigorous analysis method may be able to determine re-centring ratios for this structure. One option would be to create a separate model using only post-tensioning. This method would be complicated by issues with combining non-linear moment-displacement curves. As the structure is clearly fully re-centring the extra effort was not deemed worthwhile.

The DBD for this structure predicted a damping of 1.7%. The observed value is much greater than this. This should lower the theoretical seismic demand that this structure is subjected to.

Table 7.10: Re-centring ratios for Structure C

Load Case	Ultimate Drift	Ductility (μ)	Hysteretic Damping (ξ_{visc})	Re-centring Ratio (λ)
SLS	0.39%	-	-	-
ULS	1.9%	1.06	5.0%	[a]
MCE	4.8%	2.67	6.6%	[a]

[a] Conservative re-centring ratio formulation did not work with high damping and low ductilities.

7.5.3 Response history analysis

Non-linear response history analyses were performed on each model. These subjected each structure to ground motion records from observed earthquakes.

Selection of earthquake records

A suite of 16 ground motion records were selected from the PEER Ground Motion Database. These comprised 8 far-field and 8 near-field motions. The records were selected to have similar magnitude and soil characteristics to the assumed site of the case study buildings.

These records were scaled according to the procedure in NZS1170.5. This matched the ground motion spectra to the code spectra near the structure's fundamental period. Periods were estimated using the ADRS analyses described above. Separate effective secant periods were obtained for each limit state. This ensured that the appropriate period was used to scale the ground motions.

The results of these dynamic analyses were used to verify that:

- Inter-storey drift limits were respected
- Floor accelerations were within acceptable levels
- Residual displacements were minimal
- Joint rotations were below failure levels

Seismic analyses were conducted simulating earthquakes at SLS, ULS and MCE levels.

A summary of the records used is given in Table 7.11

Table 7.11: Summary of ground motion records

Event	Year	Mag	Station	Sequence ID	Source Distance (km)	$V_{s,30}$ (m/s)
Imperial Valley	1979	6.5	EC County Center	NGA170	29	192
			Meloland Overpass	NGA171	19	186
			El Centro Array 11	NGA174	29	196
			El Centro Array 12	NGA175	32	197
			El Centro Array 03	NGA178	29	163
			Westmorland Fire Stn	NGA192	53	194
Superstition Hills	1987	6.54	Westmorland Fire Stn	NGA728	20	194
Coalinga	1983	6.36	Parkfield	NGA326	56	185
Morgan Hill	1984	6.19	Foster City	NGA452	54	116
			SF Intern. Airport	NGA469	71	190
San Fernando	1971	6.61	Shandon Array 2	NGA60	224	185
Superstition Hills	1987	6.54	Salton Sea Wildlife Refuge	NGA726	26	191
Loma Prieta	1989	6.93	Redwood City	NGA732	63	133
			Alameda Naval Air Stn	NGA738	91	190
			Emeryville	NGA758	97	199
El Centro	1940	6.9	Peknold	-	-	-

Structure A

The inter-storey drift profile of the structure subject to SLS, ULS and MCE earthquakes is shown in Figure 7.23. The maximum drift profile for each earthquake record is shown and the maximum from all records is highlighted. Additionally, the mean and a range of one standard deviation is shown. The ULS maximum drift is obtained from the NLTHA is similar to that predicted by the ADRS and pushover. Some SLS records were larger than the 0.4% predicted by the ADRS analysis, although none reaches levels where joint activation occurs. There is a large spread in the drifts for MCE events. The maximum drift profile observed is less than the 4.9% predicted by the ADRS analysis.

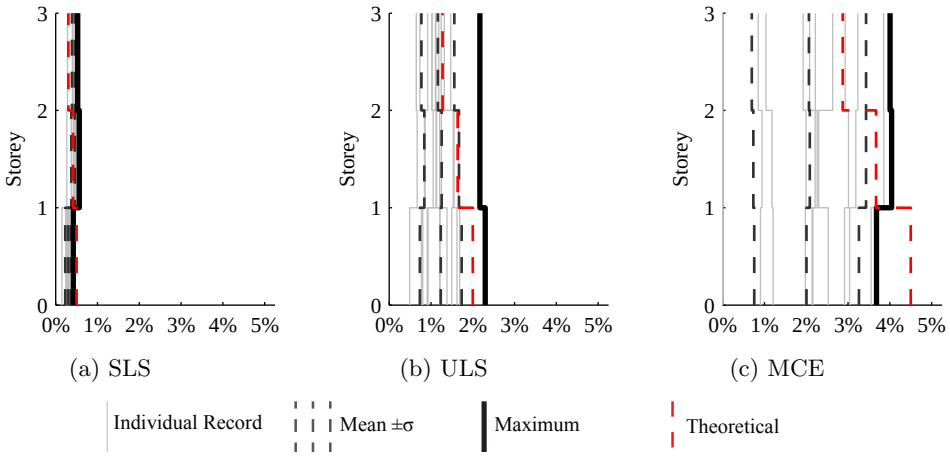

Figure 7.23: Maximum inter-storey drift profile

The maximum shear force in each storey of the structure is shown in Figure 7.24. This shows that the force sustained is far less than the shear capacity of the columns.

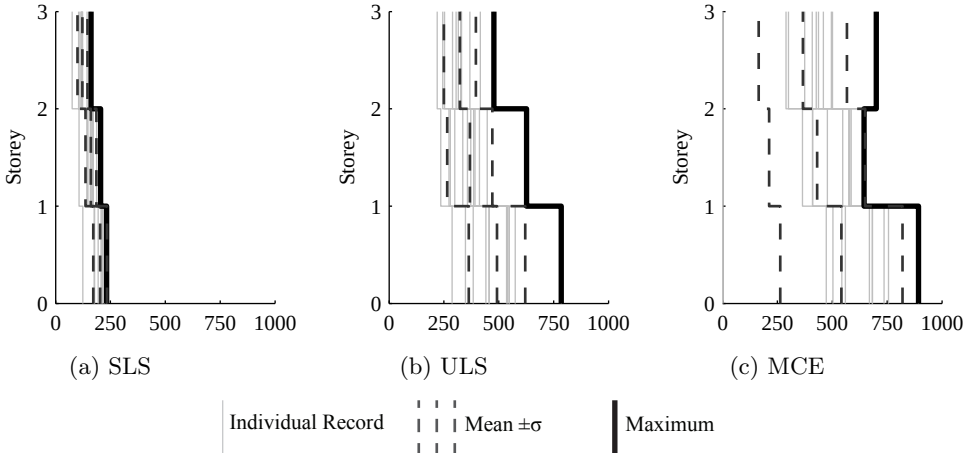

Figure 7.24: Maximum storey shear profile (kN)

The maximum rotation sustained by joints at each level of the structure is shown in Figure 7.25. The maximum rotation predicted by the ADRS analysis for the MCE level earthquakes was 3.2%, above the joint's capacity of 2.9%. Results of the NLTHA show maximum rotations less than predicted. Joint rotations seen in this analysis are beneath the ultimate capacity of the joints as predicted by the MMBA design procedure.

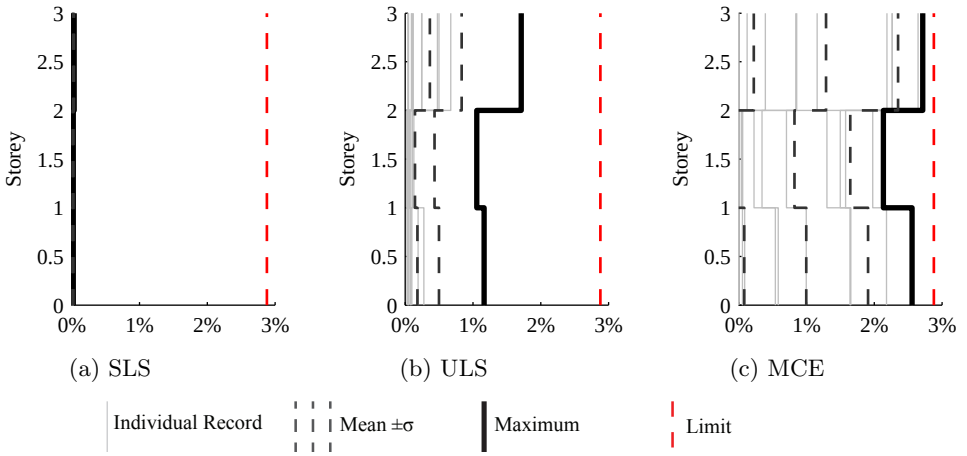

Figure 7.25: Maximum joint rotation

Peak storey acceleration for each earthquake record is shown in Figure 7.26. Due to the transient nature of this signal, the 95th percentile value for each record is shown. This filters out large accelerations which occur for only short periods of time.

A comparison to the floor accelerations prescribed in the parts and portions section of NZS1170.5 (Standards New Zealand, 2004) is shown on each plot. This shows that the peak storey accelerations are below code levels for the majority of cases. Because of this, the loadings for parts from the code should be conservative for design.

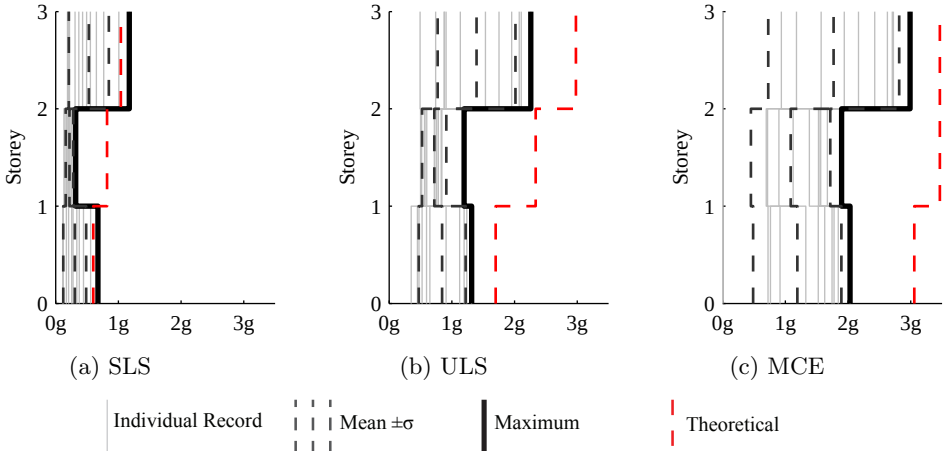

Figure 7.26: Peak storey acceleration profile

Structure B

The maximum inter-storey drift experienced by each level of the structure is shown for each record. These are compared with the predicted profile from the DBD procedure. The increased higher mode effects present in this structure can be seen in the deviation from this profile.

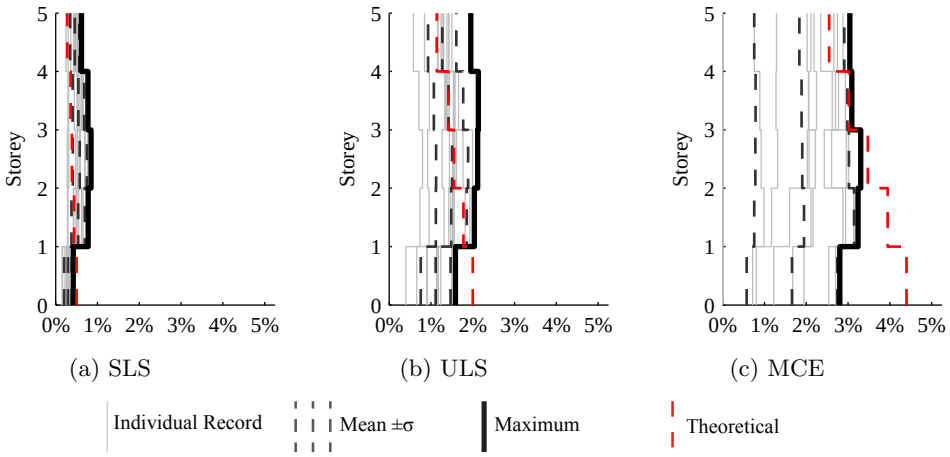

Figure 7.27: Maximum inter-storey drift profile

The shear force in the columns at each level is shown for each record in Figure 7.28. This data can be used to assess the capacity of the timber columns against earthquake demands. In this case, the 1500 kN maximum storey shear under MCE is far less than the capacity of around 2700 kN.

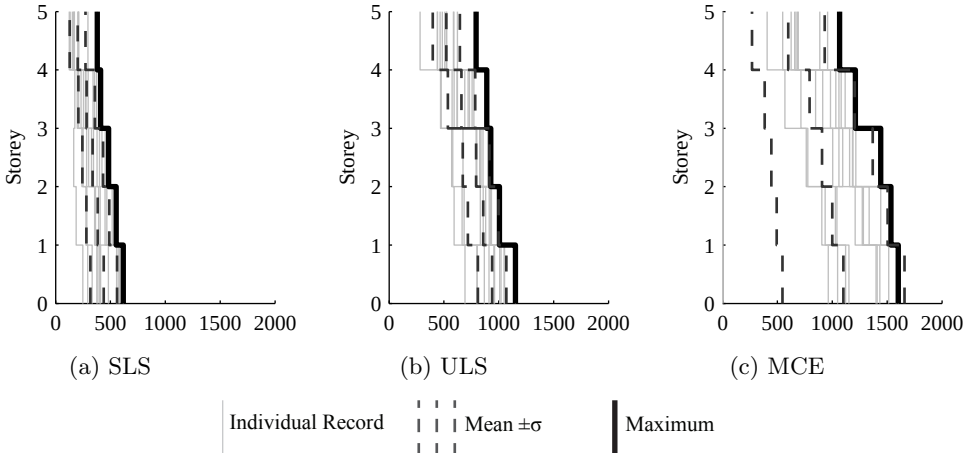

Figure 7.28: Maximum storey shear profile (kN)

The maximum joint rotation from each record is shown in Figure 7.29. The minimum rotation capacity is also shown. SLS and ULS joint rotations are far below capacities for all records. The maximum rotations of some records approach or slightly exceed capacity for the MCE case. This is not thought to be critical as the joints were designed to force a failure in the mild steel components rather than post-tensioning or timber. This means that there is significant residual capacity in each joint. Additionally, there is significant redundancy built into the structure and a failure of a single joint does not imply collapse of the building. The rotation capacity is further than 1 standard deviation from the mean recorded joint rotation. This means that there is less than a 15% chance of the joint reaching ultimate rotation in an MCE event similar to those considered.

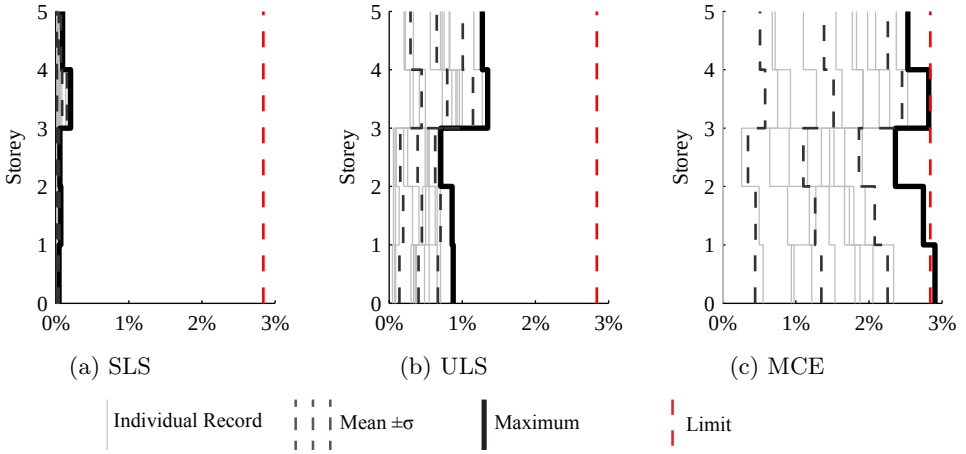

Figure 7.29: Maximum joint rotation

The maximum accelerations recorded at each storey are shown in Figure 7.30. These are compared with the design accelerations for parts and portions loadings in NZS1170.5. The predicted floor accelerations are less than code design requirements for all performance levels. This again means that code provisions provide conservative design advice for parts loadings.

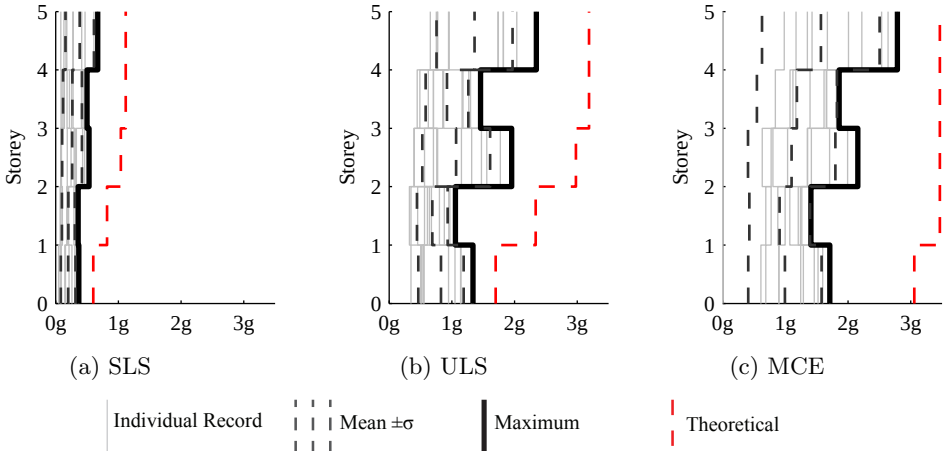

Figure 7.30: Maximum storey acceleration profile

Structure C

The ULS drift predictions from the ground motion records are all less than the predictions from the ADRS.

SLS drifts are centred around the ADRS prediction, with some records exceeding predicted levels. All of the SLS records remained under drifts where joint activation is predicted to occur.

The MCE drifts were widely distributed. The 5.0% limit proposed for MCE drifts was exceeded by one record. This is still greater than one standard deviation from the mean of the records assessed so has only a 15% chance of occurrence for records similar to those assessed.

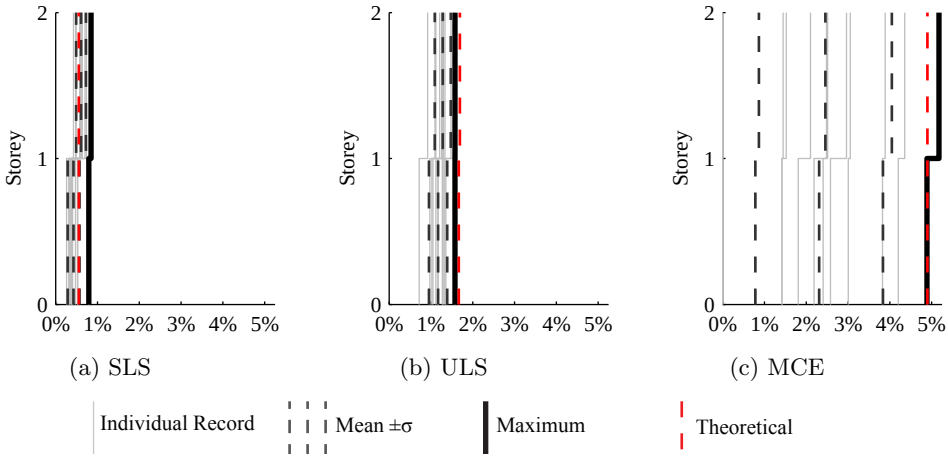

Figure 7.31: Maximum inter-storey drift profile

The maximum shear forces in the columns of each storey are shown in Figure 7.32 for the ground motions simulated. These are all significantly below the shear capacity of the columns in this frame.

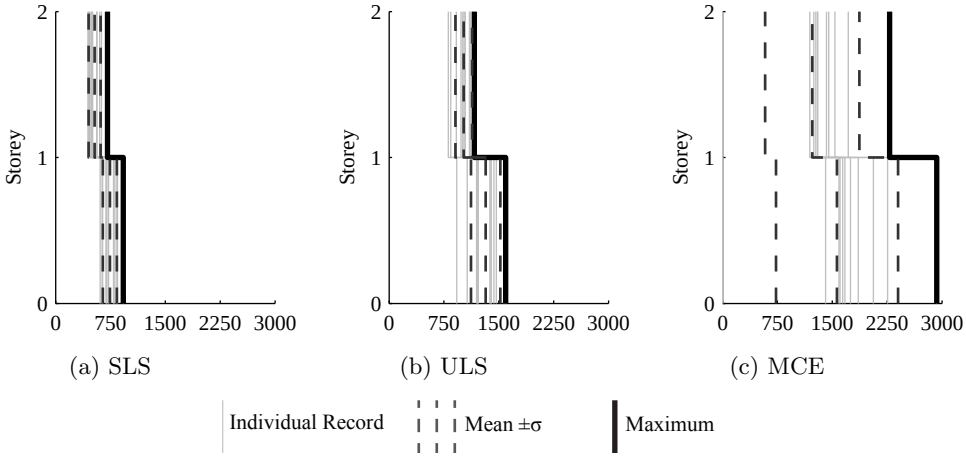

Figure 7.32: Maximum storey shear profile (kN)

Joint rotations for SLS and MCE records are well below the rotation capacity of the joints as shown in Figure 7.33. For MCE events, the rotation capacity was exceeded by two records. A single record produced joint rotation demands of nearly 6%, twice the rotation capacity of the joint. This outlying value may be the result of a numerical anomaly due to ground motion record scaling. If it were to occur, it would be unlikely to cause a collapse of the structure as there is still significant residual capacity within the joints as they have been designed for a failure in the steel dissipative elements rather than in the timber or post-tensioning. The large standard deviation of the records means that the mean minus one standard deviation line ($\mu - 1\sigma$) is not visible on the plot.

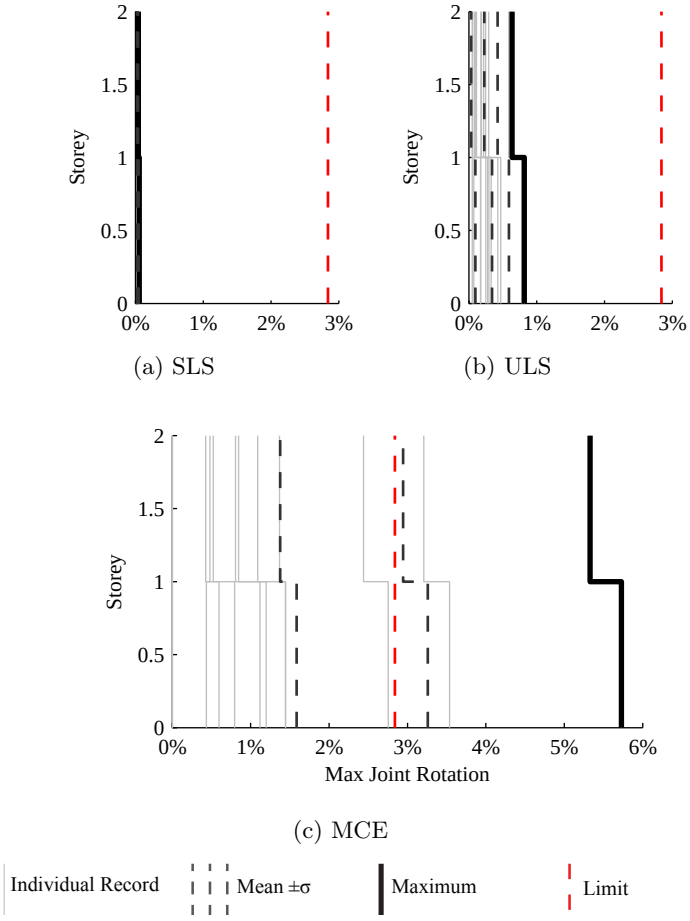

(a) SLS (b) ULS

(c) MCE

Figure 7.33: Maximum joint rotation

The peak storey accleration profile of the records is shown in Figure 7.34. These are compared with the acceleration derived from the parts and portions loading from NZS1170.5. MCE and ULS accelerations are below the value shown by the code. The SLS accelerations are below code levels for all but one record.

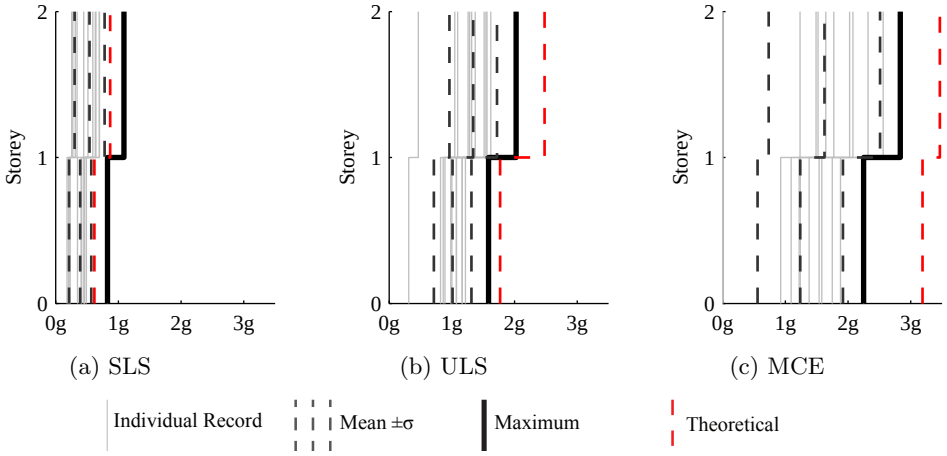

Figure 7.34: Peak storey acceleration profile

7.6 Results

DBD procedures were used to design these structures. Yield drift formulations taking into account timbers flexibility must be used for this. The yield drift estimations proposed in literature (Priestley *et al.*, 2007) were devised for concrete frames and grossly under-predict timber frame's yield drift. Proposed modifications to the method(Newcombe, 2007) were used to account for this. Had these not been used, predictions of damping would have been artificially large.

Connections were detailed for the joints in each structure. Options for joint reinforcement, dissipation and connection systems were combined to create these joints. Screw based joint reinforcing was used for the majority of these designs. Due to the large moments in the joints designed, steel joint reinforcing would have meant accepting some damage to the timber. NPD and Plug and Play dissipaters were able to be used with a range of connection systems to produce designs with almost identical performance. Connections were detailed using each of these dissipation options.

Non-linear pushover analyses gave insight into the performance of the designs under various drift levels. This resulted in changes to the designs of some structures. This analysis type is an excellent design tool as it allows a comparison of performance at each limit state. Additionally, the effect of design changes to meet requirements can be readily assessed.

Control of SLS drifts often governs member sizing. Joint design has little effect on performance at SLS as the designer should prevent joint activation for this limit state.

Interstorey drift profiles were generally consistent between the ADRS and NLTHA analyses for SLS and ULS records. There was a large variance for MCE and the ADRS drifts were exceeded for some records at this limit state. This may be due to differences between the code spectra and earthquake records being amplified for this limit state.

Storey shears were calculated for each record in the NLTHA. These were used to assess the capacity of the columns of the frame. This was not seen to govern the behaviour of the structure in any of the cases considered.

The maximum rotation demand of a joint at each level was recorded. These were compared with the minimum dependable rotation capacity of the joints from the MMBA design. There were no issues with joint rotation for SLS and ULS excitations as all demands were significantly below capacity. The rotational capacity of some joints was exceeded for some MCE records. This is unlikely to cause collapse of the structure as there is significant redundancy in the structure. Minimum dependable capacities are shown, and joints were designed to exhibit a failure in the mild-steel elements rather than in timber or tendons.

Storey accelerations were recorded for each ground motion used in the NLTHA. These were compared with the floor accelerations prescribed in NZS1170.5 for parts and portions loadings. The code accelerations were greater than calculated accelerations for the majority of the records simulated. This gives confidence to designers that non-structural elements within these buildings can be designed according to code provisions.

7.7 Conclusions

DBD is recommenced for the design of seismic resisting post-tensioned timber frame structures. Alterations to the procedure are necessary to capture the increased flexibility of timber members.

Non-linear pushover analyses should be undertaken to assess the structure's behaviour at each limit state. These ADRS analyses give good estimations of drifts however a NLTHA should be performed if more precise estimates are required. Members sizes are often controlled by SLS drift limits.

Single and multi-bay one-way frame systems have been demonstrated to work for case study structures up to five stories tall.

NPD and Plug and Play dissipaters give very similar structural performance.

Chapter 8

Discussion

This chapter details findings from each section of the research presented in this thesis. Discussions and comparisons are made based on:

- Construction and fabrication,
- Experimental testing,
- Numerical and analytical modelling of joints,
- Design considerations and case study structures.

Considerations for the components of each joint are further detailed in each section. This was done to produce evaluation matrices for aspects of each component and an overall summary matrix for each joint configuration.

8.1 Fabrication and Assembly

An experimental testing campaign was undertaken to evaluate the performance of six configurations of beam column joints. Full-scale specimens were designed to test two types of joint reinforcement and three types of energy dissipation devices. Joints without additional dissipation were also tested. Joints using dissipation were designed to match the moment capacity of the first, reference joint. All joint designs were able to meet this demand. The re-centring ratio was altered between joints using different reinforcement, changing the shape of the flag-shaped hysteresis produced.

Construction and modification of all but the initial specimen was conducted by the author in the University of Canterbury structures laboratory. This enabled the relative difficulty of construction to be assessed and other related issues identified for each joint type.

8.1.1 Joint Reinforcement

The installation of reinforcing screws was time consuming due to the number and length of the screws to be installed. For this option to be used effectively in a building, it is likely that an automated system would be required to raise efficiency. Such systems are common in Europe and are beginning to become available in the New Zealand marketplace. Computer Numeric Control (CNC) pre-drilling is also likely to increase the accuracy with which screws are installed

into the timber. This is particularly important for minimising clashes when screws are installed from several directions into the joint.

The steel reinforced joint was constructed by external fabricators rather than in the laboratory. Because of this, it was not possible to directly assess the ease of fabrication of this joint detail. The manufacture of this detail used mainly standard steel fabrication techniques. Because of this, it is likely to be considerably easier to fabricate than the joint with screw reinforcing. This could lead to cost and time savings over a screw based system in building scale projects. The steel fabrication industry in New Zealand is well developed and the details used for joint reinforcement are familiar to the industry. This should enable time savings in fabrication and a reduction in cost due to decreased uncertainty. Steel reinforcing may be used where constructibility considerations are paramount and moderate moment capacities are required.

A ranking of joint reinforcement options considering the factors outlined above is provided in Table 8.1.

Table 8.1: Joint reinforcement summary matrix for construction considerations

Criteria	Steel Based	Screw Based
Ease of Installation	1	2
Accuracy Requirements	1	2
Contractor Familiarity	1	2
Tolerance Requirements	2	1
Overall Rank[1]	1	2

[1] Lower rank is better

8.1.2 Dissipation Devices

Three types of dissipation devices were considered. These were:

- Plug and Play dissipaters,
- Necked Plate Dissipaters
- Timber plus dissipaters,

These dissipaters were connected to the beam and column using:

- Threaded couplers
- Fully threaded screws
- Timber rivets.

Steel based dissipaters were straightforward to fabricate. The construction of these dissipaters utilises techniques already familiar to the industry. Machined parts were fabricated from stock steel grades and sizes. The epoxy or grout used in the Plug and Play dissipaters is also a commodity product. This should enable these dissipaters to be produced competitively.

Robust fabricator validation and construction monitoring are required due to the dependence of dissipater performance on tight tolerances and steel grade. The suitability of the steel grade used must be established. Appropriate controls must be in place to ensure the specified material is

used. Adequate quality of workmanship must be maintained to ensure dissipaters meet design requirements.

NPDs and Plug and Play dissipation systems were simple to fabricate using standard workshop technology.

The Timber Plus dissipaters were more complex and time consuming to fabricate and install than the other options considered. These dissipaters added significant apparent bulk to the joint. Conservative assumptions were made for these specimens and it is likely that the size of these dissipater blocks could be reduced significantly. This may provide an option to designers when aesthetic considerations govern the design.

Plug and Play dissipaters incorporate buckling resistance into the removable dissipater units. The grout or epoxy filled tubes are attached in the workshop and can arrive on-site as a complete unit. This may provide time savings on site.

NPDs require buckling resisting plates and screws to be installed after installation of the dissipaters. This was not very time consuming for a single joint, but may add significant extra work for a building project.

The Timber Plus dissipaters must be connected once the joint is assembled. Because of the number of screws required, this requires significant effort. This may cause large additional costs due to increased work required on-site.

Little design advice was available for the Timber Plus dissipaters. The dissipaters constructed for testing used a concrete crack injection epoxy to fix the mild steel rods to the timber. This was clearly outside of the specifications for both the epoxy and Timber Design Guide (Buchanan, 2007). However, consultation with the manufacturer suggested that this product would be appropriate. It is likely that further testing of this connection would be required by consenting authorities before use in a building project. This adds to the complexity and cost of using this dissipation system.

Each joint detail was tested twice. This enabled an assessment of the repairability and any loss in performance to be made. No substantial damage was observed in the tests. This meant that repairs consisted of re-stressing the joint and replacing yielded dissipative elements.

Removal of some dissipaters after testing was difficult, due to buckling or elongation of dissipaters resulting in residual stresses. Simply cutting dissipaters in half was an easy way to remove them from the joint.

The Plug and Play dissipaters were the simplest to replace. The threaded coupler and slotted plate arrangement created a tight connection, while allowing some flexibility during installation.

The NPDs installed with riveted plates were more difficult to replace. The two groups of bolts did not line up after testing. This was overcome by over-sizing one group of holes in the dissipater and fitting a site welded washer to the dissipater to ensure a snug connection.

The NPDs connected with ZD plates were more time consuming to replace. Adjustments to the position of each of the eight connectors per dissipater were made by tightening and/or loosening the screws attaching them to the beam and column. This was time consuming as multiple iterations were required to achieve a good fit.

The Timber Plus dissipaters were not considered to be replaceable due to the large number of screws installed in opposing directions.

A comparison of practical considerations of energy dissipation options and connection systems is provided in Table 8.2.

Table 8.2: Dissipation device and connection type summary matrix for construction considerations

Criteria	Plug and Play	NPDs		Timber Plus
	Couplers	Rivets	Screws	Screws
Ease of Fabrication	1	2	3	4
Accuracy Requirements	1	2	3	4
Contractor Familiarity	1	3	2	4
Replaceability	1	2	3	4
Overall Rank[1]	1	2	3	4

[1] Lower rank is better

8.2 Experimental Results

The results from the experiments undertaken are used to evaluate the performance of each joint configuration. Each joint was subjected to a fully reversing monotonically increasing displacement history up to inter-storey drift levels of ±3%. Observations regarding both connection reinforcement and dissipation systems are outlined below.

8.2.1 Joint Reinforcement

The moment capacity of both joint types matched design values well. Differences observed were within ±15%.

Joints with a high stiffness to yield will limit displacements in serviceability level earthquakes. Reducing inter-storey drifts will limit damage to non-structural elements in the building. The screw reinforced joint had a stiffness around 50% larger than the steel reinforced joint. This is due to the screws passing through the centre of the joint and providing a more direct load path.

Minor timber damage was observed during testing of the steel reinforced joint with Plug and Play dissipation. Stiffness incompatibilities between parallel load paths meant that an epoxy joint split in this case. The epoxy was only included to aid fabrication and not as part of the intended load path. Because of this, there was not a large reduction in the strength or stiffness of this joint.

Table 8.3: Joint reinforcement summary matrix for experimental testing considerations

Criteria	Steel Based	Screw Based
Moment-Rotation response	2	2
Joint stiffness	2	1
Damage observed	2	1
Overall Rank[1]	2	1

[1] Lower score is better

8.2.2 Dissipation Devices

External mild steel dissipaters contributed to the joint's moment capacity. The difference between design and observed moments at 3% drift levels do not show a significant difference between Plug and Play or NPDs. The Timber Plus dissipater had a larger moment capacity than designed. This may be undesirable as larger forces will be carried by the structure due to a decrease in ductility.

Some dissipater buckling occurred at large drift levels This was particularly evident in the first test of the NPDs. A reduction of around 8% of the ultimate moment capacity of the joints was observed following this damage. A revised design using large anti-buckling plates was tested with no evidence of buckling. The ranking for NPDs in Table 8.4 has been based on the dissipaters with this additional restraint.

The stiffness increases from dissipation devices are proportional to the area of yielding steel. Because of the different design parameters for the two joints, no conclusions can be drawn directly, particularly when comparing dissipation devices. However, even with the increase in post-tensioning, a clear increase in joint zone stiffness was observed in the screw reinforced joint.

Each of the dissipation devices tested has been assigned a qualitative ranking according to the experimental results described above. These are summarised in Table 8.4.

Table 8.4: Dissipater summary matrix for experimental testing considerations

Criteria	Plug and Play	NPDs	Timber Plus
Moment capacity	1	1	3
Cyclic stability	1	1	3
Stiffness	1	3	3
Overall Rank[1]	1	2	3

[1] Lower score is better

8.3 Modelling

Numerical models of joint performance and analytical models of local behaviour have been created for each joint type. These were first used predictively and revised following testing.

The moment-rotation behaviour of the joints is the primary indicator of each joint's performance. Because of this, the accuracy of predictive models is of paramount importance to designers. The design moment capacity was predicted adequately by the models for all joints. This should give designers confidence that structures will perform as expected in seismic events.

8.3.1 Joint Reinforcement

The effect of joint reinforcement on model accuracy is considered in the following section. Comparisons between accuracy at ultimate and service drift levels are made.

The ability of the models to predict design level moments is fundamental to its applicability to these structures. Models for both steel and screw reinforced joints were able to capture the moment attained at 3% drift levels.

The yield point of the system can be used to predict gap opening, when structures will transition into non-linear behaviour. The model for the joint using Timber-Plus dissipaters did not predict yield well. Models for the remaining screw reinforced joints gave the most accurate predictions of yield drifts.

Behaviour in structures prior to gap activation is largely governed by member sizing and joint reinforcing detailing. The ability of the models to accurately predict pre-yield stiffness is key to capture this behaviour. The steel based joint's initial stiffness was over predicted by the models. This is likely to lead to structures which exhibit larger SLS drifts. The screw based joint was modelled with far more accuracy. This difference is due to the non-linear response of the steel joint before gap opening. It is thought that this was caused by interference with the shear key.

There was more variability in the accuracy of predictions of the pre-yield behaviour of the joints. This was seen in predictions of yield moment and yield rotation as well as secant stiffness to yield. Joints using the screw reinforcing matched predicted behaviour well. The steel reinforced joint did not conform as closely to predictions. This is particularly evident in the case without additional dissipation and may be due to lower than predicted interface stiffnesses of the steel reinforced joint.

A comparison of the modelling of each joint reinforcing type is shown in Table 8.5.

Table 8.5: Joint reinforcement summary matrix for modelling considerations

Criteria	Steel Based	Screw Based
Design Level Accuracy	2	1
Pre-yield Accuracy	2	1
Variability	2	1
Overall Rank[1]	2	1

[1] Lower score is better

8.3.2 Dissipation Devices

Effective models of the response of dissipation devices are needed to accurately predict the behaviour of Pres-Lam beam column joints. The efficacy of numerical and analytical models at predicting behaviour for each of the dissipation systems test is compared below.

The moment capacity provided to the joint by dissipative devices must be modelled accurately. The model's ability to predict moment at 3% drift was used to compare this for each dissipation system. Both the NPD and Plug and Play dissipaters were predicted to within ±10%. The model for the Timber Plus dissipation system was the least accurate.

Yielding mild steel provides additional energy dissipation to these systems. This lowers the seismic demand on structures. Both of the joints without dissipation developed nominal amounts of damping. Nevertheless, designers should not rely on this for their structures. The hysteretic damping for NPDs was predicted the most consistently. The updated model for Plug and Play

dissipaters was very accurate with an error of 7%, the initial model was less accurate. The Timber Plus dissipaters were predicted the least accurately with errors of up to 40%.

Dissipater performance was assessed by comparing numerical joint models to data and by using analytical models of local behaviour. Both types of models conclude that 'simpler' dissipaters, with more direct load paths, exhibit both better and more easily predictable responses.

Connections using threaded couplers were the simplest to assess and exhibited the least losses due to connection slip and flexibility. The Timber Plus dissipaters had a far more complex load path involving screws, timber blocks and epoxy. This is reflected in the reduced performance predicted by analytical models as well as the inaccuracies in predictions of the numerical model.

Model predictions for joints designed for complete re-centring were more accurate than for those where only partial re-centring was targeted. Because of this it is not possible to directly assess the effectiveness of models in predicting residual displacements. Where full re-centring was targeted, the models predicted residual displacements acceptably.

A comparison of models for each dissipation type is shown in Table 8.6.

Table 8.6: Dissipater type summary matrix for modelling considerations

Criteria	Plug and Play	NPDs	Timber Plus
Numerical Model Accuracy	2	1	2
Connection Losses	1	2	3
Residual Displacement	3	3	3
Overall Rank[1]	1	1	3

[1] Lower score is better

8.4 Design Guidance

Comprehensive and robust design guides and advice for each component of the joint are necessary for the design of these joints and the wider adoption of Pres-Lam technology. The New Zealand timber design standard (NZS3603) (Standards New Zealand, 1993) does not contain up-to-date methodologies for designing all of the components required in these joints. European Technical Approvals, manufacturers' product literature and design guides (STIC, 2013) can be used to provide guidance to designers.

8.4.1 Joint Reinforcement

Reinforcement systems are necessary to protect the LVL in the column against perpendicular to grain compression. There is little specific design guidance available directly related to reinforcing joints with controlled gap opening. Designers of this reinforcement must therefore adopt conservative design assumptions, considering stiffness as well as strength. Both steel and screw based options have been considered in this research.

This section compares steel and screw based reinforcement systems based on:

- Design guidance availability

- Ease of design
- Joint capacity
- The body of research surrounding each system
- The system's impact on connection systems.

Screw based joint reinforcement is straightforward to design. Design guides (Würth GmbH & Co, 2011, SPAX Construction, 2012, Rotho Blaas s.r.l, 2012) produced by screw manufacturers include this procedure as well as tabulated design data. Large stresses imposed on the joint at high imposed drifts may mean that a large number of screws are required. This can mean that dimensioning considerations including spacing and minimum edge distances govern design.

The steel based reinforcement solutions require careful detailing to ensure that rocking behaviour is not negatively affected. This includes considerations of both relative stiffness of components and construction tolerances.

Screw based reinforcing acts similarly to piled foundations. Maximum joint reinforcement capacity charts are provided in Chapter 6. These show that screw based reinforcing systems can achieve far greater capacities than detailing using steel plates, when bearing plates are provided.

A large body of research surrounds both steel and screw based reinforcement systems. Research performed on screw based reinforcement has been undertaken by manufacturers. This may increase designer's confidence in this research and the reinforcing system.

The steel based system is well suited for use with threaded couplers and Plug and Play dissipaters. Steel plates are unobtrusive and don't impact on dissipater connections. The high density of screws required in some joints may impact on screwed dissipation connectors. Riveted connections are unlikely to be affected by either reinforcement option.

A comparison of screw and steel based joint reinforcement systems is provided in Table 8.7.

Table 8.7: Joint reinforcement summary matrix for design considerations

Criteria	Steel Based	Screw Based
Guidance availability	1	1
Ease of design	2	1
Joint capacity	2	1
Body of research	2	1
Connection Options	1	2
Overall Rank[1]	2	1

[1] Lower score is better

8.4.2 Dissipation Devices

The availability and ease of use of design guides has been considered when evaluating dissipation options and connection methods.

Dissipaters

Design guidance for detailing energy dissipation devices is not as comprehensive as for connections and reinforcement.

While these devices are generally straightforward to design, complications in their detailing can affect behaviour. The buckling resistance of these devices is particularity critical to their cyclic performance. An issue with the designing of these dissipaters is the lack of a simple method of sizing buckling restraint. Uncertainties are compounded by the plastic elongations the dissipaters undergo during use. Generally, conservative design approaches have been taken to the detailing of dissipaters. These are often not based on clear design principles, rather on rules of thumb. While this leads to workable designs, it may reduce cost effectiveness.

The dissipation devices tested are conceptually very simple. This makes them well suited to analytical and numerical modelling. Simple models can predict their behaviour well. This simplifies their design. The NPD and Plug and Play dissipaters are less complex than the Timber Plus system due to having fewer yielding locations.

The design of discrete energy dissipation devices deviates from traditional accepted design solutions. The body of research surrounding each dissipater type will therefore be an important factor in designer's decisions around dissipation systems. Dissipation devices with a large number of tests confirming their behaviour will enable designers and consenting authorities to have greater confidence in the system. Conversely, less thoroughly tested options may require further verification before use.

Plug and Play dissipaters have been thoroughly tested in previous research campaigns. These have been seen to perform well for a large range of joint designs. NPDs have not been as thoroughly tested, however a number of positive results have been recorded. Timber Plus dissipation is relatively untested. Because of this, the system is likely to require more strenuous validation before its use in a building.

A comparison of the design issues associated with each dissipater type is shown in the assessment matrix presented in Table 8.8

Table 8.8: Dissipater type summary matrix for design considerations

Criteria	Plug and Play	NPDs	Timber Plus
Ease of design	2	2	3
Conceptual simplicity	1	1	3
Body of research	1	2	3
Overall Rank[1]	1	2	3

[1] Lower score is better

Connection Systems

Design advice available for connection systems was compared in order to provide qualitative rankings for each system. Table 8.9 shows a comparison of design considerations of dissipation connection options.

Threaded couplers are the simplest to design of the connection systems considered. They are widely supported by manufacturers' product literature. Considerations are codified and designers are already familiar with them.

Design guidance for fully threaded screws is readily available from manufacturers. These guides give design criteria for inclined screws acting in tension as well as screws acting as compression reinforcement. Some alteration may be beneficial for use with New Zealand LVL due to differences in density compared with European Kerto.

ZD plates are a proprietary system. Guidance for their design is therefore based on manufacturer provided ETA (SWG Schraubenwekr Gaisbach GmbH, 2011). The design methodology presented in this document is simple and straight-forward.

The design guide for timber rivets (Quenneville & Zarnani, 2013) is particularly comprehensive. Spreadsheet based design tools are straight forward to develop and, in some cases, already available. This greatly eases the rapid assessment of connection types, allowing for a faster, more efficient design. The factors described above have been used to develop the assessment matrix for connection types shown in Table 8.9

Dissipater performance and load path simplicity are linked. Simple load paths from the yielding element of the dissipater to the beam and column ease design and limit opportunities for performance losses to arise. The simplest of the options considered were the threaded couplers. Screws and rivets introduced more elements to the load path and decreased connection stiffness. The Timber Plus dissipaters had the most complex load path, using inclined screws, epoxy, and the LVL blocks.

Designer familiarity with connection systems will affect their inclusion on building projects. Threaded couplers are widely used in the construction industry and practitioners are comfortable designing and specifying them. Fully threaded screws are widely used overseas, although less so in New Zealand. Other systems including rivets are less commonly used.

The suitability of the various connection types considered for each dissipater may also limit design options. While the number and type of suitable connection options may not govern the choice of dissipation system, it should be considered as part of joint design.

Threaded couplers are best suited to Plug and Play dissipaters. Screw based connection systems are able to be used with both Timber Plus and NPDs. Rivets are best suited to NPDs. Designers are likely to decide on dissipation options prior to assessing connection systems. This will therefore guide their choice of connections. As such, there is little difference between the options from this perspective.

Table 8.9: Connection type summary matrix for design considerations

Criteria	Couplers	Screws	ZD Plates	Rivets
Guidance availability	1	1	1	1
Load path simplicity	1	3	3	2
Ease of design	1	2	3	3
Designer familiarity	1	2	4	4
Dissipater options	3	2	2	1
Overall Rank[1]	1	2	4	3

[1] Lower score is better

8.5 Case Study Structures

Complete Pres-Lam structural systems were investigated in Chapter 7. These structures incorporated the joints tested in this research. DBD methods were used to arrive at initial designs. Joints were developed to meet the requirements from these designs. Some modifications to the initial designs were required to meet performance specifications. Modifications were not dependant on the joint reinforcement or dissipation system chosen.

Plug and Play and NPD systems were both able to be designed satisfactorily. Timber Plus dissipaters were not considered for the case study structures due to the increased complexity associated with their design, fabrication and installation. Because of the decision to exclude Timber Plus dissipaters from the design of case study structures, no ranking is given in this regard.

Some of the joints designed were subject to large moment demands. This placed heavy perpendicular to grain compression loading on the LVL in columns. Screw reinforced joints were able to be detailed with a larger capacity than steel reinforced joints. This meant that screw reinforced joints were detailed for most of the joints in the structures.

8.6 Summary of Joint Designs

Findings from the design, construction, performance, and repair of each of the joint options assessed are summarised in the performance matrices below. These tables are aimed at allowing an overall comparison to be made between each joint type. Comparisons of joint reinforcement and dissipation options are also presented separately. Each element is compared based on:

- Constructibility,
- Experimental results
- Modelling
- Guidance available to designers

The rankings provided do not consider a weighting factor for each criteria. Designers may wish to prioritise certain aspects of the matrix to fulfil design requirements.

8.6.1 Joint Reinforcement

Steel and screw based joint reinforcement options were compared based on the criteria above. The results of these are shown in Table 8.10. This table highlights the compromise between performance and constructibility that must be made when choosing between each reinforcement type.

Table 8.10: Summary matrix for joint reinforcement

Criteria	Steel Based	Screw Based
Constructibility	1	2
Experiential results	2	1
Modelling considerations	2	1
Design Advice Availability	2	1
Case study structures	2	1
Overall Rank[1]	2	1

[1] Lower rank is better

8.6.2 Dissipation Devices

Plug and Play, NPDs and Timber Plus dissipation devices are compared in Table 8.11. Plug and Play dissipaters have been the most commonly used in previous testing and building projects. These dissipaters have benefits over the others in terms of constructibility and design advice availability. NPDs are compatible with a number of connection systems and joint reinforcement options. These may become more widely used if more design advice is produced and contractors become more familiar with the screwed or riveted connection systems used. The Timber Plus dissipater was the most complex to design and construct. Its complex load path also reduced performance.

Table 8.11: Summary matrix for dissipater types

Criteria	Plug and Play	NPDs	Timber Plus
Constructibility	1	2	3
Experiential results	1	1	3
Modelling considerations	1	1	3
Design Advice Availability	1	3	3
Overall Rank[1]	1	2	3

[1] Lower score is better

8.6.3 Joint Designs

The joint designs tested are evaluated in Table 8.12. This matrix provides a ranking of joint designs based upon the individual component matrices described above.

Each of the factors described in the sections above has been used to provide rankings for dissipation and joint reinforcement systems. These have been combined to provide the joint rankings shown.

The best ranked joints were those using Plug and Play dissipaters with steel reinforcing or NPD with screw based reinforcing. Designers may weight each of the factors described above differently or value alternative criteria. This may change the ultimate ranking of each joint design. As such the rankings provided are indicative only and should not preclude the use of any of the systems detailed.

Table 8.12: Summary matrix combined joint designs

Item (Rank)	Steel (2)	Screw (1)
Plug and Play (1)	1	-
NPD (2)	3	1
Timber Plus (3)	-	4

[1] Lower rank is better

Chapter 9

Conclusions

Details of the fulfilment of the objectives set out in Chapter 1 are provided in this chapter. These are compared to the overarching aim of providing detailing guidance to designers.

These objectives were to:

- Design, construct and assemble a selection of joint details, to gain insights about their constructibility, complexity and repairability.
- Undertake an experimental testing campaign to assess each joint's seismic performance.
- Compare the observed behaviour with predictive models of joint response.
- Provide design and detailing recommendations for beam column joints.
- Show how these joints can fit into structural systems by designing and assessing case study structures.

9.1 Joint Design and Construction

- Seven joint configurations were designed and constructed.
- Joints were designed to match the moment capacity of a benchmark joint used in a building in Christchurch.
- Joint design was completed using state of the art procedures from previous Pres-Lam research and industry.
- Issues around fabrication and constructibility were identified.
  - tolerance issues are key to ensuring the joint can be assembled efficiently.
  - construction time can be significant depending on connection type.
  - fabrication techniques should be suited to the construction environment e.g. avoid installing many screws on site.
- Contractor's familiarity with the techniques and products required may affect the choice of reinforcing or dissipation system.

9.2 Joint Testing

- Each joint configuration was subjected to a cyclic displacement history up to 3% inter-storey drift.
- The Moment-Rotation response was recorded for each joint. Observed moment capacity at targeted drifts was within 15% of the design value.
- Some minor damage was observed in the tests. This was mainly limited to epoxy included for constructibility and did not significantly affect the response of these joints.
- The stability of the hysteresis loops produced was assessed to investigate possible degradation of seismic performance. The stiffness reductions observed are believed to be due to a combination of connection slip and dissipaters not fully recovering plastic elongations after each cycle.
- Screw based joint reinforcing increased joint stiffness compared to steel armouring.

9.3 Comparison of Joint Behaviour with Numerical Predictions

- Numerical models were compared with experimental data.
- Numerical predictive models provided accuracy when compared to experiential results
  - Design level moments were matched to within ±10% for all but the Timber Plus joint.
  - Yield stiffness was matched to within ±15% for most joints.
- The models were not able to capture cyclic stiffness degradation or unloading stiffness accurately. Energy dissipated by the system was slightly lower than predicted due to this. Error in hysteretic damping predictions was 15-45%.
- Data for neutral axis depth was widely scattered. MMBA based models qualitatively predicted this behaviour with some accuracy.
- Localised models of dissipater connections showed the importance of minimising slip to achieve efficient dissipation.

9.4 Design Recommendations

- Variability in materials and construction accuracy will affect joint performance. Designers should consider the effect of these uncertainties on joint performance.
- Connections between energy dissipation devices and timber must minimise slip and elastic deformations while considering constructibility.
- The design of energy dissipation devices must include adequate buckling resistance to ensure satisfactory performance.
- Screw based reinforcing should be used where maximum performance is required. Screw based reinforcing was able to achieve capacities 3-5 times larger than steel armoured joints.

- Steel based reinforcing should be considered where ease of fabrication and assembly govern design.
- Design charts showing maximum achievable moment capacities for use as an initial design were produced.
- A range of typical connections and reinforcing designs are provided to designers for preliminary sizing.

9.5 Case Study Structures

- Three case study Pres-Lam frame structures were considered, designs were produced for structures up to five stories tall.
- DBD procedures are recommended for the seismic design of post-tensioned timber frames.
  - These procedures require modification for use with timber structures, in particular, incorporating the increased flexibility of the timber frame system. Previous research provides guidance on this.
- Non-linear pushover analyses should be undertaken to validate expected seismic performance.
  - The structure should be assessed at SLS, ULS and MCE levels.
  - SLS conditions often governed member sizing.
- NPD and Plug and Play dissipation systems were able to be designed to achieve very similar performance levels.
- Screw based reinforcement was required for most of the joints due to the large moment demands.

9.6 Further Research

Several areas where further research would be beneficial were identified in this research. These included:

- More comprehensive guidance for buckling resistance of yielding steel dissipaters.
- Accurate stiffness predictions for dissipater connections to timber including screws, rivets and proprietary connection systems.

More information in these regards would give greater confidence to designers when specifying Pres-Lam frame systems.

Constructing an increased number of Pres-Lam frames and disseminating the knowledge gained is increasingly important as this technology transitions from the laboratory to the construction site. This will likely prove the most effective way of discovering and addressing shortcomings in the body of knowledge supporting Pres-Lam structures.

References

ACI. 2001. *Acceptance Criteria for Moment Frames Based on Structural Testing (ACIT1.1-01) and Commentary (ACI T1.1R-01).* Tech. rept. Innovation Task Group 1, American Concrete Institute and Collaborators, Farmington Hills, MI.

Baird, A, Smith, T, Palermo, A, & Pampanin, S. 2014. Experimental and numerical Study of U-shape Flexural Plate (UFP) dissipators. *In: NZSEE.*

Beck, J. L., & Skinner, R. I. 1973. The seismic response of a reinforced concrete bridge pier designed to step. *Earthquake Engineering and Structural Dynamics*, **2**(4), 343–358.

Blandon, Carlos Andres. 2004 (Oct.). *Equivalent Viscous Damping Equations for Direct Displacement Based Design.* M.Phil. thesis, European School of Advanced Studies in Reduction of Seismic Risk, Università degli Studi de Pavia.

Buchanan, Andrew Hamilton. 2007. *Timber design guide.* Wellington, N.Z.: New Zealand Timber Industry Federation. Book, Whole.

Canterbury Earthquakes Royal Commission. 2012. *Final Report. Volume 3. Low-Damage Building Technologies.* Vol. 3. Canterbury Earthquakes Royal Commission.

Carr, A. J. 2008. *RUAUMOKO program for inelastic dynamic analysis - user's manual.*

Cattanach, A, & Pampanin, S. 2008. 21st century precast: the detailing and manufacture of NZ's first multi-storey PRESSS-Building. *In: NZ Concrete Industry Conference, Rotorua.*

Chopra, Anil K, & Goel, Rakesh K. 1999. Capacity-demand-diagram methods based on inelastic design spectrum. *Earthquake Spectra*, **15**(4), 637–656.

Cormack, Gavin. 1988. The Design and Construction of the Major Bridges on the Mangaweka Rail Deviation. *Transactions of the Institution of Professional Engineers New Zealand: Civil Engineering Section*, **15**(1), 17–23. Journal Article.

Cusiel, M. R., Newcombe, M., Pampanin, S., Buchanan, A., & Palermo, A. 2010. The Effect of Joint Flexibility on the Seismic Response of Post-Tensioned LVL Frames. *In: ECEE.*

Devereux, C. P., Holden, T. J., Buchanan, A. H., & Pampanin, S. 2011. NMIT Arts & Media Building-Damage Mitigation Using Post-tensioned Timber Walls. *In: Proceedings of the 9th Pacific Conference on Earthquake Engineering.*

Dominion Post. 7 Feb 2012. *New Massey building to spring back.*

European Committee for Standardization. 2004. *Eurocode 5: Design of timber structures.* Tech. rept. EN 1995-1-1:2004+A1:2008. Brussels.

EXPAN. 2012. Screw-Gluing (Screw-Lamination). *In: Guidelines for Fabricators.* EXPAN.

FEMA. 2006. *Next-Generation Performance-Based Seismic Design Guidelines: Program Plan for New and Existing Buildings.* Applied Technology Council.

fib. 2003. Alternative design philosophies and seismic response of precast concrete buildings. *fib-news*, Dec., 1–4.

Gelagoti, F., Kourkoulis, R., Anastasopoulos, I., & Gazetas, G. 2012. Rocking-isolated frame structures: Margins of safety against toppling collapse and simplified design approach. *Soil Dynamics and Earthquake Engineering*, **32**(1), 87. Journal Article.

Gledhill, SM, Sidwell, GK, & Bell, DK. 2008. The damage avoidance design of tall steel frame buildings–Fairlie Terrace student accommodation project, Victoria University of Wellington. *In: New Zealand Society of Earthquake Engineering Annual Conference.*

Housner, G W. 1963. The behavior of inverted pendulum structures during earthquakes. *Bulletin of the Seismological Society of America*, **53**(2), 403. Journal Article.

Iqbal, A, Pampanin, S, Buchanan, A, & Palermo, A. 2007. Improved seismic performance of LVL post-tensioned walls coupled with UFP devices. *In: 8th Pacific conference on earthquake engineering, Singapore.*

Iqbal, A., Pampanin, S., & Buchanan, A. 2008. Seismic Behaviour of Prestressed Timber Columns under Bi-directional Loading. *In: WCTE.*

Iqbal, Asif, Buchanan, A. H., & Pampanin, S. 2010. Seismic Performance of Prestressed Timber Beam Column Sub-Assemblies. *In: NZSEE.*

Iqbal, Md Asif. 2011. *Seismic response and design of subassemblies for multi-storey prestressed timber buildings.* Ph.D. thesis, Department of Civil/Natural Resources Engineering, University of Canterbury.

Jacobsen, L.S. 1960. Damping in Composite Structures. *Pages 1029–1044 of: Proceedings, 2nd World Conference on Earthquake Engineering*, vol. 2.

Kam, WY, Pampanin, S, Palermo, A, & Carr, A. 2008. Design procedure and behaviour of Advanced Flag-Shape (AFS) MDOF systems. *In: New Zealand Society of Earthquake Engineering Annual Conference.* University of Canterbury. Civil and Natural Resources Engineering.

Kelly, J. M., Skinner, R. I., & Heine, A. J. 1972. Mechanisms of Energy Absorption in Special Devices for use in Earthquake Resistant Structures. *Bulletin of the New Zealand Society for Earthquake Engineering*, **5**(3), 63–88.

Kelly, Trevor. 2011. Tentative Seismic Design Guidelines for Rocking Structures. *SESOC journal: journal of the N.Z. Structural Engineering Society*, **24**(1), 59–106. Journal, Physical.

Lowes, Laura. 1999. *Finite Element Modeling of Reinforced Concrete Beam-Column Bridge Connections.* Ph.D. thesis, University of California, Berkley.

Ma, Kun. 2010 (Feb.). *Effects of Reinforcing Screws on Shear Deformation in Timber Columns.* Experimental testing report. Department of Civil/Natural Resources Engineering, University of Canterbury.

Ma, Q. T., & Khan, M. H. 2008. Free vibration tests of a scale model of the South Rangitikei Railway Bridge. *In: Proceedings of the New Zealand Society for Earthquake Engineering Annual Conference, Engineering an Earthquake Resilient NZ.*

Massey University. 2012. *World-first building opens tomorrow.* `http://www.massey.ac.nz/massey/about-massey/news/article.cfm?mnarticle_uuid=7E033A84-B860-05D3-E0B8-A0E42BD9F729`.

McKenna, Frank, McGann, Christopher, Arduino, Pedro, & Harmon, Joseph Allen. 2014 (Feb). *OpenSees Laboratory.*

McManus, K. J. 1980. *The seismic response of bridge structures free to rock on their foundations.* Ph.D. thesis, Department of Civil/Natural Resources Engineering, University of Canterbury. Masters Thesis.

Mergos, Panagiotis Elia, & Kawashima, Kazuhiko. 2005. Rocking Isolation of a Typical Bridge Pier on Spread Foundation. *Journal of Earthquake Engineering*, **9**(sup2), 395–414.

Metsä Wood. 2012. *KERTO® for Load-Bearing Structures.*

Nakaki, SD, Stanton, JF, & Sritharan, S. 1999. An overview of the PRESSS five-story precast test building. *PCI JOURNAL*, **44**(2), 26. Journal Article.

Nelson Pine Industries Limited. 2012 (May). *Nelson Pine Laminated Vaneer Lumber (LVL) Specific Engineering Design Guide.*

Newcombe, M. 2005. *Beam to Column and Wall to Foundation Tests with Internal Dissipaters.* Lab Test Report. University of Canterbury.

Newcombe, M. 2007 (Dec.). *Seismic Design of Multistorey Post-Tensioned Timber Buildings.* Masters Thesis, Istituto Universitario di Studi Superiori di Pavia Università degli Studi di Pavia, Pavia, Italy.

Newcombe, M. P., Pampanin, S., & Buchanan, A. H. 2010a. Design, Fabrication and Assembly of a Two-Storey Post-Tensioned Timber Building. *In: Conference Proceedings, World Conference on Timber Engineering.*

Newcombe, M. P., Pampanin, S., & Buchanan, A. H. 2010b. Experimental Testing of a Two-Storey Post-Tensioned Timber Building. *In: 9th US National & 10th Canadian Conference on Earthquake Engineering, Toronto, Canada*, vol. 8.

Newcombe, M.P. 2011. *Seismic Design of Post-Tensioned Timber Frame and Wall Buildings.* Ph.D. thesis, University of Canterbury, Christchurch, New Zealand.

Newcombe, MP, Pampanin, S, & Buchanan, AH. 2010c. Experimental Testing of a Two-Storey Post-Tensioned Timber Building. *In: 9th US National & 10th Canadian Conference on Earthquake Engineering, Toronto, Canada*, vol. 8.

Newcombe, M.P., S. Pampanin, & A.H. Buchanan. 2010d. Numerical Modelling and Analysis of a Two-Storey Post-Tensioned Timber Frame with Floor Diaphragms. *In: ECEE.*

NIWA. 2007. *CliFlo: NIWA's National Climate Database on the Web.*

Palermo, A., Pampanin, S., & Calvi, M. 2004. Use of "Controlled Rocking" in the Seismic Design of Bridges. *In: 13th World Conference on Earthquake Engineering.*

Palermo, A., Pampanin, S., Buchanan, A., & Newcombe, M. 2005. Seismic design of multi-storey buildings using laminated veneer lumber (LVL). *In: NZSEE*. University of Canterbury. Civil Engineering. Conference Proceedings.

Pampanin, Stefano, Marriott, Dion, Palermo, Alessandro, & Society, New Zealand Concrete. 2010. *PRESSS design handbook*. Auckland, N.Z: NZCS. Book, Whole.

Pampanin, Stefano, Weng Yeun, Kam, Haverland, Gary, & Gardnier, Sean. 2011 (Aug.). Expectation Meets Reality: Seismic Performance of Post-tensioned Precast Concrete Southern Cross Endoscopy Building During the 22nd Feb 2011 Christchurch Earthquake. *In: New Zealand Concrete Industry Conference, Rotorua, August*.

Priestley, M. J. N., Sritharan, S., Conley, J. R., & Pampanin, S. 1999. Preliminary results and conclusions from the PRESSS five-story precast concrete test building. *PCI journal*, **44**(6), 42–67.

Priestley, M. J. N., Kowalsky, Mervyn J., & Calvi, G. M. 2007. *Displacement-based seismic design of structures*. Pavia, Italy: IUSS Press. Book, Whole.

Quenneville, Pierre, & Zarnani, Pouyan. 2013. *Timber Rivet Connections Design Guide, in LVL, Glulam and lumber*.

Ringfeder. 2010. *Damping Technology*.

Rotho Blaas s.r.l. 2012 (Nov.). *European Technical Approval ETA-11/0030*. European Technical Approval ETA-11/0030. European Organisation for Technical Approvals, Denmark.

Smith, T., Wong, R., Newcombe, M., Carradine, D., Pampanin, S., Buchanan, A., Seville, R., & McGregor, E. 2011. The Demountability, Relocation and Re-use of a High Performance Timber Building. *In: NZSEE*.

Smith, T, Pampanin, S, Di Cesare, A, Ponzo, FC, Simonetti, M, Nigro, D, & Carradine, D. 2014. Shaking table testing of a multi-storey post-tensioned timber building. *In: NZSEE*.

Smith, Tobias. 2006. *Work performed during summer research scholarship on LVL beam column joint*. Lab Report. University of Canterbury, Christchurch, New Zealand.

Smith, Tobias, Simonetti, Michele, Di Cesare, Antonio, Carlo Ponzo, Antonio, Carradine, David, Pampanin, Stefano, & Nigro, Domenico. 2013. *Angle dissipaters Experimental campaign and analytical study - Interim Internal Report*. Research Report 2013-XX. Departimento di Stutture, Geotecnica, Geologia Applicata Universits degli Studi della Basilicata, Potenza, Italia, Potenza, Italy.

SPAX Construction. 2012. *Dimensional notes, Notes on the dimensioning of load-bearing SPAX connections*.

Standards New Zealand. 1993. *NZS 3603 Timber Structures Standard*. New Zealand Standard NZS 3603. Wellington.

Standards New Zealand. 2004. *NZS 1170 Structural Design Actions*. New Zealand Standard NZS 1170. Wellington.

Standards New Zealand. 2006. *NZS 3101 Concrete Structures Standard*. New Zealand Standard NZS 3101. Wellington.

Stewart, Stephen, Transit New Zealand, & Works Consultancy Services Ltd. 1994. *Bridge manual: prepared by Works Consultancy Services Limited for Transit New Zealand.* Wellington [N.Z.]: Transit New Zealand. Book, Whole.

STIC. 2013. *Post-Tensioned Timber Buildings - Design Guide.* Design Guide STIC - 2013-20.

SWG Schraubenwekr Gaisbach GmbH. 2011 (Dec.). *European Technical Approval ETA-11/0470.* European Technical Approval ETA-11/0470. European Organisation for Technical Approvals.

Tyler, RG. 1978. Tapered steel energy dissipators for earthquake resistant structures. *Bulletin of the New Zealand Society for Earthquake Engineering*, **11**(4), 282–294.

van Beerschoten, Wouter. 2011. Experimental Investigation on the Stiffness of Beam-Column Connections in Post-Tensioned Timber Frames. *In: Structural engineering world conference, Como, Italy.*

van Beerschoten, Wouter. 2013. *Structural Performance of Post-tensioned Timber Frames under Gravity Loading.*

White, Samuel Lewis. 2014. *Controlled Damage Rocking Systems for Accelerated Bridge Construction.* M.Phil. thesis, Department of Civil/Natural Resources Engineering, University of Canterbury.

Würth GmbH & Co. 2011 (Aug.). *European Technical Approval ETA-11/0190.* European Technical Approval ETA-11/0470. European Organisation for Technical Approvals, Germany.

Zhu, S., & Zhang, Y. 2007. *Seismic analysis and design of steel concentrically braced frames with self-centering friction damping brace.* ATLSS Reports 97.

Appendices

Appendix A

Drawings

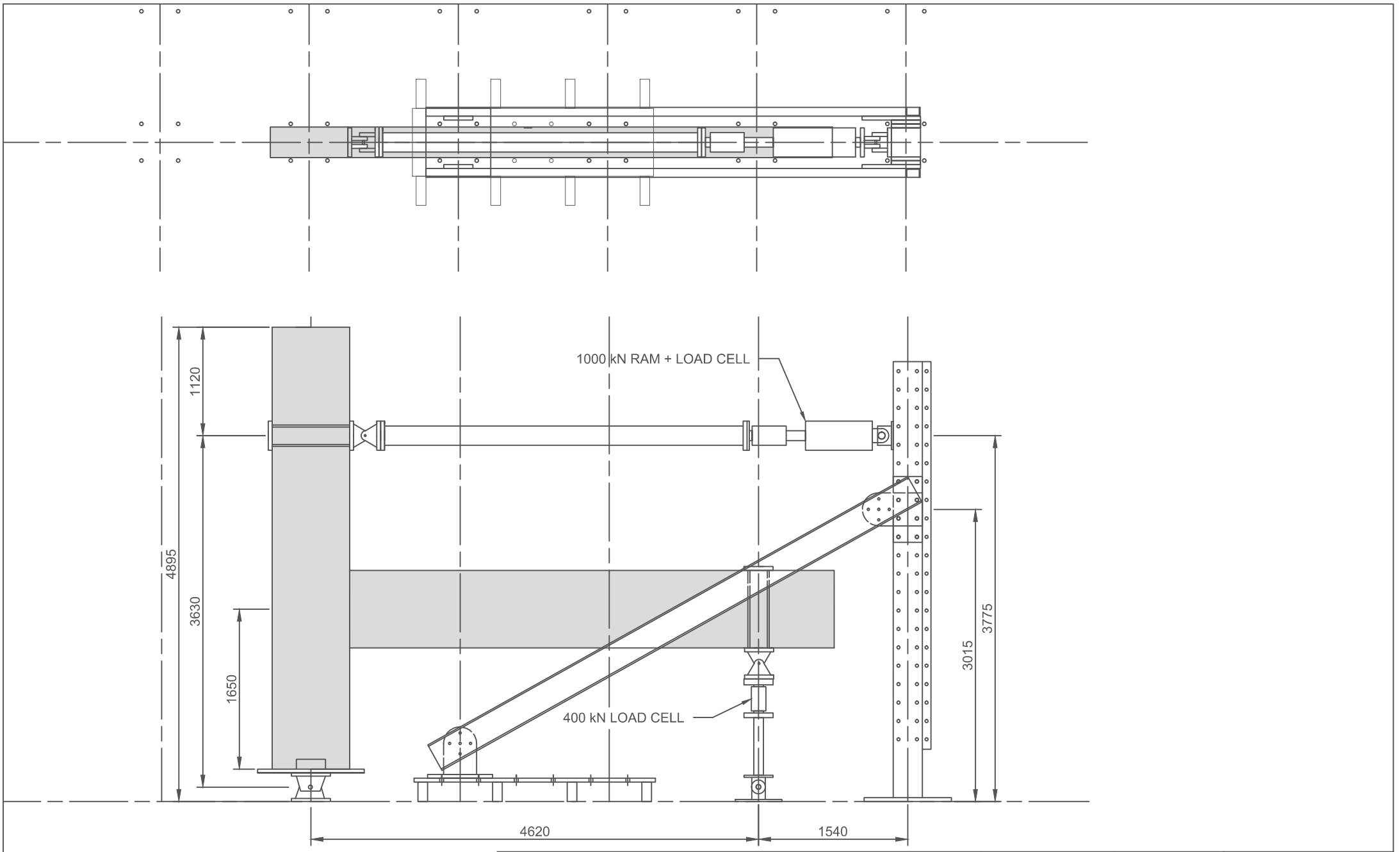

TITLE: TEST SPECIMEN AND APPARATUS ARRANGEMENT		NUMBER: DRG-1000	DATE: 18/07/2014
PROJECT: PRESLAM BEAM COLUMN JOINT LAB TESTING		BY: T. ARMSTRONG	SCALE: 1:50 (AT A4)

UNIVERSITY OF CANTERBURY
Te Whare Wānanga o Waitaha

NOTE:

1 TO BE READ IN CONJUNCTION WITH KIRK ROBERTS DRAWINGS

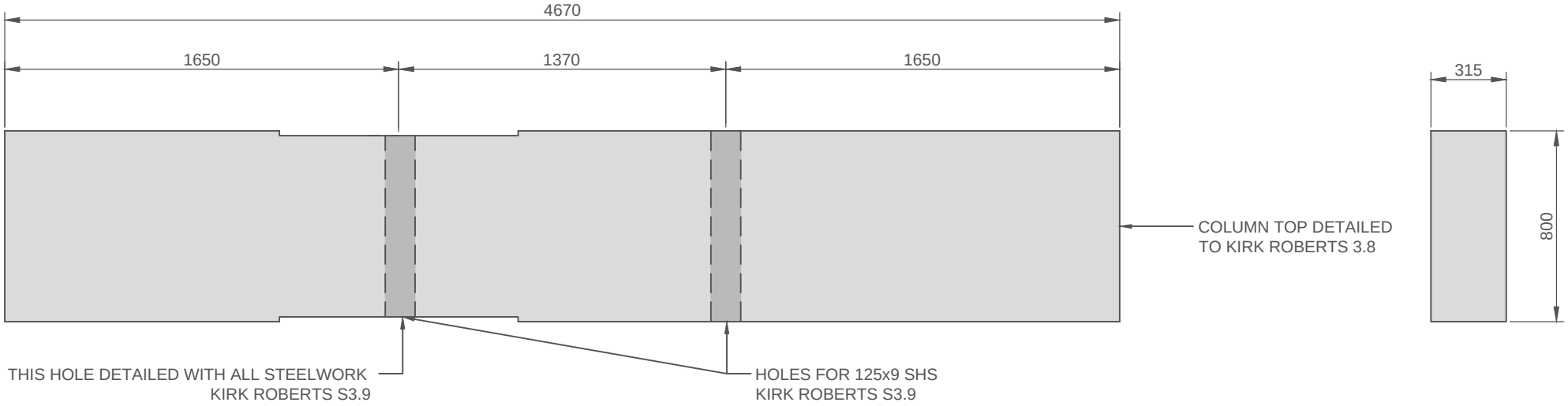

COLUMN

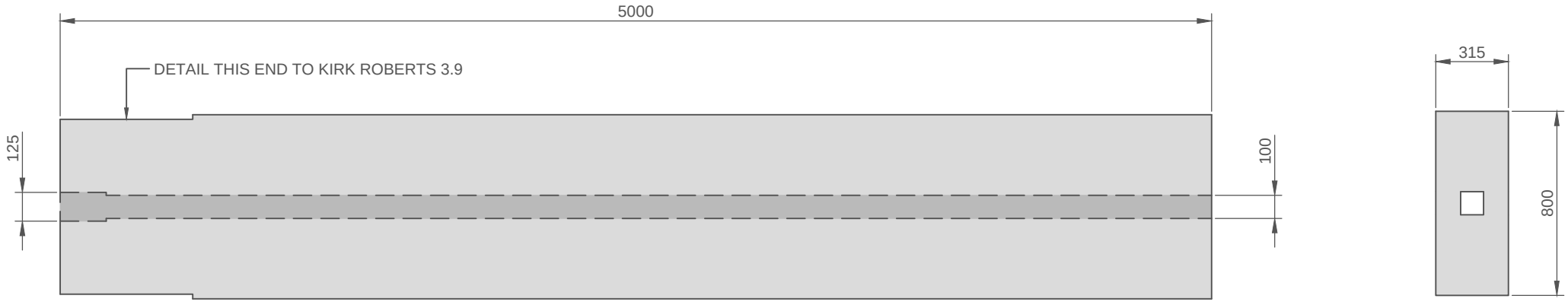

BEAM

TITLE: TIMBER MEMBER DETAILS	NUMBER: DRG-110	DATE: 29/06/12	UC UNIVERSITY OF CANTERBURY Te Whare Wānanga o Waitaha
PROJECT: PRESLAM BEAM COLUMN JOINT LAB TESTING	BY: T. ARMSTRONG	SCALE: 1:25 (AT A4)	

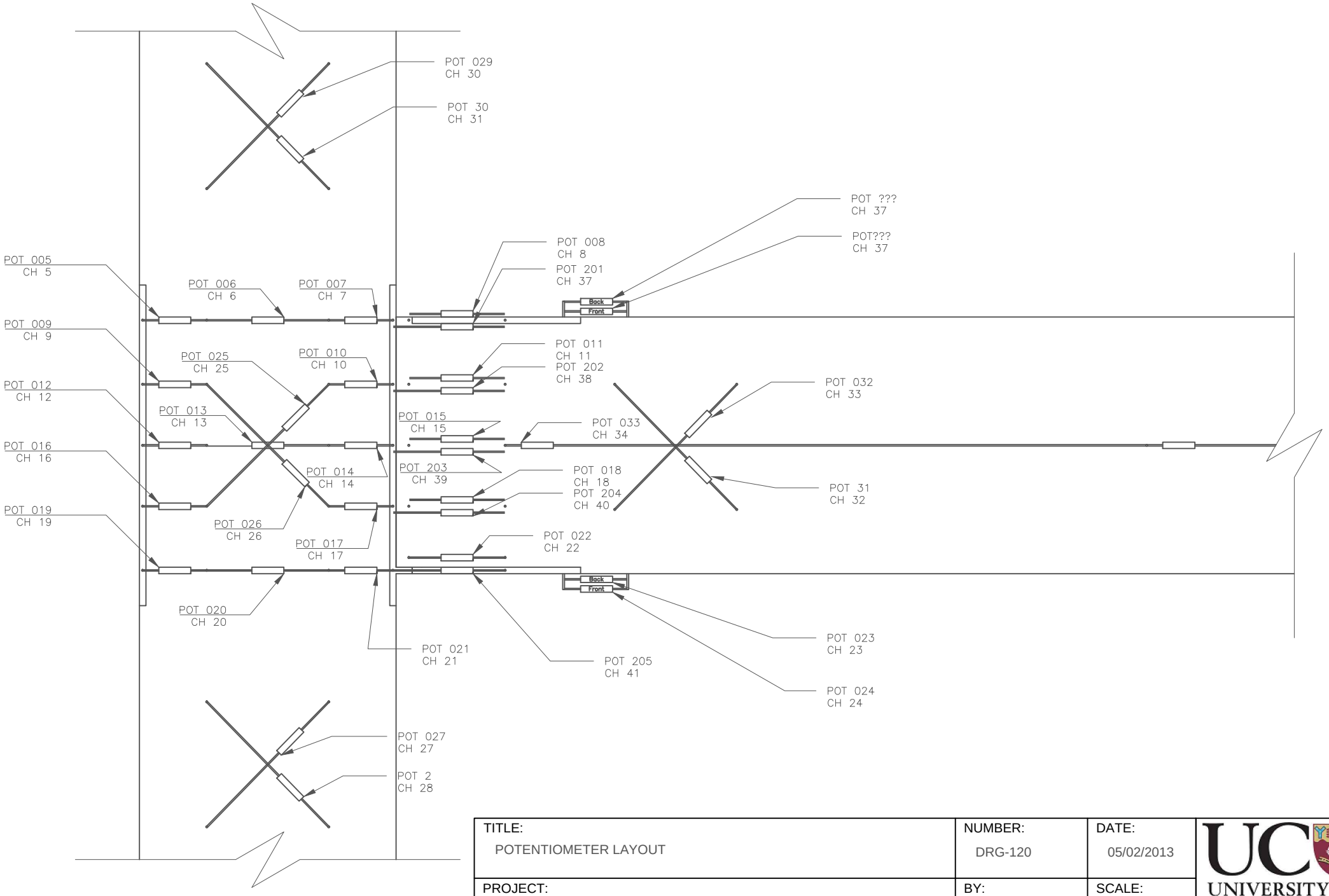

TITLE: POTENTIOMETER LAYOUT	NUMBER: DRG-120	DATE: 05/02/2013	UNIVERSITY OF CANTERBURY Te Whare Wānanga o Waitaha
PROJECT: PRESLAM BEAM COLUMN JOINT LAB TESTING	BY: T. ARMSTRONG	SCALE: 1:15 (AT A4)	

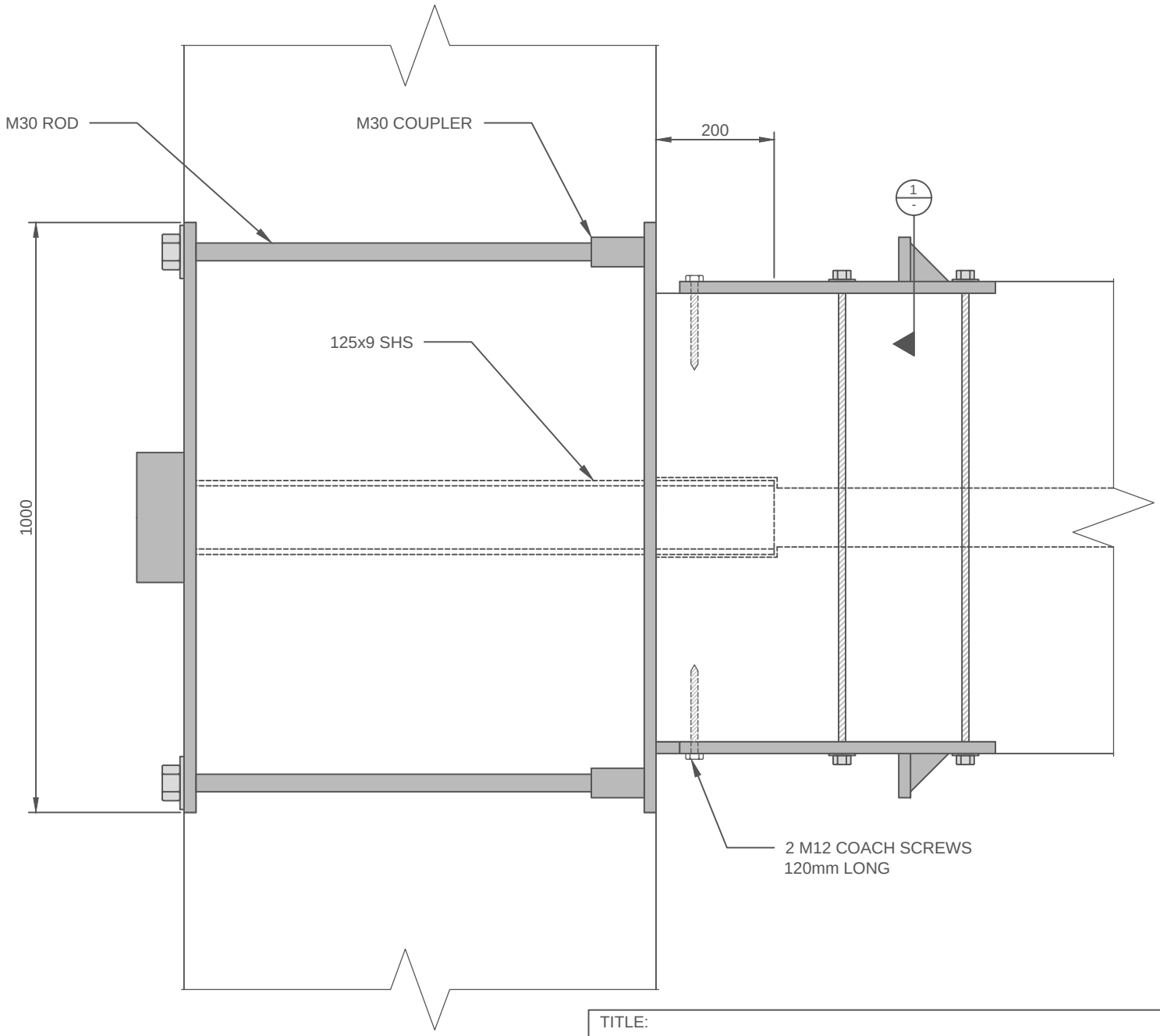

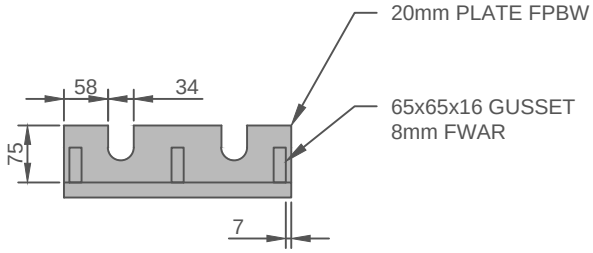

1
-
DISSIPATER ATTACHMENT PLATE

TITLE:	NUMBER:	DATE:
STEEL REINFORCING DETAILS	DRG-210	02/06/2012
PROJECT:	BY:	SCALE:
PRESLAM BEAM COLUMN JOINT LAB TESTING	T. ARMSTRONG	1:10 (AT A4)

UC UNIVERSITY OF CANTERBURY
Te Whare Wānanga o Waitaha

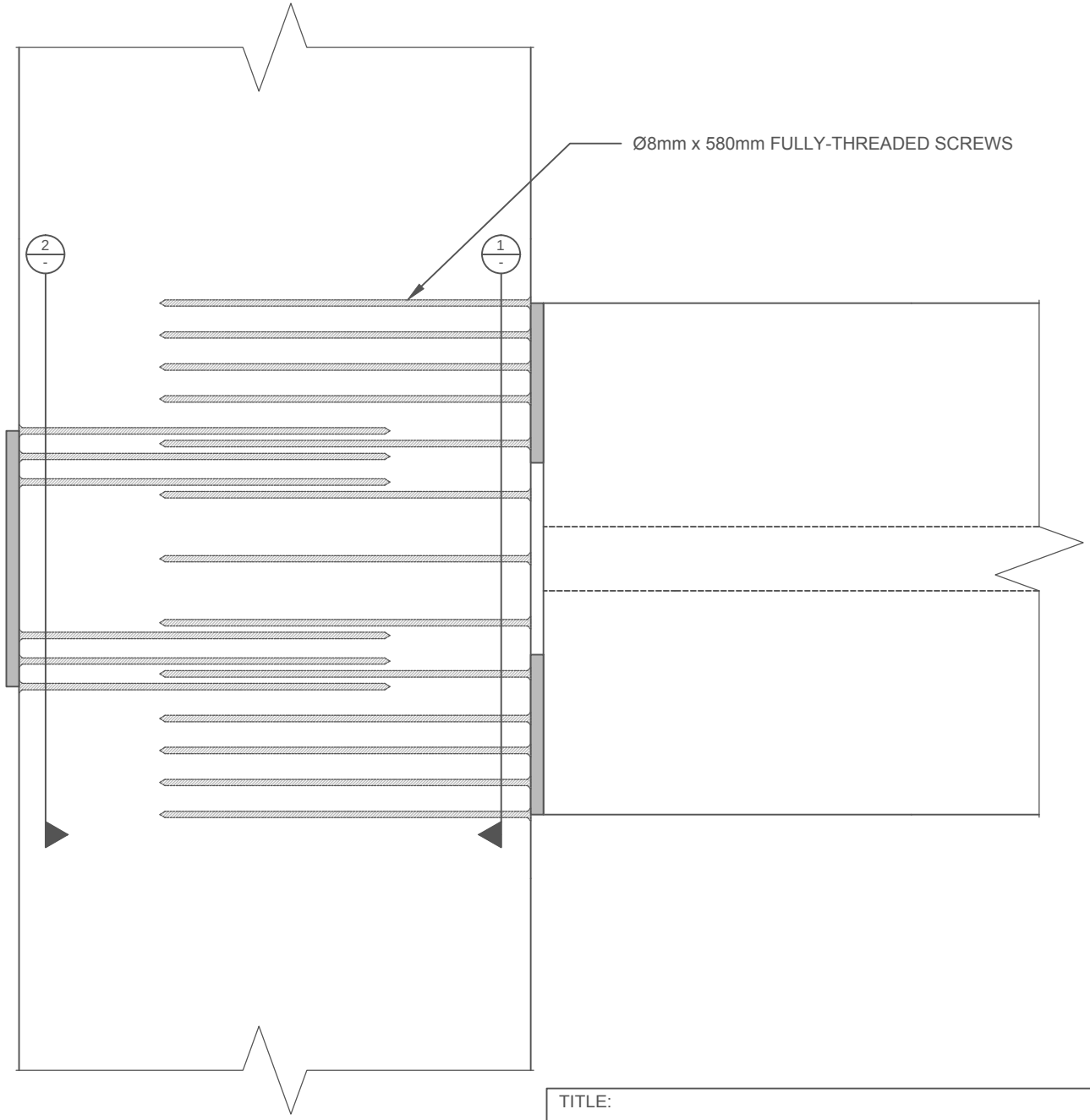

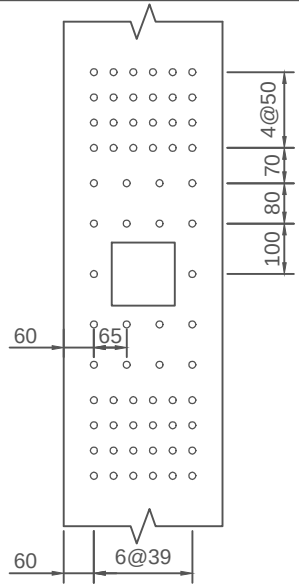

1 - INTERFACE REINFORCING
1:20

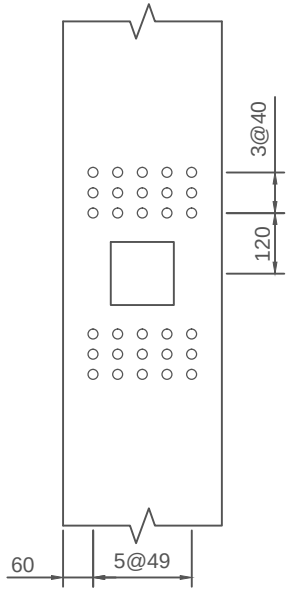

2 - POST-TENSIONING REINFORCING
1:20

TITLE:	NUMBER:	DATE:
STEEL REINFORCING DETAILS	DRG-220	02/06/2012
PROJECT:	BY:	SCALE:
PRESLAM BEAM COLUMN JOINT LAB TESTING	T. ARMSTRONG	1:10 (AT A4)

UNIVERSITY OF CANTERBURY
Te Whare Wānanga o Waitaha

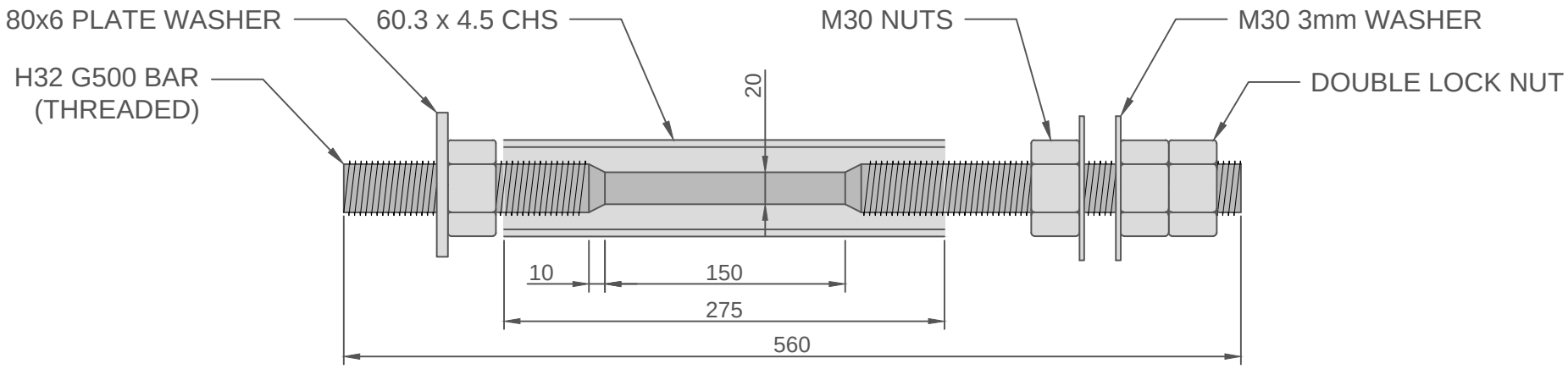

20mm DIAMETER PLUG AND PLAY DISSIPATER

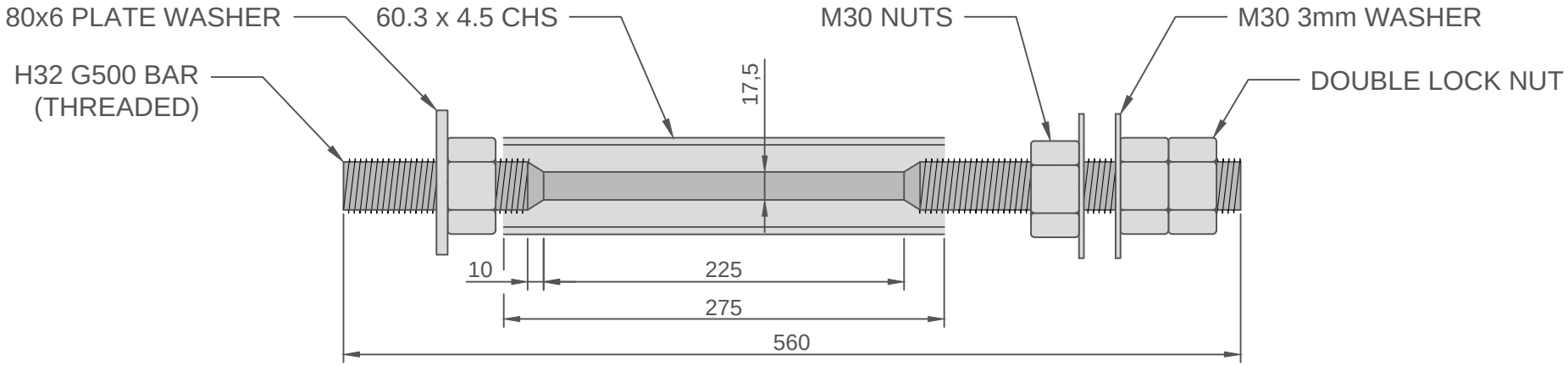

17.5mm DIAMETER PLUG AND PLAY DISSIPATER

TITLE: PLUG AND PLAY DISSIPATER DETAILS	NUMBER: DRG-310	DATE: 1/1/2012	UNIVERSITY OF CANTERBURY Te Whare Wānanga o Waitaha
PROJECT: PRESLAM BEAM COLUMN JOINT LAB TESTING	BY: T. ARMSTRONG	SCALE: 1:4 (AT A4)	

NOTE:

1 DISSIPATER G300 PLATE ONLY

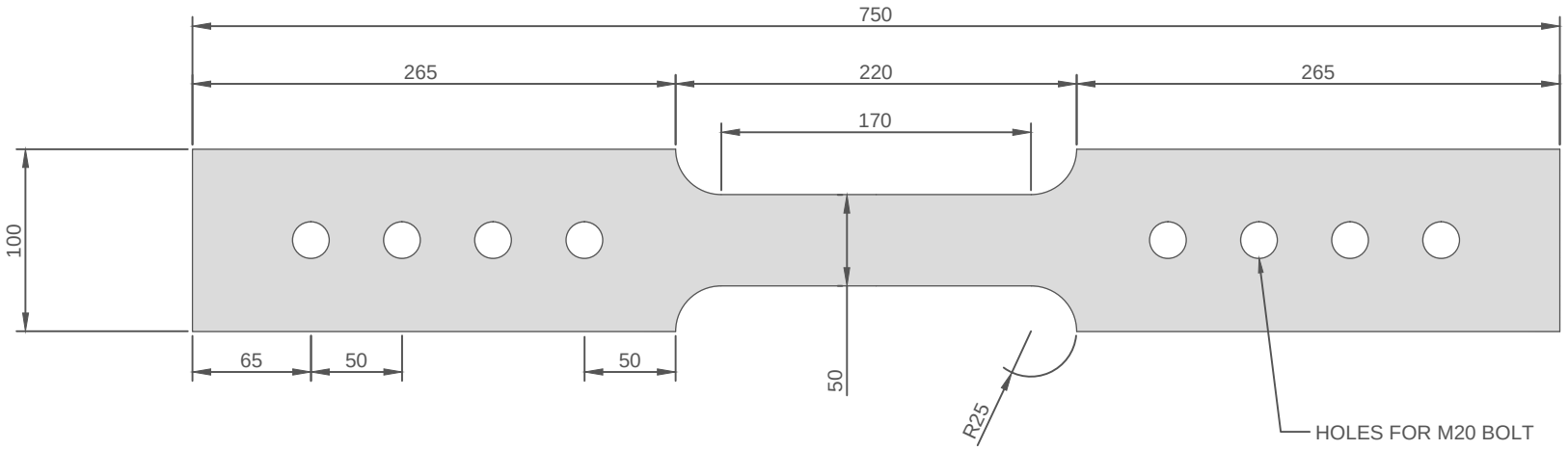

TITLE: NPD 1 DETAILS	NUMBER: DRG-320	DATE: 02/06/2012	UNIVERSITY OF CANTERBURY Te Whare Wānanga o Waitaha
PROJECT: PRESLAM BEAM COLUMN JOINT LAB TESTING	BY: T. ARMSTRONG	SCALE: 1:4 (AT A4)	

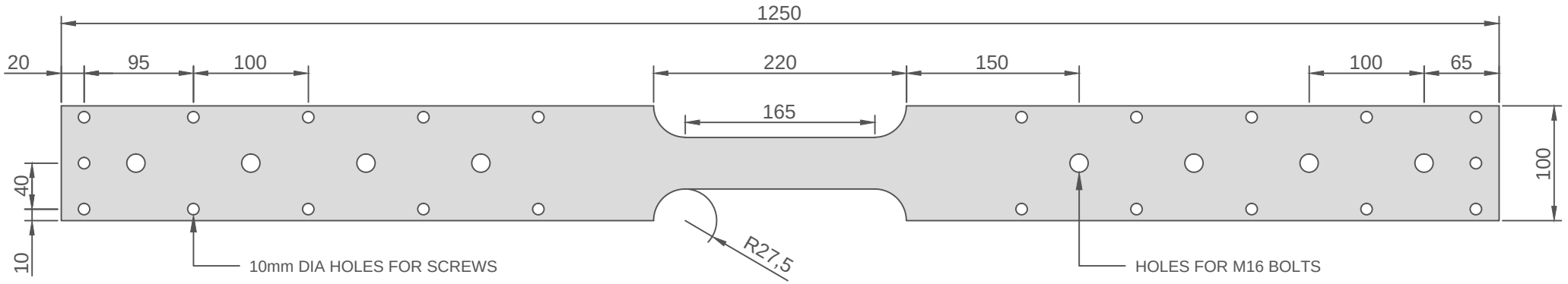

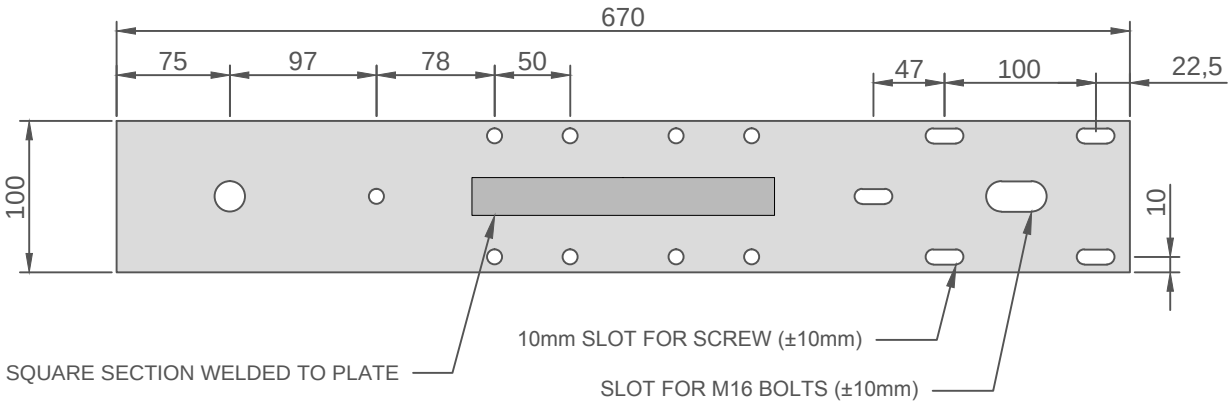

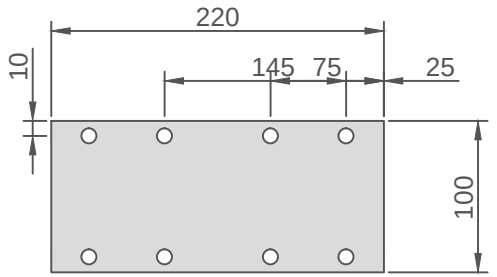

TITLE: NECKED PLATE DISSIPATER DETAILS	NUMBER: DRG-325	DATE: 02/06/2012	UC UNIVERSITY OF CANTERBURY Te Whare Wānanga o Waitaha
PROJECT: PRESLAM BEAM COLUMN JOINT LAB TESTING	BY: T. ARMSTRONG	SCALE: 1:5 (AT A4)	

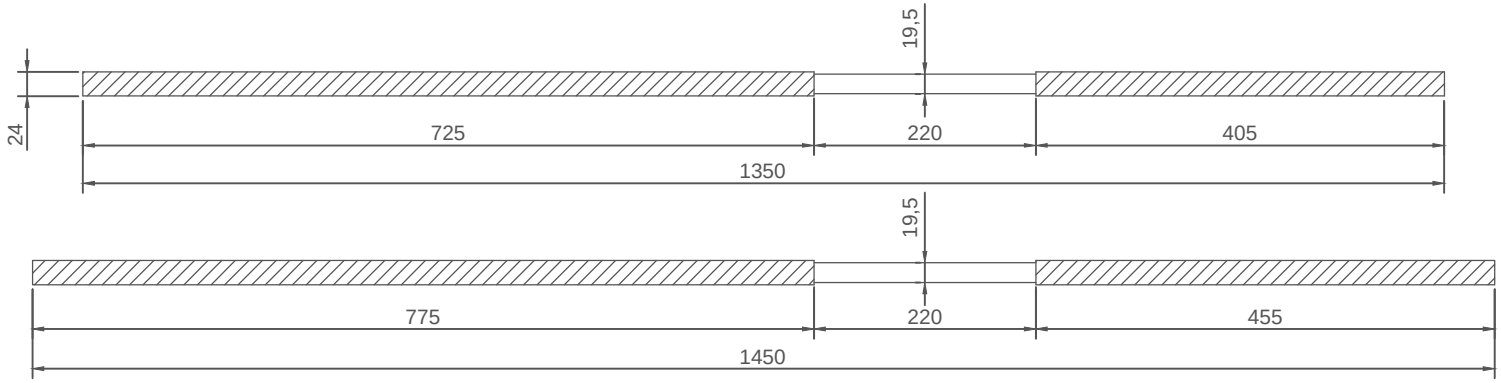

NOTE:

1. DISSIPATER RODS TO BE FABRICATED FROM G300 PLAIN ROUND BAR ONLY.
2. THREADED ROD NOT TO BE USED. CUT THREADS INTO PLAIN BAR AS REQUIRED
3. LVL BILLETS TO BE SCREW LAMINATED AND SLOTS ROUTED PRIOR TO INSTALLATION OF RODS
4. HIGHLY FLOWABLE EPOXY TO BE USED TO FIX RODS. SILICON AND BOND-BREAKER AT GAP INTERFACE
5. SCREW ARRANGEMENT MAY BE SLIGHTLY MODIFIED TO SUIT COLUMN REINFORCING SCREWS

- DISSIPATER ROD DETAILS

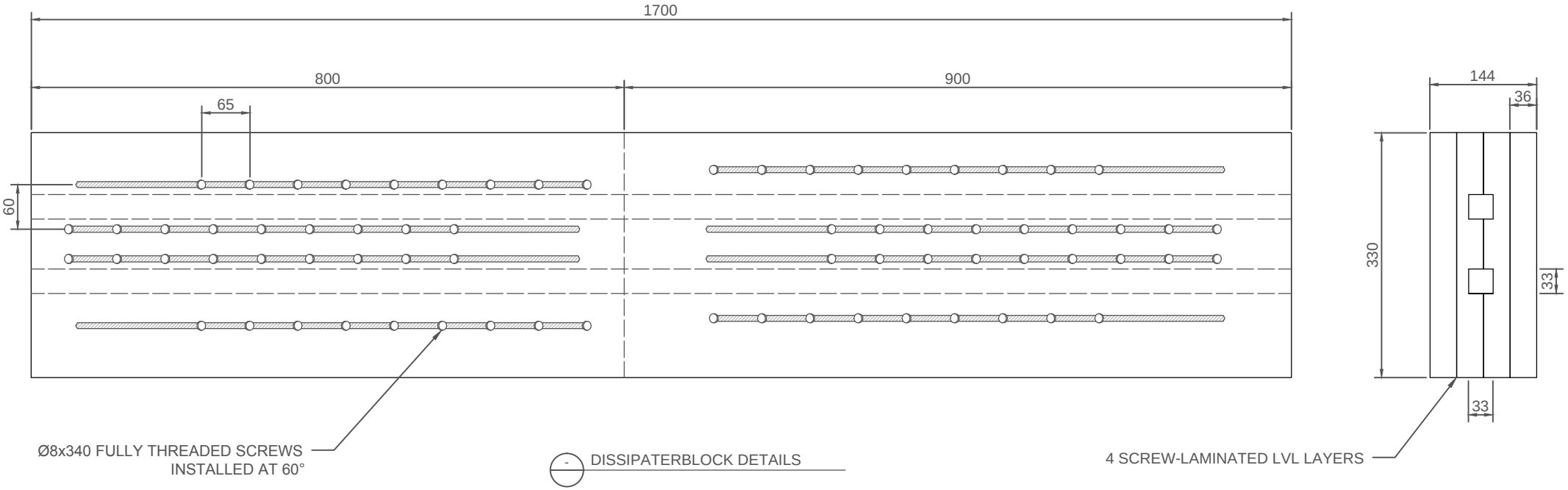

- DISSIPATERBLOCK DETAILS

TITLE: TIMBER PLUS DISSIPATER DETAILS	NUMBER: DRG-330	DATE: 02/06/2012
PROJECT: PRESLAM BEAM COLUMN JOINT LAB TESTING	BY: T. ARMSTRONG	SCALE: 1:7.5 (AT A4)

UNIVERSITY OF CANTERBURY
Te Whare Wānanga o Waitaha

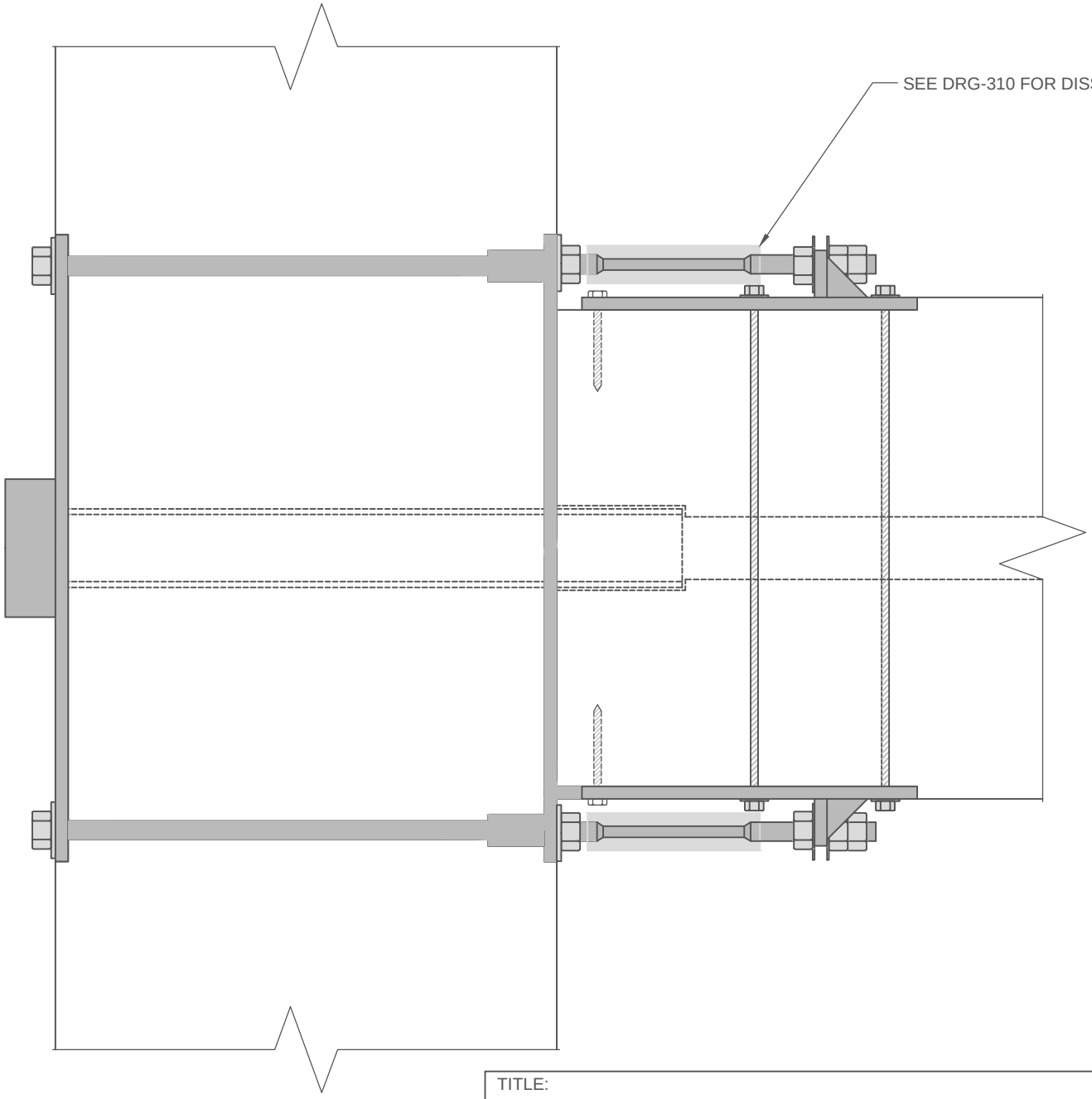

DISSIPATER DIAMETER	
TEST	DIAMETER
A-P1	17.5mm
A-P2	20.0mm (TOP) 17.5mm (BOTTOM)

TITLE: JOINT A-P DETAILS	NUMBER: DRG-420	DATE: 02/06/2012	UNIVERSITY OF CANTERBURY Te Whare Wānanga o Waitaha
PROJECT: PRESLAM BEAM COLUMN JOINT LAB TESTING	BY: T. ARMSTRONG	SCALE: 1:10 (AT A4)	

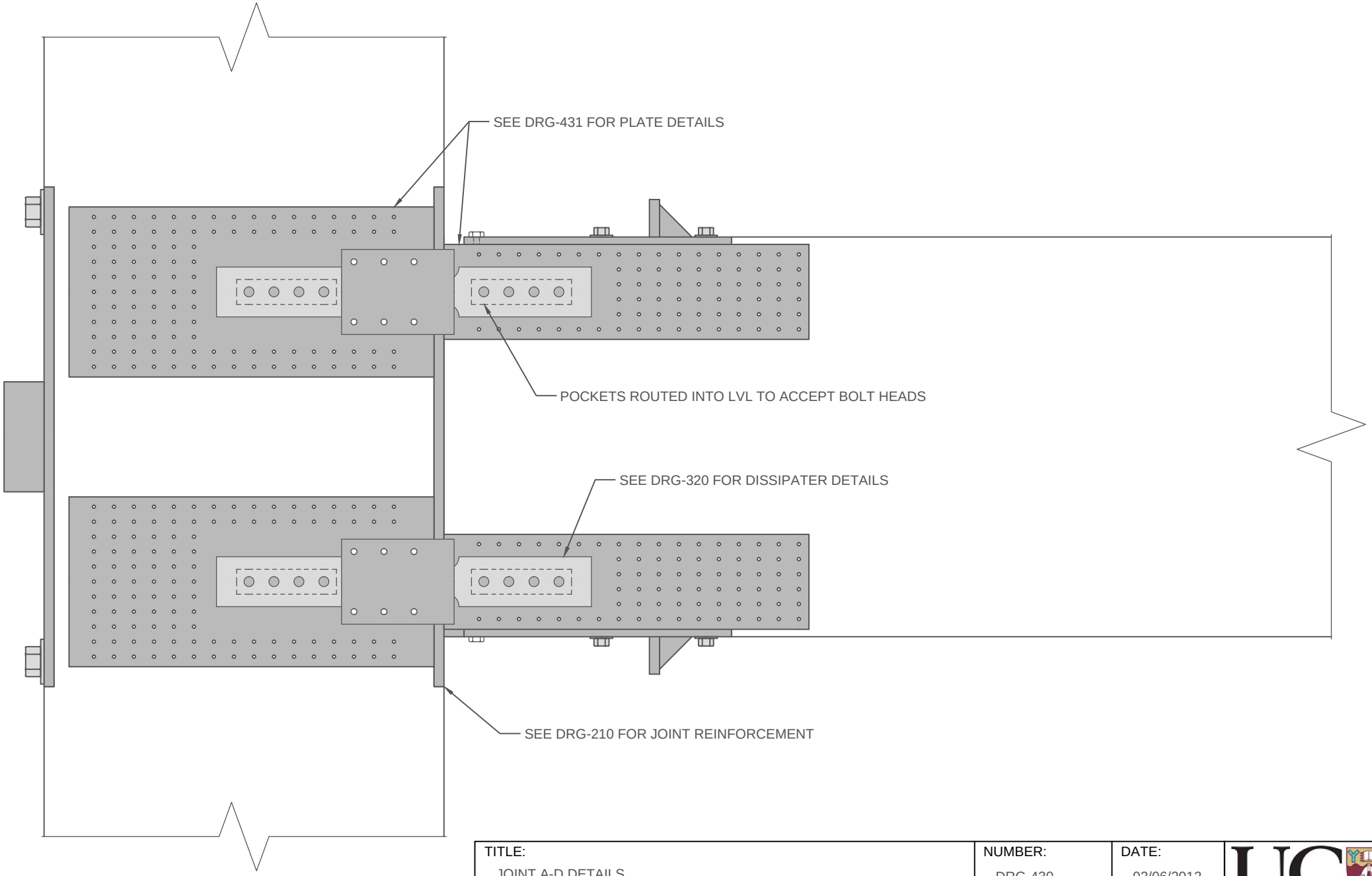

TITLE: JOINT A-D DETAILS	NUMBER: DRG-430	DATE: 02/06/2012	UNIVERSITY OF CANTERBURY Te Whare Wānanga o Waitaha
PROJECT: PRESLAM BEAM COLUMN JOINT LAB TESTING	BY: T. ARMSTRONG	SCALE: 1:10 (AT A4)	

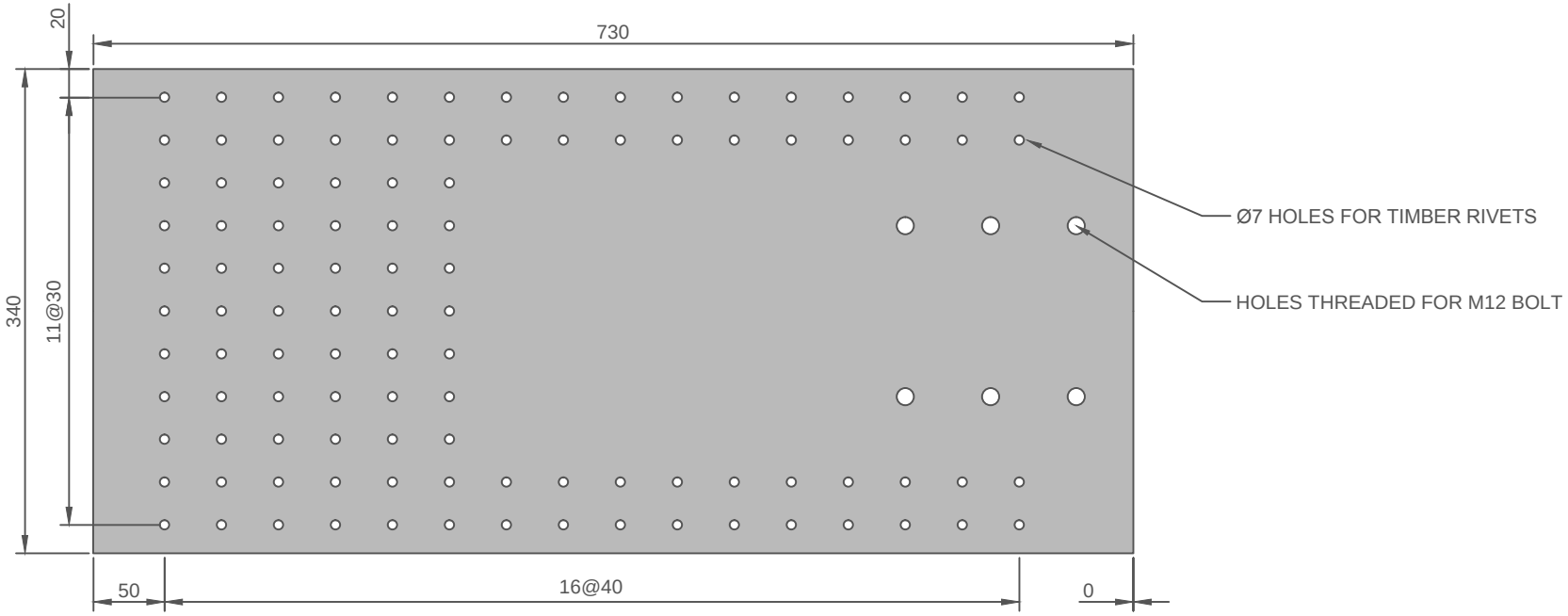

COLUMN ATTACHMENT PLATE

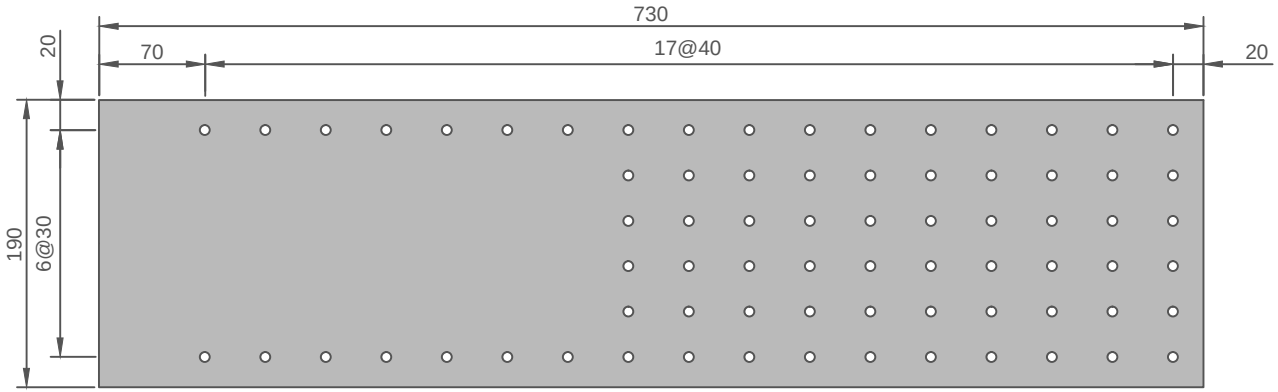

BEAM ATTACHMENT PLATE

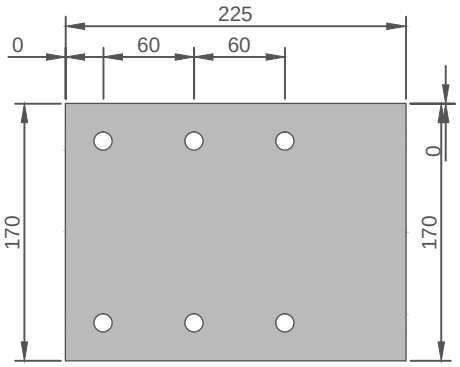

ANTI-BUCKLING COVER PLATE

NOTE:

1. ALL PLATE IS G250 UNO
2. RIVETS TO BE INSTALLED IN ACCORDANCE WITH DESIGN GUIDE

TITLE: NPD RIVET ATTACHMENT PLATE DETAILS	NUMBER: DRG-431	DATE: 02/06/2012
PROJECT: PRESLAM BEAM COLUMN JOINT LAB TESTING	BY: T. ARMSTRONG	SCALE: 1:10 (AT A4)

UNIVERSITY OF CANTERBURY
Te Whare Wānanga o Waitaha

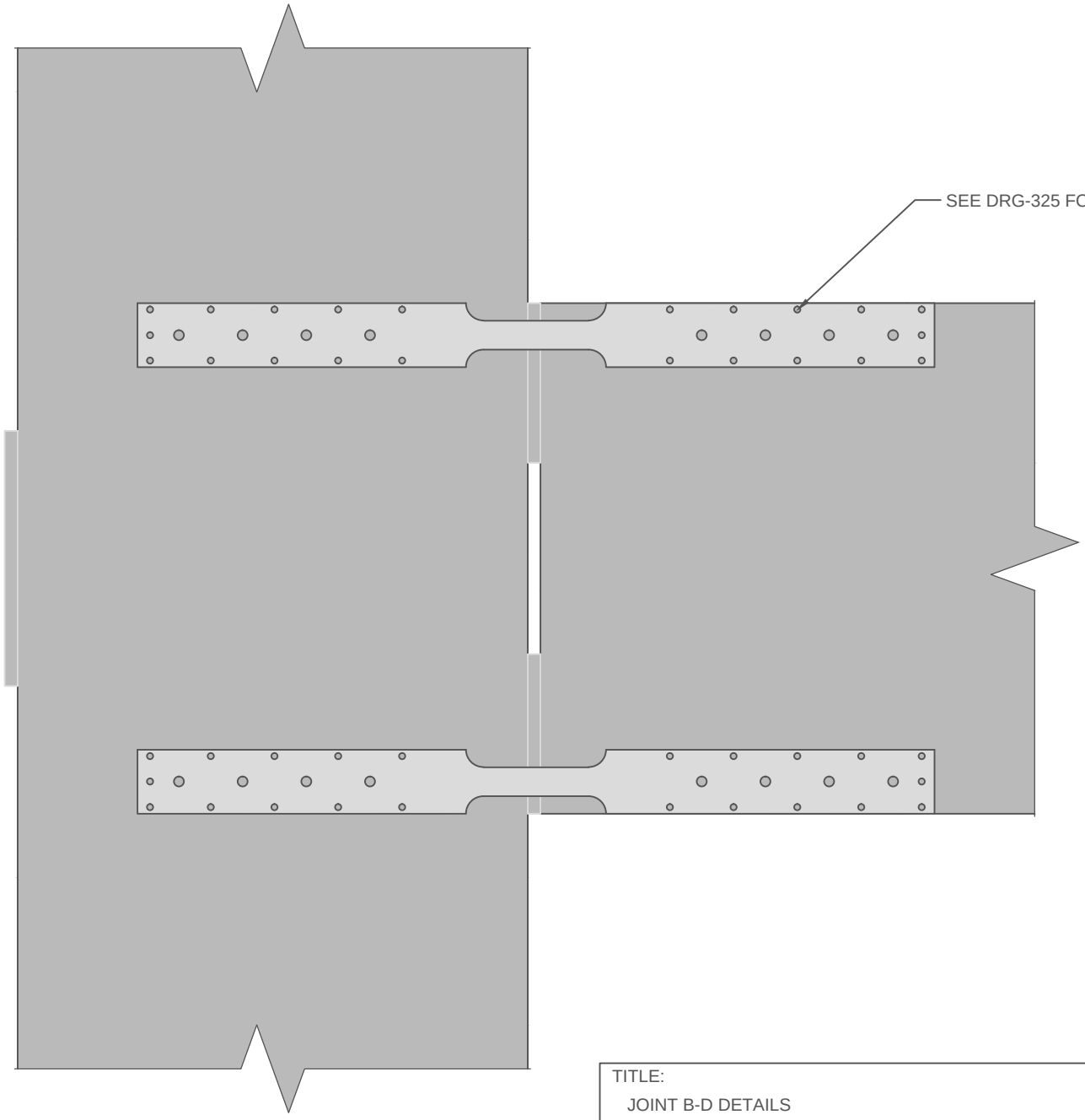

TITLE: JOINT B-D DETAILS	NUMBER: DRG-450	DATE: 02/06/2012	UNIVERSITY OF CANTERBURY Te Whare Wānanga o Waitaha
PROJECT: PRESLAM BEAM COLUMN JOINT LAB TESTING	BY: T. ARMSTRONG	SCALE: 1:10 (AT A4)	

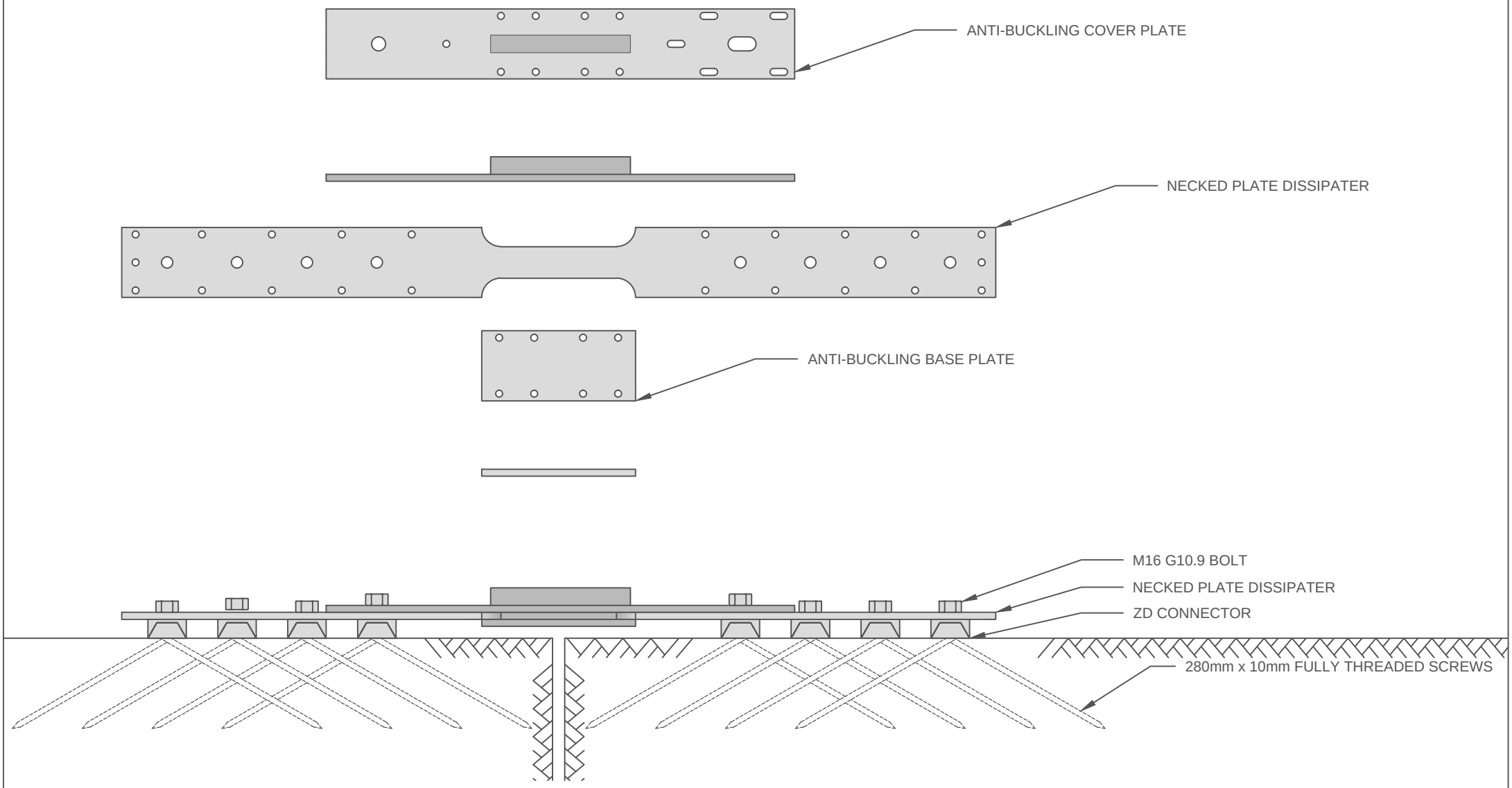

TITLE: NECKED PLATE DISSIPATER ASSEMBLY DETAILS	NUMBER: DRG-451	DATE: 02/06/2012
PROJECT: PRESLAM BEAM COLUMN JOINT LAB TESTING	BY: T. ARMSTRONG	SCALE: 1:5 (AT A4)

UNIVERSITY OF CANTERBURY
Te Whare Wānanga o Waitaha

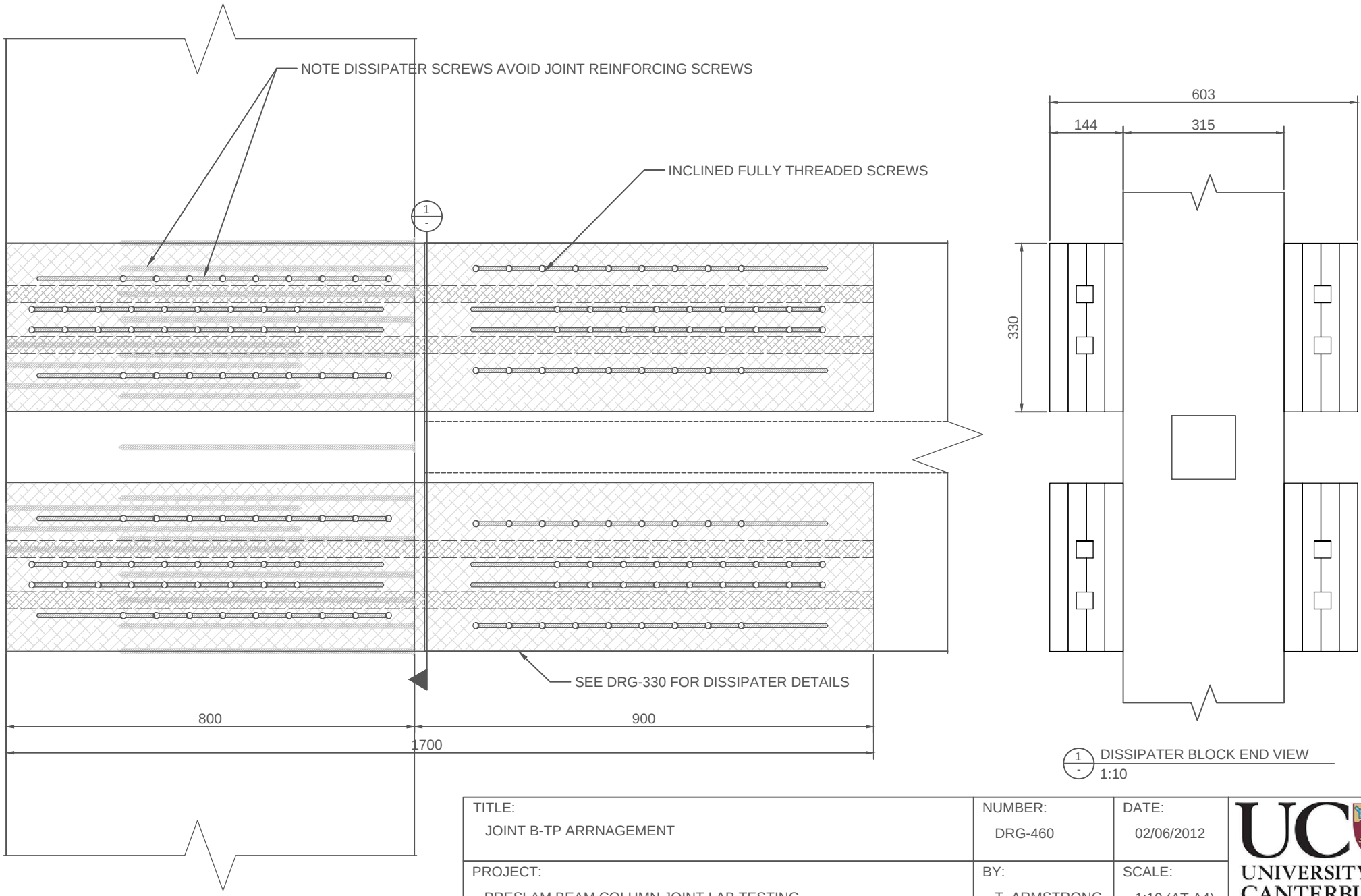

1 - DISSIPATER BLOCK END VIEW
1:10

TITLE: JOINT B-TP ARRNAGEMENT	NUMBER: DRG-460	DATE: 02/06/2012	UC UNIVERSITY OF CANTERBURY Te Whare Wānanga o Waitaha
PROJECT: PRESLAM BEAM COLUMN JOINT LAB TESTING	BY: T. ARMSTRONG	SCALE: 1:10 (AT A4)	

Appendix B

Analytical Model For Armouring Plate Bending

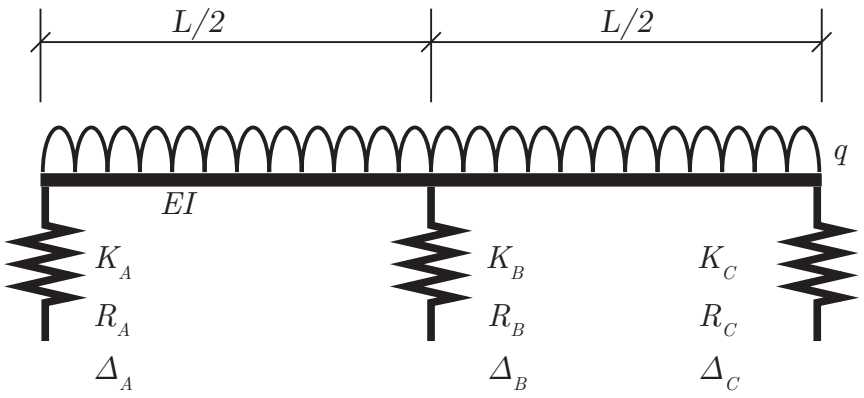

Figure B.1: Spring Beam model of Plate Bending

The model was derived from first principles, in the procedure outlined below.

Shear Force:

$$EIu''' = R_A - qx + R_B < x - \frac{L}{2} >^0$$

Integrate to get Moment:

$$EIu'' = R_A x - \frac{1}{2}qx^2 + R_B < x - \frac{L}{2} > + C_1$$

Moment at $M(x = 0) \Rightarrow$

$$C_1 = 0$$

Integrate to get Rotation:

$$EIu' = \frac{R_A x^2}{2} - \frac{qx^3}{6} + \frac{R_B < x - \frac{L}{2} >^2}{2} + C_2$$

Rotation at $\theta(x = \frac{L}{2}) = 0 \Rightarrow$

$$C_2 = \frac{qL^3}{48} - \frac{R_A L^3}{8}$$

Integrate to get Displacement:

$$EIu = \frac{R_A x^3}{6} - \frac{qx^4}{24} + \frac{qL^3 x}{24} - \frac{R_A L^2 x}{8} + \frac{R_B < x - \frac{L}{2} >^3}{6} + C_3$$

Displacement at $u(x = 0) = \frac{R_A}{k_A} \rightarrow$

$$C_3 = \frac{R_A}{k_A}$$

Solve sum of forces:

$$R_B = qL - 2R_A$$

Displacement equation:

$$\Delta(x) = R_A \left[\frac{x^3}{6} - \frac{xL^2}{8} - \frac{EI}{K_B} - \frac{< x - \frac{L}{2} >^3}{3} \right] + q \left[\frac{L^3 x}{48} - \frac{x^4}{24} + \frac{L < x - \frac{L}{2} >^3}{3} \right]$$

Now, R_A is the only unknown, solve for $\Delta(x = \frac{L}{2})$:

$$\Delta(x = \frac{L}{2}) = \frac{1}{EI} \left(R_A \left[\frac{L^3}{48} - \frac{L^3}{16} - \frac{EI}{K_B} \right] + q \left[\frac{L^4}{96} - \frac{L^4}{384} \right] \right) = \frac{R_B}{K_B} = \frac{qL - 2R_A}{K_B}$$

Solving for R_A:

$$R_A = \frac{3qL}{16} \left[\frac{(128EI - K_A L^3) K_B}{48EIK_B + 24EIK_A - L^3 K_A K_B} \right]$$

Expressions for displacement ($u(x)$) and the reaction at A (R_A) were implemented in a MATLAB script. This was used to computationally compare a variety of conditions relating to the stiffness of the beam and of the spring supports. When the properties for the tested joint were used as inputs, the deflection profile shown in Figure B.2 was produced. The results of this model were verified against a linear elastic model developed using the software package SpaceGass.

The differential displacement was determined according to:

$$\Delta_u = u(x = L/2) - u(x = 0)$$
$$\Delta_u = R_A \left[-\frac{L^3}{24} - \frac{EI}{K_B} \right] + q \left[\frac{L^4}{128} \right] - R_A \frac{EI}{K_B}$$

which simplifies to:

$$\Delta_u = \frac{L^3}{24EI}\left[\frac{3qL}{16} - R_A\right]$$

Substuting R_A from above and simplifying yields:

$$\Delta_u = \frac{-qL^4}{16}\left[\frac{3K_A - 10K_B}{48EIK_B + 24EIK_A - L^3K_AK_B}\right]$$

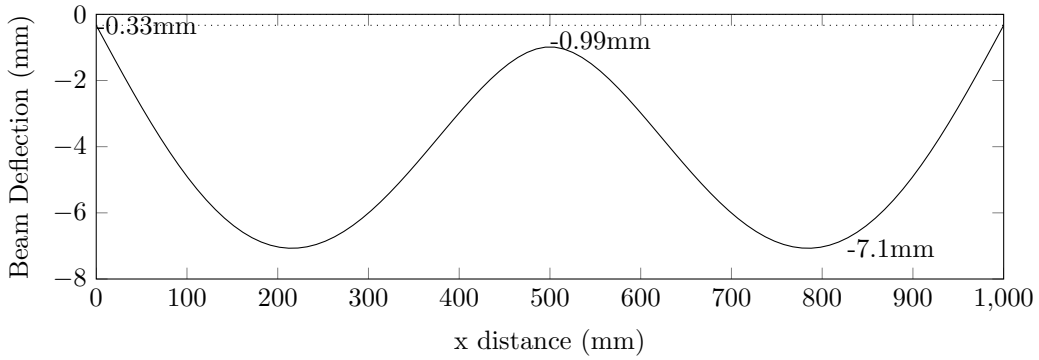

Figure B.2: Beam Deflection as modelled for Joint with details as tested

The code was run multiple times to investigate the effect of changing the support input parameters. The results of one of these iterations is shown in Figure B.3, Figure B.4 and Figure B.5. This clearly shows the asymptotic behaviour of the system, where increasing the stiffness of the outer support brings the supports closer to simple supports.

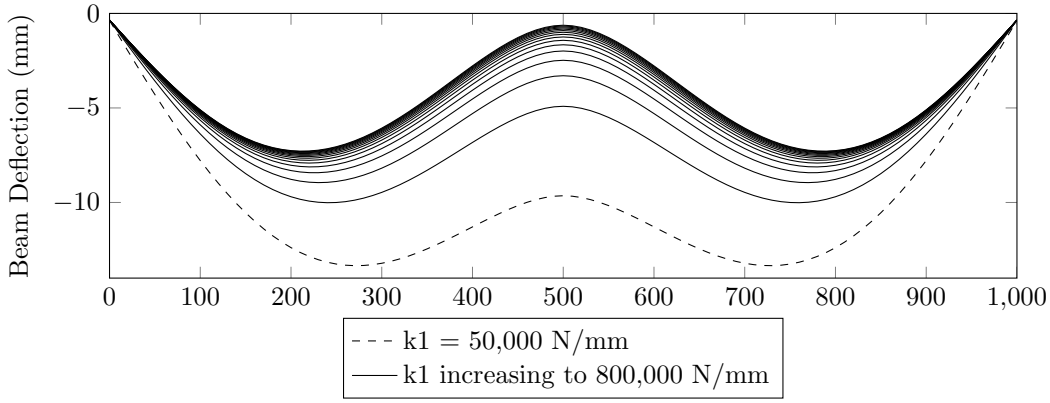

Figure B.3: Changing Beam deflections given changing Outer Support Stiffness (K_A)

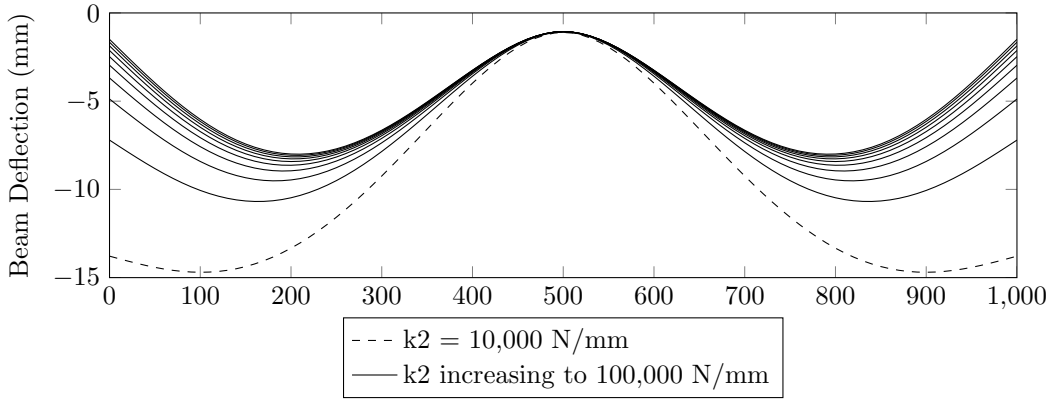

Figure B.4: Changing Beam deflections given changing Inner Support Stiffness (K_B)

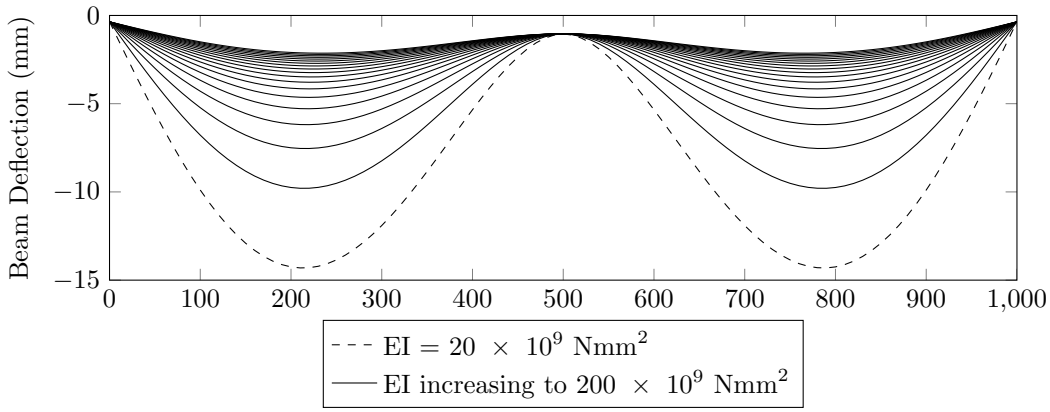

Figure B.5: Changing Beam deflections given changing Beam Stiffnesses (EI)

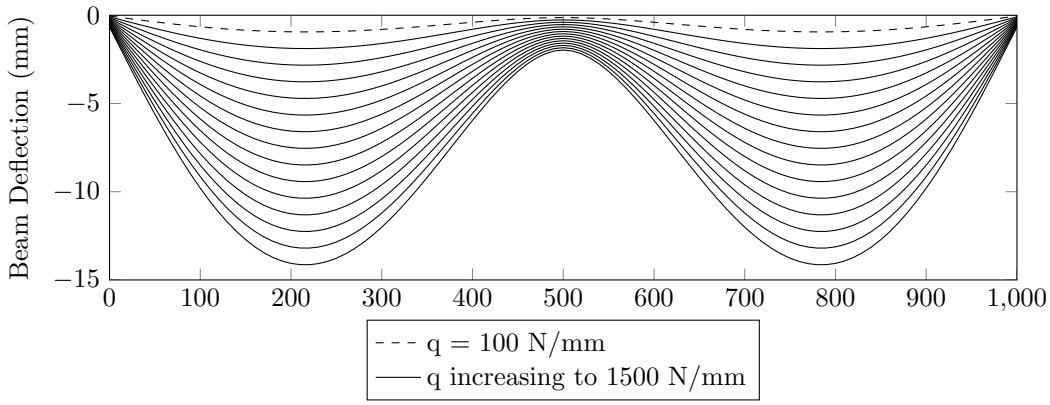

Figure B.6: Changing Beam deflections given changing applied load (q)

The closed form of the differential displacement equation presented above provides for two ways to decease the relative displacement.

- Increasing the stiffness of the plate (EI).
- Detailing the external supports to be approximately three times as stiff as the internal support.

Appendix C

Design Options for Dissipation Connections and Reinforcement

C.1 Steel Reinforcing Options

Table C.1: Steel reinforcing maximum moment capacities ($\phi = 0.9$)

Depth \ Width	252 mm	315 mm	378 mm	441 mm	504 mm
600 mm	119 kNm	149 kNm	179 kNm	208 kNm	-
800 mm	167 kNm	208 kNm	250 kNm	292 kNm	333 kNm
1000 mm	-	269 kNm	321 kNm	375 kNm	429 kNm
1200 mm	-	327 kNm	393 kNm	458 kNm	524 kNm

600mm DEEP BEAMS/COLUMNS

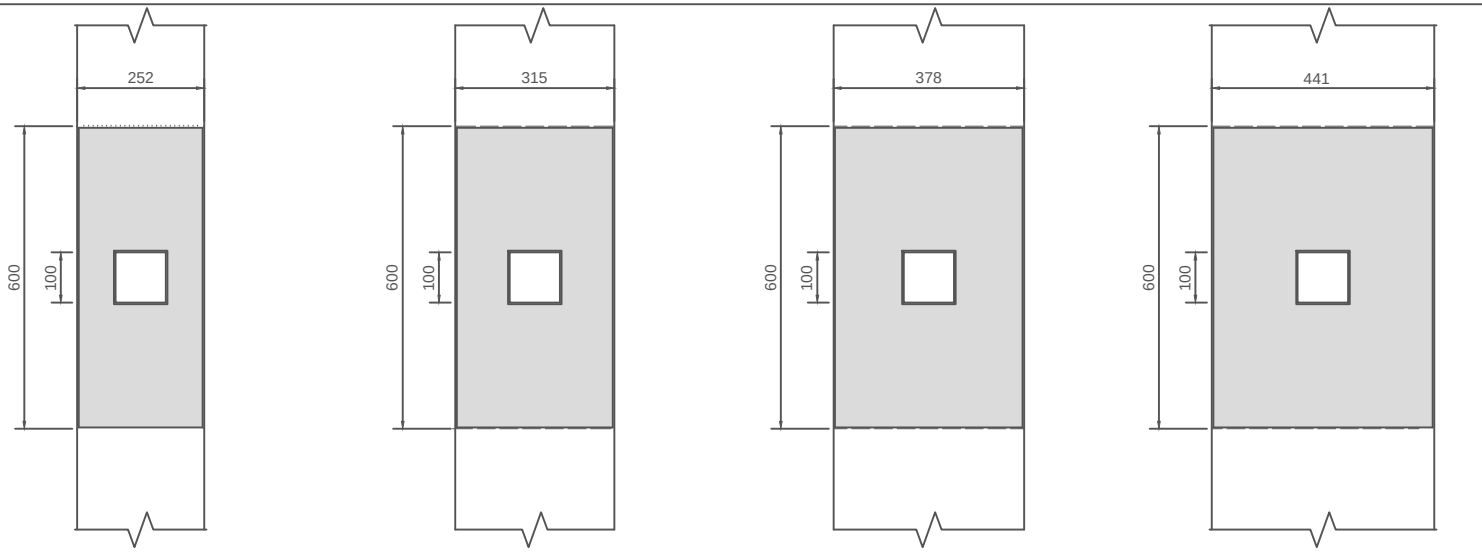

$ØM_n$ = 119 kNm | $ØM_n$ = 149 kNm | $ØM_n$ = 179 kNm | $ØM_n$ = 208 kNm

NOTE:

1. DESIGNS ARE PRESENTED FOR PRELIMINARY SIZING ONLY. DETAILED CALCULATIONS MUST BE UNDERTAKEN BY DESIGNERS ON A PROJECT SPECIFIC BASIS

800mm DEEP BEAMS/COLUMNS

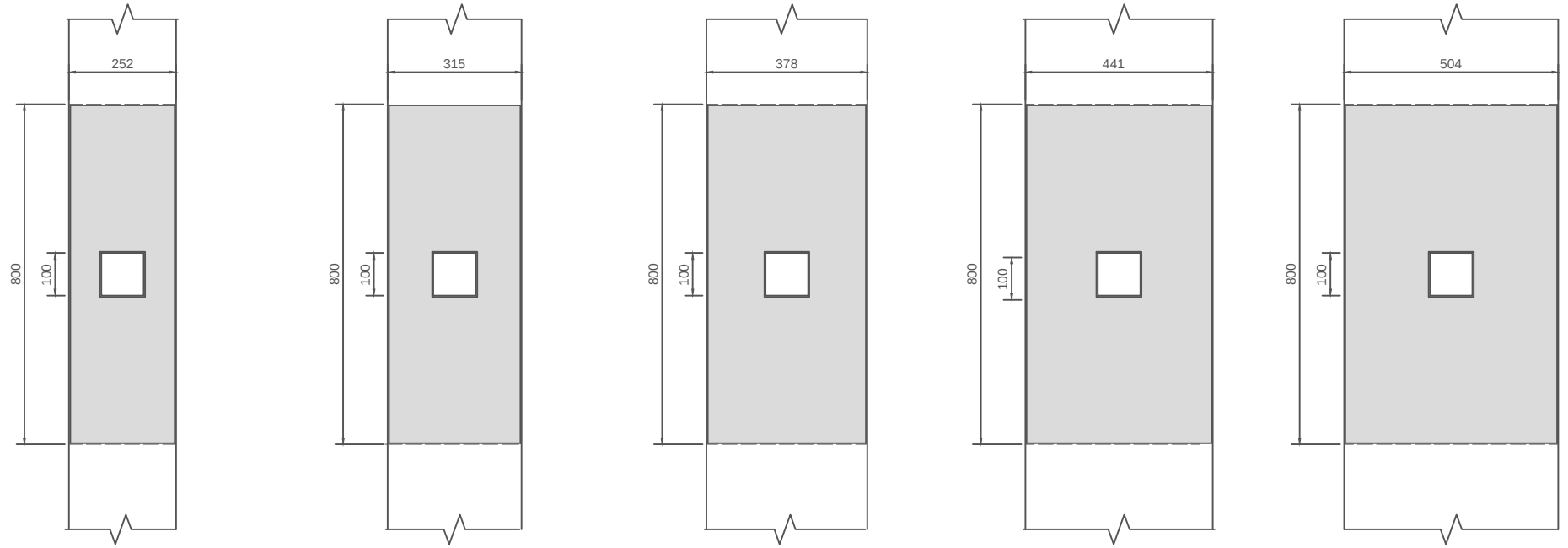

$ØM_n$ = 167 kNm | $ØM_n$ = 208 kNm | $ØM_n$ = 250 kNm | $ØM_n$ = 292 kNm | $ØM_n$ = 333 kNm

TITLE:	NUMBER:	DATE:
STEEL REINFORCING - SHEET 1 OF 3	DRG-1101	11/08/2014
PROJECT:	BY:	SCALE:
DETAILING OPTIONS	T. ARMSTRONG	1:15 (AT A4)

UNIVERSITY OF CANTERBURY
Te Whare Wānanga o Waitaha

NOTE:

1. DESIGNS ARE PRESENTED FOR PRELIMINARY SIZING ONLY. DETAILED CALCULATIONS MUST BE UNDERTAKEN BY DESIGNERS ON A PROJECT SPECIFIC BASIS

1000mm DEEP BEAMS/COLUMNS

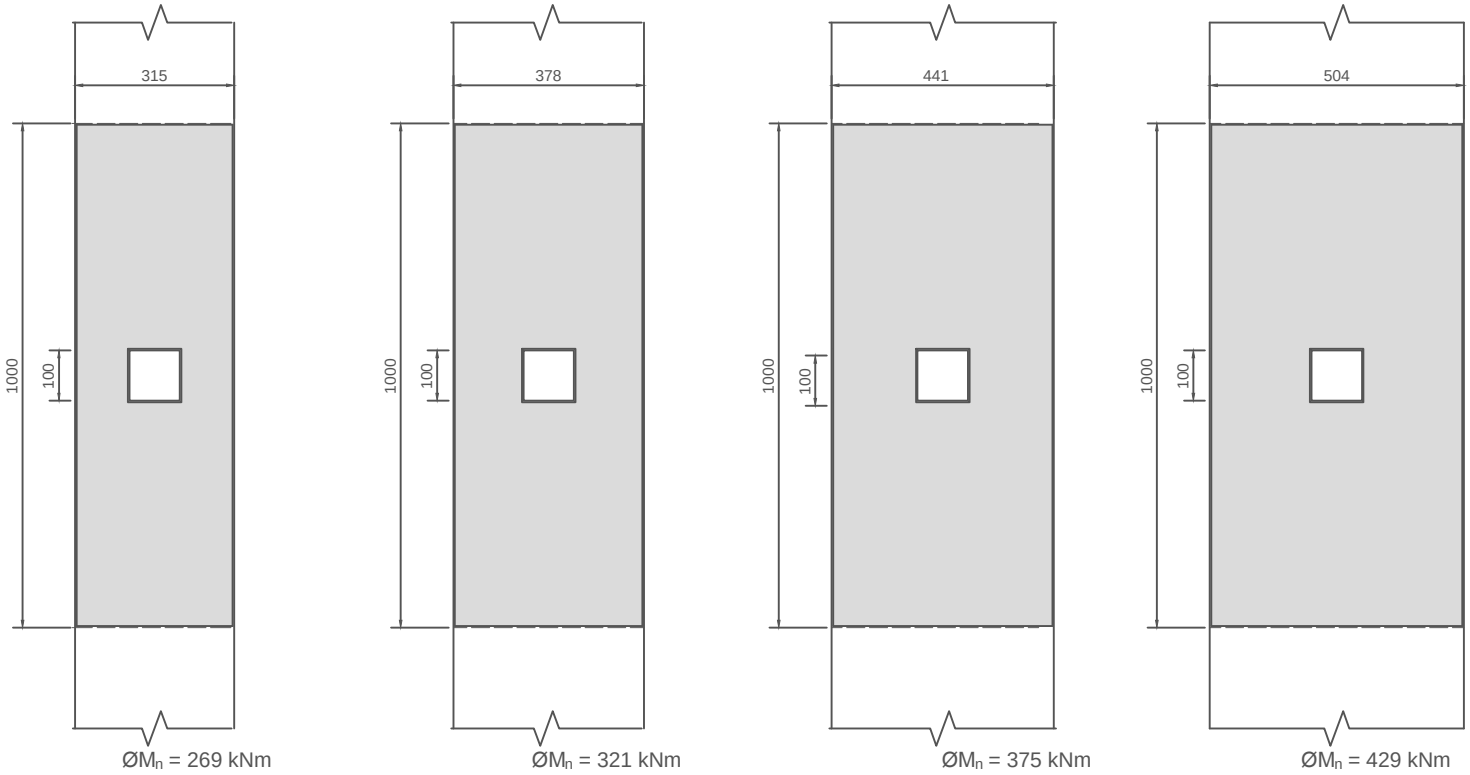

$ØM_n$ = 269 kNm

$ØM_n$ = 321 kNm

$ØM_n$ = 375 kNm

$ØM_n$ = 429 kNm

TITLE: STEEL REINFORCING - SHEET 2 OF 3	NUMBER: DRG-1102	DATE: 11/08/2014	UC UNIVERSITY OF CANTERBURY Te Whare Wānanga o Waitaha
PROJECT: DETAILING OPTIONS	BY: T. ARMSTRONG	SCALE: 1:15 (AT A4)	

NOTE:

1. DESIGNS ARE PRESENTED FOR PRELIMINARY SIZING ONLY. DETAILED CALCULATIONS MUST BE UNDERTAKEN BY DESIGNERS ON A PROJECT SPECIFIC BASIS

1200mm DEEP BEAMS/COLUMNS

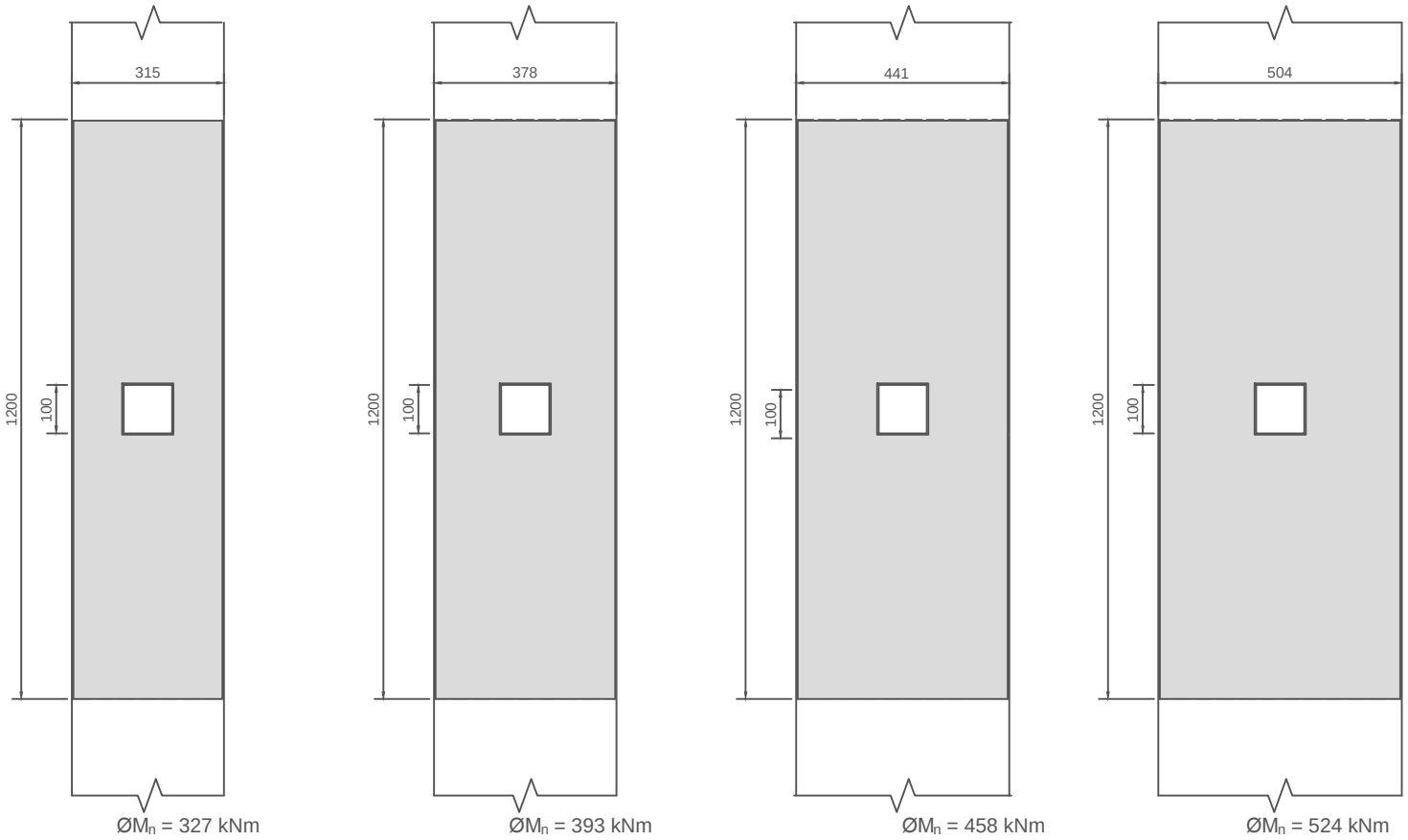

TITLE: STEEL REINFORCING - SHEET 3 OF 3	NUMBER: DRG-1103	DATE: 11/08/2014	UC UNIVERSITY OF CANTERBURY Te Whare Wānanga o Waitaha
PROJECT: DETAILING OPTIONS	BY: T. ARMSTRONG	SCALE: 1:15 (AT A4)	

C.2 Screw Reinforcing Options

Table C.2: Screw reinforcing maximum moment capacities

Depth \ Width	252 mm	315 mm	378 mm	441 mm	504 mm
600 mm	428 kNm 380 ×8[a] 5 × 11[b]	523 kNm 380 ×8 5 × 14	633 kNm 380 ×8 5 × 17	743 kNm 380 ×8 5 × 20	-
800 mm	740 kNm 580 ×8 7 × 11	925 kNm 580 ×8 7 × 14	1110 kNm 580 ×8 7 × 17	1295 kNm 580 ×8 7 × 20	1480 kNm 580 ×8 7 × 23
1000 mm	-	1422 kNm 520 ×8 10 × 14	1706 kNm 520 ×8 10 × 17	1991 kNm 520 ×8 10 × 20	2275 kNm 520 ×8 10 × 23
1200 mm	-	2007 kNm 650 ×10 10 × 11	2408 kNm 650 ×10 10 × 13	2810 kNm 650 ×10 10 × 16	3221 kNm 650 ×10 10 × 18

[a] Screw length and diameter (mm)
[b] Screw layout ($n_{rows} \times n_{columns}$).

600mm DEEP BEAMS/COLUMNS

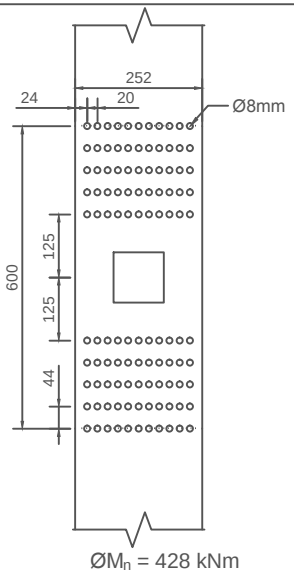

$ØM_n$ = 428 kNm

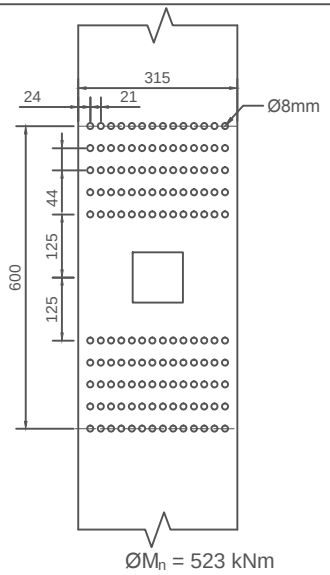

$ØM_n$ = 523 kNm

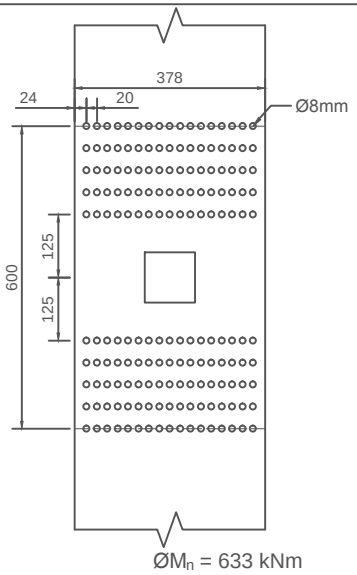

$ØM_n$ = 633 kNm

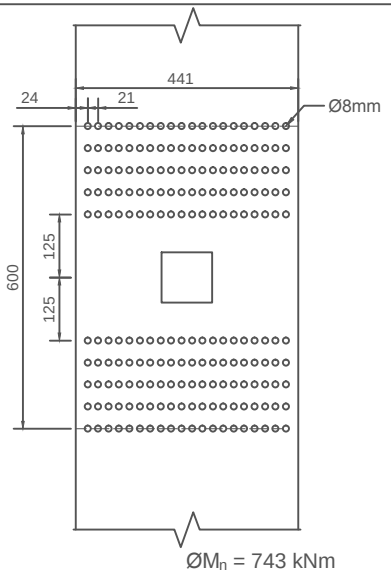

$ØM_n$ = 743 kNm

NOTE:

1. DESIGNS ARE PRESENTED FOR PRELIMINARY SIZING ONLY. DETAILED CALCULATIONS MUST BE UNDERTAKEN BY DESIGNERS ON A PROJECT SPECIFIC BASIS
2. SCREWS TO EXTEND AT LEAST HALF THE COLUMN DEPTH
3. STEEL BEARING PLATES TO BE PROVIDED COVERING ALL SCREW HEADS

800mm DEEP BEAMS/COLUMNS

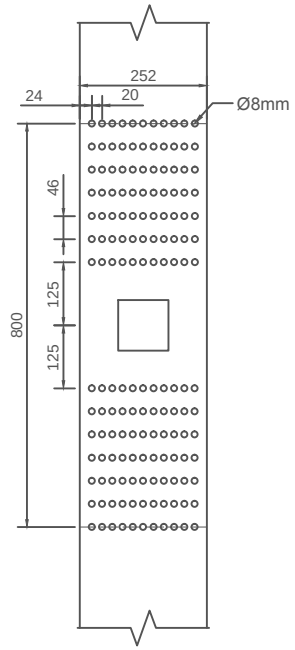

$ØM_n$ = 740 kNm

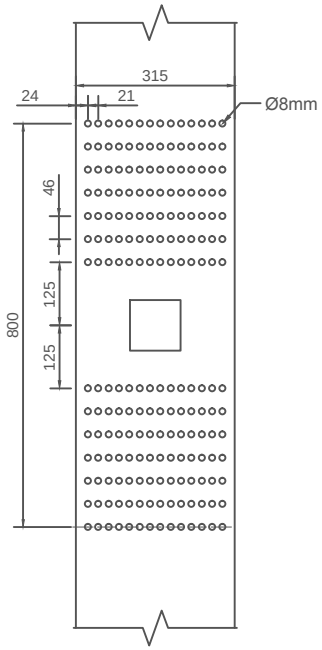

$ØM_n$ = 925 kNm

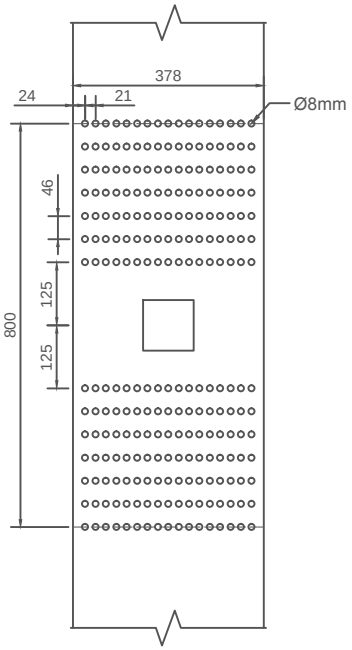

$ØM_n$ = 1110 kNm

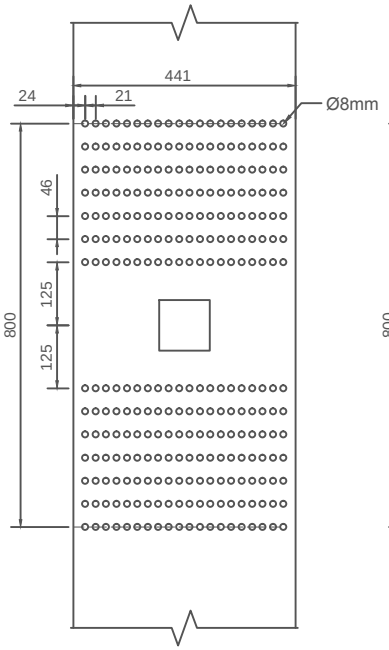

$ØM_n$ = 1295 kNm

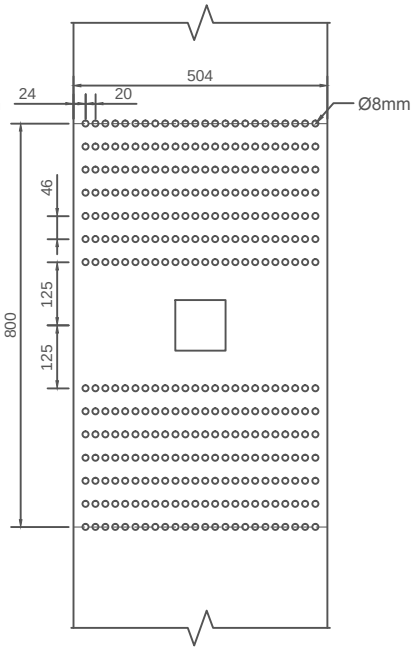

$ØM_n$ = 1480 kNm

TITLE: SCREW REINFORCING - SHEET 1 OF 3	NUMBER: DRG-1201	DATE: 11/08/2014
PROJECT: DETAILING OPTIONS	BY: T. ARMSTRONG	SCALE: 1:15 (AT A4)

UNIVERSITY OF CANTERBURY
Te Whare Wānanga o Waitaha

1000mm DEEP BEAMS/COLUMNS

NOTE:

1. DESIGNS ARE PRESENTED FOR PRELIMINARY SIZING ONLY. DETAILED CALCULATIONS MUST BE UNDERTAKEN BY DESIGNERS ON A PROJECT SPECIFIC BASIS
2. SCREWS TO EXTEND AT LEAST HALF THE COLUMN DEPTH
3. STEEL BEARING PLATES TO BE PROVIDED COVERING ALL SCREW HEADS

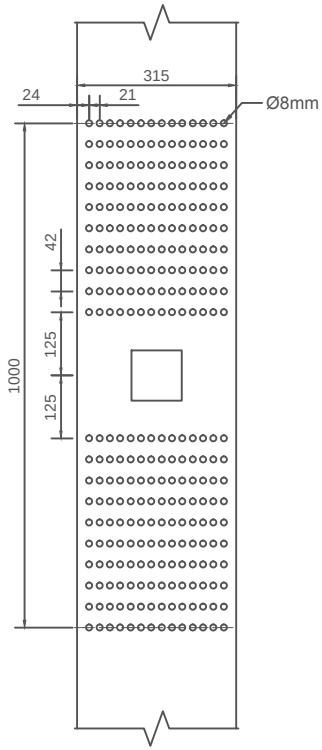

$ØM_n$ = 1422 kNm

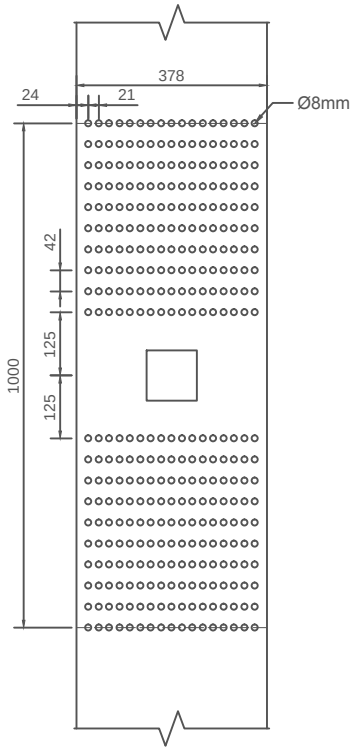

$ØM_n$ = 1706 kNm

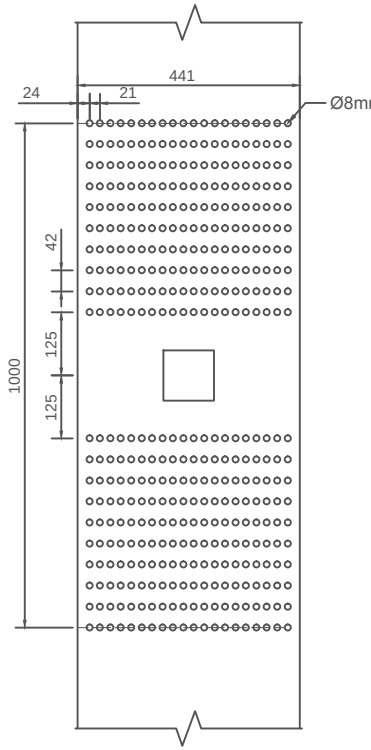

$ØM_n$ = 1991 kNm

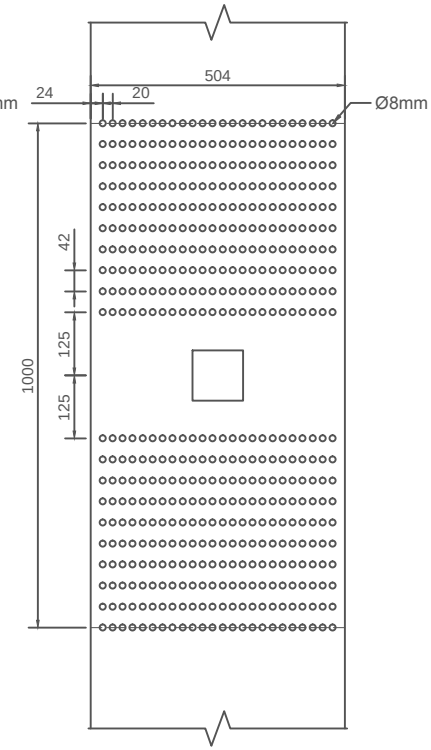

$ØM_n$ = 2275 kNm

TITLE: SCREW REINFORCING - SHEET 2 OF 3	NUMBER: DRG-1202	DATE: 11/08/2014	UNIVERSITY OF CANTERBURY Te Whare Wānanga o Waitaha
PROJECT: DETAILING OPTIONS	BY: T. ARMSTRONG	SCALE: 1:15 (AT A4)	

1200mm DEEP BEAMS/COLUMNS

NOTE:

1. DESIGNS ARE PRESENTED FOR PRELIMINARY SIZING ONLY. DETAILED CALCULATIONS MUST BE UNDERTAKEN BY DESIGNERS ON A PROJECT SPECIFIC BASIS
2. SCREWS TO EXTEND AT LEAST HALF THE COLUMN DEPTH
3. STEEL BEARING PLATES TO BE PROVIDED COVERING ALL SCREW HEADS

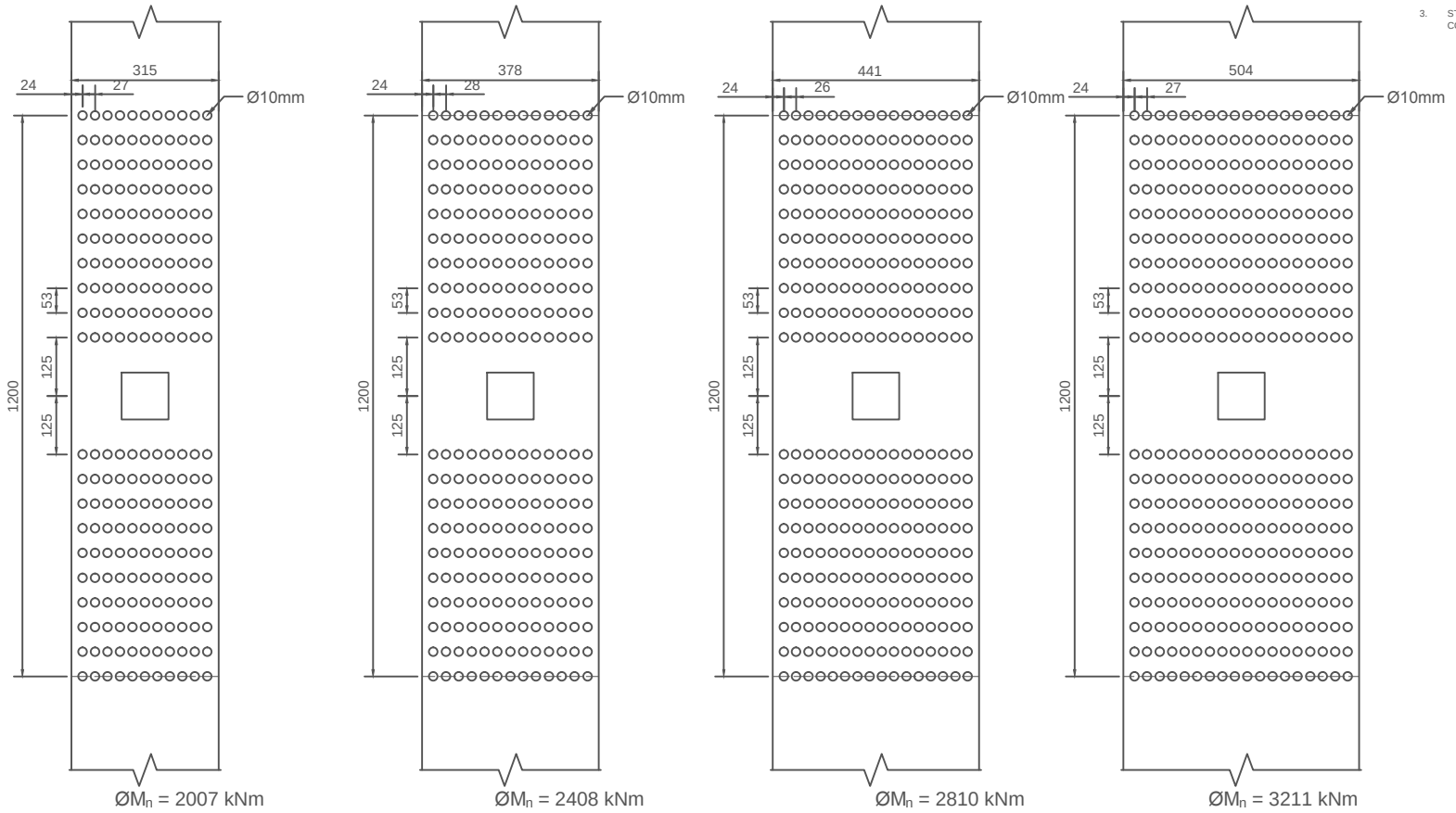

TITLE: SCREW REINFORCING - SHEET 3 OF 3	NUMBER: DRG-1203	DATE: 11/08/2014	UNIVERSITY OF CANTERBURY Te Whare Wānanga o Waitaha
PROJECT: DETAILING OPTIONS	BY: T. ARMSTRONG	SCALE: 1:15 (AT A4)	

Appendix D

Construction Monitoring

The Merritt Building was under construction in Christchurch while this research was being undertaken. The joints tested in this experimental campaign were derived from designs for this building as discussed in Chapter 3. A laser range finder was used to measure the length between column faces while the building was under construction. The locations where measurements were taken are depicted in Figures D.1 and D.2. The data collected is provided in Table D.1. Not all locations were safely accessible on each monitoring visit.

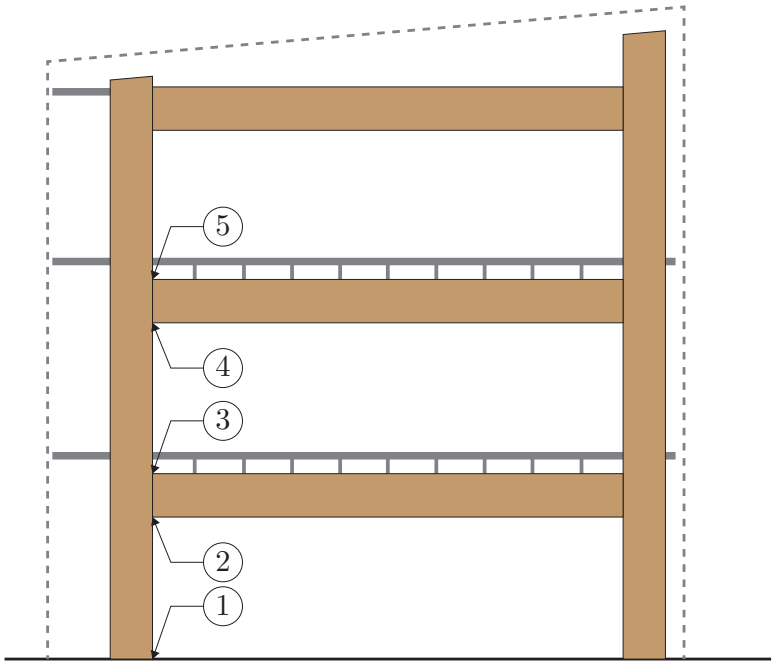

Figure D.1: Typical frame elevation showing recording station numbering

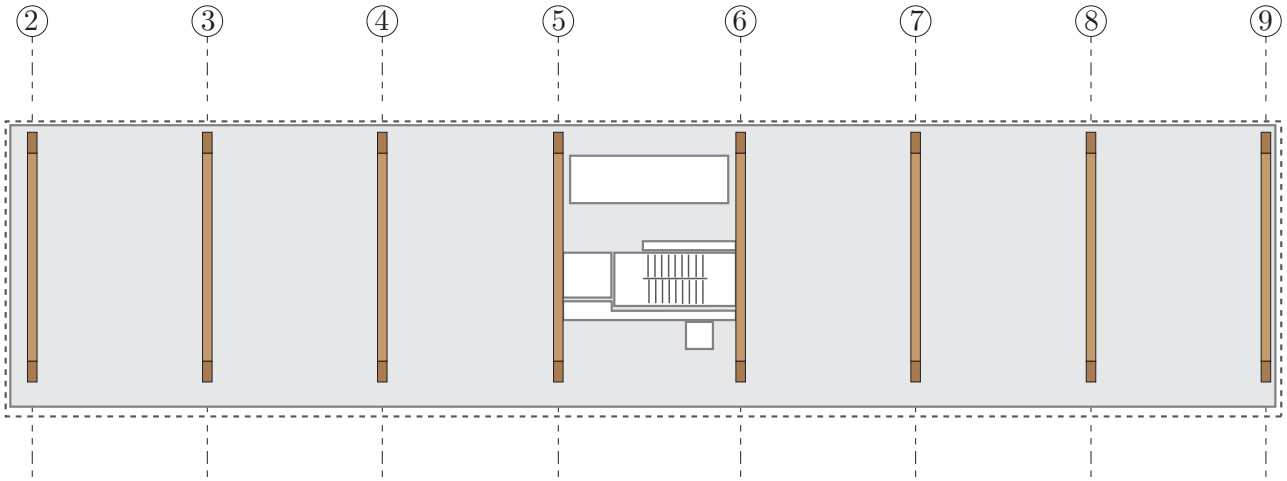

Figure D.2: Typical floor plan showing grid numbering

Table D.1: Measured beam lengths (mm) from Merritt Building monitoring

Frame	Date / Position	09/10/12 (0 days)	16/10/12 (7 days)	24/10/12 (8 days)	01/11/12 (8 days)	12/11/12 (11 days)	28/11/12 (16 days)	14/12/12 (16 days)	17/04/13 (124 days)
2	1		8805	8805	8805	8805	8805	8805	8805
	2			8803	8803			8801	8801
	3			8803	8803		8803	8803	8803
	4							8801	8800
	5							8802	8802
3	1		8798	8797	8797	8798	8798	8796	8797
	2			8797	8797		8795	8796	8795
	3			8800	8800		8800	8800	8801
	4							8799	8799
	5							8804	8804
4	1	8800	8800	8800	8800	8800	8801	8804	8801
	2	8799		8799	8799			8798	
	3	8800		8801	8800		8800	8800	8801
	4	8797						8797	8795
	5	8797						8797	8804
5	1	8796	8796	8796	8796	8796	8796	8794	8796
	2	8795	8795	8794	8796			8795	8793
	3	8795			8796		8795	8795	8796
	4	8794						8791	
	5	8796						8795	
6	1		8795	8793	8795	8795	8795	8747	8794
	2		8795	8794	8794		8792	8793	8792
	3		8795		8794		8795	8795	8794
	4								8792
	5							8797	8796
7	1		8794	8796	8795	8795	8795	8795	8795
	2		8794	8794	8794		8794	8792	8792
	3		8800	8794	8794		8794	8794	8975
	4							8790	8794
	5							8796	8794
8	1	8797	8799	8800	8800	8801	8800	8801	8801
	2	8799	8798	8798	8798			8797	8796
	3	8799		8801	8800		8800	8800	8801
	4	8800						8795	8793
	5	8799						8799	8799
9	1		8800	8799	8800	8800	8800	8799	
	2	8800	8799	8798	8798		8798	8797	8799
	3	8795	8799	8799	8799		8798	8799	8800
	4								8796
	5	8798						8798	8798